UNIVERSITÀ DEGLI STUDI DI MILANO

Department of Pharmaceutical Sciences

Doctoral Program in Pharmaceutical Sciences – XXXV Cycle

A4β2 neuronal nicotinic acetylcholine receptor ligands: from subtype selective to stoichiometric isoform selective partial agonism

CHIM/08 – Medicinal Chemistry

PhD thesis of Rebecca APPIANI

Reg. Number: R12544

Supervisor: Prof. Cristiano BOLCHI

Co-Supervisor: Prof. Marco PALLAVICINI

PhD Coordinator: Prof. Giancarlo ALDINI

Academic Year 2021-2022

Мама всегда хотела, чтобы из меня вышел толк.
Так и получилось — толк вышел, а бестолочь осталась.

Mio padre mi ha fatto il più bel regalo che qualcuno
poteva fare a un'altra persona: ha creduto in me.

Я могу рассказать бабушке все, что угодно. И знаю,
что ее уши всегда слушают, а руки всегда поддерживают.

Preface

This dissertation entitled “A4β2 neuronal nicotinic acetylcholine receptor ligands: from subtype selective to stoichiometric isophorm selective partial agonism” describes the research performed as part of the PhD program of Pharmaceutical Sciences at the Department of Pharmaceutical Sciences at Università degli Studi di Milano from October 2019 to September 2022, that resulted in 6 publications. In addition to the PhD project, some time was dedicated to green chemistry topics, which are not included in this thesis, but resulted in 3 publications. The chemistry experimental work was performed at the department of Pharmaceutical Sciences, Universitià degli Studi di Milano, and was supervised by Professors Cristiano Bolchi and Marco Pallavicini.

The time period from August 2021 to December 2021 was spent at the Pharmacy Department, University of Texas at Tyler, under the supervision of Professor Ayman K. Hamouda performing pharmacological analysis included in this thesis.

The PhD program was financed by Università degli Studi di Milano.

Publication list

1) Bavo F, Pallavicini M, Pucci S, Appiani R, Giraudo A, Eaton B, Lucero L, Gotti C, Moretti M, Whiteaker P, Bolchi C. From 2-Triethylammonium Ethyl Ether of 4-Stilbenol (MG624) to Selective Small-Molecule Antagonists of Human α9α10 Nicotinic Receptor by Modifications at the Ammonium Ethyl Residue. *J Med Chem.* 2022 Jul 28;65(14):10079-10097. doi: 10.1021/acs.jmedchem.2c00746.
2) Appiani R, Morano C, Roda G, Pallavicini M, Bolchi C. 4-, 5-, 6-, and 7-Hydroxybenzofuran: a unified strategy for a two-step synthesis of versatile benzofuranic building blocks. *Arkivoc*. 2022 Jun 259-269. doi: 10.24820/ark.5550190.p011.791.
3) Appiani R, Pallavicini M, Hamouda AK, Bolchi C. Pyrrolidinyl benzofurans and benzodioxanes: Selective α4β2 nicotinic acetylcholine receptor ligands with different activity profiles at the two receptor stoichiometries. *Bioorg Med Chem Lett.* 2022 Jun 1;65:128701. doi: 10.1016/j.bmcl.2022.128701.
4) Bertolini V, Appiani R, Pallavicini M, Bolchi C. Green Oxidation of Ketones to Lactones with Oxone in Water. *J Org Chem.* 2021 Nov 5;86(21):15712-15716. doi: 10.1021/acs.joc.1c01469.
5) Bavo F, Pallavicini M, Appiani R, Bolchi C. Determinants for α4β2 vs. α3β4 Subtype Selectivity of Pyrrolidine-Based nAChRs Ligands: A Computational Perspective with Focus on Recent cryo-EM Receptor Structures. *Molecules*. 2021 Jun 12;26(12):3603. doi: 10.3390/molecules26123603.
6) Bolchi C, Appiani R, Roda G, Bertolini V, Arnoldi S, Pallavicini M. Efficient conversion of D-mannitol into 1,2:5,6-diacetonide with Aquivion-H as a recyclable catalyst. *Carbohydr Res*. 2021 Jan;499:108229. doi: 10.1016/j.carres.2020.108229.
7) Bavo F, Pallavicini M, Gotti C, Appiani R, Moretti M, Colombo SF, Pucci S, Viani P, Budriesi R, Renzi M, Fucile S, Bolchi C. Modifications at C(5) of 2-(2-Pyrrolidinyl)-Substituted 1,4-Benzodioxane Elicit Potent α4β2 Nicotinic Acetylcholine Receptor Partial Agonism with High Selectivity over the α3β4 Subtype. *J Med Chem.* 2020 Dec 24;63(24):15668-15692. doi: 10.1021/acs.jmedchem.0c01150.

8) Bolchi C, Bavo F, Appiani R, Roda G, Pallavicini M. 1,4-Benzodioxane, an evergreen, versatile scaffold in medicinal chemistry: A review of its recent applications in drug design. *Eur J Med Chem.* 2020 Aug 15;200:112419. doi: 10.1016/j.ejmech.2020.112419.
9) Braida D, Ponzoni L, Moretti M, Viani P, Pallavicini M, Bolchi C, Appiani R, Bavo F, Gotti C, Sala M. Behavioural and pharmacological profiles of zebrafish administrated pyrrolidinyl benzodioxanes and prolinol aryl ethers with high affinity for heteromeric nicotinic acetylcholine receptors. *Psychopharmacology.* 2020 Aug;237(8):2317-2326. doi: 10.1007/s00213-020-05536-6.
10) Airoldi V, Piccolo O, Roda G, Appiani R, Bavo F, Tassini R, Paganelli S, Arnoldi S, Pallavicini M, Bolchi C. Efficient One-Pot Reductive Aminations of Carbonyl Compounds with Aquivion-Fe as a Recyclable Catalyst and Sodium Borohydride. EurJOC. 2020 Jan;2:162-168. doi: 10.1002/ejoc.201901614.

Abstract

This PhD thesis focuses on the study of the α4β2 nicotinic acetylcholine receptors (nAChRs). This dissertation is divided into two parts. The first part is centred on the design, synthesis, and biological evaluation of compounds selective for the orthosteric and unorthodox binding sites of the α4β2 nAChRs. In the second part, attention is paid to the study of a photoactivatable α4β2 nAChRs full agonist.

Part 1

The first goal of Part 1 was the mutational studies of Ser108 residue of the hydrophilic pocket of the β2(-) side of the α4β2 orthosteric binding site with the purpose of studying the importance of the hydroxyl group of serine residue and the steric encumbrance in the pocket. For this reason, binding experiments were performed on the heterologously expressed human α4β2 receptor and its three Ser108→Leu, Ser108→Phe and Ser108→Ala mutants using the most promising partial agonists synthesized previously.

The second goal was the synthesis and pharmacological evaluation of the naked and hydroxy/methoxy decorated benzofuran-based compound in order to study the implications of the flexibility reduction, abolishment of cycle stereogenic and of the one of the two oxygen in comparison with previously tested benzodioxane derivatives. Subsequently, the most promising benzodioxane compounds and the obtained benzofuran derivatives were evaluated for their affinity and activity on the two distinct α4β2 nAChR isoforms: $(\alpha4)_2(\beta2)_3$ and $(\alpha4)_3(\beta2)_2$.

The third goal was the study of the *in vivo* effects of prolinol aryl ethers and pyrrolidinyl benzodioxanes full and partial agonists. These compounds were tested for their effects on zebrafish behaviour. In particular, full agonists were tested for their ability to improve spatial memory and attention, and partial agonist for its ability to block the rewarding effects of nicotine and therefore its potential use for smoking cessation.

The fourth goal was the design, synthesis and pharmacological evaluation of selective agonists for the α4α4 unorthodox binding site of the α4β2 nAChR based on the structure of NS9283, an α4α4selective compound, described in the literature. The main aim was to identify new hit

compounds potentially selective at the $(\alpha4)_3(\beta2)_2$ receptor isoform with a better pharmacological profile.

Part 2

Regarding the second part of this thesis, it focuses on the synthesis of a photoactivatable α4β2 nAChR full agonist with the purpose to spatiotemporally control its release with light at the specific site of action. To follow this strategy, 8-bromo-7-hydroxy-2-methylquinoline (BHQ) and 8-cyano-7-hydroxy-2-methylquinoline (CyHQ) protecting groups were synthesized and used to cage a previously synthesized full agonist. Subsequently, its release after the irradiation with the UV light at 365 nm was followed using HPLC in order to obtain a full photo-chemical characterization of the caged compounds to get necessary information for *in vitro/in vivo* experiments.

Abbreviations and acronyms

1PE	one-photon excitation
2PE	two-photon excitation
Å	angstrom
α-Bgtx	α-bungarotoxin
Ac	acetyl
ACh	acetylcholine
AChBPs	acetylcholine binding proteins
AChE	acetylcholinesterase
ACN	acetonitrile
AcOH	acetic acid
AD	Alzheimer's disease
BBB	blood-brain barrier
BHQ	8-bromo-7-hydroxyquinoline
Bn	benzyl
Boc	tert-butyloxycarbonyl
BODIPY	boron-dipyrromethane
Bu	butyl
Cbz	benzyloxycarbonyl
ChAT	choline acetyltransferase
Ci	Curie
CNS	central nervous system
cRNA	complementary ribonucleic acid
CryoEM	cryo electron microscopy
CTD	C-terminal extracellular domain
CyHQ	8-cyano-7-hydroxyquinoline
DA	dopamine
DCM	dichloromethane
dFBr	desformylflustrabromine
DMA	dimethylacetamide

DMED	Dulbecco's modified eagle medium
DMSO	dimethylsulfoxide
e.g.	exempli gratia
EC_{50}	half maximal effective concentration
EDTA	ethylenediaminetetraacetic acid
EGTA	ethylene glycol-bis(β-aminoethyl ether)-N,N,N’,N’-tetraacetic acid
Et	ethyl
EtOAc	ethyl acetate
EtOH	ethanol
Fab	high-affinity antigen-binding fragment
FBDD	fragment-based drug discovery
fs	femtosecond
g	gram
GABA	γ-aminobutyric acid
GM	Göppert-Mayer
GPCR	G protein coupled receptor
h	hour
HBA	hydrogen-bond acceptor
HBD	hydrogen-bond donor
HEK	human embryonic kidney
HEPES	4-(2-hydroxyethyl)-1-piperazineethanesulfonic acid
HS	high sensitivity
Hz	hertz
i.p.	intraperitoneal
*i*PrOH	isopropanol
kcal	kilocalorie
Kd	dissociation constant
kg	kilogram
Ki	inhibition constant
kJ	kilojoule
LBD	ligand binding domain

LC	liquid chromatography
LDT	laterodorsal tegmental nucleus
LGIC	ligand gated ion channel
LS	low sensitivity
Ls-AChBP	*Lymnaea stagnalis* AChBP
mAChR	muscarinic acetylcholine receptor
mCi	millicurie
Me	methyl
MEM	methoxyethoxymethyl
MeOH	methanol
mg	milligram
µg	microgram
MHz	megahertz
min	minute
mL	millilitre
mol	mole
MOPS	3-(N-morpholino)propanesulfonic acid
mm	millimetre
mM	millimolar
µM	micromolar
mmol	millimole
mp	melting point
Ms	Methansulfonyl
MS	mass spectrometry
mV	millivolt
MWC	Monod-Wyman-Changeux
N.A.	not available
NAc	nucleus accumbens
nAChR	nicotinic acetylcholine receptor
NAM	negative allosteric modulator
NBS	*N*-bromosuccinimide

NIS	*N*-iodosuccinimide
nm	nanometre
nM	nanomolar
NMR	nuclear magnetic resonance
NNAL	4-(methylnitrosamino)-1-(3-pyridyl)-1-butanol
NNK	4-(metylnitrosamino)-1-(3-pyridyl)-1-butanon
NNN	*N*'-nitrosonornicotine
NTD	N-terminal extracellular domain
OT	olfactory tubercle
PAM	positive allosteric modulator
PBS	phosphate-buffered saline
PD	Parkinson's disease
PFC	prefrontal cortex
pH	potential of hydrogen
Ph	phenyl
pic-BH3	2-picoline borane complex
pLGIC	protein ligand gated ion channel
pM	picomolar
PNS	peripheral nervous system
PPG	photoremovable protecting group
p-TSA	p-toluenesulfonic acid
R_f	retention factor
RNA	ribonucleic acid
rpm	revolutions per minute
rt	room temperature
SAM	silent allosteric modulator
SAR	structure-activity relationship
sat	saturated
Saz-A	sazetidine-A
SD	standard deviation
s	second

sec	second
SNc	substantia nigra pars compacta
T	tritium
TEA	triethylamine
THF	tetrahydrofuran
TLC	thin layer chromatography
TM	transmembrane
TMD	transmembrane domain
TPP	tegmental pedunculopontine nucleus
UV	ultraviolet
VAChT	vesicular acetylcholine transporter
VDB	vesicle dialysis buffer
VORT	virtual object recognition test
VTA	ventral tegmental area
W	watt
WT	wild type

The 3-letter and 1-letter IUPAC nomenclature are used for the 21 proteinogenic amino acids.

Table of Contents

1. Nicotinic acetylcholine receptors (nAChRs)

1.1. Structure and function

Acetylcholine (ACh) is one of the most important neurotransmitters in both the central nervous system (CNS) and peripheral nervous systems (PNS). There are two main classes of ACh receptors: nicotinic acetylcholine receptors (nAChRs) and muscarinic acetylcholine receptors (mAChRs). Their names derive from compounds that selectively bind and activate one of the receptor types. Nicotine is selective for nAChRs and muscarine for mAChRs *(Figure 1)*. They are responsible for different physiological and pathological effects.

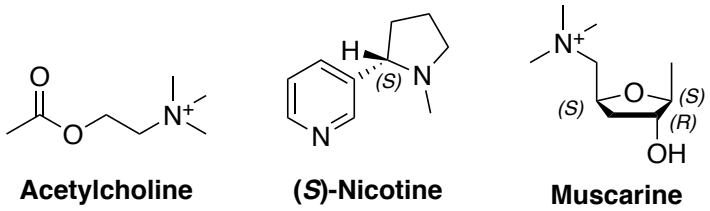

Acetylcholine **(*S*)-Nicotine** **Muscarine**

Figure 1. The endogenous neurotransmitter ACh, the exogenous agonist of nAChRs (S)-Nicotine and of mAChRs Muscarine.

mAChRs are seven-transmembrane domain receptors (7TM) belonging to the superfamily of G-coupled receptors (GPCRs). The activation of these receptors through the neurotransmitter binding mediate a metabotropic response.[1]

On the other hand, nAChRs are ligand-gated ion channels (LGICs). They are transmembrane proteins that allow a regulated flux of ions. Neurotransmitters, such as ACh, or agonists, such as nicotine, allows the pore opening and so, the channel gating.[2]

nAChRs are hetero- or homopentameric ion channels made up of 5 different or identical polypeptide subunits assembled to form diverse collection of subunits with a central pore permeable to mono- and/or divalent cations such as Na^+, K^+ or Ca^{2+}. All the subunits have a common structure. They are polypeptides formed by 500-600 amino acid residues. Each subunit begins with a short C-terminal extracellular domain (CTD), four α-helix hydrophobic transmembrane domains (TMD) and an N-terminal extracellular domain (NTD). This last domain contains a loop formed by circa 13 amino acids, constrained by a disulphide bridge between two cysteines, C192 and C193, but only in α subunits. This particular structure gives

the name to Cys-loop receptors and its integrity is essential for the architecture and function of the receptor.[3] On the extracellular domain, at the interface between two adjacent subunits, there is the ligand binding domain (LBD) which contains the orthosteric binding sites (*Figure 2*). The ion flux is regulated by ligand binding at the orthosteric binding site. Agonist binding induces channel opening with the consequent cation flux according to their electrochemical gradient (K^+ outward, Na^+ and Ca^{2+} inward), causing the membrane depolarization. Instead, antagonist binding stabilizes a non-conductive receptor conformation. Cation selectivity is determined by some negatively charged amino acids placed near the channel entrance.[4]

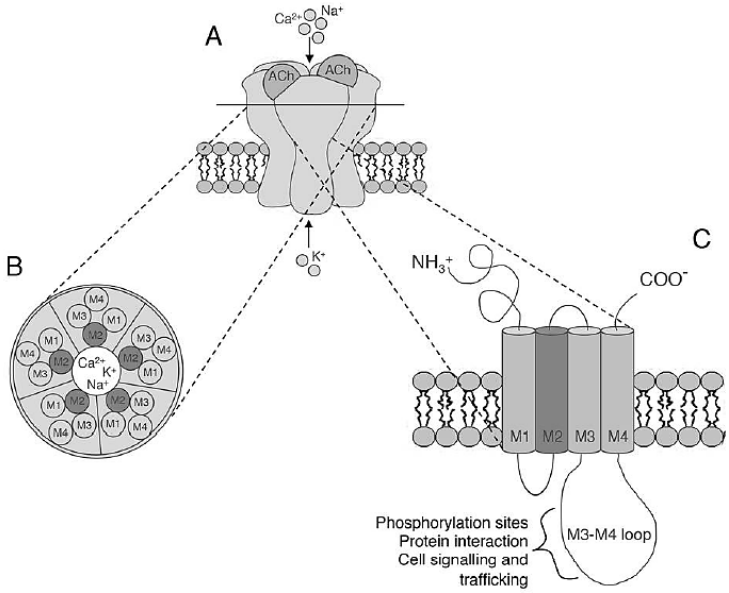

Figure 2. The structure of neuronal nAChR. A) Structure showing the arrangement of nAChR subunits and the location of the two ACh-binding sites. B) A section of the nAChR with the five subunits arranged around a central cation-conducting pore. C) A single nAChR subunit embedded in the membrane. The extracellular amino acid terminal portion is followed by three hydrophobic transmembrane domains (M1-M3), a large intracellular loop, and a fourth hydrophobic transmembrane domain (M4). The transmembrane M2 segments lining the ion path wall are shown in dark grey. Adapted from Zoli et al.[5]

nAChRs, as said previously, are called Cys-loop receptors and belong to a large superfamily of homologue receptors called Cys-loop LGIC superfamily that includes also $GABA_A$, $GABA_A$-r, glycine, 5-HT_3 and zinc-activated receptors.[6]

The physiological consequences of membrane depolarization depend on the localization of nAChRs. nAChRs are classified based on their tissue distribution: muscle-type nAChRs and neuronal-type nAChRs. Muscle nAChRs are involved in muscle contraction due to their activation in the neuromuscular junction. Neuronal nAChRs are distributed mostly in pre- and post-synaptic ganglia, hippocampus, retina, cortex, hypothalamus and striatum nucleus.[7] They

mediate the fast synaptic transmission in both CNS and PNS by controlling the release of different neurotransmitters and influence the cell excitability.[3,8] The activation of nAChRs is involved in various physiological processes, such as cell differentiation, proliferation and inflammatory responses.[5] In fact, they are associated with different cognitive and pathological conditions, such as anxiety, pain, depression, epilepsy, Alzheimer's and Parkinson's diseases, nicotine and alcohol addiction.[9] Neuronal nAChRs are also distributed in non-neuronal cells and tissues like endothelial cells and immune system, glial cells, cancer cells, lung epithelium and epithelial cells of the digestive tract.[5]

1.2. Classification

During the years, different classifications of nAChRs were proposed. All of them are based on structural, phylogenetic or pharmacological approaches. So far, 16 nAChR subunits have been described in humans, which can combine into homo- or heteropentameric structures. These subunits are classified based on their structural similarity: α (α1-7, α9-10), which contains a disulphide bridge in the ECD and non-α, which are β (β1-4), γ, δ and ε. 11 subunits (α2-7, α9-10, β2-4) assemble to form neuronal nAChRs. The remaining ones assemble into muscle nAChRs (*Figure 3*).[10] Different combinations of subunits are possible, forming homo- or heteromeric receptors with different pharmacological functions.[11]

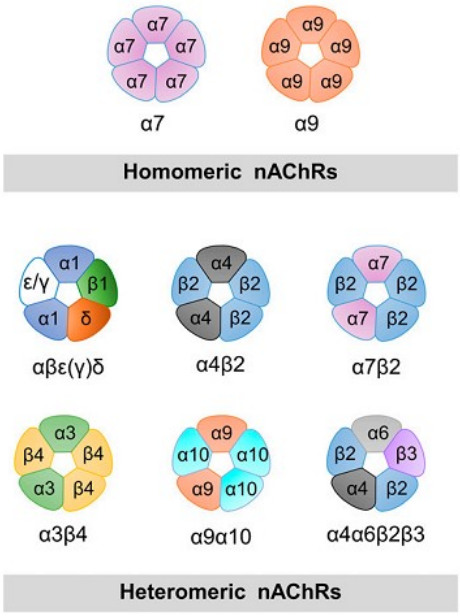

Figure 3. Examples of different combinations of subunits to form homomeric and heteromeric nAChRs. Adapted from Bouzat et al.[11]

These subunits can also be classified based on phylogenetic characteristics into 4 subfamilies (I-IV), where the subfamily III is further divided into 3 subgroups (*Figure 4*).[8]

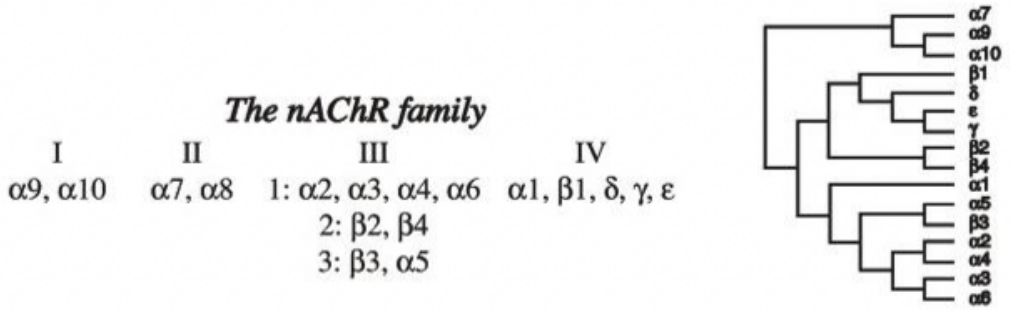

Figure 4. Phylogenetic classification of nAChRs. Adapted from Jensen et al.[4]

A pharmacological classification has been proposed in 1949 by Barlow, Ing, Paton and Zaimis, who distinguished muscle-type nAChRs from neuronal ones. They saw the decamethonium (C10) was a more effective antagonist of muscle nAChRs than hexamethonium (C6), which turned out to be the ganglionic nAChRs antagonist (Figure 5).[12,13]

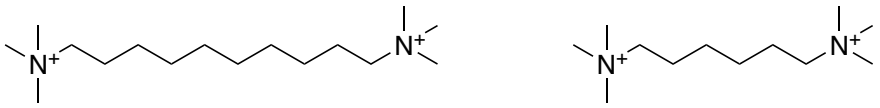

Decamethonium **Hexamethonium**

Figure 5. nAChRs antagonists used for the pharmacological classification.

Another classification of nicotinic receptors is based on the sensitivity towards the natural neurotoxin α-bungarotoxin (α-Bgtx) and (*S*)-nicotine. Some receptors have a high affinity for α-Bgtx and low affinity for (*S*)-nicotine, such as α7, α9 and α9 α10, and receptors that bind α-Bgtx with low affinity and (*S*)-nicotine with high (different combination of α2-6 and β2-4).[6,14]

1.3. Electrophysiology

As the result of the binding of an agonist, such as ACh, to the orthosteric binding pocket, the receptor changes its conformation going towards the channel opening and subsequent cationic influx. Due to the prolonged and/or repeated exposure to the agonist, the receptor loses its functional response. This phenomenon was discovered in 1957 by Katz and Thesleff. They called it "desensitization" and proposed a two-state model for muscle nAChRs.[15] According to this model, the receptor can exist in two different conformations. The first one is resting and activable state (R), and the second is desensitized non-conductive state (D). In a

ligand-free receptor, these two states are in equilibrium. The R conformation was considered to have a low agonist affinity because it requires a high concentration of agonists, such as ACh or nicotine, to open the channel. Contrariwise, the D conformation was considered to have a high affinity for agonists, because a low concentration of them desensitizes the receptor. Based on this model, the incubation of an agonist with the receptor takes the receptor to an agonist-bound desensitized conformation (AD), because the agonist preferentially binds the pre-existing desensitized state due to its higher affinity. Consequentially, R conformation turns to D to restore the equilibrium between the two states (*Figure 6A*).

In 1984, Monod-Wyman-Changeux (MWC) cyclical model was described.[16] This model suggests that there are four different receptor conformations in equilibrium with each other. There are a resting state (R), a desensitized state (D), an opened and activated state (A) and an intermediate desensitized state (I). This state I takes place when the receptor is exposed to an agonist for a short time, and it has a faster recovery time to the R state than the D state (*Figure 6B*).

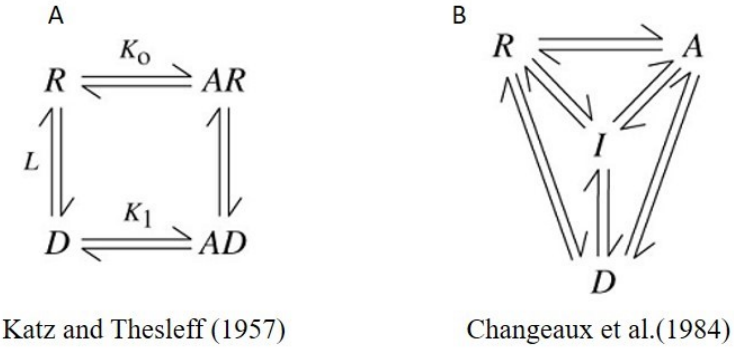

Figure 6. (A) Katz and Thesleff model, standard cyclical model; (B) MWC model, complete cyclical model. Adapted from Quick and Lester.[17]

2. α4β2 nAChRs

2.1. Introduction

The α4β2 and the α7 subtypes, are the predominant nAChRs in the CNS. The α4β2 subtype binds with high affinity the most common nicotinic agonists, such as ACh and (*S*)-nicotine. This subtype was found in different brain areas, such as the cerebral cortex, lateral geniculate nucleus, striatum, superior colliculus, cerebellum.[6]

nAChRs are pentamers, so heteromeric receptors are present in different stoichiometries. The α4β2 assembles in two stoichiometries of α- and β-subunits (2α:3β and 3α:2β), one with two α4 and three β2 subunits, the other one with three α4 and two β2. Both isoforms have two orthosteric ACh-binding sites at α/β subunit interfaces. However, it was discovered that the receptor isoform with three α4 subunits has an additional ACh site on the α4/α4 subunit interface that was defined as an unorthodox binding site.[18–20] These two stoichiometries differ in agonist sensitivity and rate of desensitization, and this difference can be attributed to the presence of an unorthodox α4/α4 binding site. The ACh EC_{50} in 3α:2β is 87 μM while in 2α:3β is 4 μM.[21] For this reason, they are commonly named low-sensitivity (LS) and high-sensitivity (HS) α4β2 nAChRs. In 2011, Harpsøe *et al.* using mutational and electrophysiological studies explains the different receptor sensitivities related to the receptor stoichiometries. The LS isoform has two different binding sites and, therefore, biphasic concentration-response curves with high- and low-sensitivity components corresponding to agonist binding at two different binding sites, where α4/α4 agonist site shows low agonist sensitivity to ACh and α4/β2 sites have high agonist sensitivity.[22] This additional site, named unorthodox binding site, increases the receptor activation by 5-folds and accelerates its desensitization (*Figure 7*).[23,24] Also, the two stoichiometries have different Ca^{2+} permeability: 3α:2β is 3-times more permeable than 2α:3β and has a higher single channel conductance. The agonist binding to this unorthodox site is insufficient to active the receptor, but it synergizes with orthosteric binding sites to promote the receptor conformation changing with subsequent activation.[20,25–27]

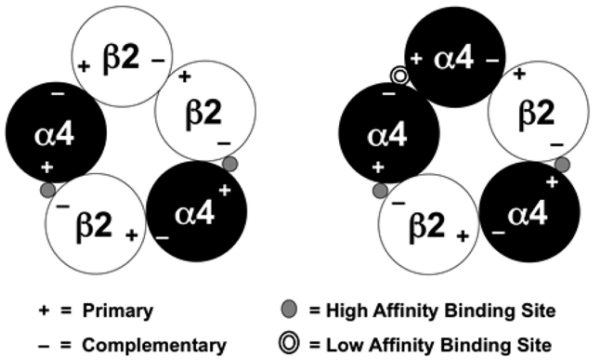

Figure 7. Graphic representation of the high affinity (left) and low affinity (right) α4β2receptors. Adapted from Marotta et al.[21]

2.1.1. α4β2 Architecture

The muscular nAChR of the *Torpedo Marmorata* is considered a prototype for all the nAChRs due to its similarity with receptors present in humans.[28] Between the '80s and '90s, Unwin studied *Torpedo Marmorata* postsynaptic membranes of electric organs and provided the first information regarding the structure of nAChRs using electron microscopy.[29–31] In 2001, the first X-Ray structures of Acetylcholine Binding Proteins (AChBPs) of *Lymnaea Stagnalis* and *Alypsia Californica* proteins were published. These proteins regulate the ACh synaptic transmission in snails.[32] AChBPs can be considered as structural surrogates of nAChR-ECDs because they share 15-25% identities.[33] Thanks to these similarities, it was possible to obtain a higher resolution of the nAChR binding site. Also, the X-Ray structure of other pLGIC members, such as the human β3 $GABA_A$ receptor[34], the mouse 5-HT_3 receptor[35], the human α3 Gly receptor[36], the zebrafish α1 Gly receptor[37] the invertebrate glutamate-gated chloride channel (GluCl)[38] and two bacterial pLGICs[39,40] were used as surrogate models or as templates for homology modelling to determine the architecture of the nicotinic receptor. An important thing is that the above structures revealed different possible states of the channel, providing information about gating transition and desensitization.

In 2016, R.E.Hibbs reported the first X-Ray structure of nicotinic α4β2 receptor (HS isoform). This α4β2 crystallized receptor retains function comparable to the full-length protein. The best crystal was obtained by co-crystallization with nicotine and a cholesterol analogue. The obtained resolution was 3.9 Å. The receptor is formed of five subunits arranged pseudo-symmetrical around a channel axis to form a cylinder. The subunits follow α-β-β-α-β order around the pentameric ring (*Figure 8*).[41] Each subunit has a large ECD with an N-terminal α-

helix and ten β-strands wrap inwards to form a sandwich. The C-terminal part has three TM α-helices (M1-M3), an amphipathic or intracellular MX helix, and a final transmembrane α-helix (M4). This architecture is similar to that discovered in the other Cys-loop receptors.[42]

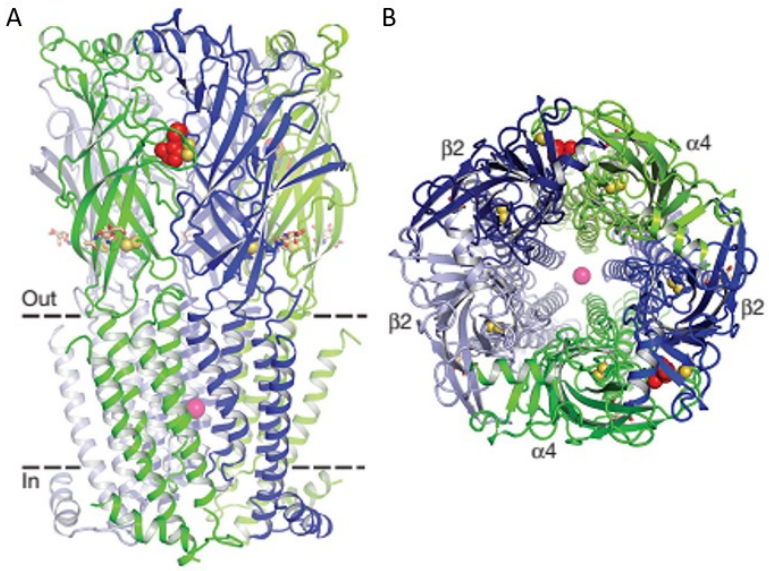

Figure 8. The architecture of the α4β2 nicotinic receptor. (A) Side view (α4 subunits are in green and β2 in blue) with nicotine (red) and sodium (pink); (B) Axial. Adapted from Morales-Perez et al.[41]

Consequently, in 2018, the same authors published the Cryo-Electron Microscopy (cryoEM) structure of two different stoichiometries of the α4β2. The α- and β- subunits have similar structural features, and so makes them indistinguishable at low resolution. For this purpose, Walsh *et al*. raised monoclonal antibodies against the recombinant α4β2 nicotinic receptor and isolated high-affinity antigen-binding fragments (Fab) to structurally distinguish different subunits in the pentamer. They then produced a mixed population of both stoichiometries and co-purified the receptor-Fab complex. Fabs can interact only with the ECD of the β2 subunits. Therefore, single particle cryoEM revealed two distinct populations of receptors, one with two Fabs and one with three Fabs bound. These two populations correspond to LS and HS stoichiometries. The cryoEM maps have a 3.5 Å resolution for the receptor and 4 Å resolution for the entire complex with Fab (*Figure 9*).[26]

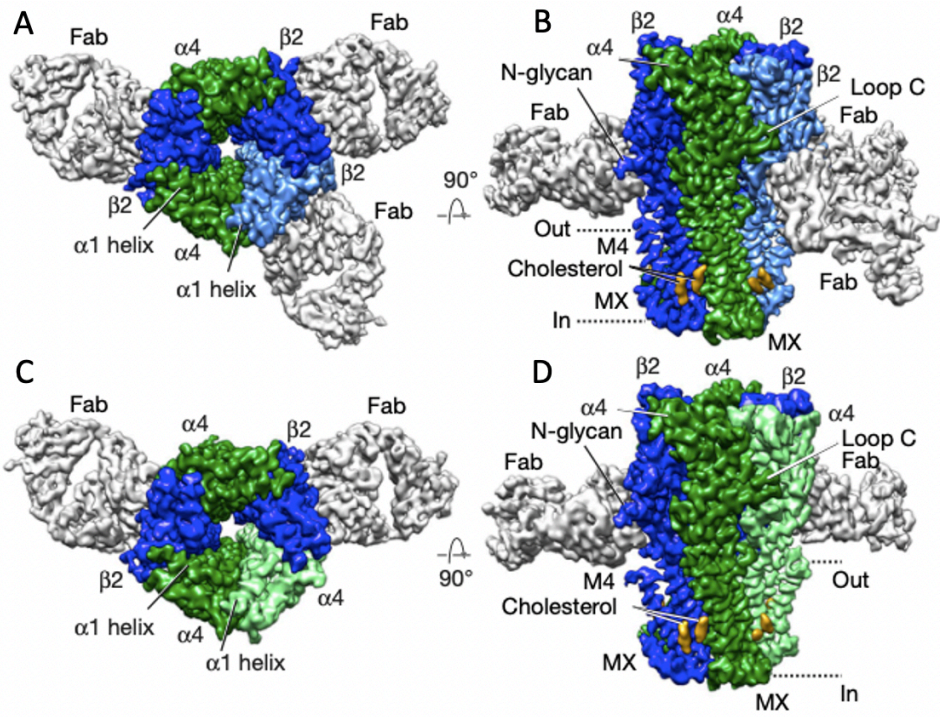

Figure 9. (A, B) 2α:3β–Fab complex reconstruction; Fab fragments are grey, density corresponding to cholesterol is yellow, and the α4 and β2 subunits are green and blue, respectively, with a lighter shade of green or blue denoting the subunit position that is unique between the two stoichiometries; (C, D) 3α:2β–Fab complex reconstruction. Adapted from Walsh et al.[26]

The calculation of interfacial free energies revealed that the preferable assemblies are α-β, β-α and α-α. The β-β interface is the least favourable. Hence, the interfaces α-β and β-α assemble first with the consequent incorporation of the fifth subunit. These considerations indicate that 3α:2β would be the preferable stoichiometry in the absence of other factors, such as low temperature and nicotine presence. For example, nicotine added to the cell culture favours the expression of 2α:3β stoichiometry, but the mechanism is unclear. Also, it is impossible to have other types of stoichiometries because, from the free energy studies, only one α-α and β-β interface can be accommodated in the pentameric structure.[26]

2.1.2. α4β2 Electrophysiology

When the receptor is exposed for a prolonged time to an agonist, it desensitizes, adopting a high-affinity non-conducting conformation.[42] In their studies, Morals-Perez *et al.* had performed patch-clamp electrophysiology experiments to compare the responses of full-length WT and crystallized α4β2 receptor to ACh and had found a similar behaviour (*Figure 10*).

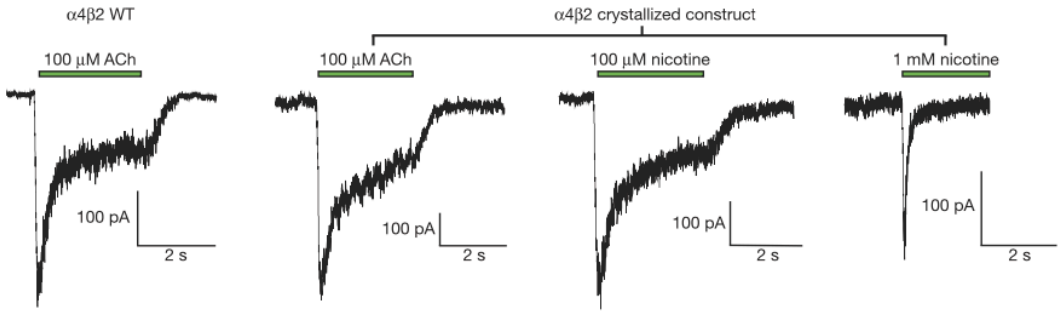

Figure 10. Patch-clamp recordings of the wild type (WT) and crystallized α4β2 receptor with ACh. Adapted from Morales-Perez et al.[41]

Also, the response to 1mM nicotine was measured, and the receptor desensitization in a few milliseconds was observed. The X-Ray structure shows a constriction point of 3.8 Å in diameter. This point is formed by glutamate side chains at the -1' position of the M2 α-helix (*Figure 11*). This diameter is smaller than the minimum consensus pore diameter of 6-8 Å which allows the movement of ions. The α4β2 receptor is a non-selective cation channel permeable to Na^+, K^+ e Ca^{2+}. Of these cations, Na^+ is the smallest one, with the diameter of 1.9 Å, which with the single equatorial water molecule of 2.8 Å diameter, would have the diameter above (4.7 Å) the constriction point. Thus, this structural analysis suggested that the X-Ray structure of the α4β2 receptor represent a desensitized, non-conducting state.[41]

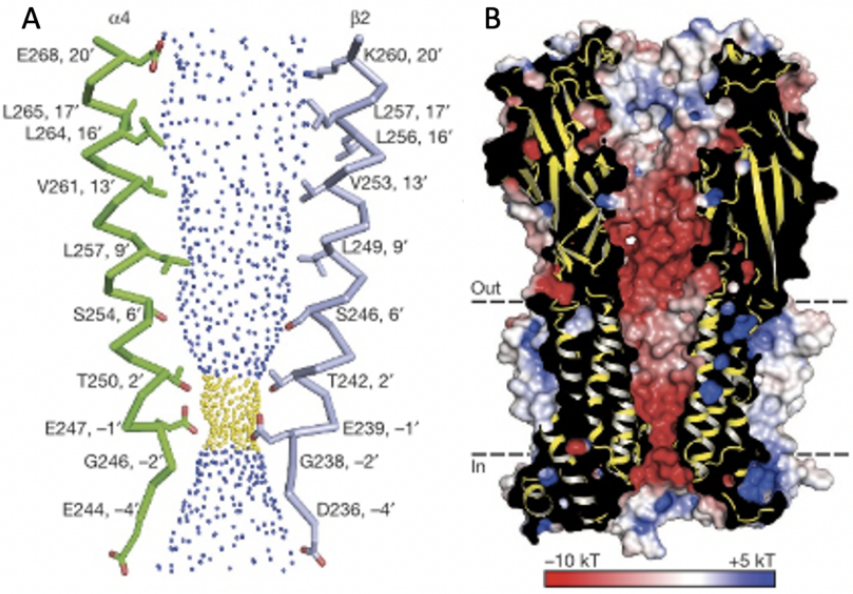

Figure 11. (A) Pore diameter of LS isoform; blue spheres indicate pore diameters >5.6 Å; yellow are >2.8 Å and <5.6 Å; (B) Cutaway of the receptor showing the permeation pathway coloured by electrostatic potential. Adapted from Morales-Perez et al.[41]

2.1.3. α4β2 Orthosteric binding sites

Nicotine, ACh and other orthosteric ligands bind at the α-β interface. This site is called the orthosteric binding site. There are two orthosteric binding pockets in both isoforms. This binding pocket is lined by α4(+) subunit and β2(-) subunits. Three loops from each side contribute to form the binding pocket, A, B and C from (+) side, and D, E and F from the (-) side.

Residues from these latter loops form a so-called "aromatic box". This boxes floor is lined by tyrosine Y100 of loop A and tryptophane W57 of loop D. The back walls are formed by leucine L121 of the loop E and tryptophane W156 of loop B. The front wall is defined by the flexible loop C with its vicinal cysteines C199 and C200, and tyrosines Y197 and Y204. The top of the hydrophobic box is lined by valine V111 and phenylalanine F119 of loop E. All these residues contribute to aromatic and hydrophobic interactions with the ligand. Furthermore, nicotine forms a hydrogen bond between its positively charged nitrogen of the pyrrolidine ring and the oxygen of the carbonyl backbone of W156. This nitrogen is also positioned to form a cation-π interaction with the indole ring of W156.[43] Loop F does not contribute to the binding of the ligands to the aromatic box, but it seems that aspartic acid D170 stabilizes loop C via hydrogen bond to the nitrogen of cysteine C199 (*Figure 12*).[41]

Furthermore, nicotine does not bind to β-α and β-β where β2 is a (+) side because of the different structure of the binding site. In this case, the small glycine G154 of the α4 subunit is substituted with a bulky arginine R149 of β2. Its side chain occupies the binding pocket and remains trapped between two tyrosines, twisting away the crucial W151 residue from the pocket (*Figure 12*).[41]

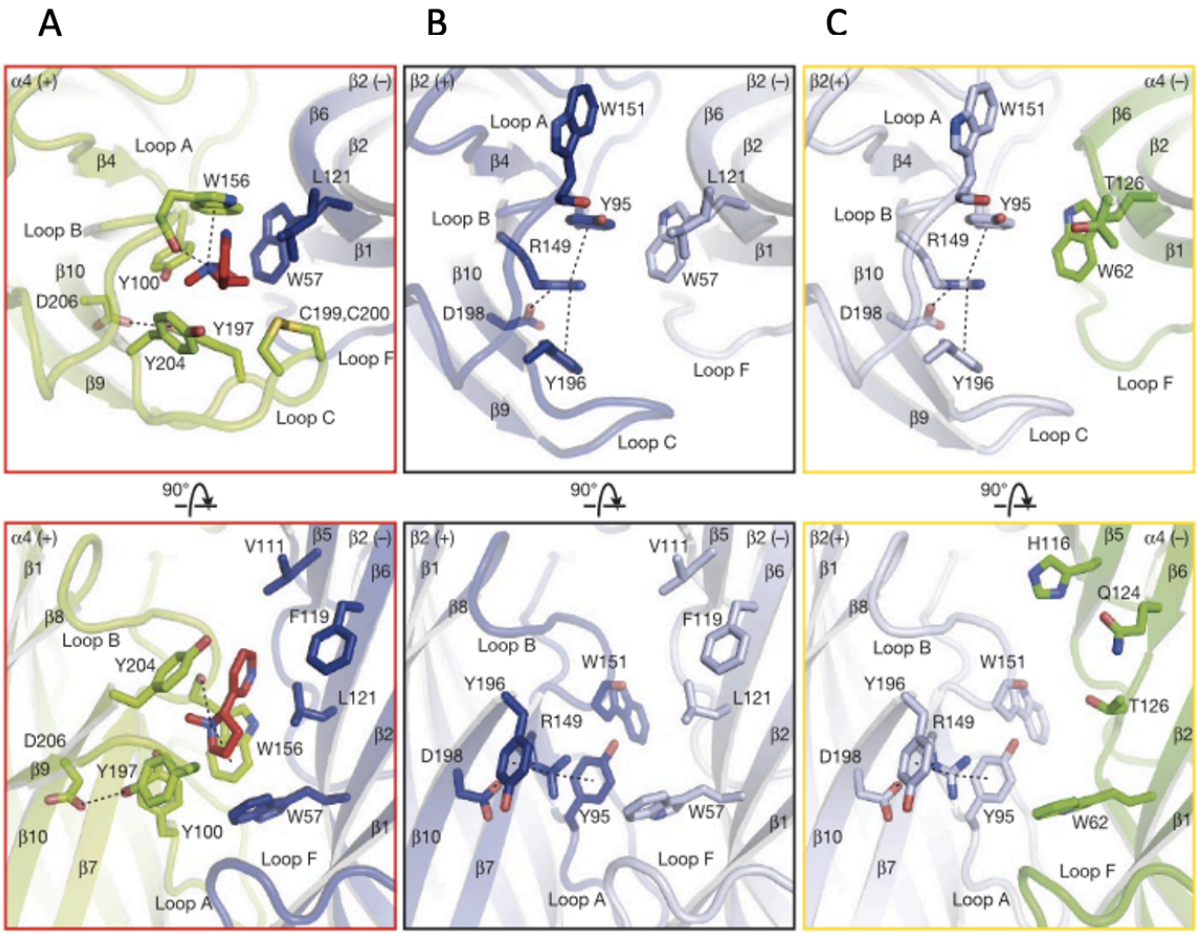

Figure 12. (A) Nicotine binds at the α4β2 interface; (B) Nicotine doesn't bind to the β2β2 and (C) to the β2α4 interface. Adapted from Morales-Perez et al.[41]

2.1.4. α4β2 Functions

The α4β2 nAChRs are the most abundant receptor subtype in CNS and are involved in many different physiological and pathological functions. This receptor subtype plays an important role in memory, learning, attention, mood, and nociception. Also, they are involved in several neurological conditions such as epilepsy, Alzheimer's and Parkinson's diseases, depression, schizophrenia, drug abuse, alcohol and nicotine addiction.[44–47]

2.1.4.1. Nicotine addiction

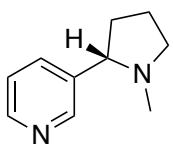

(*S*)-Nicotine

Nicotine is a chiral alkaloid derived from the leaves of tobacco plants (*Nicotiana tabacum* and *Nicotiana rustica*), and it is a primary addictive agent in tobacco products. It is nAChRs exogenous agonist which interacts with both CNS and PNS. Prolonged exposure leads to addiction development with consequent memory, learning and other cognitive pathways modulation.[48] It is predominantly

used recreationally as a stimulant throughout cigarette smoking, chewing tobacco, holding moist snuff in the mouth, inhaling dry snuff through the nose, inhaling smoke from a water pipe and inhaling vapour from an electronic cigarette.[49]

In 2020, National Institute on Drug Abuse reported that approximately one-fourth of the population uses tobacco products, and 20% circa smoke cigarettes.[50] Globally, about 57% of men and 10% of women smoke tobacco products. Nowadays, tobacco smoking is the cause of ~5–6 million deaths per year, counting 31% and 6% of all cancer deaths (affecting 18 different organs) in middle-aged men and women, respectively. It is estimated that smoking leads to about 480000 deaths yearly in the USA. Lung cancer is the dominant malignancy caused by smoking. The total number of cases is estimated to be 1.2 million annually, with about 90% attributed to smoking. Nicotine itself can be genotoxic and tumour-promoting. Moreover, at least 69 chemicals in tobacco smoke are carcinogenic. The overall rates of death from cancer are twice as high among smokers as non-smokers. Smoking increases the risk of all histologic types of lung cancer such as squamous cell carcinoma, small cell carcinoma, adenocarcinoma and large cell carcinoma, but also of head and neck, gastric, pancreatic, gallbladder, liver, colon, breast, cervical, urinary bladder and kidney cancers. [50–53]

Nicotine is involved in biological processes such as regulation of cell proliferation, apoptosis, migration, invasion, angiogenesis, inflammation, and cell-mediated immunity in a wide variety of cells including foetal, embryonic and adult stem cells, adult tissues as well as cancer cells.[52] During cigarette burning, different carcinogenic compounds are produced, such as tobacco-specific *N*-nitrosamines. NNN (*N*'-nitrosonornicotine) and NNK (4-(metylnitrosamino)-1-(3-pyridyl)-1-butanon) are among the most important and most potent carcinogens. NNAL (4-(methylnitrosamino)-1- (3-pyridyl)-1-butanol) is a metabolite of NNK (*Figure 13*).[54]

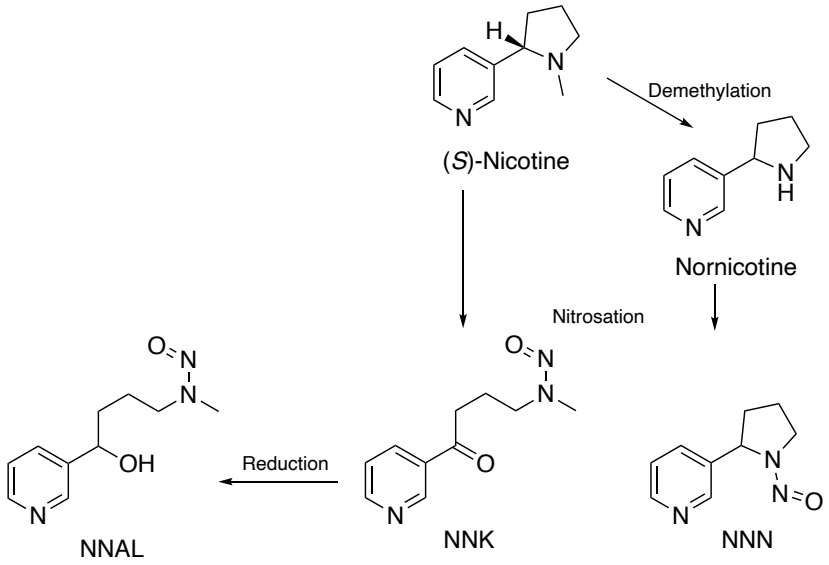

Figure 13. Formation of NNN, NNK and NNAL.

Nicotine is a tertiary amine composed of pyridine and pyrrolidine rings. It is a weak base with a pKa of 8.0, and at physiological pH, about 30% of nicotine is non-ionized which allows it to readily cross cell membranes, including the blood-brain barrier (BBB). Nicotine is rapidly absorbed in the small airways and alveoli, and its concentration rises quickly and peaks after cigarette smoking. Nicotine is rapidly metabolized in the liver, but also the lung.[55] Once delivered to the brain, nicotine activates and desensitizes nAChRs at a dose of 20-100nM.[10]

Particularly, nicotine exercises its action on dopamine (DA) and GABA pathways in the midbrain, especially on the mesostriatal and mesocortical dopamine pathways. The mesostriatal system includes the mesolimbic and nigrostriatal dopamine projections. The mesolimbic pathway connects the ventral tegmental area (VTA) to the ventral striatum. The ventral striatum includes the nucleus accumbens (NAc) and the olfactory tubercle (OT). The nigrostriatal pathway connects the substantia nigra pars compacta (SNc) with the dorsal striatum. The mammalian VTA is involved in the rewarding effects of different drugs, alcohol, and nicotine. The mesocortical pathway connects VTA to the prefrontal cortex (PFC). Also, there is a population of VTA GABA neurons that provides inhibitory input to DA neurons. There are descending projections to the brainstem mesopontine region, including the tegmental pedunculopontine nucleus (TPP). TPP is a brain region that is important in DA independent reward signalling. The VTA also receives excitatory glutamatergic and cholinergic projections

from both the TPP and the adjacent laterodorsal tegmental nucleus (LDT), as well as inhibitory GABA inputs from the TPP (*Figure 14*).[10,56,57]

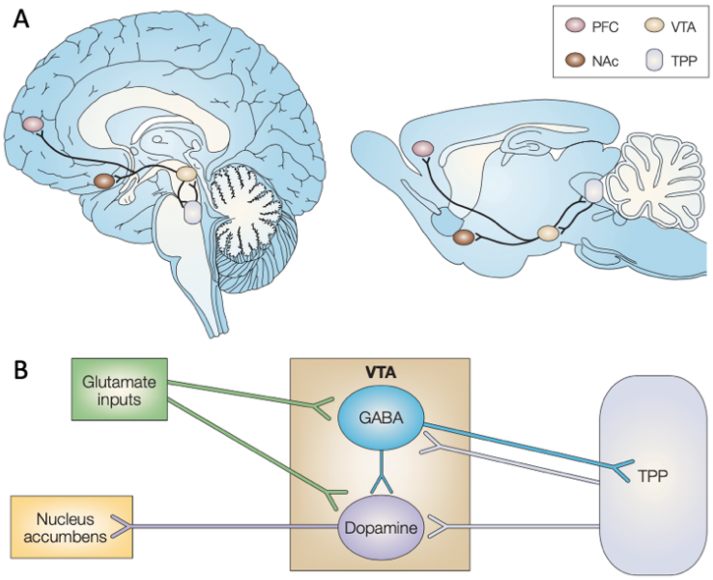

Figure 14. (A) Human (on the left) and rat (on the right) brains with mesolimbic and mesocortical DA pathways; (B) Schematic representation of dopaminergic and GABAergic neurons in VTA. Adapted from Laviolette et al.[56]

Acute effects of nicotine in the VTA affect primary GABA neurons, which rapidly desensitize leading to a long-lasting DA neurons excitation through the removal of the GABA inhibitory effect. Moreover, this desensitization is correlated to the enhancement of glutamatergic input to the DA neurons. To sum up, nicotine activation of GABAergic neurons initially increases inhibitory input to the DA neurons, but after prolonged exposure to the nicotine with a consequent depolarization of nAChRs on GABA neurons, nicotine bypass these inhibitory cells and acts directly on the DA neurons.[56]

2.1.4.2. Alzheimer's disease

Alzheimer's disease (AD) is one of the most common neurodegenerative disorders in the world. It has affected approximately 47 million people, and the tendency is that this number will increase to 62% by 2030. The most affected segment of the population is the over 65. AD is characterized by the deposit of β-amyloid (Aβ) plaque in the extracellular surface of neurons, the arising of neurofibrillary tangles from the intracellular accumulation of hyperphosphorylated Tau protein. These factors are associated with a gradual memory deterioration in its early stages, and problems with language, disorientation, mood swings,

loss of motivation, behavioural issues, and self-neglect in the advanced phase. AD is also associated with the deficit of ACh and oxidative stress caused by exacerbation of glutamatergic transmission.[58]

In AD there is a constant reduction of α4β2 nAChRs within the hippocampus, frontotemporal cortices, and basal forebrain. This reduction is most pronounced within the mesial temporal cortex of the hippocampus and basal forebrain. Also, in AD, there is a relationship between the decrease of α4β2 nAChRs and loss of memory.[59] Cholinergic neurons at the nucleus basalis of Meynert (basal forebrain) are the most affected in the disease. It was demonstrated that in the advanced patients there are 5 times fewer neurons than in healthy adults. Furthermore, the transcription of choline acetyltransferase (ChAT), an enzyme responsible for the synthesis of ACh, is drastically decreased in the remaining neurons. This leads to less ACh synthesis and dementia progression. Moreover, through molecular modelling it seems that acetylcholinesterase (AChE), an enzyme that catalyses the breakdown of ACh, interacts with Aβ peptide, promoting the amyloid fibril formation.[60]

Currently, only two classes of pharmacological therapy are available for AD. The first class of drugs is inhibitors of ChAT, such as donepezil, rivastigmine, and galantamine. They are recommended for all types of patients. Another drug is memantine with a non-competitive N-methyl-D-aspartate receptor antagonist and a dopamine agonist, and it is approved for the treatment of patients with moderate to severe AD.[61]

2.1.4.3. Parkinson's disease

Parkinson's disease (PD) is a neurodegenerative disorder that affects 1 out of 1000 persons over 50, and 19 out of every 1000 over 80. The most common symptoms are involuntary movements, tremors, rigidity, and bradykinesia. Cognitive and behavioural problems may occur, such as mood disorder, sleep alteration, anxiety, depression, dysautonomia, etc. PD is characterised by progressive loss of the nigrostriatal dopaminergic pathways and other dopaminergic neurons in the SNc. This neuron reduction explains typical motor symptoms.[62]

In the PD there are lesions on the expression of nAChR subtypes in the striatum. In the health striatum α4β2 are located on dopaminergic terminals and comprise 30 to 50% of the α4β2

striatal population. In a brain with a complete lesion all α4β2 and other nAChRs disappear from nigrostriatal dopaminergic terminals (*Figure 15*).[17] Furthermore, nAChRs damage in SNc is important. Studies on rats' and monkeys' brains suggested that nAChR binding is decreased in the lesioned brain. α4β2 are present on dopaminergic neurons and GABAergic interneurons afferents from substantia nigra pars reticulata are decreased.

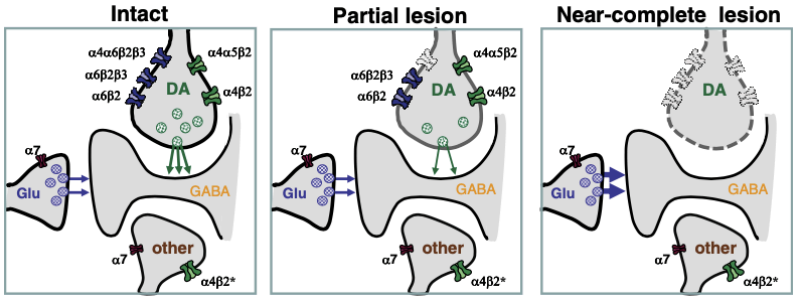

Figure 15. Schematic representation of intact, partial, and near-complete dopaminergic lesioning in the striatum. Adapted from Quick et al.[17]

As said previously, PD is associated with the abnormalities of the nigrostriatal dopaminergic pathway which interacts with the nicotinic cholinergic system. This interaction can help to understand a possible and efficient therapy. It is possible to intervene on two different mechanisms: 1. protect nigrostriatal damage to improve motor control; 2. directly stimulate the dopaminergic system using nAChR ligands. Administration of levodopa to parkinsonian patients has been considered the most effective symptomatic treatment for the last 40 years.[17]

2.2. α4β2 Ligands

All the nAChRs orthosteric ligands are classified based on their electrophysiological effects in full agonists, partial agonists, antagonists, inverse agonists, and desensitizing agonists. Ligands could be both endogenous and exogenous molecules. The orthosteric binding site is a primary, unmodulated binding site. Full agonists are ligands able to bind the receptor binding site and activate it resulting in a strong biological response (100% intrinsic activity). A partial agonist is a compound that cannot activate the receptor with maximal efficacy, even with its maximal binding (intrinsic activity <100%). Whereas antagonists bind the receptor but without activating it. As the result of this binding, there is a receptor blockade and inhibition of the agonist effect. Inverse agonists are ligands able to reduce the active conformation of the receptor with consequent inhibition of the activity.

In addition to the orthosteric binding sites, nAChRs have allosteric binding sites that are topologically and functionally distinct. Their presence allows more additional interactions between a ligand and the receptor, giving rise to an allosteric regulation which translates into possible new therapeutic approaches for different pathological conditions. Allosteric ligands do not activate the receptor alone but can stabilize it in different electrophysiological conformations.[63] Allosteric ligands can be positive allosteric modulators (PAMs), negative allosteric modulators (NAMs) or silent allosteric modulators (SAMs). PAMs enhance the binding affinity between the orthosteric binding site with the ligand. NAMs, on the other hand, reduce the binding affinity between the ligand and the orthosteric site. SAMs do not affect the binding of the orthosteric ligands but can block the action of other allosteric modulators.

2.2.1. α4β2 Full agonists

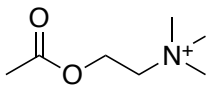

Acetylcholine

Acetylcholine is a fast-acting neurotransmitter at the neuromuscular junction and in the autonomic ganglia. It is synthesized in cholinergic nerve terminals from choline and acetyl coenzyme A by ChAT. ACh is transported using vesicular ACh transporter (VAChT) into synaptic vesicles, where it is stored. After an electrical depolarization of the neuron terminal, ACh is released by exocytosis, exerting its physiological effects by binding and activating neuronal and muscular nAChRs on pre- and postsynaptic membranes. In the end, ACh is hydrolysed in choline and acetate by acetylcholine esterase (AChE), and choline is then reuptake into cells. ACh is a non-selective AChRs full agonist.[64–66]

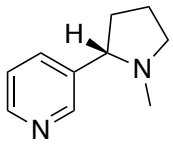

(*S*)-Nicotine

Nicotine is an exogenous ligand that activates nAChRs located on neurons in both CNS and PNS. Its action exerts different physiological effects such as diarrhoea, miosis, nausea, vomiting, blood pressure elevation, amnesia, tremor, and convulsion. Nicotine acts as a nAChR competitive full agonist specifically at the α3β4 ganglion type nicotinic receptor and α4β2 in CNS, rather than at the α7.[67–69]

Epibatidine is a very potent antinociceptive alkaloid isolated and characterized in 1992 from the frog *Epipedobates anthonyi*. It is 100 times more potent than morphine as an analgesic agent from activation of nicotinic receptors, but its analgesic effect occurs at doses like those causing severe hypertension, convulsion, and respiratory depression. This does not permit to use it in therapy, but it has become one of the most well-studied alkaloids. Epibatidine is a non-selective very potent full agonist (200 times more potent than nicotine). Epibatidine has a much higher affinity at nAChRs than ACh or nicotine. It predominantly binds α4β2 and α3β4 receptors with very high affinity (20 times higher than nicotine). It has less affinity for α7 receptors (300 times less than for α4β2 subtype). It also binds the muscle-type nicotinic receptors producing a paralyzing effect.[69–71]

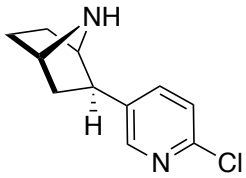

Epibatidine

2.2.2. α4β2 Partial agonists

The use of α4β2 nAChRs agonist for the treatment of smoking addiction is based on their nicotine-like action which replaces the effects of nicotine during a quit attempt. Although, given the reinforcing effects of inhaled nicotine, nAChRs agonists cannot substitute the rapid increase of nicotine concentrations from smoking, and this is translated into the possibility to eliminate withdrawal symptoms with consequent relapse. In 1991, Rose and Levin proposed an "agonist-antagonist" approach to reduce the rewarding effects of nicotine. This approach consists of the co-administration of a nicotine replacement therapy with a nAChR antagonist, such as mecamylamine (channel blocker). Thanks to this combination it is possible to reduce withdrawal symptoms and attenuate the reinforcing effects of nicotine through mecamylamine's antagonist effect during a relapse.[72] Partial agonists can have both nicotine-replacing agonist and nicotine-blocking antagonist activities. Therefore, nAChR partial agonist can replace nicotine and reduce craving by mimicking the effects of nicotine ("agonist activity"). On the other hand, during a relapse, the nAChR partial agonist can compete with nicotine for the same binding site and attenuate the reinforcing effect of inhaled nicotine. ("antagonist activity"). The advantage of this strategy is that a partial agonist acts as a competitive nicotine antagonist and not as an antagonist, which means that its binding slightly activates the receptors, both in the absence and in the presence of nicotine from smoking (*Figure 16*).[73]

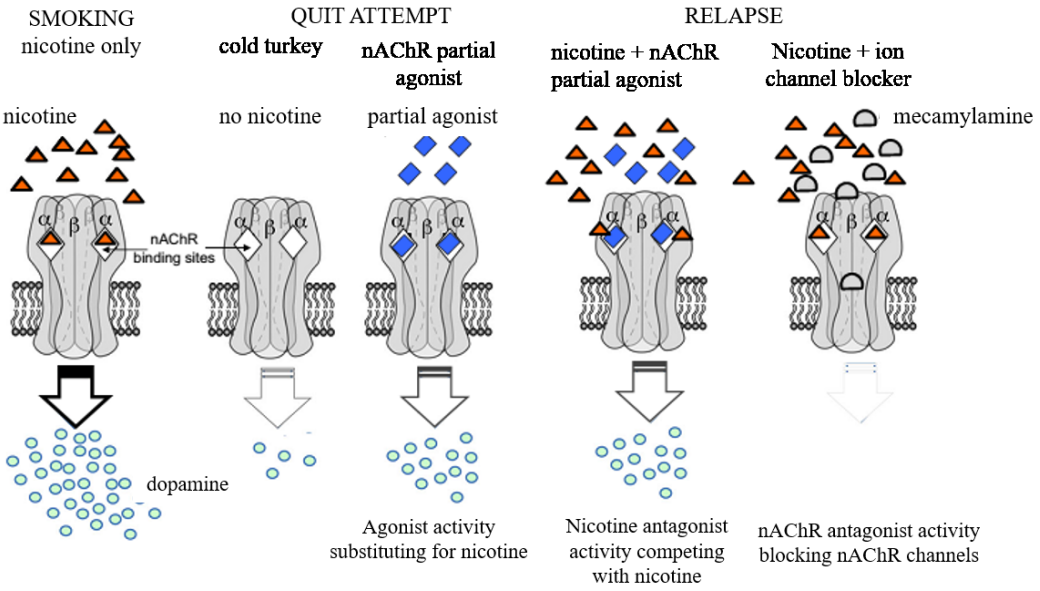

Figure 16. Schematic representation of agonist and antagonist effect of nAChR partial agonist during a quit attempt and a relapse. Adapted from Rollema et al.[73]

Cytisine is an alkaloid found in all parts of the *Laburnum* and *Cytisus*. It has a molecular structure similar to that of nicotine and it acts as an α4β2 partial agonist. Also, it acts as a full agonist at the α7 and α3β4 nAChRs. Because of its affinity to the nicotinic receptors, cytisine has been used as a model for the development of new drugs for the treatment of nicotine addiction. Since 1964, cytisine was used as a smoking cessation drug in Eastern European countries under the name Tabex®. Unfortunately, it has not been available for clinical use outside Eastern European countries, probably due to limited access to the clinical studies conducted in East Europe which were also not published in English. [21,74–76]

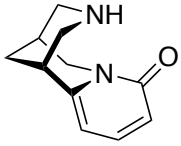

Cytisine

Varenicline is a drug developed by Pfizer in 2005 as a cytisine analogue for smoking cessation. It is commercialized with the name of Chantix® in the USA and Champix® in the EU and Canada. Varenicline is a highly selective and potent α4β2 partial agonist. *In vivo* studies have demonstrated its ability to attenuate the central dopaminergic response to nicotine and providing a sufficient dopaminergic tone to limit withdrawal.[77] It is selective for LS stoichiometry. It has similar hydrogen-bond donor interaction to that of nicotine but different from all other compounds hydrogen-bond donor acceptor interaction. This may be due to the capacity of the protein to adjust itself to the geometry of varenicline without altering its function.[76]

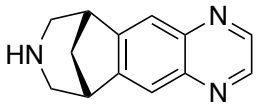

Varenicline

Sazetidine-A (Saz-A) was synthesized and characterized in 2006 by the research group of Kozikowski as a new nicotinic ligand with very high affinity and selectivity for nAChRs containing β2 subunits. Saz-A has a very high affinity for rat and human α4β2 nAChRs. Also, it has a 24000 times higher affinity for the rat α4β2 rather than for rat α3β4. Saz-A has a unique activation profile. Contrary to the cytisine and varenicline, Saz-A selectively activated HS stoichiometry over LS. It was shown that the pyridine ring gives the compound receptor and subunit selectivity, while the hydroxyl groups does not affect it. The β2(-) face with its Val109, Phe117 and Leu119, generate a hydrophobic pocket while the α4(-) face residues His114, Gln122 and Thr124, create a hydrophilic pocket. Mutational studies on the α4(-), where the three residues were modified to make them resemble β2(-), allowed to generate receptor response for Saz-A in the mutated LS receptor, while this was not possible in the wild type LS isoform. Also, mutation to make the β subunit similar to the α subunit abolished the actiavion of the HS isoform. These results suggest that the α4(-) is too polar and incompatible with the hydrophobic side chain of Saz-A, not allowing the interaction with the receptor subtype and its further activation.[21,78,79]

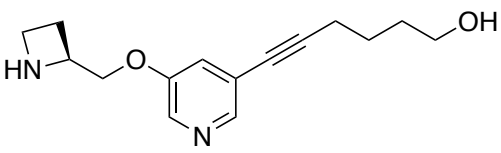

Sazetidine-A

2.2.3. α4β2 Antagonists

α**-Conotoxines** are a large family of disulfide-rich peptides derived from the venom of carnivorous marine cone snails of the genus *Conus.* They act as competitive antagonists at the ACh binding site. They are divided into different structural subfamilies with different selectivity for nAChR subtypes. α3/5-conotoxins are selective for muscle-type nAChR, while α4/6 and α4/7 are selective for neuronal nAChRs.[80]

Mecamylamine is a secondary amine that belongs to "ganglionic blockers" drugs. It is a nonselective and non-competitive antagonist of both peripheral and central nAChRs. It acts as an open-channel blocker, decreasing the duration of the open-channel state by interacting with the pore binding site of the open nAChR channel. Mecamylamine is a racemic mixture. (*S*)-mecamylamine in more effective than (*R*)-mecamylamine at inhibiting the LS stoichiometry. However, on the HS isoform, (*S*)-mecamylamine amplifies, while *R*)-mecamylamine blocks agonist-induced activation. In pre-

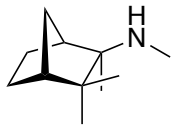

Mecamylamine

clinical studies, (*S*)-mecamylamine resulted to be more effective in blocking nicotine-induced seizures, showed better antidepressant and anxiolytic effects than its (*R*) enantiomer.[81]

2.2.4. α4β2 Positive allosteric modulators (PAMs)

As mentioned previously, PAMs can increase the affinity and/or the efficacy of an orthosteric ligand.[82] PAMs can increase receptor binding in different ways. Normally, at the baseline equilibrium, nAChRs is in its closed state, and it shifts to an open state when a high concentration of agonist binds. One of the ways of PAM exerts its activity is by increasing the agonist binding to the closed state of the receptor, increasing in this way the potency of the agonist. This modulation is advantageous with a low concentration of the agonist that otherwise would not give a maximal response. Also, with this strategy, it is possible to use lower concentrations of the agonist to limit unwanted side-effects.[83] PAMs are generally classified into two types based on the effects on nAChR gating kinetics and ACh-mediate response. Type I PAMs are compounds that increase the sensitivity to ACh and the peak ion current but do not modify the channel kinetics. Type II PAMs, on the other hand, can modify the channel gating kinetics. They can also transiently reactivate the desensitized state. For these reasons and because nAChRs have numerous allosteric binding sites, PAMs represent a possible therapeutic approach to limit side-effects of agonists.[84]

Physostigmine and **galantamine** are AChE inhibitors and first identified PAMs. They are able to potentiate both muscle and neuronal type nAChRs but have no effect on muscarinic AChRs. Physostigmine binds at both agonist binding and non-agonist binding sites. Mutiational studies have shown that it is selective for LS α4β2. Galantamine binds at α4β2 and α7 nAChRs enhancing the DA signaling. It is not clear if AChE inhibition or allosteric modulation of nAChRs mechanism of galantamine is responsible for the smoking cessation, but it represent a potential therapy for smoking addiction.[84]

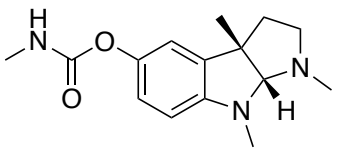

Physostigmine

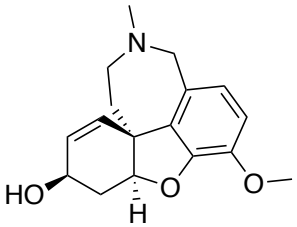

Galantamine

Desformylflustrabromine (dFBr) is a monomethyltryptamine derivative isolated as a secondary metabolite from marine bryozoan *Flustra foliacea*. It is one of the most investigated nAChRs PAMs, and a large library of its analogues was described and used to study the structure-activity relationship (SAR) of this pharmacophore, identify binding sites and *in vitro* nAChR effects. dFBr itself does not elicit nAChR-mediated current in two-electrode voltage-clamp and patch-clamp electrophysiological studies, but it enhances the ACh response of α4β2. It potentiates both HS and LS isoforms with an EC_{50} of ∼0.4 and ∼1.6 μM and potentiation I_{max} of ∼400 and ∼300%, respectively. dFBr increases the efficacy of nAChR agonists and so it is considered a Type II PAM of the α4β2 because it enhances the peak current of low and saturated concentrations of ACh and modifies the channel gating.[84]

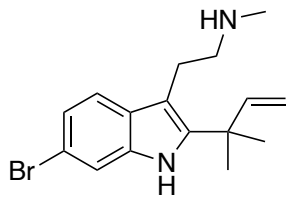

Desformylflustrabromine

LY2087101 ([2-[(4-Fluorophenyl)amino]-4-methyl-5- thiazolyl]-3-thienylmethanone) was developed by Eli Lilly and Company in 2006 by high-throughput screening. It selectively potentiates human α4β2, α4β4, α2β2 and α7 nAChRs but not α3β4. It increases ACh maximal response of α4β2 nAChRs while has little or nor effect on its potency.[85] It potentiates both the isoform in the same way (EC_{50} ∼1 μM), but it is 2-fold less efficacious at high-sensitivity isoform rather than at low-sensitivity. It was supposed that these results are due to the additional α4 subunit. Subsequently, mutational and computational studies were performed, and it was identified that LY2087101 has two distinct binding sites. One site is at the interface between two adjacent α4 subunits and the other within the α4 subunit. LY2087101 is a Type I PAM because it increases peak agonist-evoked response of nAChRs with practically no effect on the receptor desensitization. It is also an equipotent potentiator of both isoforms but with higher efficacy at LS nAChR.[84–86]

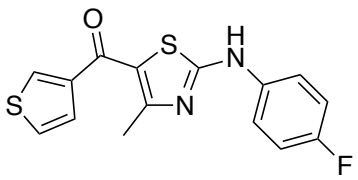

LY2087101

2.2.5. α4β2 Unorthodox ligands

Recently an additional ACh site was identified at the α4/α4 subunit interface in the LS α4β2 nAChRs. This additional site was defined as the unorthodox binding site. It was known that LS and HS isoforms have different sensitivity to the agonists and a different rate of desensitization, but the discovery of an additional α4/α4 site has permitted to better understand these differences. This binding site increases the activation of the orthodox α4/β2

sites by 5-fold and accelerates the receptor desensitization. This unorthodox site has a 100-fold lower sensitivity than the classic orthodox site. Moreover, unorthodox sites synergize with orthodox sites to promote receptor activation. The only one interaction with the α4/α4 sites is insufficient to trigger a global conformation change to the activated state, but different mutational studies performed during the years in which three amino acids of β2 subunit were muted to give three α4/α4-like ACh sites have shown the possibility of the activation of the receptor with an unorthodox-selective agonist. It was generated the LS β2 triple mutant, with V109H, F117Q and L119T mutations, and the application of NS9283 alone was tested. It was seen the response in a dose dependent manner, suggesting that it acts as a partial agonist, however not very potent or efficacious.[20,21] It was recently established that these compounds are neither allosteric nor modulators because they act as selective agonists at the ACh binding site formed at the α4/α4 interface. Because they achieve their effects by occupying a third ACh site, just as any other full agonist would at that site, they are not a modulator.[24] However, it is not an error to call these compounds PAMs because, in the presence of an orthodox agonist, they act as allosteric modulators to all effects.

NS9283 (3-(3-(pyridine-3-yl)-1,2,4-oxadiazol-5-yl)benzonitrile) is the unorthodox α4/α4 agonist which has no effect at orthodox α4/β2 sites, that means that it potentiates the LS isoform and not the HS. It was discovered by Neurosearch A/S. This molecule represents a new class of selective ligands for α4β2 nAChRs, which are useful in increasing the action of nAChR agonists in the treatment of neuropathic pain and increasing cognitive functions.[24] It was initially erroneously defined as PAM because alone it cannot activates the receptor by itself but increases the activity of α4β2 receptors in response to stimulation of an agonist. Through the mutation of the α4/β2 sites into α4/α4-like, it was discovered that NS9283 could activate the receptor, this allowed to define it as an agonist selective for the α4/α4 ACh site. NS9283 increases the potency without affecting the maximum efficacy and does not alter the rate of desensitization of currents evoked with ACh and it decrease the rate of receptor recovery from a desensitized state.[20,84,87] In 2016, Maurer *et al.* discovered that acute and repeated administration of NS9283 attenuated nicotine seeking in rats. These results demonstrate that the unorthodox α4/α4 agonists can modulate addiction-like behaviours in rats and it possible to hypothesize that the action on α4/α4 binding site may

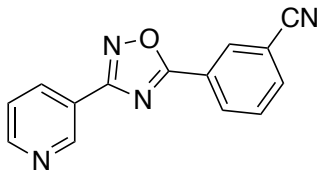

NS9283

reduce chronic smoking and relapse in humans. In fact, co-administration of NS9283 and a subthreshold dose of an α4β2 agonist produce a nicotine-like effects in rats, suggesting that lower doses of agonist could be used to treat smoking addiction.[88] Furthermore, in 2011 Lee *et al.* studied the co-administration of NS9283 with ABT-594, an α4β2 agonist for treatment of pain, which is poorly tolerated at the efficacious doses for its side effects. They demonstrated in preclinical models (ferrets and dogs) that the analgesic efficacy of well-tolerated doses of ABT-594 in humans can be significantly enhanced by co-administration with NS9283.[89] Moreover, in 2012, Timmermann *et al.* showed promising results in the treatment of cognitive dysfunction in rodents. NS9283 was administered to rats and their behaviour was observed in different cognitive tests. They observed, as recently reported that NS9283 augment the anti-hyperalgesic effects of α4β2 agonists but was ineffective alone. However, the pro-cognitive efficacy of NS9283 did not require co-administration of exogenous agonist, suggesting that the level of cholinergic tone in the cognitive circuitry is sufficient to drive allosteric modulator efficacy. Comparing with other agonists, NS9283 action potentially gives the same effects of nicotine but with better selectivity.[90]

CMPI (3-(2-chlorophenyl)-5-(5-methyl-1-(piperidin-4-yl)-1*H*-pyrazol-4-yl)isoxazole) was developed at Amgen Inc. It selectively potentiates α4β2 nAChR and not the other subtypes. Especially it potentiates LS α4β2 and has no effect on HS α4β2. As NS9283, it is an agonist selective for α4/α4 ACh site with the binding site at the extracellular domain ad the α4/α4 subunit interface. It enhances the ACh potency at the LS isoform by ∼100 fold without significantly modifying its efficacy.[84]

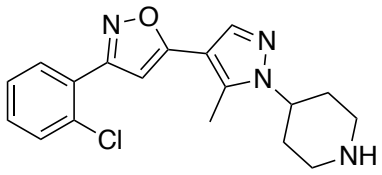

CMPI

3. Part 1: Orthosteric and unorthodox binding sites studies

3.1. State of the art

3.1.1. Orthosteric binding site studies

In 1996 Abreo *et al.* from Abbott Laboratories reported two potent nAChR ligands with a 3-pyridyl ether structure that possesses a subnanomolar affinity for neuronal nAChRs. **A-85380** and **A-84543** resulted to be full agonists with pM (measured by [^{3}H]-(-)-Cytisine displacement in the rat brain) affinity and increased efficacy compared to nicotine to stimulate ion flux.[91] The same year, Elliot *et al.*, also from Abbott Laboratories, have reported two bioisosteres of **A-85380** and **A-84543**, where the 3-pyridyl ring was substituted with a phenyl ring, (*S*)-**I** and (*S*)-**II**. This substitution maintains a good but decreased binding affinity (*Table 1*).[92]

Compound	Structure	Ki (nM)
A-84543	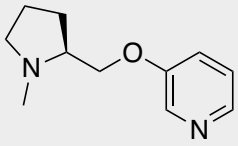	0.15 ± 0.01
A-85380	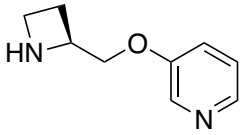	0.052 ± 0.0001
(*S*)-**I**	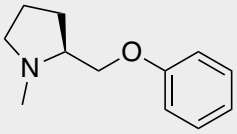	42 ± 1.45
(*S*)-**II**	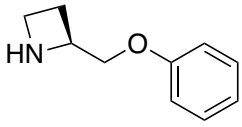	52 ± 4.3
(*S*)-**Nicotine**	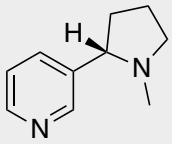	1 ± 0.01
(±) **Epibatidine**	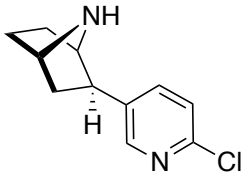	0.043 ± 0.006

Table 1. The compounds were tested for nAChR binding in a whole rat brain preparation using [^{3}H]-Cytisine. Values represent mean ± S.E.M.[91,92]

In 2006, Pallavicini *et al*. synthesized two rigid analogues of (*S*)-**I** with a benzodioxane scaffold, namely N-methyl-2-(2-pyrrolidinyl)benzodioxanes (*S,R*)-**III** and (*R,S*)-**III**. The decision to introduce a rigid structure was taken to study a possible stereochemical complication in the proximity of the critical cationic head. The replacement of hydrogen-bond acceptor/π (HBA/π) moiety of nicotine (pyridine ring) by 1,4-benzodioxane was chosen considering HBA/π proprieties of both systems.[93] In 2009, they extended the synthesis to all four stereoisomers. The affinity of all four compounds towards the α4β2 and α7 nAChR subtypes were evaluated in rat cortex membranes by binding studies using [^{3}H]-Epibatidine and [^{125}I]-α-Bgtx. Only compounds with the absolute configuration (*S*) at the pyrrolidine stereocenter maintained the α4β2 affinity and good selectivity against α7 (*Table 2*).[94]

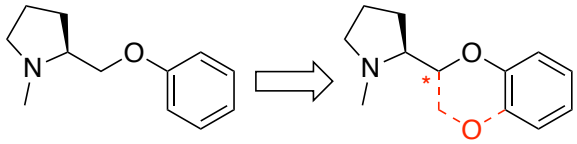

(*S*)-**I** * New stereocenter

Compound	Structure	α4β2 Ki (μM)	α7 Ki (μM)
(*S,R*)-**III**	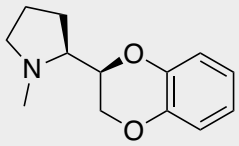	0.26	21
(*R,S*)-**III**	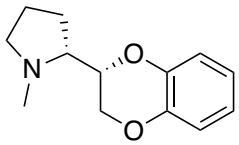	12.5	35
(*S,S*)-**III**	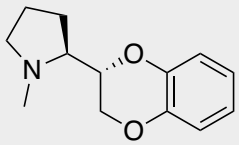	0.47	14.6
(*R,R*)-**III**	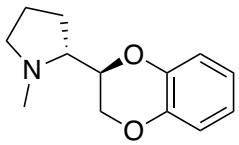	43.8	14.8

Table 2. The compounds were tested for nAChR binding in whole rat brain membranes using [^{3}H]-Epibatidine and [^{125}I]-α-Bgtx.

Subsequently, to better understand the receptor binding pocket and to discover new pharmacophoric elements, different substituents at the aromatic ring were introduced. Based on SAR studies conducted on **A-84543** and (*S*)-**I**, where the most advantageous position for

the affinity and selectivity is at the *meta*-position, Pallavicini's group synthesized different 7-substituted analogues of (*S*,*R*)-**III**. The most promising compound was 7-hydroxy substituted derivative (*S*,*R*)-**IV**. The introduction of OH group in that position increases the affinity at the α4β2 nAChRs from 0.26 to 0.012 μM, maintaining a good selectivity towards α4β2 receptors rather then α3β4. Furthermore, this compound resulted to act as a partial agonist on α4β2 nAChRs measured by the induced [^{3}H]DA release from striatal slices with a maximum effect at circa 50% (*Figure 17*).[95]

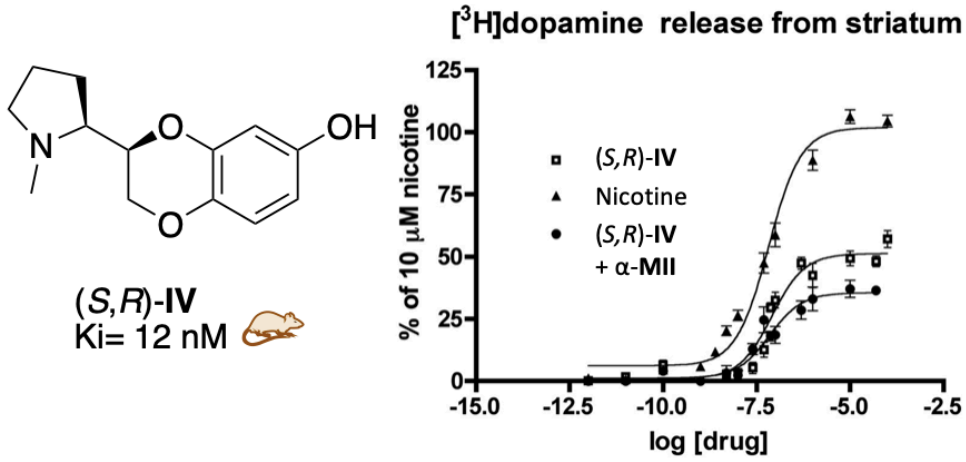

*Figure 17. (S,R)-**IV** structure. Ki value derived from [^{3}H]-Epibatidine competition binding on rat brain membranes (left); concentration response curves of agonist-induced [^{3}H]DA release from rat striatal slices (right).*

All the other substitutions in the 7-position resulted in loss or poor affinities. Small apolar methyl, medium lipophilic bromine, bulky aromatic phenyl or bulky polar hydroxymethyl, acetyl and methoxy substituents led to the loss of the affinity. These results suggested that there is a small hydrophilic subpocket that can accommodate the hydroxyl group. In 2015, Bolchi *et al*. reported that (*S*,*R*)-**IV** is more than 50-fold more selective at the human α4β2 nAChRs over the ganglionic α3β4 subtype (α4β2 EC_{50}= 0.3 μM; α3β4 EC_{50}= 17 μM; functional selectivity 57) (*Figure18*). In the same work, new compounds designed using **A-84543** and (*S*)-**I** as lead compounds were investigated. In particular, based on the good results obtained by the introduction of the hydroxyl group in the 7-position of the benzodioxane scaffold of compounds (*S*,*R*)-**IV**, the research group decided to introduce the OH group in *meta*-position of the aromatic ring on these compounds. The resulting compounds (*S*)-**V** and (*S*)-**VI** resulted to be highly potent α4β2 full agonists, but only (*S*)-**VI** was functionally selective towards α4β2 rather than α3β4 nAChRs (*Figure 18*).[96]

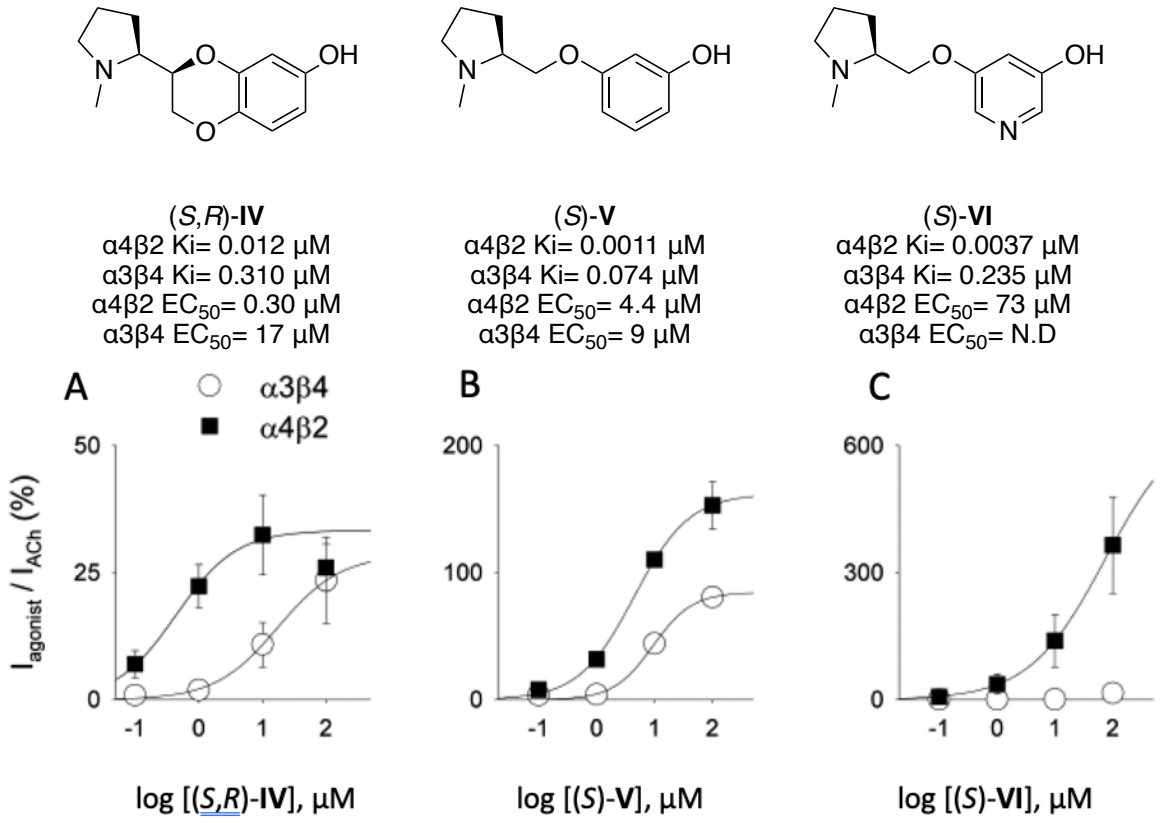

*Figure 18. (S,R)-**IV**, (S)-**V** and (S)-**VI** structures. Ki values derived from [^{3}H]-Epibatidine competition binding on rat cortex membranes for α4β2 and human α3β4 transfected cells membranes. Agonist effects on transfected human α4β2 and α3β4 subtypes normalized to the maximal response to 1mM ACh.*

The difference between the activities of (*S*,*R*)-**IV**, (*S*)-**V** and (*S*)-**VI** might be attributed to their structure. Compound (*S*,*R*)-**IV** acts as a partial agonist, while compounds (*S*)-**V** and (*S*)-**VI** are full agonists at the α4β2 nAChRs. The rigid non-flexible structure of (*S*,*R*)-**IV** occupy all the space in the binding pocket and keeps the loop C "opened". The flexible structure of phenyl- and pyridyl- ethers of prolinol permits them to position themselves in a more relaxed way in the binding pocket, keeping the loop C slightly "closed" and more flexible (*Figure 19*).

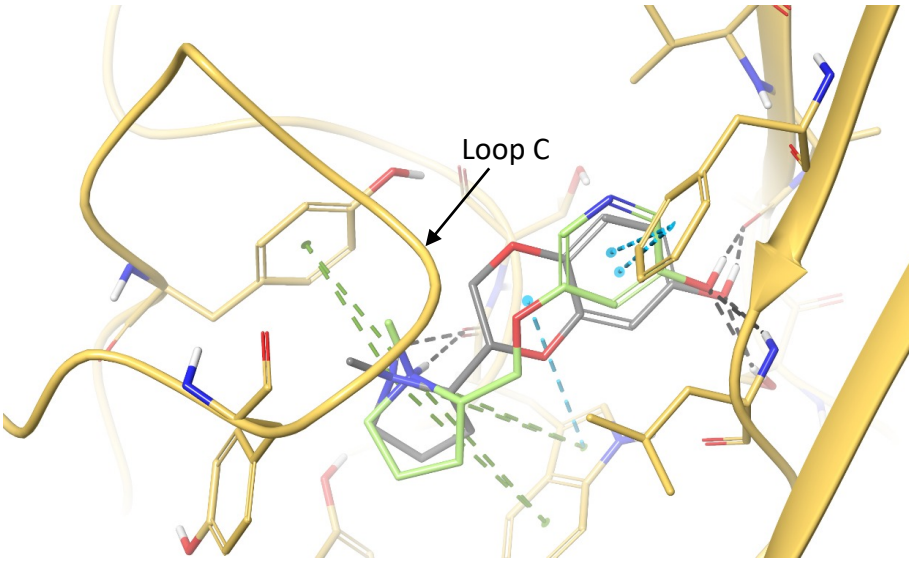

*Figure 19. Docking at the α4β2orthosteric binding site. (S,R)-**IV** (in grey) and (S)-**VI** (in green) poses with main interaction (dashed lines).*[97]

When I joined the research group, their efforts were focused on the synthesis of (*S,S*)/(*S,R*) diastereomeric pairs of pyrrolidinyl benzodioxanes substituted in 6- and 5-benzodioxane positions with groups, such as OH, NH_2, NO_2, NHAc, NMe_2 and Ph, in order to consider small or bulky and HBD or HBA substituents. All the substitutions in the 6-position are unfavourable for the affinity, probably because of their elongating effect on the shape of the molecule. In position 7, only hydroxy and amino groups are beneficial for the affinity, but only with OH the selectivity is maintained. All the other groups in that position have no ameliorative effect. Furthermore, the substituents in position 5 have a completely different behavioural profile. This position tolerates OH, NH_2, NO_2 and even Ph substituents and maintains the submicromolar affinity for α4β2 nAChRs similar to the naked derivative (*S,R*)-**IV** but with the absolute S configuration at the dioxane stereocenter and not with R configuration as for 7-OH derivative. Good results were obtained with the 5-NH_2 derivative with (*S,S*) configuration that has high α4β2 affinity and selectivity, and also acts as a weak α3β4 antagonist (*Scheme 1*).[98]

Compound	Structure	α4β2 [^{3}H]Epi Ki (μM)	α3β4 [^{3}H]Epi Ki (μM)	α4β2 EC_{50} (μM)	α3β4 EC_{50} (μM)
(*S,R*)-**IV**	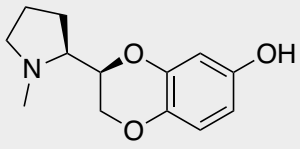	0.012	0.31	0.3	17
(*S,R*)-**VII**	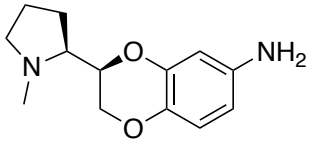	0.022	0.019	14	19
(*S,S*)-**VIII**	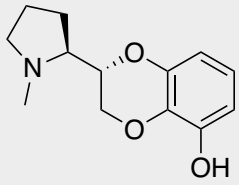	1.7	>100	N.A.	N.A.
(*S,S*)-**IX**	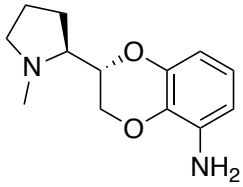	0.131	13	0.005 8.7	Antagonist

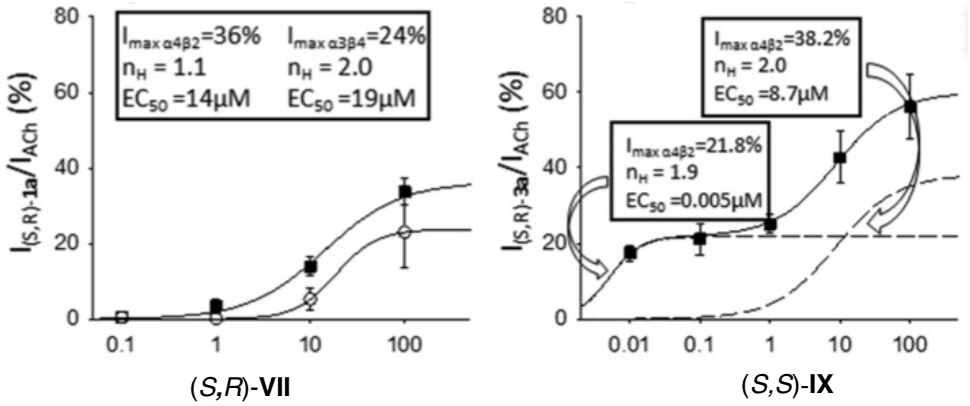

(*S,R*)-**VII** (*S,S*)-**IX**

*Scheme 1. Ki value derived from [^{3}H]-Epibatidine competition binding on rat cortex membranes for α4β2 and human α3β4 transfected cells membranes. Human α4β2 (solid square; n = , and n = 6 for (S,R)-**VII** and (S,S)-**IX**, respectively) and α3β4 (open circle; n = 7 and n = 2 for (S,R)-**VII** and (S,S)-**IX**, respectively) nAChRs were transiently transfected into the GH4C1 rat anterior pituitary cell line and the activation responses are normalized to the maximal response to 1 mM ACh.*

Furthermore, both diastereomers of all four regioisomers *N*-methyl-pyrrolidinyl-pyridodioxanes were synthesized. They were designed as bioisosteres of (*S,R*)-**III** and (*S,S*)-**III** and as rigidified analogous of previously described compound **A-84543**. They were subsequently assayed for their binding affinities and electrophysiological activities at α4β2

and α3β4 nAChRs. Only compound (*S,R*)-**X** showed high α4β2 affinity and selectivity, whereas its diastereomer and all the other regioisomers had much lower affinities (*Figure 20*).[98]

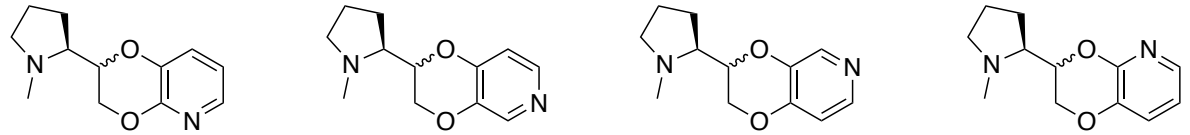

(*S*,*R*)-**X**
α4β2 Ki= 0.41 (20) μM
α3β4 Ki= 16.2 (35) μM

(*S*,*S*)-**X**
α4β2 Ki= 30.4 (34) μM
α3β4 Ki= 22 (22) μM

(*S*,*R*)-**XI** + (*S*,*S*)-**XI**
α4β2 Ki= 2.5 (30) μM
α3β4 Ki= 12.3 (37) μM

(*S*,*R*)-**XII**
α4β2 Ki= 1.64 (19) μM
α3β4 Ki= 5.8 (27) μM

(*S*,*S*)-**XII**
α4β2 Ki= 3.6 (16) μM
α3β4 Ki= 8.9 (31) μM

(*S*,*R*)-**XIII**
α4β2 Ki= 43 (29) μM
α3β4 Ki= N.A.

(*S*,*S*)-**XIII**
α4β2 Ki= 30 (21) μM
α3β4 Ki= N.A.

*Figure 20. N-Me-pyrrolidinyl-pyridodioxanes (S,R)- and (S,S)-**X-XIII** structures. Ki values derived from [^{3}H]-Epibatidine competition binding on rat cortex membranes for α4β2 and human α3β4 transfected cells membranes. Adapted from Bolchi et al.*[99]

3.1.2. Unorthodox binding site studies

In 2012, Timmermann *et al.* started with more specific studies on NS9283 (*Figure 21A*). They discovered that this compound does not activate α4β2 receptors by itself, but dramatically increases the peak width representing nicotine-induced Ca^{2+} flux in HEK293-hα4β2 cells (*Figure 21B*). In subsequent experiments it was shown that the effect of NS9283 is concentration-dependent, thus suggesting the presence of a specific and saturable binding site. To characterize the effect of the molecule on α4β2 receptors, an electrophysiological study was performed on both HS and LS isoforms, expressed in X. Laevis oocytes; the results show that NS9283 concentrations higher than 0.1 μM generate a clear increase in current spikes associated with the action of ACh in the LS receptors compared to the control trace, but no positive modulation effect on the HS isoform (*Figure 21C,D,E*). The enhancement, obtained through NS9283, on nAChRs was confirmed in a patch-clamp electrophysiological study, in which human α4β2 receptors were expressed in rat GH4C1 cells. NS9283 produces a significant increase in peak current obtained by activating nAChR at sub-saturation ACh concentrations, without producing any detectable signal when applied alone (*Figure 21F*).[90]

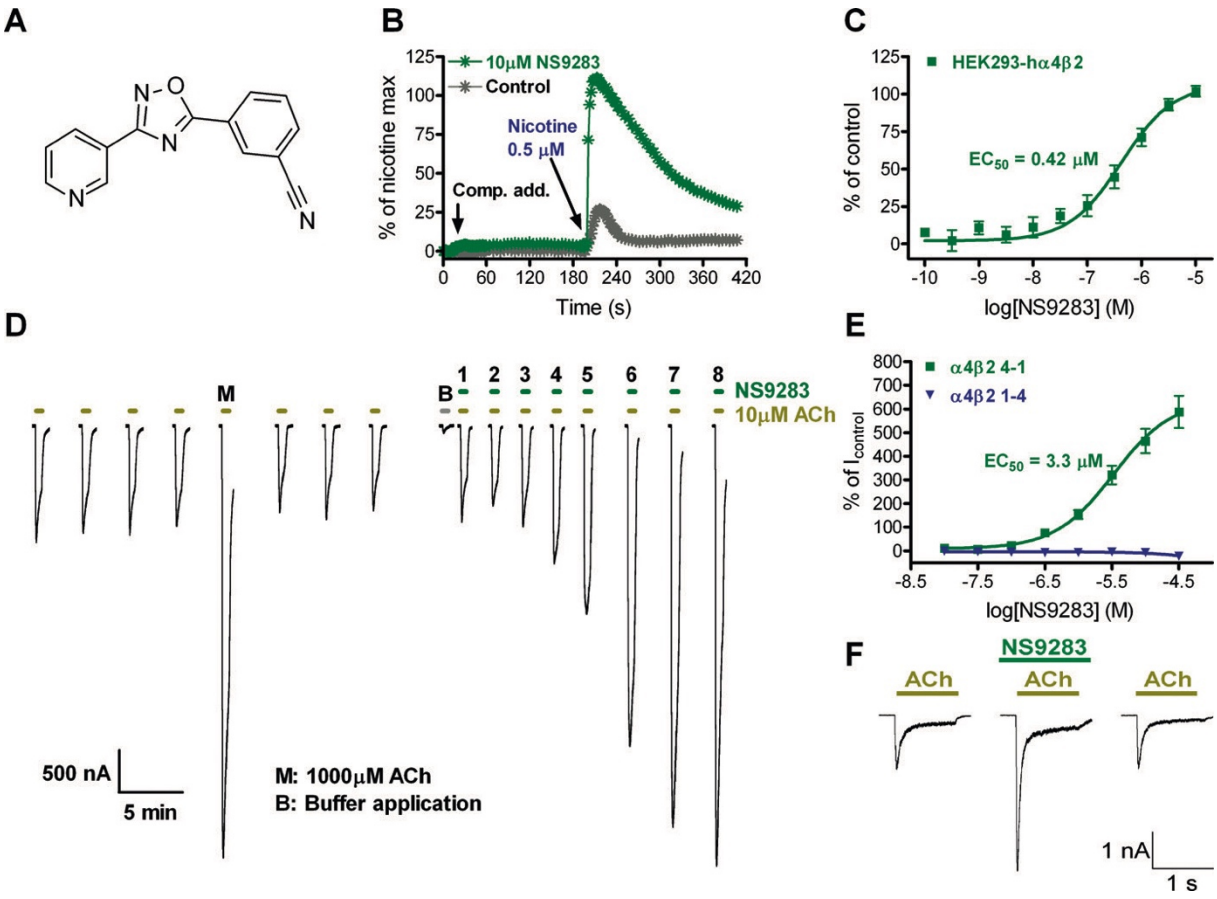

Figure 21. (A) Chemical structure of NS9283; (B) NS9283 does not activates the α4β2 nAChR alone but increases the amplitude of nicotine-evoked Ca^{2+}-response; (C) Concentration-response relationship for NS9283 allosteric modulation; (D) Current traces of ACh and NS9283+ACh in two-electrode voltage-clamp experiments in Xenopus laevis oocytes expressing LS isoform of α4β2 nAChR. NS9283 concentrations were increased in half-log unit increments starting with the lowest concentration (10 nM) in application '1' and ending with the highest concentration (31.6 mM) in application '8'; (E) Concentration–response relationships for NS9283 modulation of ACh-evoked currents in X. laevis oocytes. Oocytes were injected with α4 and β2 nACh receptor subunits in a 1:4 or 4:1 ratio to obtain $(\alpha4)_2(\beta2)_3$ or $(\alpha4)_3(\beta2)_2$ receptors, respectively. Peak current amplitudes were baseline subtracted and normalized with respect to the current induced by ACh (1 mM for $(\alpha4)_2(\beta2)_3$, 10 mM for $(\alpha4)_3(\beta2)_2$), and are presented as mean ± SEM of 11–12 experiments; (F) Representative current traces from whole-cell patch-clamp experiments on human α4β2 nACh receptors transiently expressed in GH4C1 cells stimulated with ACh (100 mM) in the absence, presence and after wash-out of NS9283 (10 mM), respectively. Adapted from Timmermann et al.[90]

In 2013, Grupe *et al.* investigated the mechanism of action of NS9283 on α4β2 receptors expressed in HEK293-hα4β2 cells. From the experiments, it emerged that this molecule increases the potency but not the effectiveness of ACh; it has no effect on the desensitizing action of the endogenous agonist nor it is able to reactivate the desensitized receptors. NS9283 also reduces the recovery rate from ACh-induced desensitization and slows the deactivation rate (*Figure 22*).[83,87]

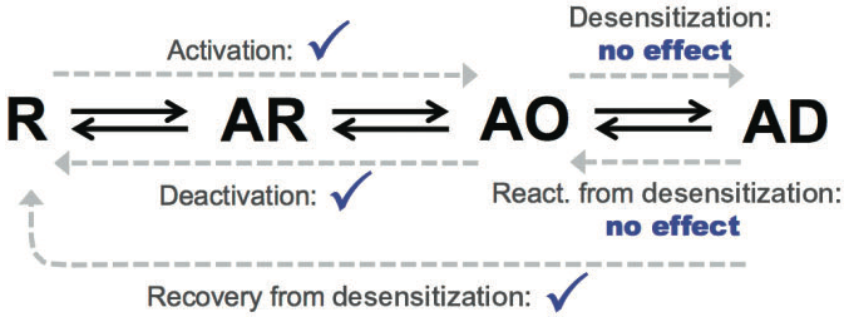

Figure 22. Activation scheme of ACh-evoked currents and modulation exerted by NS9283. R is the closed unliganded state, AR is the closed agonist-bound state, AO is the open agonist-bound state, and AD is the desensitized agonist-bound state. The ticked processes are significantly modulated by NS9283. Adapted from Grupe et al.[83]

Finally, the effect of NS9283 on "windows current" was studied. The “window current” of a ligand-gated ion channel represents the range of an agonist concentration in which several receptors can be recovered for activation despite the presence of a desensitizing agonist. The overlap between the activation and desensitization curves represents the window current. Comparison between the “window currents” of ACh in the presence (area with blue oblique lines) and absence (area with black vertical lines) of NS9283 indicates that the peak of the ACh window current alone occurs at 1.75 mM reaching a maximal response of 8% of the initial 1 mM ACh response, whereas the peak of the ACh window current with NS9283 occurs at 250 nM and reaches a maximal response of 13% of the initial 1 mM ACh response (*Figure 23*). The significance of this result lends itself to different interpretations but, in the light of what Vinson and Justice reported in 1997 and Mattinson *et al.* in 2011, on resting ACh levels in rat brains in the range between the nanomolar and low micromolar, the NS9283 could be a cholinergic transmission volume enhancing agent.[87]

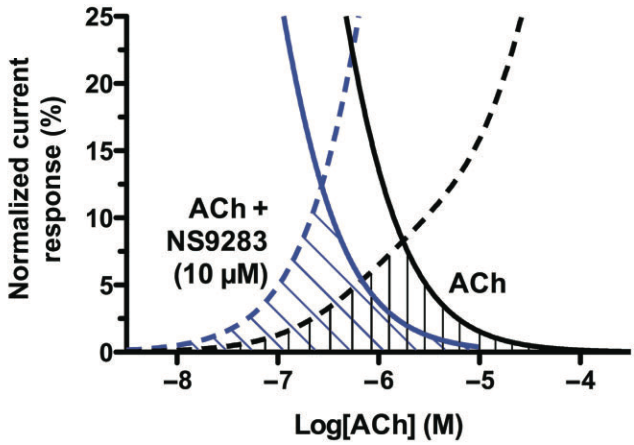

Figure 23. Window current of 1 mM ACh in the absence and presence of NS9283. Adapted from Grupe et al.[87]

In 2014, Olsen *et al.*, crystallized *Lymnaea stagnalis* AChBP (*Ls*-AChBP) with NS9283 to investigate the mechanism of action and binding of this molecule on the α4β2 LS isoform. The data obtained show that the main interactions of NS9283 with the conserved residues on the principal side of the interface: the pyridine ring which forms a π-π bond with Tyr89, the pyridine nitrogen as well as the nitrile group which establish a hydrogen bond with Tyr185 and Tyr192 respectively, and the oxadiazole group interacting with the carbonyl oxygen of Trp143. On the complementary side of the interface, on the other hand, the crystalline structure reveals a close proximity, 4 Å, between the N2 of the oxadiazole group and the centroid of Trp53; N2 also appears to be engaged in van der Waals bonds with Arg104, Leu112 and Met114. A quantum-mechanical study of the interaction between the oxadiazole group and the carbonyl oxygen of Trp143 revealed that the area around C5 and C3 appears to possess a partial positive charge, due to the descherming effect of the nitrile electron-withdrawing group, thus allowing the interaction with the unpaired electron doublets of Trp143 (*Figure 24A*). The amino acid residues of the principal (+) side are completely conserved in both AChBP and the α4 subunit. Although, the complementary part of the *Ls*-AChBP binding site appears to be aligned with the hydrophobic amino acids, corresponding to the β2 (-) subunit, but differs from the hydrophilic amino acids present in the α4 (-) subunit. Thus, to investigate the interactions between the (-) site and NS9283, a homology model was used similar to that described by Harpsøe *et al.*[22] In this model NS9283 maintains similar interaction to the ones with AChBP and it suggests potential interaction with the complementary side, such as hydrogen bond between His142 and nitrile group of the ligand (*Figure 24B*).[100]

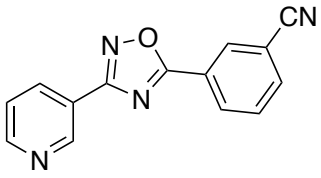

NS9283

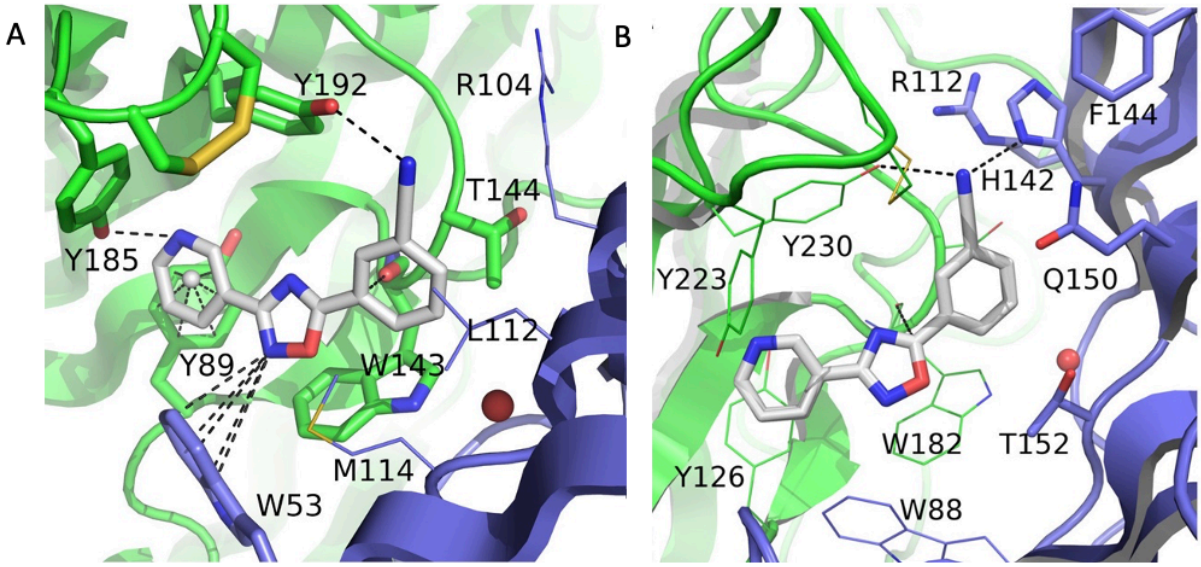

Figure 24.(A) Binding of NS9283 (in gray). Residues from the principal (+) subunit are in green and from complementary (-) side in blue. Interactions are shown with dashed lines; (B) Homology model of NS9283 binding. Non conserved residues are sticks, and conserved are lines. Adapted from Olsen et al.[100]

Also, point mutations were performed on the amino acids considered important for the interaction of NS9283: Trp88, Arg112, His142, Phe144, Gln150 and Thr152. All the mutations led to a modification of NS9283 potency. Trp88 of α4 is the only amino acid conserved in *Ls*-AChBP (Trp53) and its mutation to alanine or phenylalanine resulted in greatly reduced modulator potency indicating the importance of the Trp-specific interaction. A mutation with an arginine completely abolishes the modulation due to a steric encumbrance. Arg112, His142 and Phe144 seem to play an important role in the binding of NS9283 to the complementary part because single mutations of these amino acids in alanine lead to a loss of power of NS9283. Interestingly, the α4α4-ACh interaction is similarly affected by the same mutations thus suggesting that the interaction model of NS9283 with α4α4 mimics that of agonists. Other residues of the complementary subunit α4 (-) such as Thr109, Ser110, Thr139 and His145, were mutated and it was confirmed that they are not involved in the interaction with NS9283. Furthermore, mutation of the α4 (-) side into a β2 (-) side, where H142V, Q150F and T152L mutations were performed, abolished the activity of NS9283. When these mutations were performed individually, in the H142V mutant there was no activity, however, in Q150F and T152L mutants there was a decreased functional potency by a factor of 2 and 3, respectively (*Figure 25*). It was important to understand if the effect of H142V was due to the lack of interaction of the histidine or to a steric encumbrance. Therefore, other two mutations were

performed with valine and alanine which are less bulky. The replacement of histidine with alanine reduces the potency by about 10-times, but the replacement with valine eliminates the effect of NS9283. This means that the bulky and branched valine prevents the binding of NS9283 with the α4β2 interface due to steric hindrance, while histidine interacts directly with NS9283. Therefore, histidine suggests being the main factor in determining the α4α4 selectivity of NS9283 by forming a bridge that anchors the ligand by binding it to the binding site.[100]

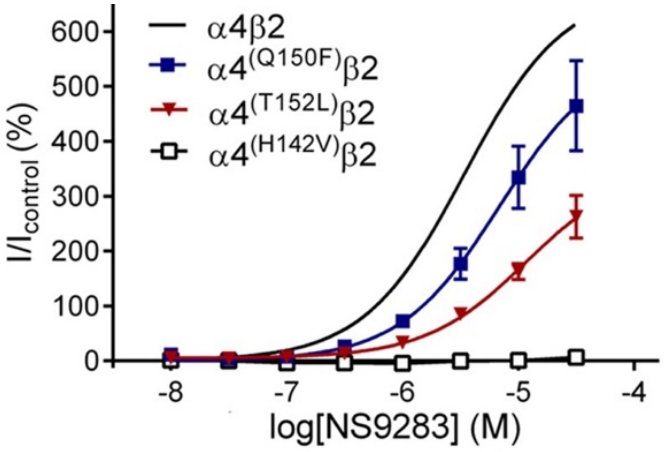

Figure 25. Mutations of the α4 (-) side lead to a decreased modulatory potency. Adapted from Olsen et al.[100]

Marotta *et al.* hypothesized that NS9283 might be able to activate alone receptors with more than one α4α4 binding site. For this purpose, they decided to mutate three amino acids of the β2(-) side: V136H, F144Q and L146T. In this way, it was obtained a receptor with 3α:2β stoichiometry but with two pseudo α4α4 sites instead of native α4β2 binding sites. Indeed, the application of NS9283 on this mutant receptor alone activates the receptor response in a dose-dependent manner.[21]

Thanks to this study it was possible to better understand the mechanism of action of NS9283 and other compounds with similar behaviour, such as CMPI. SAR studies involving NS9283 and CMPI might be useful for the discovery of new molecules that act on nAChRs as well as on other members of the Cys-loop receptor family.[100,101] In 2017, Wang *et al.* performed docking studies of NS9283 in the absence of ACh using a previously generated LS-α4β2 nAChR homology model. Two docking modes with similar interaction energies (-26.99 and -26.87 kcal/mol) were predicted. In the first docking pose, NS9283 is positioned near His116

(His142[100]), and in the second docking mode, it is tilted outward toward Gln124 and Thr126 (Gln150 and Thr152[100]) confirming mutational studies results obtained previously (*Figure 26*).

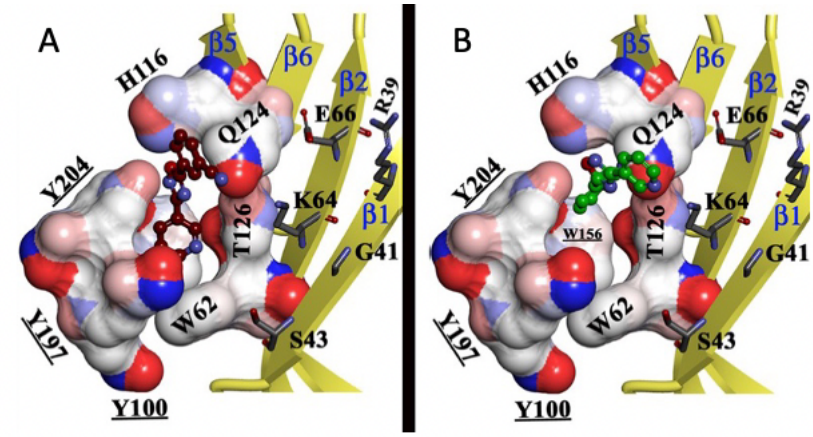

Figure 26. NS9283 docked at the α4α4 binding site of LS-α4β2 nAChR homology model based on the X-ray structure of LS-α4β2 nAChR (PDB ID: 5KXI). (A) NS9283 first docking pose; (B) NS9283 second docking pose. Adapted from Wang et al.[101]

Furthermore, these nAChRs potentiators may be useful in the treatment of diseases where agonists have shown efficacy. The co-administration of these potentiators with α4β2 agonist allows the use of lower doses of agonist with consequent decrease of side effects. This can be particularly useful with agonists with low therapeutic index and/or low receptor subtype selectivity. For example, the effectiveness of co-application of NS9283 has been demonstrated in the treatment of pain, cognitive disorders, obsessive compulsive disorder and nicotine addiction. For example, NS9283 is selective for nAChRs containing the α4 and α2 subunits, without interacting with the α3β2 ganglionic receptors, thus avoiding cardiovascular or body temperature regulatory side effects.[20]

In 2019, Mazzaferro *et al.* discovered that mutation on both principal β2 and complementary α4 sides prevent the potentiation action of currents generated by ACh in LS isoform by NS9283. This result suggest that NS9283 potentiates α4β2 receptor as a pseudo-agonist of the β2:α4 interface, as an α4α4 agonist, or both. To distinguish between these possibilities, different mutational studies were performed. Trp176 from the principal face of the β2 subunit is adjacent to the His142 from the complementary α4 side and together they can contribute to the NS9283 binding. The mutation on the β2 subunit of the amino acid W176A in both pseudo-interfaces β2α4 suppresses the enhancement while the mutation of the amino acid α4H142V on the interface α4α4 induces a significant enhancement. This reveals that the

activation of the pseudo-interface β2α4 is necessary to generate a response in the LS α4β2. However, β2:α4 interface might not be the binding site, but act as transduction elements for potentiation.[19]

3.2. Aim and objectives

Based on previous work, the main goals of this part of my thesis are:

1. Mutational studies of the hydrophilic pocket defined by Ser108, Asn109 and Leu121 in the β2 (-) side of the orthosteric binding site of the α4β2 nAChR, identified by modelling the complex α4β2/2-pyrrolidinyl-7-hydroxybenzodioxane (*S*,*R*)-**IV**.
2. Synthesis of new α4β2 neuronal nicotinic acetylcholine receptor (nAChR) partial agonists based on the benzofuran scaffold.
3. Investigation of the α4β2 HS and LS isoform selectivity of previously synthesized compounds.
4. *In vivo* studies of the most promising benzodioxanes and prolinol aryl ethers previously synthesized using a zebrafish model.
5. Design, synthesis and evaluation of potential selective agonists for α4β2 unorthodox binding site based on NS9283 structure.

3.3. Mutational studies of β2 subunit

3.3.1. Introduction and aim

Compounds (*S,R*)-**IV**, (*S,S*)-**IX** and (*S,R*)-**X** are the most promising compounds synthesized and tested for their binding affinity. They were docked into the orthosteric α4β2 binding site and it was confirmed that they are involved in hydrogen-bond interaction with Asn109 and Leu121 through 7-OH ((*S,R*)-**IV**), 5-NH_2 ((*S,S*)-**IX**) and pyridodioxane nitrogen ((*S,R*)-**X**). These two residues together with Ser108 form a hydrophilic pocket of the β2(-) side. The interactions with this site justify that in their absence, like in naked benzodioxane derivative (*S,R*)-**III**, the affinity is lower and there is a loss of agonist activity. These compounds show α4β2 affinity and agonism, and α4β2/α3β4 selectivity. Therefore, it was important to determine the critical role of substituents at the aromatic ring in the interaction with the small hydrophilic pocket on β2(-) side.[98]

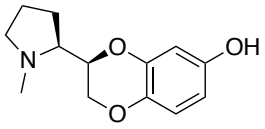

(*S,R*)-**IV**

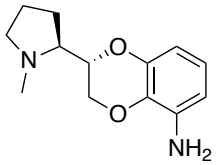

(*S,S*)-**IX**

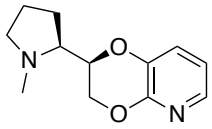

(*S,R*)-**X**

3.3.2. Biology

For this purpose, we chose to make single mutations rather than backbone mutations, which can be generically disruptive to receptor function. Considered the small capacity of the pocket, we decided to increase and decrease the volume of Ser108 side chain in order to disfavor or favor the accessibility to backbone NH of Leu121 and CO of Asn109. Ser108 residue was replaced with leucine (Leu), phenylalanine (Phe) and alanine (Ala). Binding experiments were performed on the heterologously expressed human α4β2 receptor and its three Ser108→Leu, Ser108→Phe and Ser108→Ala mutants. We also tested compound (*S,R*)-**III** and (*S,R*)-**VII** to extend the investigation. The results are shown in *Table 3*. To assess whether conserved or slightly increased binding to the Ala mutated receptor corresponds to unaltered agonist activity, compounds (*S,R*)-**IV**, (*S,S*)-**IX** and (*S,R*)-**X** were tested via whole-cell patch clamp electrophysiology with GH4C1 cell line cells transiently expressing the human α4β2 subtype and its Ser108 → Ala mutant (*Figure 27*).

3.3.2.1. Constructs of Mutated β2 Subunits.

The amino acid S108 of the human β2 subunit, identified by modeling, corresponds to S133 (due to the presence of signal peptide of 25 amino acids) in the UniProt sequence. The mutants S133A, S133L, and S133F have been generated by site-directed mutagenesis using the QuikChange Lightning Site-directed mutagenesis kit (#210519, Agilent). The template used was pCDNA3-hβ2 (a kind gift of Sergio Fucile, Università la Sapienza, Roma), which codes for the entire CDS of the human β2 subunits (protein sequence, ACHB2_HUMAN, UniProt database). In pCDNA3-hβ2-S133A, a TCC trinucleotide sequence (position 397−399) that codes for a serine is changed to GCC (one nucleotide mutated) that codes for an alanine. To obtain pCDNA3-hβ2-S133L, the TCC is converted to CTC (two nucleotides mutated) that codes for a leucine, while it is converted to TTC (one nucleotide mutated) that codes for a phenylalanine

in pCDNA3-hβ2-S133F. To obtain these substitutions, we designed the following primers (the mutated oligonucleotides in bold):

S133A upper: 5'-CGAGGTGTCCTTCTAT**G**CCAATGCCGTGGTCTCC-3'.

S133A lower: 5'-GGAGACCACGGCATTGG**C**ATAGAAGGACACCTCG-3'.

S133L upper: 5'-CGAGGTGTCCTTCTAT**CT**CAATGCCGTGGTCTCC-3'.

S133L lower: 5'-GGAGACCACGGCATTG**AG**ATAGAAGGACACCTCG-3'.

S133F upper: 5'-CGAGGTGTCCTTCTATT**T**CAATGCCGTGGTCTCC-3'.

S133F lower: 5'-GGAGACCACGGCATT**G**AAATAGAAGGACACCTCG-3'.

According to the protocol of the kit, 25 ng of the template was amplified using 125 ng of primers with the following PCR protocol: 1 cycle of 95 °C for 2 min (step 1), 18 cycles of 95 °C for 20 s, 60 °C for 10 min and 68 °C for 3.5 min (step 2), and 1 cycle of 68 °C for 5 min.

After the digestion of the parental methylated DNA with the DpnI enzyme, we transformed the mutated plasmid into XL10-GOLD Ultracompetent cells. The mutations were checked by sequencing the plasmid obtained.

3.3.2.2. Transfection and Binding Studies of WT and Mutated α4β2 Subtypes

HeLa cells were purchased from ATCC and grown in a high-glucose DMEM medium (Gibco, Thermo Fisher Scientific) supplemented with 10% heat-inactivated FBS (CARLO ERBA Reagents) of South American origin, 2 mM L-glutamine (Euro- Clone), 100 U/mL penicillin G, and 100 µg/mL streptomycin (EuroClone). The cells were maintained in a 5% CO_2 environment at 37 °C. On the day before transfection, 2.2×10^6 to 2.5×10^6 cells for each condition were plated in a 100 mm Petri dish. Each dish was transfected with 15 µg of pcDNA (7.5 µg of pcDNA for each subunit: α4 and β2 for control α4β2; α4 and β2S133A for α4β2S133A subtype; α4 and β2S133L for α4β2S133L subtype; α4 and β2S133F for α4β2S133F subtype) by employing JetPEI DNA transfection reagent (Polyplus-transfection) diluted with a 150 mM NaCl solution by following the manufacturer's instructions. The culture medium was replaced with fresh medium just before transfection. After 24 h, the transfected cells were washed once with PBS, harvested, and immediately frozen. For [^{3}H]epibatidine saturation binding experiments,

aliquots of the membrane homogenate obtained from transfected HeLa cells were used and binding was performed as described above. For competition studies, the inhibition of [^{3}H]epibatidine binding was measured by incubating the membranes of HeLa cells transfected with the appropriate subtype with increasing concentrations of compounds for 5 min followed by overnight incubation at 4 °C, with 0.1 nM [^{3}H]epibatidine. At the end of the incubation time, the samples were processed as described above. [^{3}H]Epibatidine binding was determined by liquid scintillation counting in a β counter. Ki values were obtained by fitting three independent competition binding experiments, each performed in duplicate for each compound on each subtype.

3.3.2.3. Electrophysiological Experiments

The human α4β2 and α4β2S108A nAChRs were expressed by transient transfection in the rat anterior pituitary GH4C1 cell line. Transient transfection was achieved by adding to each well 0.5 µg of each subunit cDNA, along with 2 µL of Magnetofection reagent NeuroMag (OZ Biosciences, France). All culture media were purchased from Invitrogen (Italy). Whole-cell current recordings were performed 2−3 days after transfection. Recordings and data analysis were performed by using a borosilicate glass patch pipette (3 to 6 MΩ tip resistance) connected to an Axopatch 200A amplifier (Axon Instruments, Foster City, CA). Data were stored on a PC computer by using PCLAMP10 software (Molecular Devices). During the recording period, the cells were bathed in the following solution: 140 mM NaCl, 2 mM $CaCl_2$, 2.8 mM KCl, 2 mM $MgCl_2$, 10 mM Hepes/ NaOH, and 10 mM glucose (pH 7.3). The patch pipettes were filled with a solution containing 140 mM CsCl, 2 mM MgATP, 10 mM Hepes/CsOH, and 5 mM BAPTA (pH 7.3). Whole-cell capacitance and patch series resistance (5−15 MΩ) were estimated from slow transient compensations. A series resistance compensation of 85− 90% was obtained in all cases. The cells were voltage-clamped at a holding potential of −70 mV and continuously perfused with a gravity-driven system using independent external tubes for the control and agonist-containing solutions. These tubes were positioned 50−100 µm from the patched cell and connected to a fast exchanger system (RSC-160, BioLogic, France). Dose−response relationships were constructed by sequentially applying different concentrations of agonists and normalizing the obtained current

amplitudes to the value obtained by applying 100 µM ACh on the same cell. For quantitative estimations of agonist actions, dose−response relationships were fitted by the equation:

$$I = I_{max} ([C]^{nH} / (EC_{50}{}^{nH} + [C]^{nH})),$$

where I is the peak current amplitude induced by the agonist at concentration [C], I_{max} is the maximum response of the cell, n_H is the Hill coefficient, and EC_{50} is the concentration for which a half-maximum response is induced. Dose−response curves were fitted with separate or shared parameters for α4β2 and α4β2S108A nAChRs (I_{max}, EC_{50}, and n_H) and then compared with F statistical analysis. No significant difference was found; thus, a single dose−response curve was shown for each compound.

3.3.3. Results and discussion

Western blot analysis of the mutated receptors showed that none of the three mutations affected the expression of the receptors. However, the substitution of Ser108 with Leu and Phe residues completely abolished the binding of the [^{3}H]epibatidine, not allowing the determination of the K_i of our compounds. Contrastingly, the mutation to Ala had a beneficial effect on the binding of the two 7-substituted derivatives (*S,R*)-**IV** and (*S,R*)-**VII**, and it was insignificant to the binding of other 3 compounds (*Table 3*).

Compound	Structure	Wild-type α4β2 nAChR Ki (μM)	Mutated α4β2S108A nAChR Ki (μM)	Ratio (wild type/mutant)
(*S,R*)-**IV**	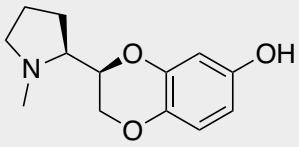	0.0067 (0.001)	0.0012 (0.0004)	5.6
(*S,S*)-**IX**	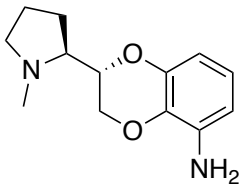	0.373 (0.049)	0.156 (0.017)	2.4
(*S,R*)-**X**	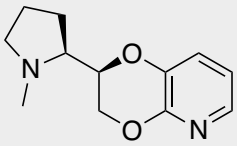	0.114 (0.026)	0.265 (0.091)	0.43
(*S,R*)-**III**	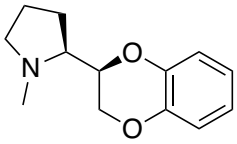	1.175 (0.16)	0.912 (0.29)	1.29
(*S,R*)-**VII**	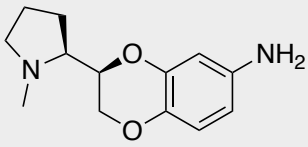	0.046 (0.008)	0.006 (0.001)	7.7

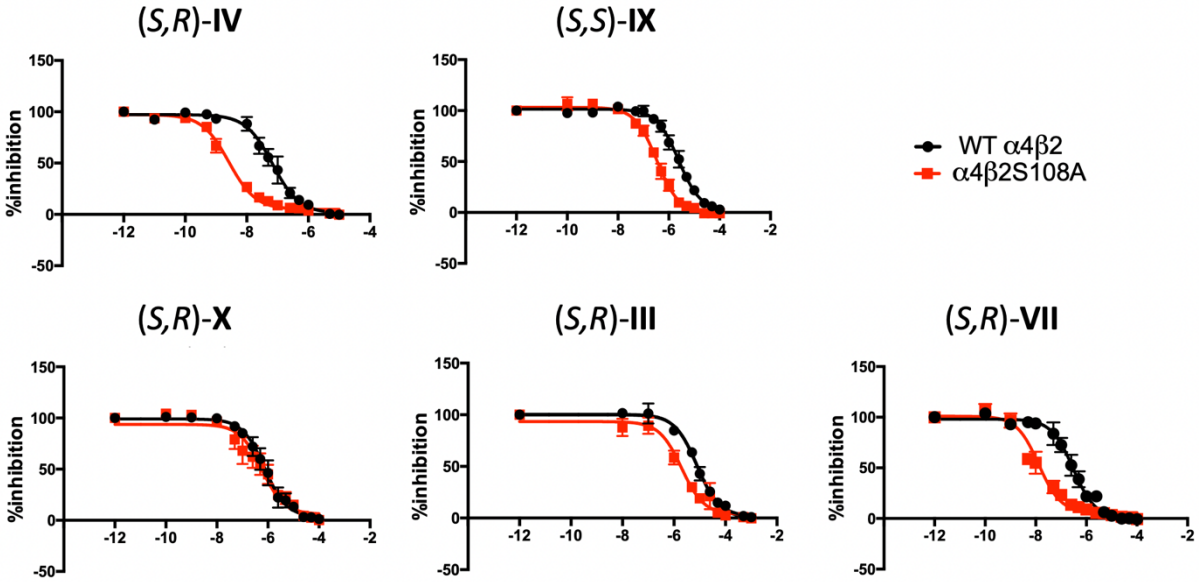

Table 3. The Kd and Ki values were derived from [3H]epibatidine saturation and three competition binding experiments using human WT α4β2 and mutated α4β2S108A subtypes. Data from saturation and competition binding curves were evaluated by one-site competitive binding curve-fitting procedures using GraphPad Prism version 5 (GraphPad Software, Inc., CA, USA). Each compound was tested in three separate competition binding curves for both wild-type and mutated receptors and the inhibition constant (Ki) was estimated in reference to the Kd of the radioligand according to the Cheng–Prusoff equation. The numbers in brackets represent the standard error.[98]

As shown in *Figure 27A-C*, the three compounds maintain partial agonism responses with almost identical efficacies at the wild-type and mutated receptors, confirming the binding results.

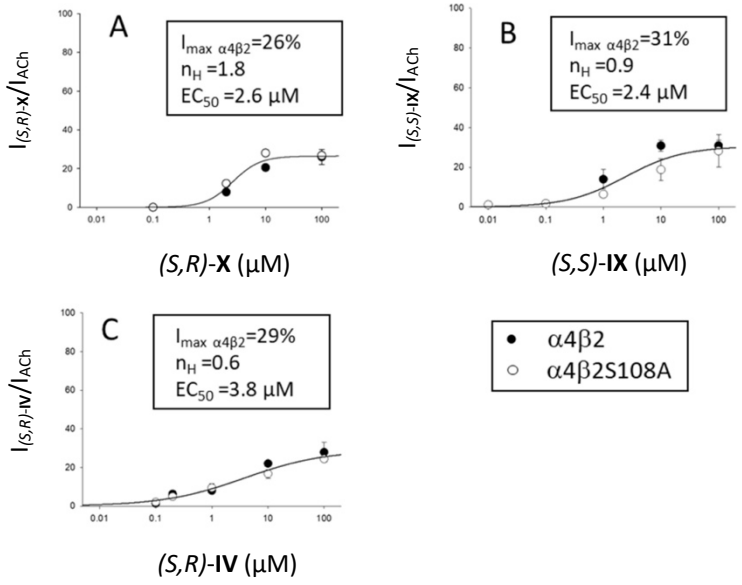

*Figure 27. Agonist properties of (S,R)-**X** (A), (S,S)-**IX** (B), and (S,R)-**IV** (C) do not differ on human α4β2 and α4β2S108A nAChRs. (A) (S,R)-**X** dose−response relationship (normalized with respect to the response elicited by 100 µM ACh) for human α4β2 nAChR (black circle; n = 3) and for human α4β2S108A nAChR (white circle; n = 2). A single Hill equation was best fitted to all data, yielding I_{max} = 26 ± 2%, EC_{50} = 2.6 ± 0.6 µM, and nH = 1.8 ± 0.8; (B) (S,S)-**IX** dose−response relationship (normalized as in A) for human α4β2 nAChR (black circle; n = 3) and for human α4β2S108A nAChR (white circle; n = 4). A single Hill equation was best fitted to all data, yielding I_{max} = 31 ± 5%, EC_{50} = 2.4 ± 1.7 µM, and nH = 0.9 ± 0.4; (C) (S,R)-**IV** dose−response relationship (normalized as in A) for human α4β2 nAChR (black circle; n = 4) and for human α4β2S108A nAChR (white circle; n = 8). A single Hill equation was best fitted to all data, yielding I_{max} = 29 ± 3%, EC_{50} = 3.8 ± 2.1 µM, and nH = 0.6 ± 0.1.*

Replacement of the hydroxymethyl side chain of Ser108, one of the amino acid residues lining the small hydrophilic β2 pocket, with the little less bulky methyl of Ala increases the affinity of the 7-OH and 7-NH_2 derivatives without significantly modifying that of the benzodioxane derivatives unsubstituted or 5-modified and, in any case, it does not affect α4β2 partial agonism. On the contrary, replacement of the hydroxymethyl side chain of Ser108 even just with the little bulkier isopropyl of Leu abolishes the labeled epibatidine binding so as to hinder α4β2 affinity determination. These results indicate that the small β2 pocket is well receptive to OH and NH_2 substituents and to pyridodioxane nitrogen, which are indispensable to elicit the agonist activity, but with very strict occupancy limits.[98]

3.4. Design, synthesis and pharmacological evaluation of new α4β2 partial agonists

3.4.1. Introduction and aim

As discussed in the previous chapter 2.3, a series of pyrrolidinyl-benzodioxanes and analogues were synthesized, and their pharmacological profiles were investigated. Their activity strictly depends on the conformation and the configuration of -C-O- linker between the pyrrolidine ring and the aryl moiety and on the substitution pattern of the latter. In smoking cessation, the partial agonist approach combines agonist activity to relieve craving during abstinence with attenuation of the rewarding effects of smoking by blocking nicotine's access to the α4β2 nAChR. From the results obtained with the mutational studies, we decided to further investigate the importance of the hydrophilic pocket and the interaction of hydroxyl group with it. Therefore, we were interested to find new α4β2 potential partial agonists based on the benzofuran scaffold in place of benzodioxane system previously synthesized in our research group to further investigate the implications of the flexibility reduction, abolishment of stereogenic centre and of the one of the two oxygen in comparison with previously tested benzodioxane derivatives. For this purpose, we designed and synthesized compounds **1**-**6** with naked or hydroxy/methoxy decorated benzofuran scaffold (*Figure 28).*

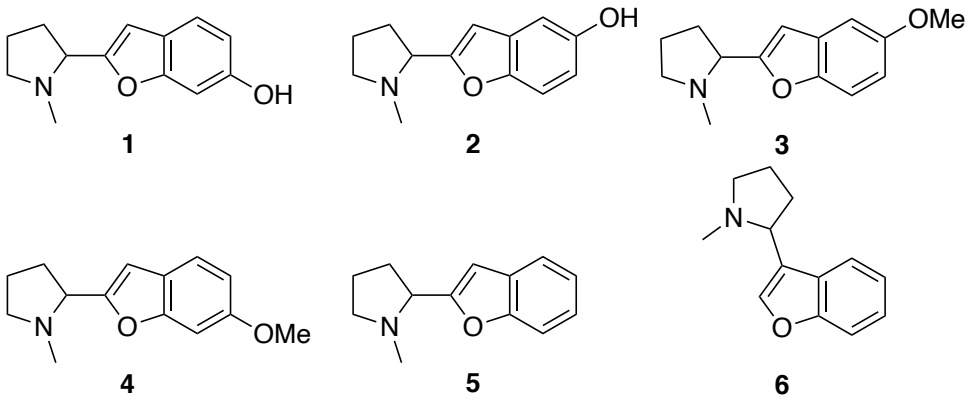

*Figure 28. Potential α4β2 partial agonists **1**-**4** and antagonists **5** and **6**. All the compounds are racemic.*

We performed docking in the orthosteric binding pocket of the α4β2 receptor starting from the new Cryo-EM structure of the full-length human receptor (6CNJ) now available. Docking was performed using the Glide XP Ligand Docking Protocol docking in Maestro, Schrodinger, with default settings (van der Waals radius scaling factor: 0.8, partial cutoff: 0.15, XP precision, OPLS3e forcefield, flexible sampling), with a grid centered on the present ligand. It is possible

to observe that our most interesting benzodioxane derivative, (*S,R*)-**IV,** places the hydroxyl group deep in the hydrophilic pocket. Otherwise, the hydroxyl group of the benzofuran analogues **1** and **2** were slightly out of the pocket. These docking results prompted us to synthesize a series of pyrrolidinyl benzodioxanes differently substituted, at the benzene ring, in order to better evaluate the role of such interactions with the hydrophilic pocket (*Figure 29*).

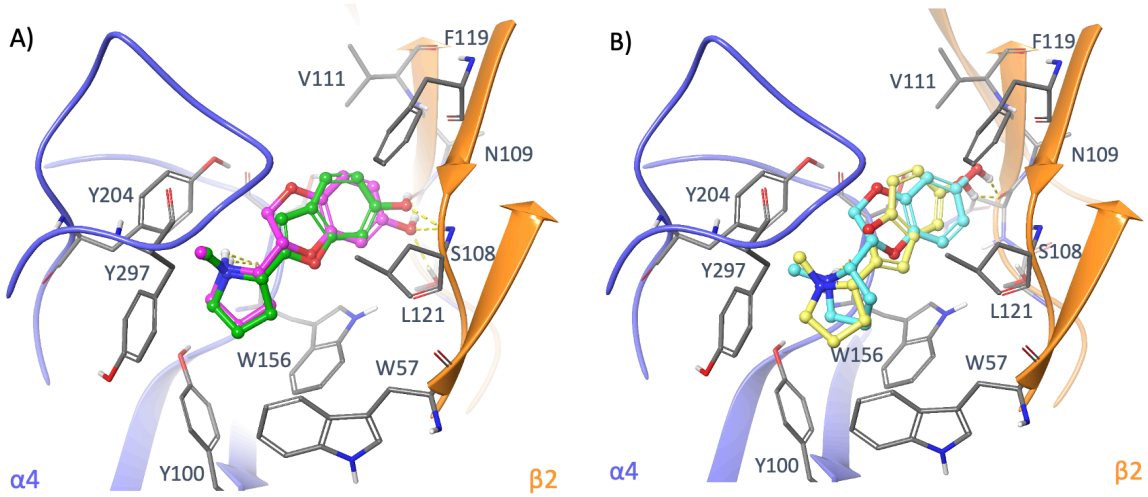

*Figure 29. A) Binding modes of (S,R)-**IV** (pink) and **1** (green) and of B) (S,R)-**IV** (cyan) and **2** (yellow) at the α4β2-nAChR orthosteric binding site (PDB ID: 6CNJ). The backbone of the receptor is represented with blue (α4) and orange (β2) cartoons, and amino acids of the binding sites are shown in dark grey. For clarity, only H-bonds are depicted (yellow dashed lines). Whereas the pyrrolidine rings and aromatic cores of (S,R)-**IV** and **1** are similarly positioned, the terminal hydroxyl group of **1** does not access completely the small hydrophilic subpocket, and interacts only with the backbones of S108 and N109, but not with the side chain of S108. Repositioning of the terminal OH group to (S,R)-**IV** and **2** disallows H-bond interactions with both S108 and N109 of the hydrophilic subpocket and an overall upwards shift of the ligands.*

3.4.2. Chemistry

For the synthesis of these compounds, I started with *N*-Boc protection of commercially available pyrrolidine performed by treatment with di-tert-butyl decarbonate (Boc_2O). This is the main intermediate which will then react with properly substituted 2- or 3-bromobenzofurans in a Catalytic Lithiation Trapping-Negishi Coupling reaction to give the desired products.

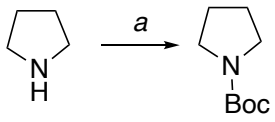

7

Scheme 2. Reagents and condition (a) DCM, TEA, Boc_2O, rt, overnight, 98%.

The synthesis of 2-bromobenzofuranol scaffolds is based on the Ramirez olefination reaction followed by the intramolecular cyclization of the formed dibromoolefine to benzofuran. The properly substituted dihydroxybenzaldehyde (compounds **8** and **9**) was reacted with CBr_4 and PPh_3 in presence of Zn powder, used as a scavenger of acidity, to give the correspondent *gem*-dibromoalkene. This latter was found to decompose on isolation and for this reason, the crude of the reaction was submitted directly to the cyclization step by treatment with CuI and K_2CO_3 o Cs_2CO_3, giving compounds **10** and **11**. Many efforts have been made for the optimization of this step by trying different bases, solvents, and temperatures. I also tried to use a heterogenous Copper-catalyst based on AquivionH polymer, which gave higher yields. Unfortunately, every attempt to recover this cataluyst at the end of the reaction was not effective, so I decided to use CuI, which is less expensive. Compounds **10** and **11** were then *O*-alkylated by reaction with BnBr or MeI to obtain compounds **12**-**15** (*Scheme 3*).

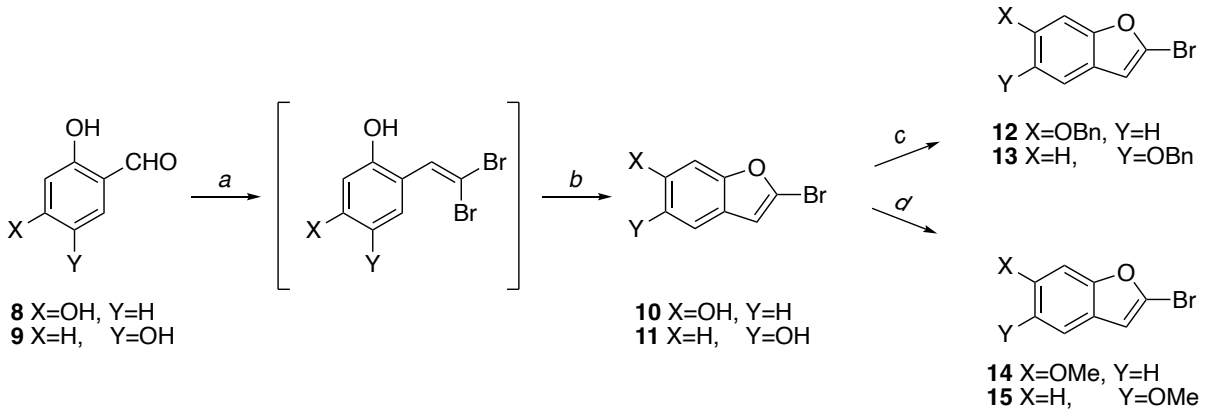

*Scheme 3. Reagents and conditions (a) ACN, CBr_4, Ph_3, Zn, rt, 1h; (b) NH_4Cl, rt, 30min; Cs_2CO_3 or K_2CO_3, CuI reflux 3h, 43% (**10**), 36% (**11**); (c) dry THF, NaH, BnBr, rt, overnight, 84% (**12**), 73% (**13**); (d) dry THF, NaH, MeI, rt, overnight, 70% (**14**), 86% (**15**).*

The obtained benzofurans **12**-**15** were then coupled with *N*-Boc pyrrolidine in a lithiation trapping – Negishi reaction giving compounds **16-19**. Compounds **20**, **21** and **3** were then obtained by *N*-Boc deprotection and subsequent *N*-methylation of pyrrolidine ring by reductive amination. Compound **4** was obtained by N-Boc deprotection of **19** with $LiAlH_4$.

Compounds **1** and **2** were obtained by catalytic hydrogenation of compounds **20** and **21** (*Scheme 4*)**.**

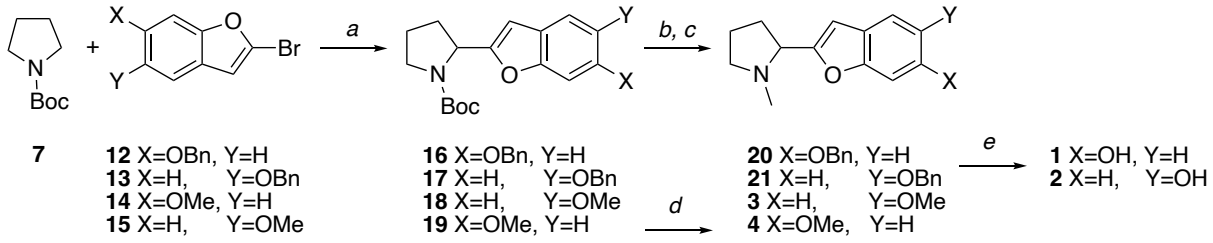

*Scheme 4. Reagents and conditions (a) dry THF, s-BuLi, $ZnCl_2$, $Pd(OAc)_2$, $^tBu_3PHBF_4$, rt, 16h, 16% (**16**), 20% (**17**), 10% (**18**), 17% (**19**); (b) HCl in MeOH 1.25N, 50°C, 3h; (c) MeOH, CH_3COOH, 37% $HCHO_{(aq)}$, pic-BH_3, rt, 4h, 60% (**20**), 41% (**21**), 37% (**3**); (d) dry THF, $LiAlH_4$, rt, 3h, 14% (**4**); (e) H_2, Pd/C 10%, MeOH, rt, 2h, 78% (**1**), 66% (**2**).*

Mechanism of the step *a*:

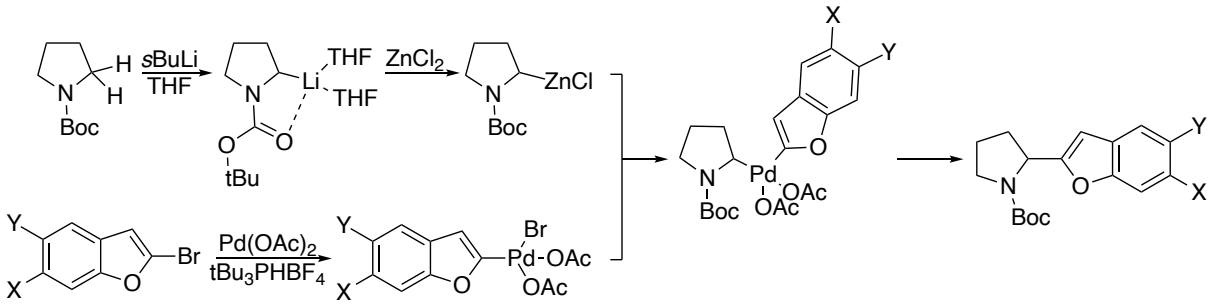

Compound **5** was synthesized using a Lewis acid promoted addition of *n*-BuLi to an intermediate imine. In this synthesis, *N*-lithiated pyrrolidine reduces benzophenone forming a lithium alkoxied and 1-pyrroline. This intermediate imine is instable on isolation, so it directly reacts with previously formed α-lithiated benzofuran, forming the α-functionalized intermediate compound **22**. The addition of Lewis acid in the condensation step activates the 1-pyrroline towards nucleophilic attack. The desired compound **5** was then obtained by *N*-methylation of pyrrolidine ring by reductive amination (*Scheme 5*).

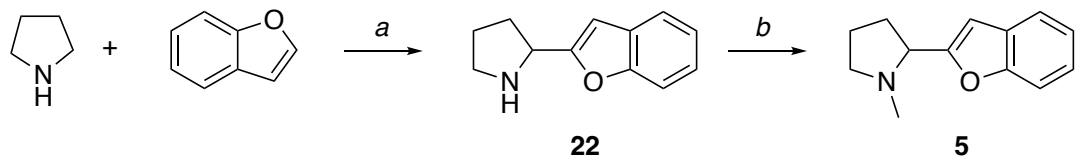

Scheme 5. Reagents and conditions (a) dry THF, dry Et_2O, n-BuLi, benzophenone, $BF_3{\cdot}Et_2O$, rt, 2h, 7%; (b) MeOH, CH_3COOH, 37% $HCHO_{(aq)}$, pic-BH_3, rt, 4h, 62%.

Mechanism of the step *a*:

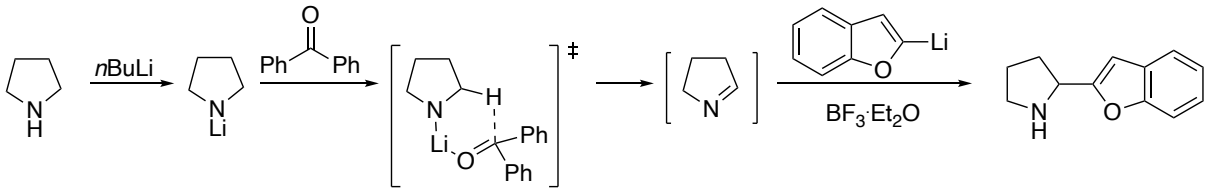

For the synthesis of compound **6**, the key intermediate is 3-bromobenzofuran, which was obtained by the treatment of the commercially available benzofuran with bromine to obtain the corresponding 2,3-dibromo derivative, that was dehydrobrominated to the desired compound **23.** Subsequently, this latter compound **23** was coupled with *N*-Boc-pyrrolidine to give intermediate **24**, which was then Boc-deprotected by treatment with HCl methanol solution and *N*-methylated using reductive amination procedure to final compound **6** (*Scheme 6*).

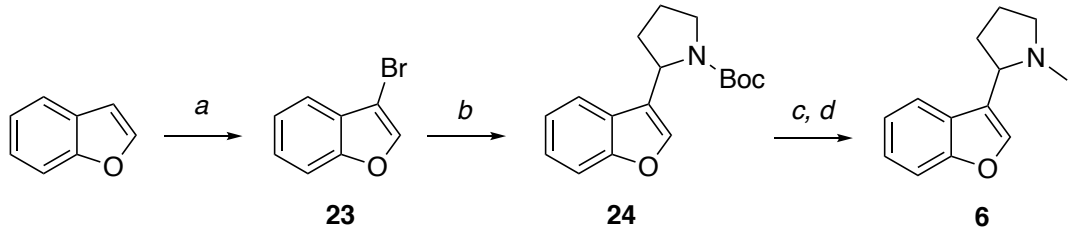

Scheme 6. Reagents and conditions (a) DCM, Br_2, rt, 30min; followed by KOH_{sat} in EtOH, reflux, 3h, 56%; (b) dry THF, N-Boc pyrrolidine, s-BuLi, $ZnCl_2$, $Pd(OAc)_2$, $^tBu_3PHBF_4$, rt, 16h, 15%; (c) HCl in MeOH 1.25N, 50°C, 3h, 33%; (d) MeOH, CH_3COOH, 37% $HCHO_{(aq)}$, pic-BH_3, rt, 4h, 26%.

3.4.3. Biology

3.4.3.1. Cell culture and membrane preparation

Culture of HEK-293 cells stably transfected with human α4β2 (HEK-α4β2) or rat α3β4 (HEK-α3β4) and membrane fractions preparation were performed as previously described.[102] HEK-α4β2 and HEK-α3β4 cells were grown at 37 °C in a humidified incubator at 5% CO_2 in 25 mL of growth medium 140 mm tissue culture dishes for 4 days. The medium consists of a 1:1 mixture of DMED and Ham's F12, supplemented with 10% fetal bovine serum, penicillin (100 units/mL), streptomycin (100 units/mL) and G418 (450 µg/mL). At 80-100% confluency, cells were treated with trypsin and harvested by gentle scraping. Cells were washed twice with phosphate buffer saline and final cell pellet was stored at -20 °C till used. At the day of membrane preparation, cells were thawed on ice in vesicle dialysis buffer (VDB; 100mM NaCl,

0.1mM EDTA, 0.02% NaN3, 10mM MOPS, pH 7.5) in the presence of protease inhibitor cocktail (Calbiochem, Millipore, San Diego, CA, USA). Cell were homogenized using glass-Teflon homogenizer and unsuspended cell debris was removed by centrifugation at 2000 rpm at 4 °C for 20 min. The supernatant was collected and centrifuged at 15K rpm at 4 °C for 1 h to pellet membrane fractions which was resuspended in VBD.

3.4.3.2. Binding assay

The affinity (Kd) of the nAChR agonist epibatidine at the α4β2 nAChR was determined using [^{3}H]epibatidine saturation binding to membranes isolated from HEK-293 cells stably transfected with human α4β2 (HEK-α4β2). The affinities (Ki) of the synthesized compounds **1-6** for the α4β2 and α3β4 nAChRs were determined using their concentration-dependent displacement of the specific binding of [^{3}H]epibatidine to HEK-α4β2 and HEK-α3β4 membranes, respectively. The total and specific bindings of [^{3}H]epibatidine were determined using a filtration based assay as described in Pinheiro *et al.*[103] and every experiment was done in triplicate. Briefly, for saturation experiments, HEK- α4β2 membranes at 0.1 mg/mL protein were incubated at room temperature for 3 h with 1- 20 nM concentrations of [^{3}H]epibatidine in the absence (total binding) or presence of 1 mM carbamylcholine (nonspecific binding). At the end of the incubation, receptor bound and free [^{3}H]epibatidine were separated by rapid filtration using polyethyleneimine-treated glass microfiber filters. Filters then washed with 5 mL of ice-cold VDB, allowed to fully dry, soaked in 5 mL of scintillation cocktail, and their 3H contents were quantified by liquid scintillation counting (liquid scintillation analyzer Tri-Carb 4810TR, PerkinElmer Life Sciences, Waltham, MA, USA). For [^{3}H]epibatidine competition studies, the inhibition of [^{3}H]epibatidine binding was measured by incubating membranes of the appropriate subtype with 1 nM [^{3}H]epibatidine and increasing concentrations of the compound to be tested at room temperature for 3 h. The Kd of the ligands for each subtype was determined by performing triplicate binding experiments for each compound for each dose. Data analysis, curve fitting and Kd determination were calculated using GraphPad Prism version 9 (GraphPad Software, Inc., San Diego, CA, USA). Inhibition constants (Ki) of newly synthesized compounds were determined using the Cheng−Prusoff equation and the Kd value for [^{3}H]epibatidine are expressed as μM values ± SD. The results are shown in *Table 4*.

3.4.3.3. Receptor expression in Xenopus oocytes

For α4β2 nAChRs, cRNA transcripts concentration were determined from absorbance at 260 nm. cRNas subunits were mixed at ratios of 8α:1β or 1α:8β to express nAChRs with subunit stoichiometries of 3α:2β or 2α:3β, respectively. For α3β4 nAChR, RNA was mixed at ratios of 1α:1β. Oocytes were injected with a volume containing 5-20 ng of cRNA mixture. Oocytes-positive female *X.laevis* were purchased from NASCO (Fort Atkinson, WI), and ovarian lobules were harvested surgically following animal use protocols approved by the University of Texas at Tyler Institutional Animals Care and Use Committee. The lobules were treated with 3 mg/mL collagenase type 2 (Worthington Biomedical) with gentle shaking for 3 h at room temperature in Ca^{2+}-free OR2 buffer (85 mM NaCl, 2.5 mM KCl, 1 mM $MgCl_2$, 5 mM HEPES, pH 7.6). Stage V and VI oocytes were selected, injected with cRNA, and incubated at 18 °C in ND96-gentamicin buffer (96 mM NaCl, 2 mM KCl, 1.8 mM $CaCl_2$, 1 mM $MgCl_2$, 5 mM HEPES, 50 µg/mL gentamicin, pH 7.6) for 24 –72 h to allow receptor expression.

3.4.3.4. Electrophysiological recording

A standard two-electrode voltage-clamp technique was used to acquire whole-cell current from *Xenopus* oocytes expressing WT nAChR in response to drugs application as described in Wang *et al.*[101] *Xenopus* oocytes were voltage-clamped at -50 mV using Oocyte Clamp OC-725C (Warner Instruments, Holliston, MA, USA) in a custom-made small recording chamber and under continuous perfusion with recording buffer (ND96; 100 mM NaCl, 2 mM KCl, 1 mM $CaCl_2$, 0.8 mM MgCl2, 1 mM EGTA, 10 mM HEPES, pH 7.5). An automated perfusion system made up of glass reservoirs and Teflon tubing (Warner Instruments, Holliston, MA, USA) was used to control recording chamber perfusion and drug application. Each recording run included 3-5 drug applications (5 s each) separated by 120 s wash intervals unless otherwise specified in the figure legends, and oocytes were washed for 3 min between runs. Each drug concentration was tested in at least three oocytes. Current traces were digitized at 50 Hz and peak current amplitudes in response to drug applications were quantified using Digidata 1550A interface/ pCLAMP 10.7 software (Molecular Devices, San Jose, CA, USA). ACh and LY2087101were prepared as 10mM stock solution in DMSO. Stock solutions were stored at -20 °C and diluted to final concentrations in recording buffer on the day of experiments. At the highest concentration tested, DMSO was present at 0.1%, which had no effect on ACh

responses. Dose-response relationships were constructed by sequentially applying different concentrations of drugs and normalized to the value obtained by applying 10µM ACh on the same oocyte unless otherwise specified in the figure legends. For quantitative estimations of agonist actions, dose−response relationships were fitted by the 4-parameter Hill equation

$$I_x = I_0 + (x^h)*(I_{max}-I_0)/(x^h + EC_{50}{}^h)$$

where I_x is the normalized ACh current in the presence of the drug at concentration x, I_0 is the bottom plateaus, I_{max} is the maximum potentiation of current, h is the Hill coefficient, and EC_{50} is the drug concentration producing 50% of maximal potentiation.

3.4.4. Results and discussion

The binding studies indicate that compounds do not bind or bind very little the α3β4 nAChRs with Ki values in µM scale, making them selective for α4β2 receptor subtype. We can observe analogies between 2-(*N*-methyl-2-pyrrolidinyl)benzofurane (**5**) and 2-(*N*-methyl-2-pyrrolidinyl)-1,4-benzodioxane ((*S,R*)-**III**): the hydroxylation at C(6) and C(7), to give, respectively, **1** and (*S*,*R*)-**IV**, increases not only the α4β2 affinity but also the α4β2 selectivity. The higher selectivity ratios of the benzofuranes **5** and **6**, compared to benzodioxane (*S,R*)-**III**, and of benzofurane **1**, compared to the benzodioxane (*S*,*R*)-**IV**, could be due also to the fact that the α3β4 affinities of **1**, **5**, and **6** were determined at the rat receptor subtype, which is, as previously underlined, more discriminating than the human receptor subtype used to determine the α3β4 affinities of (*S,R*)-**III** and (*S*,*R*)-**IV**. (*Table 4*, *Figure 30*). The most promising compounds previously synthesized were reported for the comparison.

Compound	Structure	α4β2 Ki (μM)	α3β4 Ki (μM)	α4β/α3β4 selectivity
1	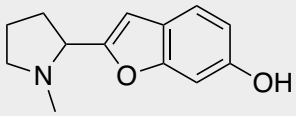	0.172 (0.025)	45.31 (13.26)	260
2	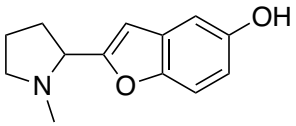	>100	>100	
3	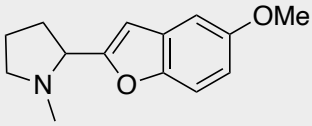	181	>100	
4	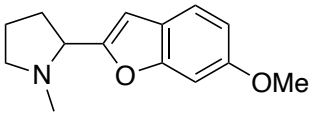	>100	27.10 (11.18)	
5	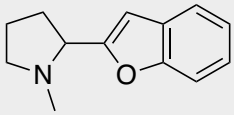	0.718 (0.98)	19.43 (2.7)	27
6	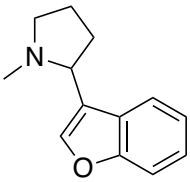	0.828 (0.32)	81.55 (69.48)	98
(S,R)-**III**	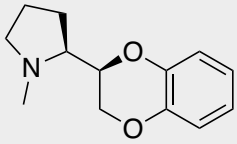	0.26 (0.08)	1.2 (0.34)	4.6
(S,R)-**IV**	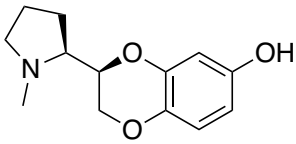	0.012 (0.002)	0.31 (0.1)	26

Table 4. The Ki values were derived from [^{3}H]epi competition binding experiments using HEK α4β2 and HEK α3β4 membranes. Data from competition binding curves were evaluated by one-site competitive binding curve-fitting procedures using GraphPad Prism version 9. Each compound was tested in triplicated for each subtype and the inhibition constant Ki was estimated using Kd of the radioligand according to Cheng-Prusoff equation. The numbers in brackets represent the standard error.

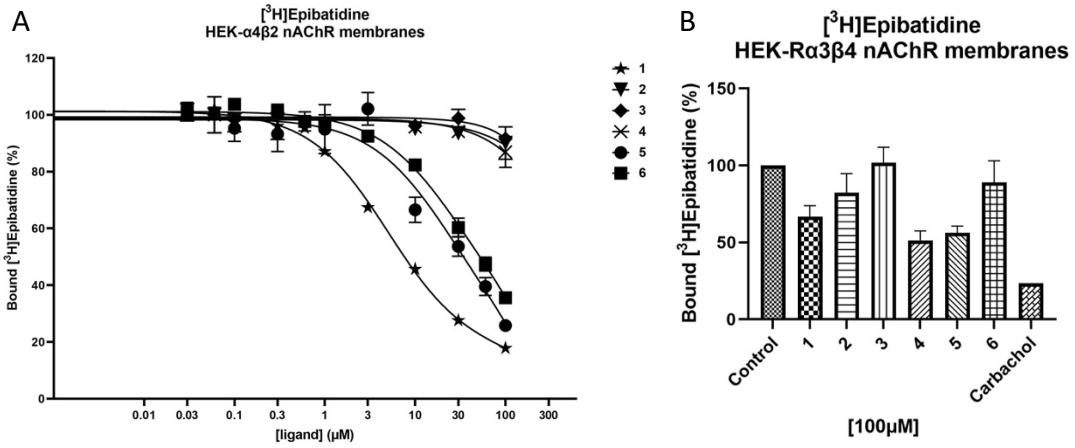

Figure 30. (A) Inhibition of [^{3}H]epibatidine binding to the α4β2 nAChR subtype by increasing compound concentration. Competition binding curves were evaluated by one-site competitive binding curve-fitting procedures using GraphPad Prism version 9 and Ki was using Kd of the radioligand according to Cheng-Prusoff equation; (B) Inhibition of [^{3}H]epibatidine binding to the α3β4 nAChR subtype at 100μM concentration of compound.

The activity at the two α4β2 isoforms, the HS and the LS, were determined for the compounds displaying the highest α4β2 affinities, namely the 6-hydroxylated pyrrolidinyl benzofurane **1** and the 7-hydroxylated pyrrolidinyl benzodioxane (*S*,*R*)-**IV**. In addition to the α4β2 partial agonist (*S*,*R*)-**IV**, we thought to test two other benzodioxane based α4β2 partial agonists, namely the 7- and 5-amino analogues of (*S*,*R*)-**III** (compounds (*S*,*R*)-**VII** and (*S*,*S*)-**IX**). These three benzodioxane derivatives have three different activity profiles. They are all α4β2 partial agonists, but (*S*,*R*)-**IV** with a moderate α4β2/α3β4 functional selectivity, (*S*,*R*)-**VII** with no α4β2/α3β4 functional selectivity and (*S*,*S*)-**IX** with no α3β4 functional activity. The functional effect was assessed using two-electrode voltage-clamp technique and measuring the whole cell current elicited in *Xenopus* oocytes expressing wild-type human LS or HS nAChRs in response to application of these ligands alone or in combination with other nAChR ligands as described by Wang *et al.*[101] and by Deba *et al.*[85] To circumvent the low current amplitudes observed with these ligands at HS and/or LS receptors, 1 μM of the positive allosteric modulator LY2087101 was coapplied. LY2087101, as underlined previously, is expected to enhance maximal responses with little effect on potencies at both stoichiometries based on its effect on the current elicited by ACh under similar experimental conditions (*Figure 31*).[85]

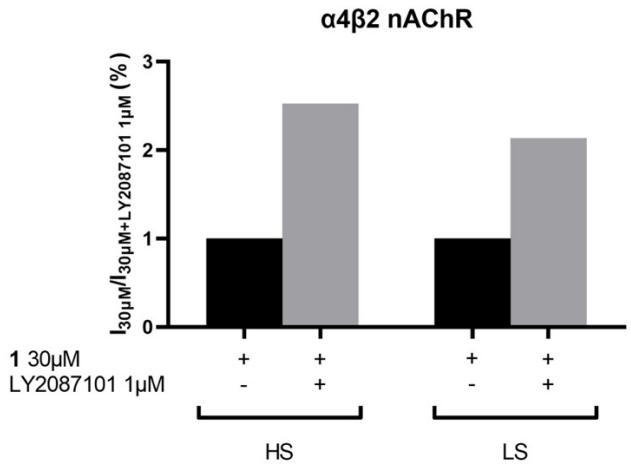

*Figure 31. Potency enhancement of **1** in the presence of PAM LY2087101 (HS left, LS right).*

From the functional tests, it is possible to notice that compound **1** has similar potency at both isoforms with EC_{50} of 2.34 ± 0.07 μM at HS and 3.0 ± 0.46 μM at LS isoform (*Figure 32A*). However, the efficacy of this compound is different at two isoforms. The I_{max} at the high sensitivity isoform is 24 ± 4.3 % while it is only 3.4 ± 1.5 % at the low sensitivity α4β2 nAChR (*Figure 32B,C*). It was also tested for its activity at the α3β4 nAChR. At the saturation dose of 100 μM, it does not elicit any current at the receptor (*Figure 32D*).

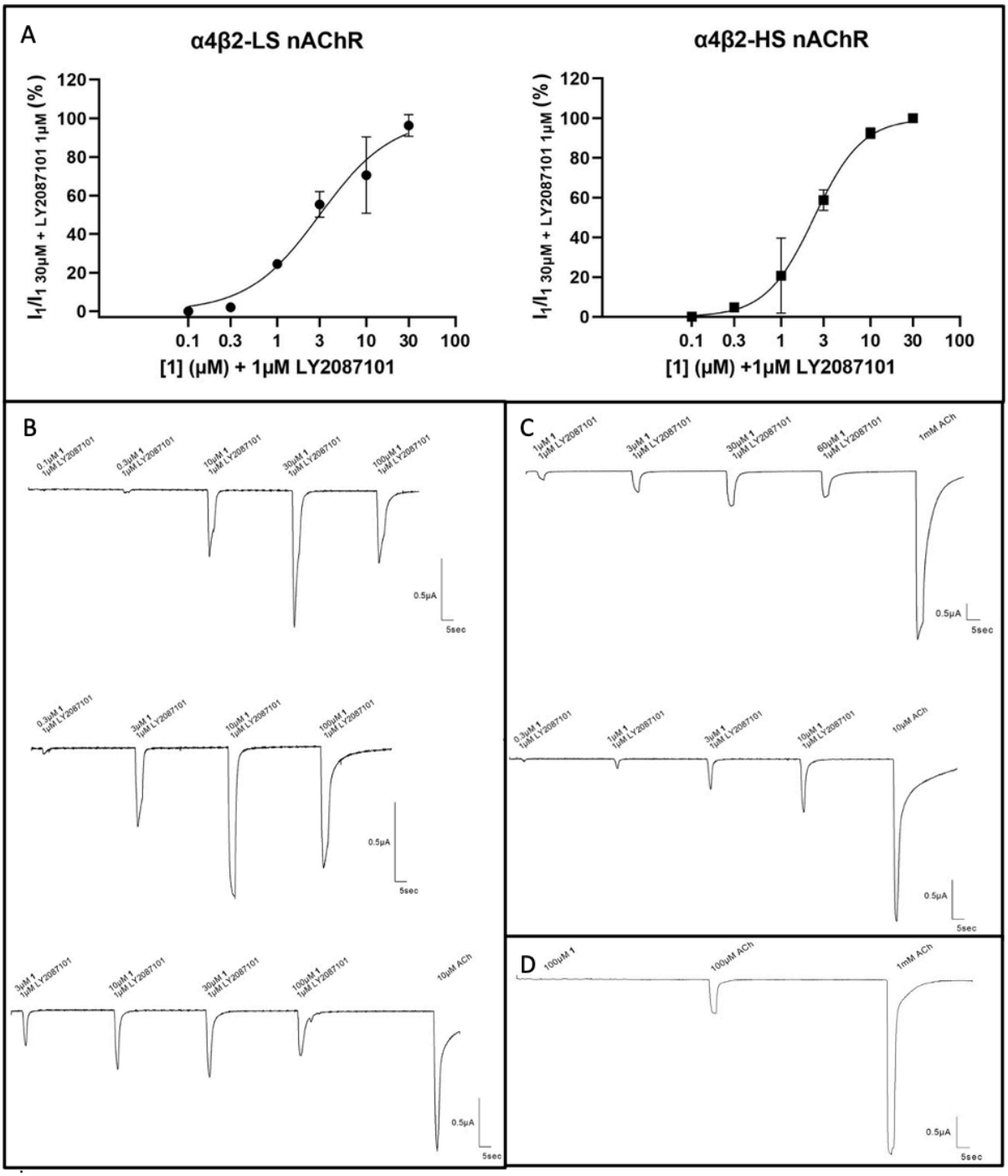

*Figure 32. (A) Current elicited by Xenopus oocytes expressing WT $(\alpha4)_2(\beta2)_3$ and $(\alpha4)_3(\beta2)_2$ nAChRs in response to 5 s applications of increasing concentrations of **1** with 1 μM LY2087101 were recorded and normalized to peak currents elicited by 30 μM **1** co-applied with LY2087101; (B, C) Representative two-electrode clamp traces showing the effects of different concentration of **1** with 1 μM LY2087101 and ACh in HS (B) and LS (C) α4β2 nAChRs; (D) Representative two-electrode clamp traces showing the effects of different concentration of ACh in α3β4 nAChRs.*

On the other hand, the three benzodioxane-based compounds (*S*,*R*)-**IV**, (*S*,*R*)-**VII** and (*S*,*S*)-**IX** exhibit three different potency profiles (*Figure 33A-C*).

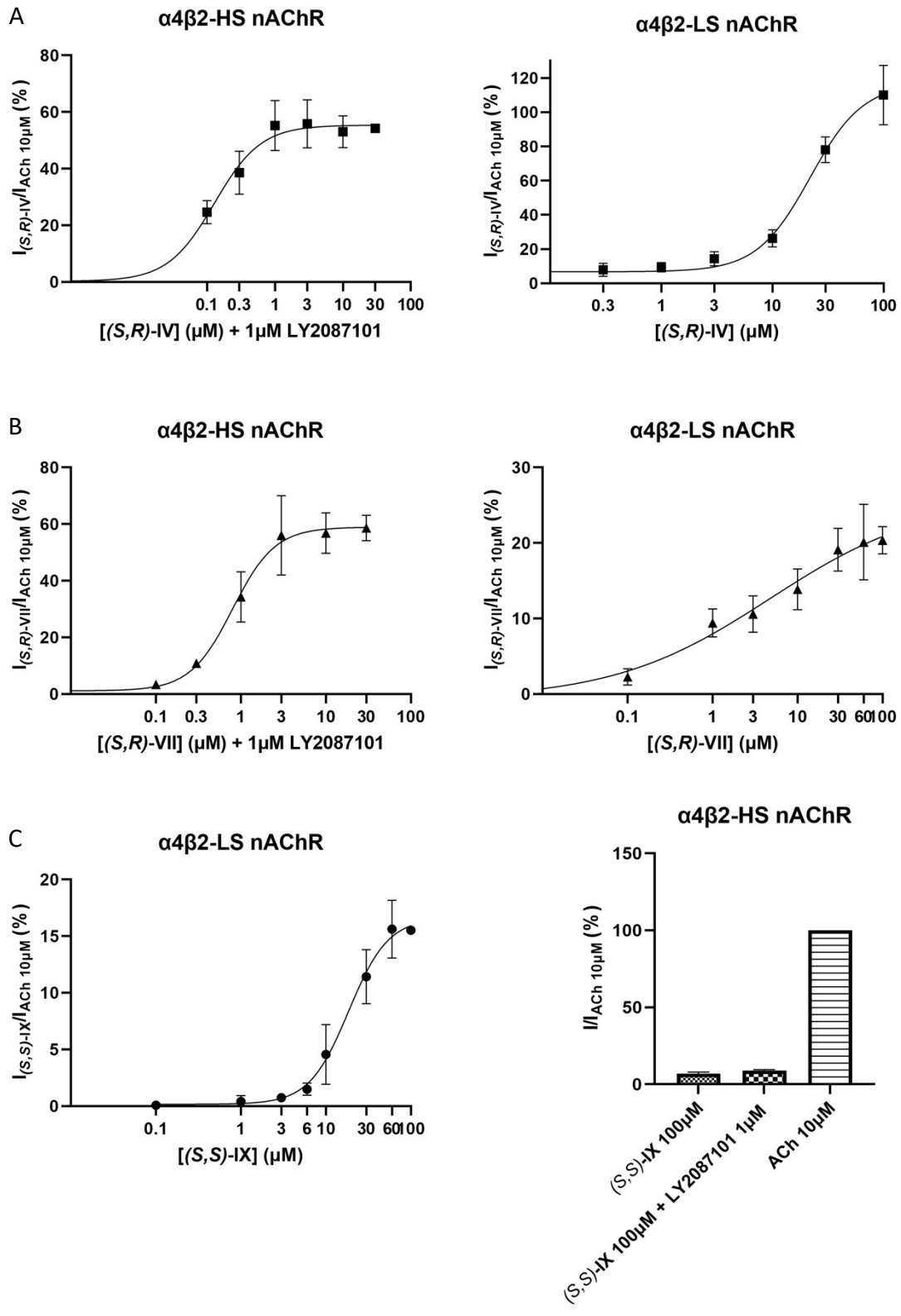

*Figure 33. Current elicited by Xenopus oocytes expressing WT $(\alpha4)_2(\beta2)_3$ and $(\alpha4)_3(\beta2)_2$ nAChRs in response to 5 s applications of increasing concentrations of compounds (S,R)-**IV** (A), (S,R)-**VII** (B) and (S,S)-**IX** (C) with 1 μM LY2087101 were recorded and normalized to peak currents elicited by 10 μM ACh.*

The 2-pyrrolidinyl-7-hydroxybenzodioxane (*S*,*R*)-**IV** is 170 times more potent at the HS isoform, the 2-pyrrolidinyl-7-aminobenzodioxane (*S*,*R*)-**VII** shows modestly different potencies, while the 2- pyrrolidinyl-5-aminobenzodioxane (*S*,*S*)-**IX** has no activity at the HS isoform. All the four compounds are partial agonists with markedly higher efficacy at the HS isoform, except for (*S*,*S*)-**IX**, which has null efficacy at the HS isoform (*Table 5*).

Compound	$(\alpha4)_2(\beta2)_3$		$(\alpha4)_3(\beta2)_2$	
	EC_{50} (μM)	I_{max} %	EC_{50} (μM)	I_{max} %
1	2.34 (0.07)	24 (4.3)	3.0 (0.46)	3.4 (1.5)
(*S*,*R*)-**IV**	0.129 (0.22)	30 (3.7)	21.8 (3.29)	12.1 (1.9)
(*S*,*R*)-**VII**	0.799 (0.07)	38 (2.9)	4.8 (4.6)	2.3 (0.2)
(*S*,*S*)-**IX**	no current		18.5 (1.92)	3.4 (1.5

*Table 5. Potency and efficacy of compounds **1**, (S,R)-**IV**, (S,R)-**VII** and (S,S)-**IX** at the two wild type human α4β2 nAChR isoforms expressed in Xenopus oocytes. Current responses by Xenopus oocytes expressing WT $(\alpha4)_2(\beta2)_3$ and $(\alpha4)_3(\beta2)_2$ nAChRs to 5 s applications of increasing concentrations compounds alone or with 1 μM LY2087101 were recorded and normalized to peak current amplitude elicited by 10 μM ACh alone. Efficacies are expressed as percentage ratio between the maximal effect of the compound, in the absence of LY2087101, and the maximal effect of ACh at the $(\alpha4)_2(\beta2)_3$ (10 μM) or $(\alpha4)_3(\beta2)_2$ (1 mM) isoform.*

The activation profile of (*S*,*R*)-**IV** resembles that of sazetidine-A, which selectively activates the HS over the LS receptor, while the behaviour of compound (*S*,*S*)-**IX** is analogous to that of cytisine. Such results indicate that substituents at benzodioxane C(7) and C(5), which are determinant for the α4β2/α3β4 selectivity, as we have previously rationalized, are involved also in the stoichiometry selectivity. This is intriguing and not surprising. In fact, the substituents at the benzodioxane aromatic ring interact mostly with the complementary β2(-), and β4(-) faces controlling the α4β2/α3β4 selectivity and it is reasonable that these substituents also interact with the α4(-) face of the third "low" affinity ACh site identified at the α4/α4 interface, unique in the LS receptor, thus being critical also for the HS/LS selectivity.[19,84,104]

Taken together, these results show how the benzofuran scaffold can take the place of the benzodioxane scaffold and how, for both, the position of the oxygens of the heterocycle and the decoration of the aromatic ring are discriminant. Furthermore, the investigation of the

two isoforms highlights how these characteristics are involved in a discriminating way in the interaction with the two α4β2 isoforms in the case of the benzodioxane scaffold.

3.5. Zebrafish in vivo studies of α4β2 nAChRs agonists

3.5.1. Introduction and aim

As discussed above, prolinol aryl ethers and pyrrolidinyl benzodioxanes have a high affinity for mammalian α4β2 nAChRs.[95,96,99,105] Their electrophysiological profiles were studied in the past years but not their *in vivo* effects. We tested them for their effects on zebrafish behaviour. We hypothesised that α4β2 receptor full agonists *(S)*-**V** and *(S)*-**VI** may reinforce learning and memory. We tested *(S)*-**V** and *(S)*-**VI** and the antagonist *(S,R)*-**III** using the T-maze and a virtual object recognition tests which respectively evaluate spatial memory and attention. We also tested the *(S,R)*-**IV** partial agonist, using conditioned place preference, in order to investigate its ability to block the rewarding effects of nicotine and therefore its potential use in smoking addiction.[106]

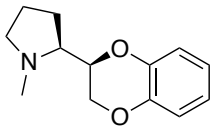

(*S*,*R*)-**III**

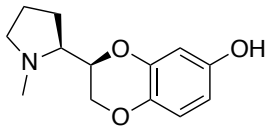

(*S*,*R*)-**IV**

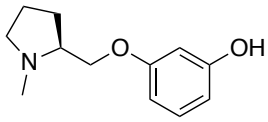

(*S*)-**V**

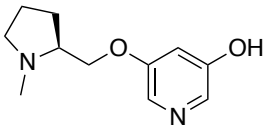

(*S*)-**VI**

3.5.2. Biology

3.5.2.1. Animals and housing

Five hundred and seventy adult male and female (approximately 50%–50%) wild-type (short fin) zebrafish (*Danio rerio*) were obtained from the Department of Life and Environmental Science of the Università Politecnica delle Marche (Ancona, Italy). The zebrafish were 6–12 months old, 3–4 cm long, that is typical of young age[107], and were housed in mixed age groups of 30 in 96 L tanks under standard conditions (28 ± 2 °C, 14–10 h day/night cycle, with lights on at 7:00 a.m.) for at least 2 weeks before the experiments. The tank water contained sea salts (Instant Ocean, Aquarium System, Sarrebourg, France) at a concentration of 0.6 g/10 L, dissolved in water obtained by means of a reverse osmosis filter system. Water quality was kept at opti- mal levels and checked for pH (6.5–7.5) every day and for nitrates (< 0.02 ppm)

every 3 days. The fish were fed twice a day (2 h before each test in the morning and late in the eve- ning) with commercial flakes (tropical fish food, Consorzio G5, Italy) supplemented with live brine shrimp. All of the fish were drug naive. All of the experiments followed the ARRIVE guidelines and were approved by the National Ethics Committee for the care and use of laboratory animals and the National Ministry of Health (Italian Government Decree N° 513/2018PR). In addition, the number of animals used and their suffering was minimised in all experiments.

3.5.2.2. Behavioural testing

Behavioural testing took place between 09:00 and 14:00 h during the light phase. Animals from different tanks were chosen using a simple randomisation method based on a spe- cific statistical random table. For each test, the tank was positioned in front of a webcam in order to ensure optimal video recording for later video-aided analysis. Each video was evaluated by three trained observers blinded to treatment. To reduce handling stress during the T-maze and VORT tasks, groups of 16 fish first underwent two habituation trials of 1 h each every day for 3 days during which they were allowed to freely explore the entire apparatus. To minimise acute social isolation stress, the number of fish was gradually reduced: starting with 16 on day 1, to eight fish on day 2 and four fish on day 3 with individual fish testing starting on day 4[108]. After each habituation trial, the fish were returned to their home tank until the next habituation. Each fish was used only for one test. Ten fish per group were used for each drug concentration based on Braida *et al.*[109,110] and Ponzoni *et al.* [111], and each fish received a single dose of only one compound.

3.5.2.3. Treatment

Zebrafish body weight was measured according to Braida *et al.* Each fish was removed from its tank using a net and placed in a container of tank water positioned on a digital balance, and its weight was determined as the weight of the container plus the fish minus the weight of the container before the fish was added. The mean of three measurements was recorded. After weighing, each fish was put into an an-aesthetic solution of tricaine methanesulfonate (Sigma- Aldrich, St. Louis, MO, USA) (150 mg/L) and, upon loss of response to touch, was placed in a supine position. The drugs were injected into the abdominal cavity using a

Hamilton syringe (Hamilton Bonaduz AG, Bonaduz, Switzerland) at a volume of 2 µL/g. No more than the tip of the needle was inserted into the abdomen of each fish in order to prevent damage to its internal organs. After injection, each fish was immediately transferred back to its tank water for recovery.

3.5.3. *In vivo* assays

3.5.3.1. T-maze test

Zebrafish possess associative learning, and they prefer to swim in vegetation enriched areas where they feel safe from predators. In this experiment, we used a transparent Plexiglas T-maze filled with 10 cm of tank water. The maze is formed by a start zone (30 x 10 cm) which is separated from the rest of the structure with a removable door. Behind the door, there is a long arm (50 x 10 cm) with two short arms (20 x 10 cm) at the end (chambers). One of the short arms contains only water, while the other one is filled with plants, shells, stones, and marbles. Each fish was subjected to two training trials of exposure in the mazed with a 24-hour interval. At the beginning of each test, the fish was placed in the start zone with the door closed for 5 min, after which the door was opened allowing the fish to enter the maze. Each subject had 10 minutes to reach one of the two chambers. The running time taken to reach the enriched chambers and stay in it for at least 20 seconds was recorded. After this time, each fish was returned to a home tank. Half of the fish were injected with saline solution during the first day and with the drug during the second. The other half received the drug on the first day and the saline on the second. The fish were then subjected to a second exposure trial after 24 hours, and the time taken to reach and stay for 20 sec in the enriched chamber was recorded. The difference between these measured times measures the memory of the spatial location of reward.

3.5.3.2. Virtual object recognition test

Virtual object recognition test (VORT) was carried out in a transparent Plexiglas tank filled with water. A central area was delimited by two removable opaque barriers which isolate the two stimuli areas. These areas consist of two identical white geometrical shapes on a black background located on the opposite walls. In this test, fish were placed for 5 minutes in the

central area, after which each fish was subjected to a familiarisation trial, called acquisition phase T1, followed by a shape recognition trial, called test phase T2, with a 5-minute interval between them. During T1, the fish was exposed for 10 minutes to two identical white geometrical shapes on a black background (square, circle, triangle, cross, etc.). After this time, the fish was placed in the home tank. At this point, one of the two shapes was replaced with a new one. After 5 minutes, the fish was placed again in the central area for the T2 phase. Shape recognition was scored with a stopwatch in terms of exploration time every time the fish directed its head toward the shape.

3.5.3.3. Conditioned place preference

For this test, we used a tank divided into two equal parts with three black polka dots in one halve and no dots in the other. Two halves were divided with a perforated wall in order to allow the fish movement. The fish was placed in the tank and the percentage of time spent on a given side during a 15-minute trial was calculated as a baseline preference. This was defined as the pre-conditioning phase. After 6 hours, the fish were injected i.p. with nicotine (0.01 mg/kg dose) or one of the doses of *(S,R)*-**IV** or vehicle (saline solution) and restricted in the least preferred side for 30 min, and after 24 hours, the fish was placed in the opposite side for 30 min. On the third day, there was a post-conditioning phase during which the fish was free to swim between in the tank for 15 minutes. The time spent on each side was recorded. Subtracting the time spent in the drug-paired compartment of the pre-conditioning phase from the post-conditioning phase reflected rewarding or aversive effects. To sum up, during the first restriction, the fish associates the rewarding effect of nicotine or the drug with the least preferred side. During the second restriction, the fish is in a kind of drug withdrawal, and it starts to associate the preferred side with a negative sensation.

3.5.4. Results and discussion

The effects of nicotine and full agonists (*S*)-**V** and (*S*)-**VI** on the memory of the spatial location are shown in *Figure 34*. (*S*)-**VI** (*Fig. 34a*) induces a significant cognitive enhancement at 10 ng/kg dose, while (*S*)-**V** (*Fig. 34b*) exercises its maximal effect at 1 µg/kg dose. Antagonist *(S,R)*-**III** alone has no effect, but when co-applied with nicotine and full agonists it drastically reduces memory improvement (*Fig. 34c*).

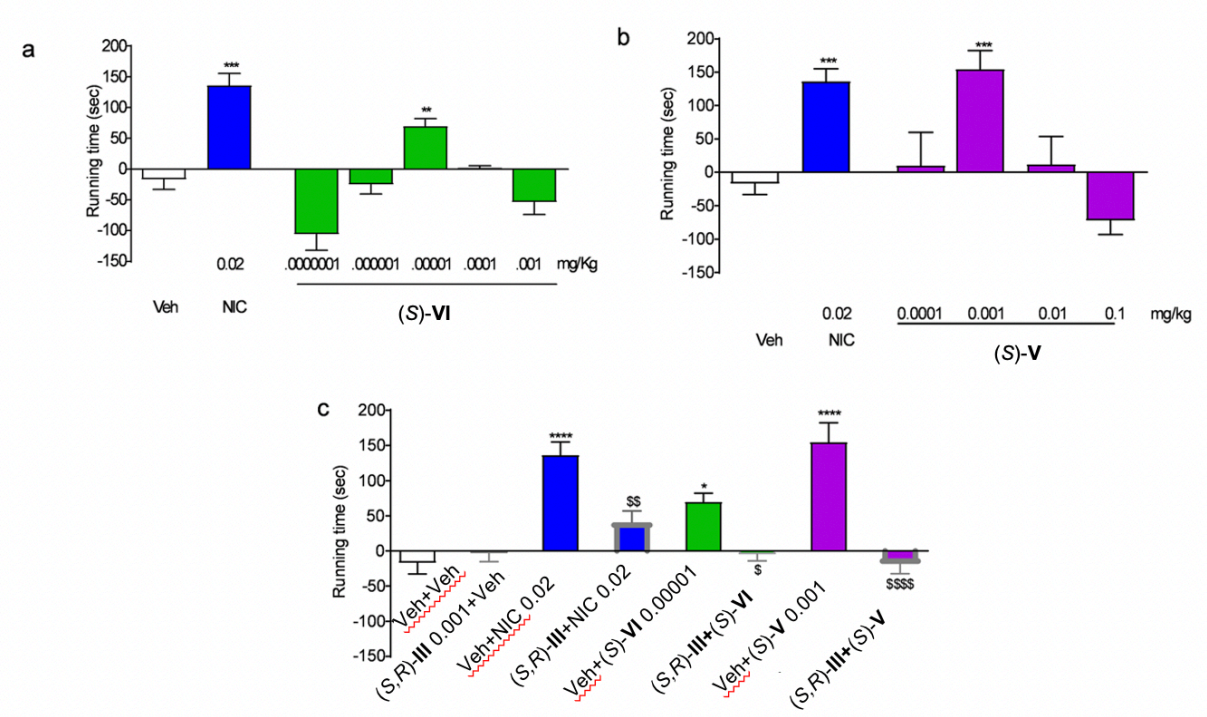

Figure 34. Cognitive improvement of zebrafish in terms of running time in a T-maze after treating with nicotine and different drugs. The antagonist was given in combination with agonists. All the drugs were injected i.p. 20 min before the test. Running time was calculated as the difference of pre-training running time at 0 h minus post-training running time evaluated at 24 h. Each value represents the mean ± SEM of 10 observations per group.

The effects of nicotine and full agonists in VORT are shown in *Figure 35*. (*S*)-**VI** at 10 ng/kg dose increases the attention in a way similar to nicotine, while higher doses progressively reduce the memory improvement *(Fig. 35a*). (*S*)-**V** has a similar behaviour but with the maximally effective dose of 0.1 mg/kg dose *(Fig. 35b*). Also, in this test, *(S,R)*-**III** applied alone has no effect, but it reduces drastically nicotine and full agonists memory improvement (*Fig. 35c*). Regarding the total exploration time, there is no difference between the T1 and T2 phases (*Fig. 35d-f*).

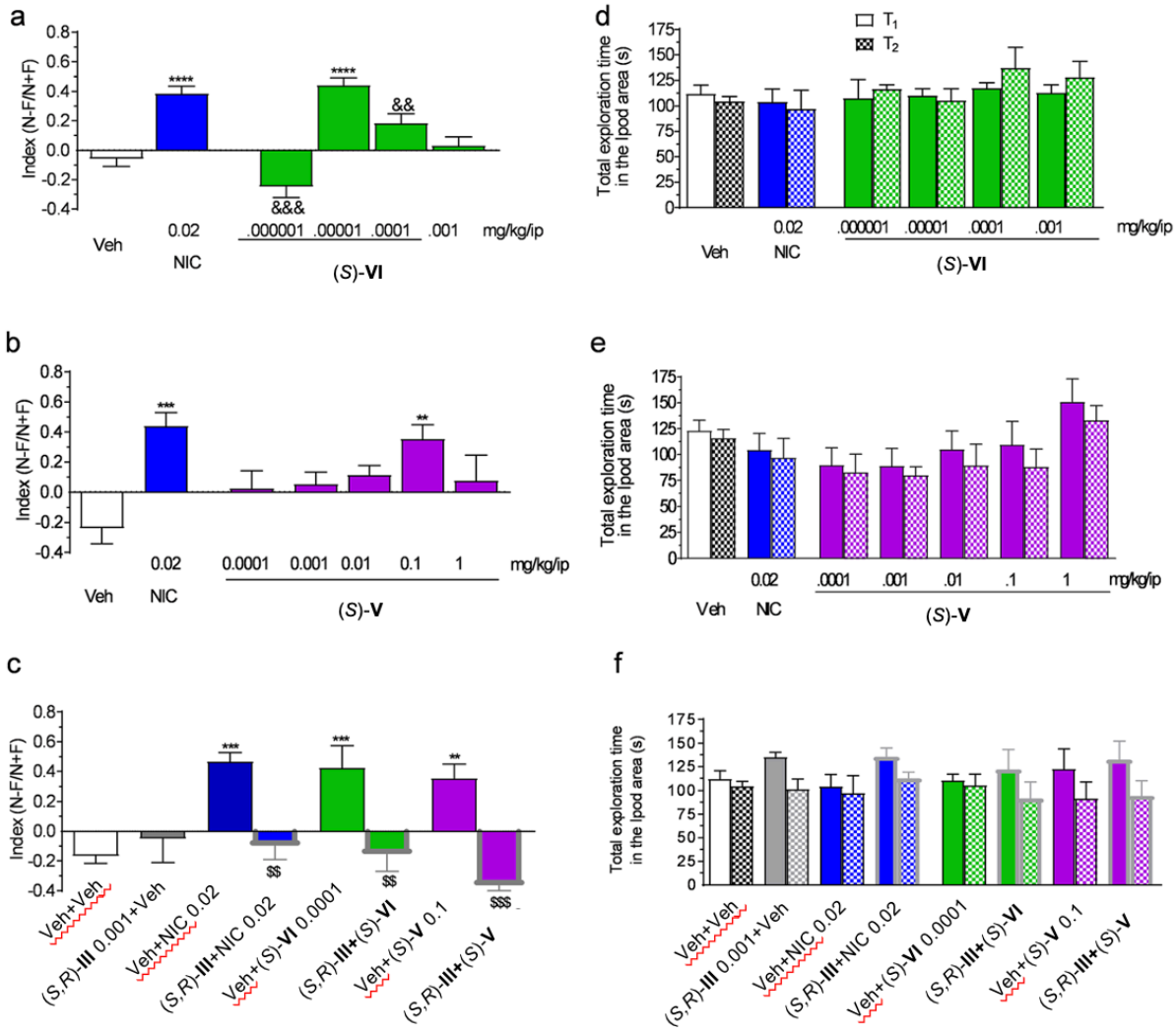

Figure 35. Effect on nicotine and different drugs on discrimination index (a-c) and exploration time (d-f) in VORT. The antagonist was given in combination with agonists. All the drugs were injected i.p. 20 min before T1. N – novel shape, F – familiar shape. Each value represents the mean ± SEM of 10 observations per group.

Nicotine and the partial agonist *(S,R)*-**IV** administration develops a conditioned place preference in zebrafish. The i.p. injection of *(S,R)*-**IV** at doses between 1 and 10 mg/kg increases the time spent in the drug-paired side during the post-conditioning phase, while lower and higher doses are ineffective. It has a similar effect to a 1 µg/kg dose of nicotine. The dose of 5 mg/kg resulted in the maximal effect. Combined treatment with nicotine and the partial agonist, given at the maximal used dose, significantly blocked the rewarding effect of nicotine (*Figure 36*).

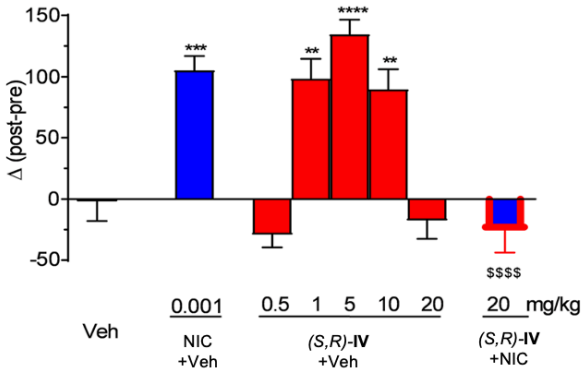

*Figure 36. Effect of (S,R)-**IV** on conditioned place preference compared to nicotine. All the drugs were injected i.p. 20 min before the conditioning session. Preference was calculated by subtracting the time (mean ± SEM) spent in the drug-paired compartment before drug-conditioning from the time spent after drug-conditioning. Each value represents the mean ± SEM of 10 observations per group.*

In conclusion, both full agonists (*S*)-**V** and (*S*)-**VI** improve attention and spatial memory in a dose-dependent manner in a way similar to nicotine. Although, the maximal effective doses of (*S*)-**V** and (*S*)-**VI** were 10.5 and 882 times lower than those of nicotine. From previous binding studies, we know that (*S*)-**VI** is a highly selective α4β2 full agonist and this can explain its low effective dose compared to (*S*)-**V**. Also, the administration of these drugs improved the attention, in terms of shape discrimination in VORT. Both (*S*)-**V** and (*S*)-**VI** are, one more time, more potent than nicotine. Moreover, their effects are completely blocked by *(S,R)*-**III**, a compound previously identified as an antagonist.

The partial agonist *(S,R)*-**IV** has the maximal reinforcing effect at the dose of 5 mg/kg with lower or higher doses less or non-effective. These results are comparable with the results obtained using other partial agonists such as cytisine or varenicline.[111] Furthermore, when *(S,R)*-**IV** is co-applied with nicotine, it prevents the maximal effect of nicotine on this response, antagonises the rewarding properties. This antagonistic activity may be explained by the intrinsic pharmacological properties of partial agonists, which may decrease the rewarding effects of nicotine by reducing the release of dopamine at the level of the mesolimbic circuit. All the data were published.[106]

3.6. Design, synthesis and pharmacological evaluation of NS9283 analogues

3.6.1. Introduction and aim

As abovementioned, NS9283 is an agonist of the unorthodox α4α4 binding site. Unfortunately, there is little information about its interactions with LS isoform and where is exactly located its binding site. Moreover only a few selective compounds for the unorthodox binding site, are described in the literature. In this context, the investigation of new hit compounds, targeting the α4α4 binding site, is of great interest and outcomes could be very useful to better understand the distribution and the drugability of the LS isoform.

3.6.2. Design of NS9283 analogues

As the first step, we decided to synthesize and investigate the activity of some NS9283 derivatives, reported by Jin *et al.* in 2014 as α4β2α5 as positive allosteric modulators (PAMs). In fact, we supposed that these compounds would bind the α4α4 binding site. NS9283 is made up of 3 different fragments: 3-pyridyl moiety, a central oxadiazole ring and a 3-CN substituted phenyl ring. In this work, they selectively modified one of the fragments to see the effects of one point change.[112] We decided to resynthesize the most promising and interesting modification from their paper (compounds **25, 28, 30-33, 35**). Furthermore, to complete our SAR investigation we design other compounds introducing other modifications to complete our SAR investigation (compounds **26, 27, 29, 34, 36-41**).

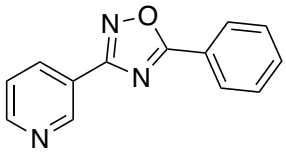

25

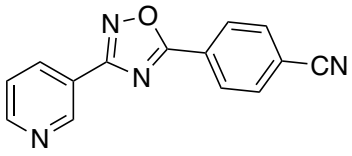

26

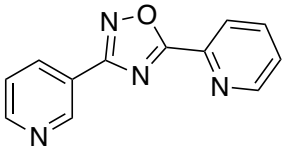

27

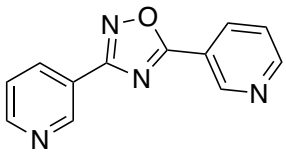

28

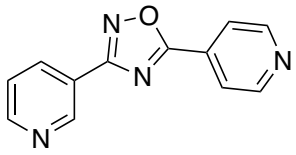

29

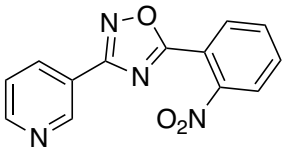

30

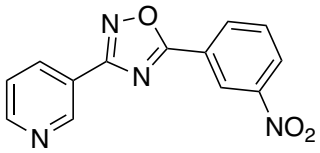

31

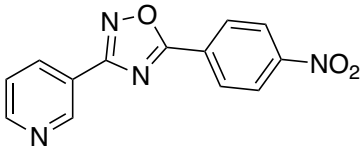

32

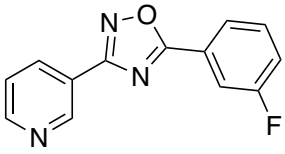

33

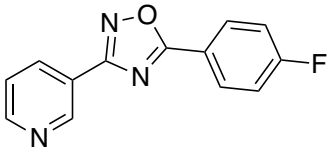

34

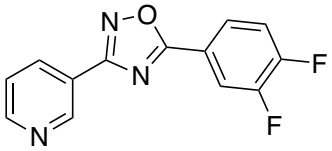

35

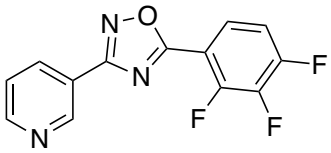

36

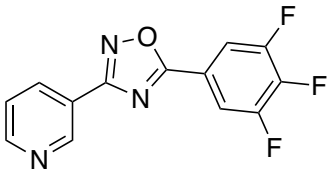

37

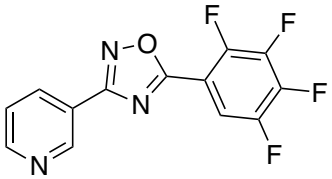

38

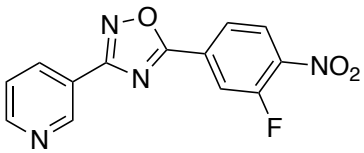

39

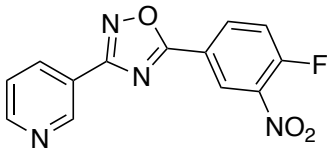

40

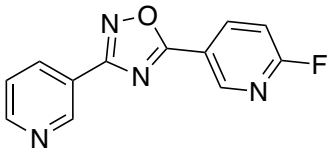

41

Afterwards, we decided to further expand our studies using virtual screening approach. We decided to use two different approaches: Fragment-based Drug Discovery (FBDD) using BROOD 3.1.2.2 software[113] and Shape Similarity Screening using Schrödinger software[114,115].

For the FBDD, we used the ChEMBL20 database which is a manually curated chemical database of bioactive molecules with drug-like proprieties. Using BROOD, we separately selected the three fragments of NS9283 and then the software substituted them with different fragments based on different values such as molecular weight, logP, polar surface area, rotatable bonds, heavy atoms, Lipinski donors and acceptors etc. After running BROOD screening the results were visualized using VIDA 4.4.0.4 software. All the potential hit compounds were divided into clusters by the software. The most interesting compounds were selected based on their shape and electronic characteristics and also synthetic complexity and availability (*Figure 37*).

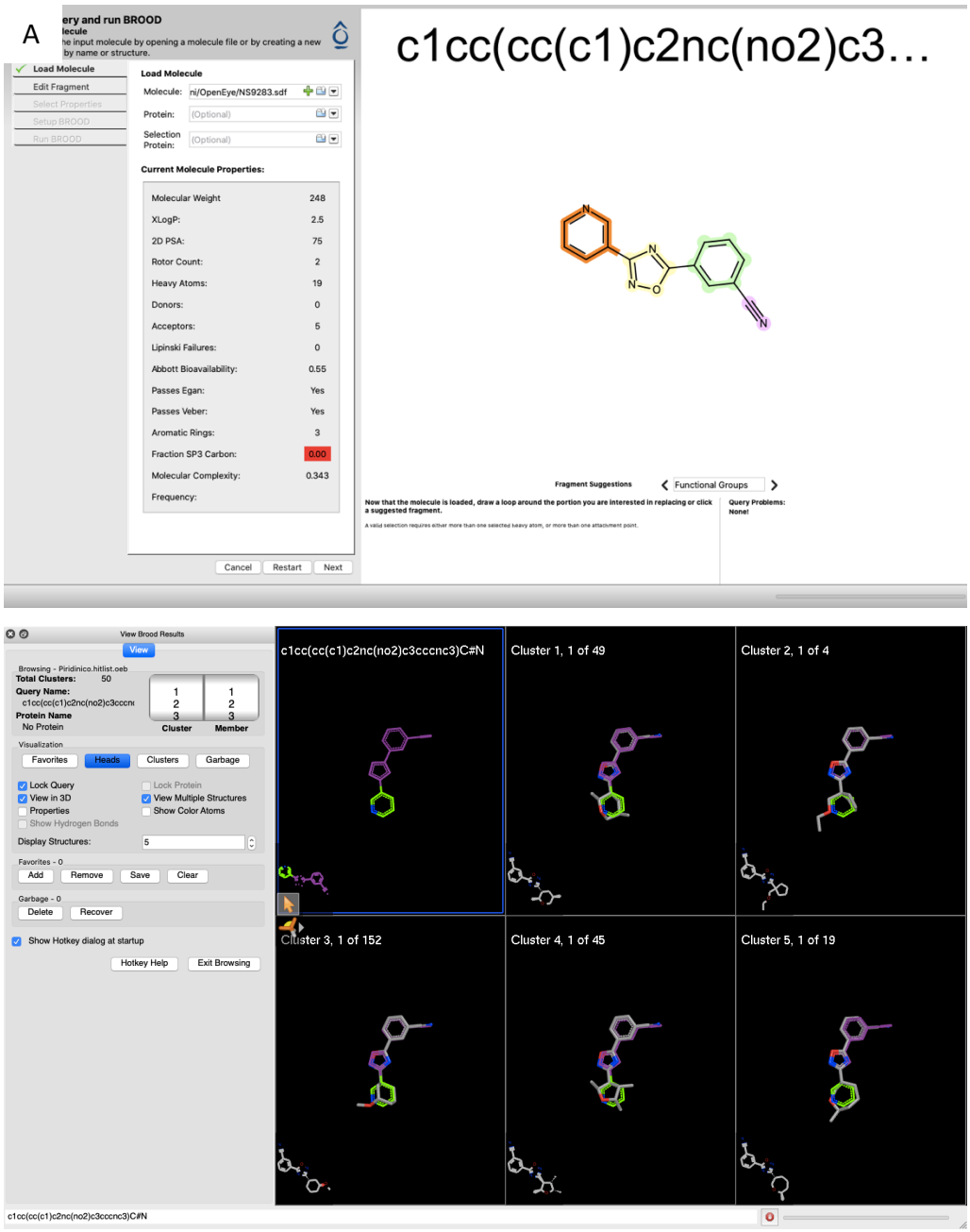

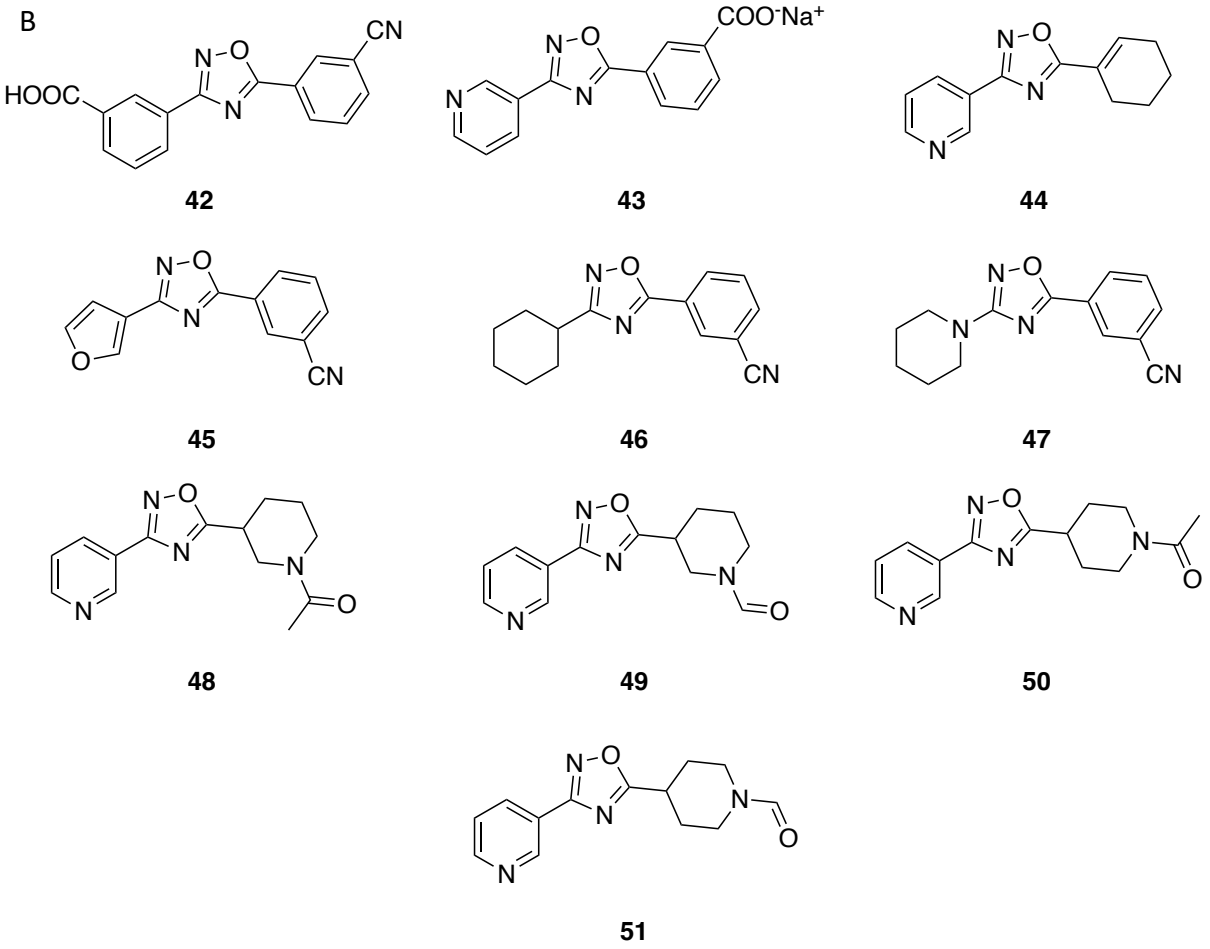

Figure 37. (A) Example of FBDD using BROOD® and VIDA® Software; (B) selected compounds for the synthesis.

For the second approach we screened 2 different databases of molecules extracted from Zinc using the Shape Similarity Screening (Maestro, Schrödinger[114]). These results were clustered the results using a Fingerprint Similarity Clustering (Canvas[115]) and then, handpicked the 24 compounds relying on chemical diversity and commercial availability. In details, for the Shape Screening, the pharmacophore type volume scoring was applied, and compound conformers were pre-generated and directly extracted online from the ZINC database previously prepared. ZINC database was developed by John Irwin from the Department of Pharmaceutical Chemistry at the University of California, San Francisco and it is free of charge database of commercially available chemical compounds prepared especially for the virtual screening. From this database, two smaller databases were prepared. Database 1 contains circa 24 million molecules and Database 2 with 6 million containing negatively charged and neutral molecules, respectively. This was done to avoid the loss of selectivity due to the positive charge against the other interfaces. The included molecules should have a MW

between 200 and 500 with a logP of 1-4.5. Furthermore, pan-assay interference compounds (PAINs) should be excluded and the selected compound should be in stock and/or custom synthesized (*Table 6*). The top 50,000 compounds of the shape screening results were retained. Of those, the top 44-45k compounds presented a very similar scaffold to the original hit compound. Therefore, the effort was focused on the last 5000 compounds from the screening results. A fingerprint similarity search was applied in Canvas using the MOLPRINT2D fingerprint, which is a radial-like fingerprint that encodes atom environments using predefined lists of atom types located at different topological distances. The atom type scheme takes into account ring sizes, aromaticity, hydrogen bond acceptors/donors, ionization potential, whether rings are terminal, and whether halogens are present. In all scenarios, bonds are distinguished by their bond orders. In cases where little information is known about the active ligands, MOLPRINT2D fingerprints have been found to produce the highest average retrieval rates of true actives when compared to other fingerprints.[116] Clustering following the "average" method was applied resulting in 349 and 43 number of clusters for Database 1 and 2 screening results, respectively. Reclustering was further applied in cases where the sub-clusters contained too many and/or too chemically similar compounds, using the "complete" method. 24 compounds were then handpicked from clusters and checked for purchase availability and were later sent for pharmacological evaluation (*Figure 38*).

	Database 1	**Database 2**
Number	24 mil (24281397)	6 mil (6396364)
Includes	Negative charge	Neutral
Why	Avoid loss of selectivity due to the + charge	
MW	200-500	200-500
Log P	1-4.5	1-4.5
Filter 1	No PAINS	No PAINS
Filter 2	Includes also the custom synthesis	In stock

Table 6. Database preparation for the virtual screening with all selected characteristics such as charges, molecular weight, logP, biological properties and availability.

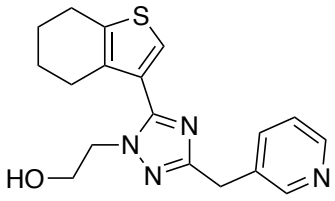

52

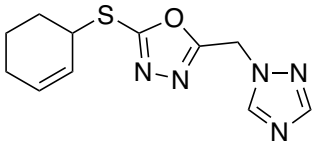

53

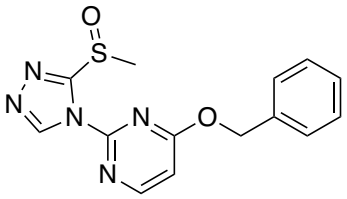

54

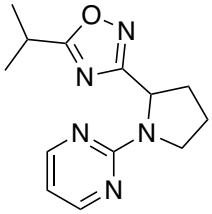

55

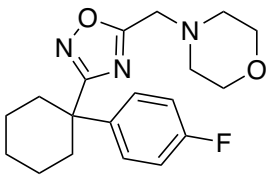

56

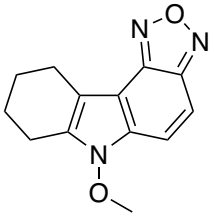

57

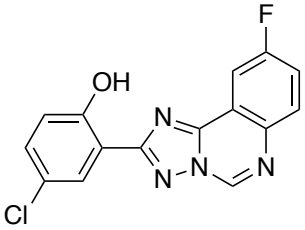

58

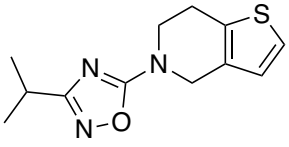

59

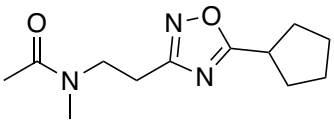

60

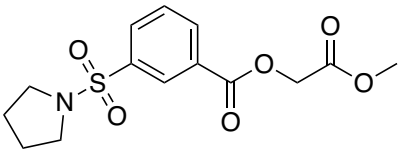

61

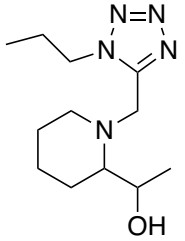

62

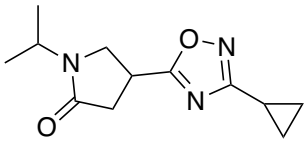

63

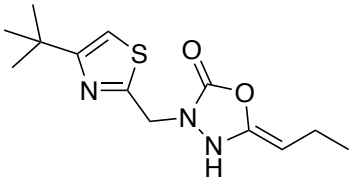

64

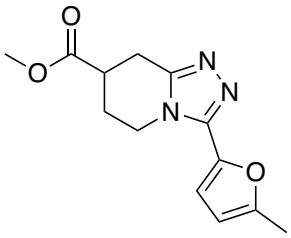

65

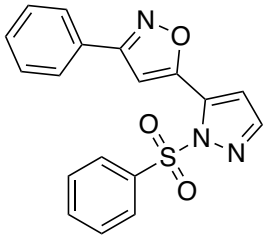

66

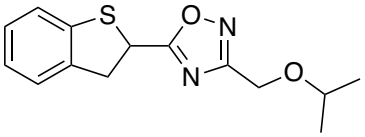

67

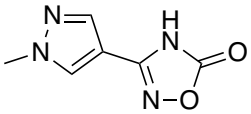

68

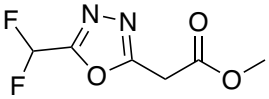

69

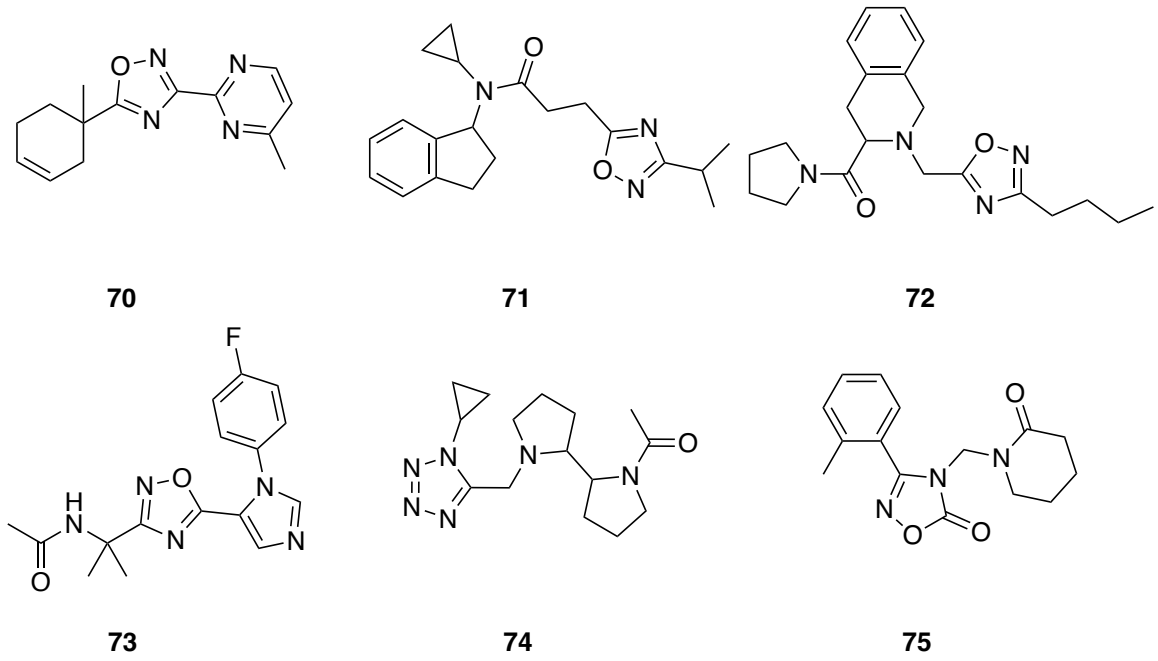

Figure 38. Selected compounds from Shape Similarity Screening with Schrodinger® Software.

3.6.3. Chemistry

For the synthesis of compounds **25-42, 44-51** the key reaction is the condensation between properly substituted amidoximes and acyl chloride (*Scheme 7*).

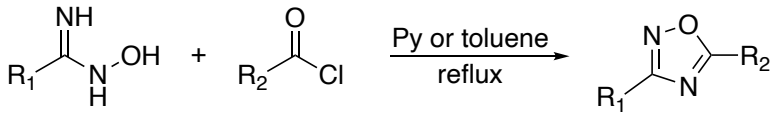

*Scheme 7. Synthetic scheme for the synthesis of compounds **25-42, 44-51**.*

The intermediates were synthesized by the treatment of properly substituted nitrile-derivatives with hydroxylamine hydrochloride in aqueous ethanol solution to give the desired amidoximes and by the treatment of different carboxylic acids with thionyl chloride obtained the intermediate acyl chlorides (*Scheme 8*).

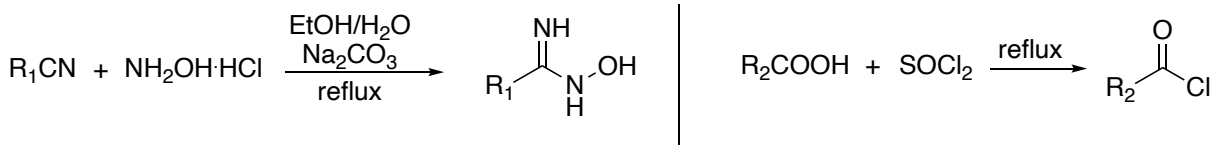

Scheme 8. Synthetic scheme for the synthesis of intermediate amidoximes and acyl chlorides.

For the synthesis of compounds **25-41, 44, 48-51**, the common intermediate **76** was synthesized as described above using commercially available 3-cyanopyridine which was

treated with hydroxylamine hydrochloride in an aqueous ethanol solution. The obtained amidoxime was coupled with previously obtained acyl chlorides (**77-98**) from differently substituted acids. For the synthesis of intermediates **99-102**, commercially available nipecotic and isonipecotic acids were first treated with acetic anhydride or acetic anhydride and formic acid to obtain acetyl or formyl derivatives respectively, which were subsequently treated with $SOCl_2$ (*Scheme 9*).

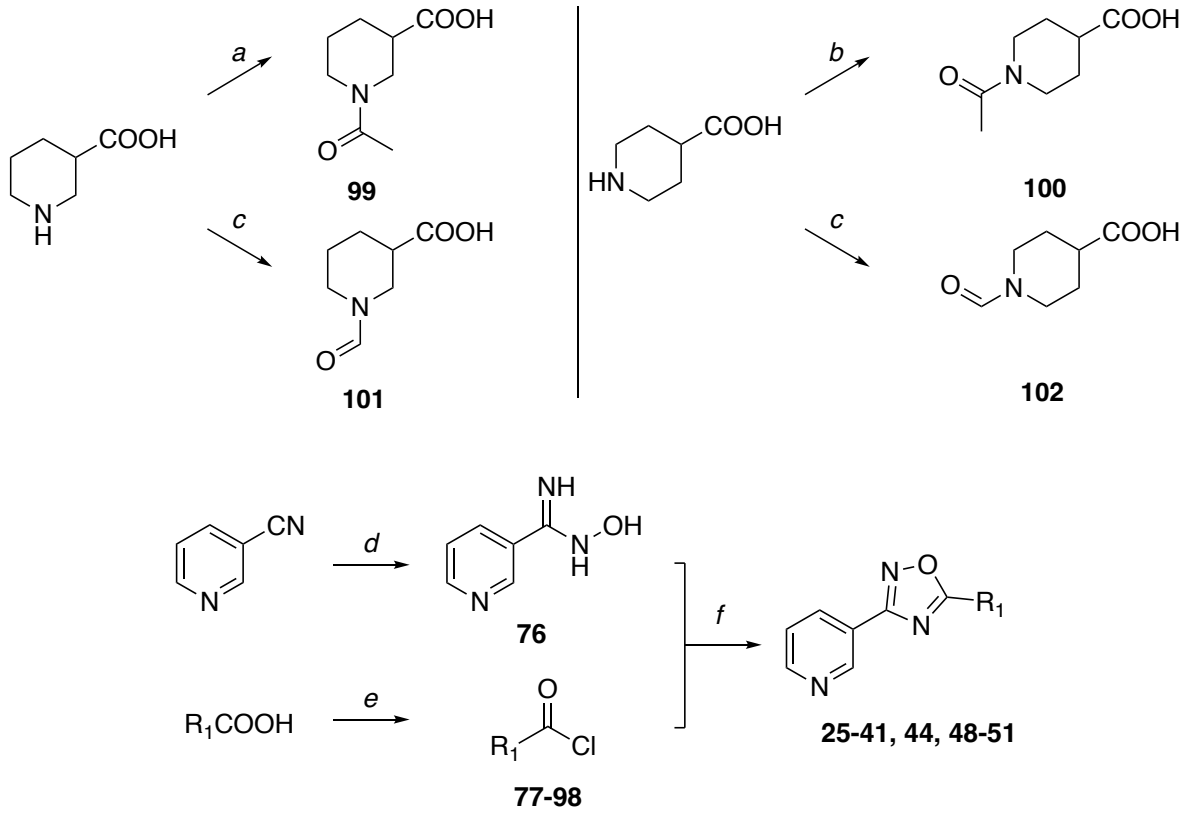

Compound	R_1	Yield %	Compound	R_1	Yield %
25	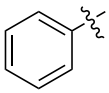	52%	**36**	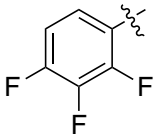	10%
26	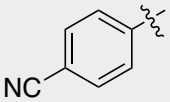	51%	**37**	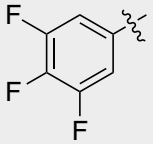	14%
27	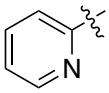	32%	**38**	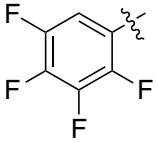	14%

28	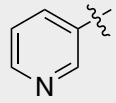	47%	**39**	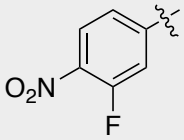	16%
29	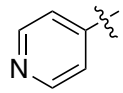	41%	**40**	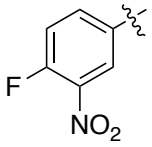	13%
30	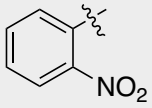	30%	**41**	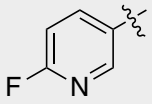	12%
31	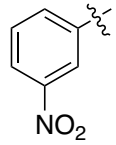	59%	**44**	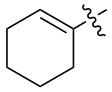	30%
32	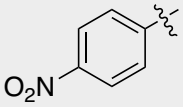	60%	**48**	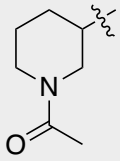	12%
33	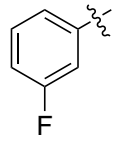	26%	**49**	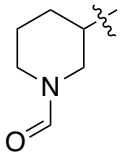	8%
34	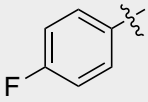	23%	**50**	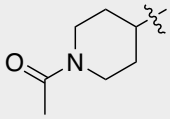	20%
35	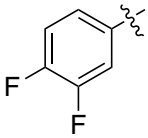	93%	**51**	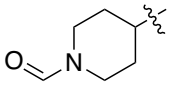	5%

*Scheme 9. Reagents and conditions. (a) DCM, acetic anhydride, rt,overnight, 80%; (b) DCM, acetic anhydride, rt, overnight, 98%; (c) formic acid, acetic anhydride, rt, 16h, 76% (**101**), 94% (**102**); (d) EtOH/H2O 1:1, $NH_2OH{\cdot}HCl$, $NaHCO_3$, reflux, 4h, 84%; (e) $SOCl_2$, reflux, 1-5h, quantitative; (f) Py or toluene, reflux, 3h-overnight.*

Compounds **42, 45-47** were synthesized in the similar way described previously. Differently substituted amidoximes derived from the reaction between commercially available cyano derivative and hydroxylamine hydrochloride in an aqueous ethanol solution (**103-106**). The obtained intermediates were coupled with 3-cyanobenzoyl chloride **107**, to give final compounds **42, 45-47** (*Scheme 10*).

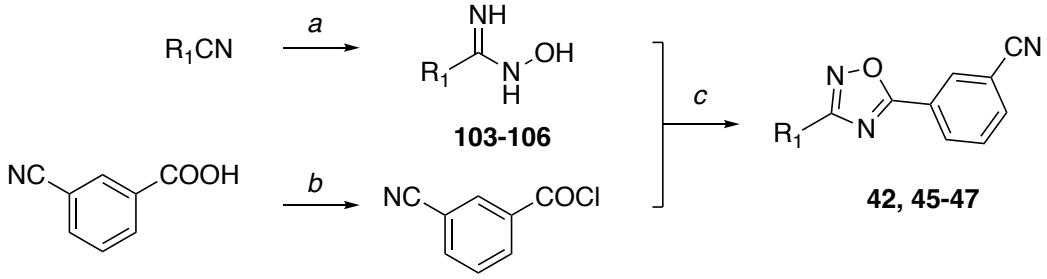

Compound	R_1	Yield %
42	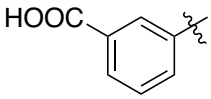	50%
45	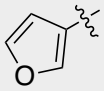	45%
46	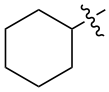	43%
47	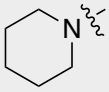	54%

*Scheme 10. Reagents and conditions. (a) EtOH/H_2O 1:1, NH_2OH·HCl, $NaHCO_3$, reflux, 4h, 53% (**103**),46% (**104**), 53% (**105**), 98% (**106**); (b) $SOCl_2$, reflux, 2h, quantitative; (f) Py or toluene, reflux, overnight.*

Compound **43** was synthesized using a different procedure. 3-cyanopyridine was treated with hydroxylamine hydrochloride in an aqueous ethanol solution to obtain the amidoxime **76** which was subsequently cycled to 3-(pyridine-3-yl)-1,2,4-oxadiazole **108** using trimethyl orthoformate and TFA. Concurrently, 3-iodobenzoic acid was methylated using H_2SO_4 in MeOH to give the intermediate compound **109**. Then, compounds **108** and **109** were coupled together using $Pd(OAc)_2$, PPh_3 and AgOAc in toluene to obtain methylated compound **110** which was, in the end, demethylated using NaOH 1M giving the final compound **43** (*Scheme 11*).

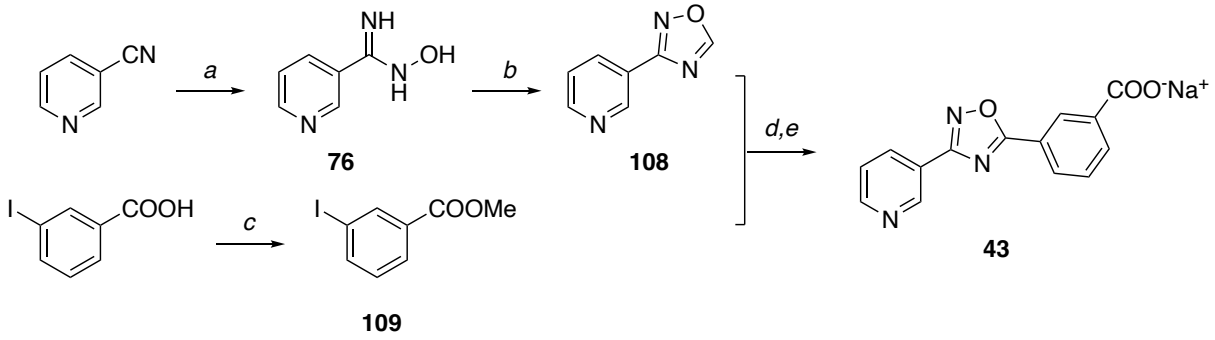

Scheme 11. Reagents and conditions. (a) EtOH/H2O 1:1, $NH_2OH{\cdot}HCl$, $NaHCO_3$, reflux, 4h, 84%; (b) $HC(OMe)_3$, TFA, 60°C, 30min, 63%; (c) MeOH, H_2SO_4, reflux, 3h, 93%; (d) toluene, $Pd(OAc)_2$, PPh_3, AgOAc, reflux, overnight, 54%; (e) MeOH, NaOH 1M, rt, 2h, 78%.

Moreover, [^{3}H]NS9283 was prepared in order to study the binding affinities of selected potential unorthodox-site selective agonists. The tritiation of NS9283 was performed in collaboration with Dr. Aleš Marek from Institute of Organic Chemistry and Biochemistry of the CAS, Prague, Czech Republic. Before the tritiation, a deutartion of the same compound was performed in order to investigate the optimal reaction conditions; in fact, the use of tritium was avoided because of its toxic radioactivity.

The [^{2}H]NS9283 was synthesized by deuteration of brominated analogue in *meta*-position of pyridine ring of NS9283 using different conditions: catalyst, solvents, time, etc. (*Table 7*). The brominated intermediated was synthesized using the same procedure described for other analogues using commercially available 3-bromo-5-cyanopyridine and 3-cyanobenzoic acid. The best conditions are described in the Exp13, using 10% Pd/C in EtOAc for 2h. These conditions were subsequently applied for the tritiation.

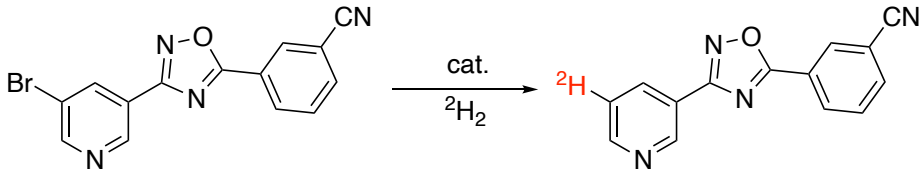

Exp	Catalyst	Solvent	Base	Time	$^2H_2$	^2H-NS9283	Over-reduced	Starting mat.
1	*10% Pd/alumina*	*MeOH*	*–*	*2,5 h*	*0,98*	*10 %*	*90 %*	*–*
2	*10% Pd/alumina*	*MeOH*	*TEA*	*1,5 h*	*–*	*–*	*100 %*	*–*
3	*10% Pd/alumina*	*MeOH*	*–*	*0,5 h*	*0,83*	*20 %*	*48 %*	*32 %*
4	*10% Pd/alumina*	*MeOH*	*–*	*1 h*	*0,88*	*5 %*	*95 %*	*–*
5	*10% Pd/alumina*	*MeOH*	*–*	*0,75 h*	*0,71*	*21 %*	*56 %*	*23 %*
6	*10% Pd/alumina*	*MeOH*	*TEA*	*1 h*	*–*	*–*	*100 %*	*–*
7	*5% Pd/$BaSO_4$*	*MeOH*	*–*	*0,75 h*	*0,77*	*18 %*	*40 %*	*42 %*
8	*5% Pd/$BaSO_4$*	*MeOH*	*TEA*	*1 h*	*–*	*3 %*	*–*	*97 %*
9	*10% Pd/C*	*MeOH*	*–*	*0,5 h*	*0,9*	*18 %*	*44 %*	*38 %*
10	*10% Pd/C*	*EtOAc*	*–*	*0,5 h*	*0,96*	*23 %*	*–*	*77 %*
11	*10% Pd/C*	*EtOAc*	*–*	*1 h*	*0,93*	*26 %*	*–*	*74 %*
12	*10% Pd/C*	*EtOAc*	*TEA*	*1 h*	*0,93*	*2 %*	*98 %*	*–*
13	*10% Pd/C*	*EtOAc*	*–*	*2 h*	*0,94*	*35 %*	*–*	*65 %*

Table 7. Screening condition for deuteration of NS9283.

The [^{3}H]NS9283 synthesis is based on the best conditions obtained in the deuteration reaction screening using as a starting compound the brominated analogue in *meta*-position of NS9283 which was treated with tritium (*Scheme 12*).

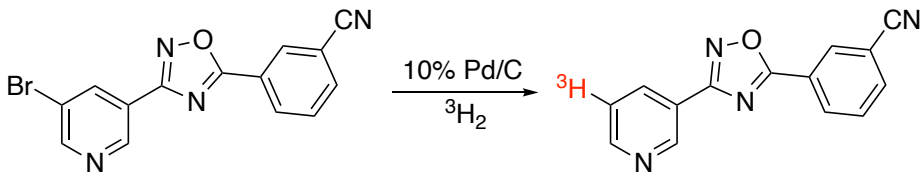

Scheme 12. Reagents and conditions. 10% Pd/C, ~950 mbar $^3H_2$, EtOAc, 2h, 22%.

Tritiated product was obtained with a 22% conversion with a specific activity of 26.08 Ci/mmol. Different formulations were prepared: 1mCi/1mL EtOH/H_2O 9:1 for binding assays and 0.5mCi/0.5mL EtOH/H_2O 9:1 for stability studies. Subsequently, [^{3}H]NS9283 was analysed

using LC-MS chromatography, radio HPLC and ^{1}H NMR as a crude and purified compound (*Figure 39*).

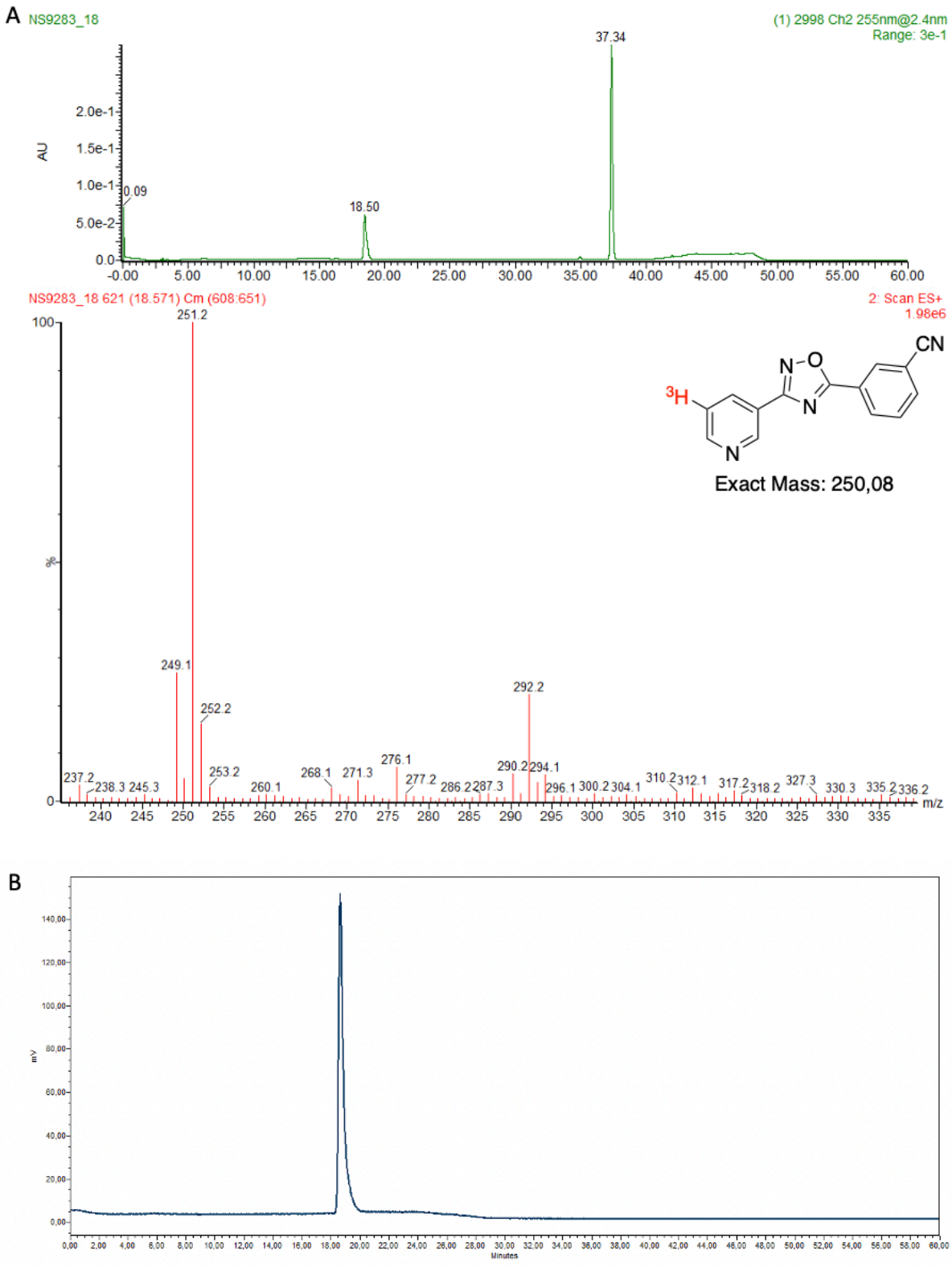

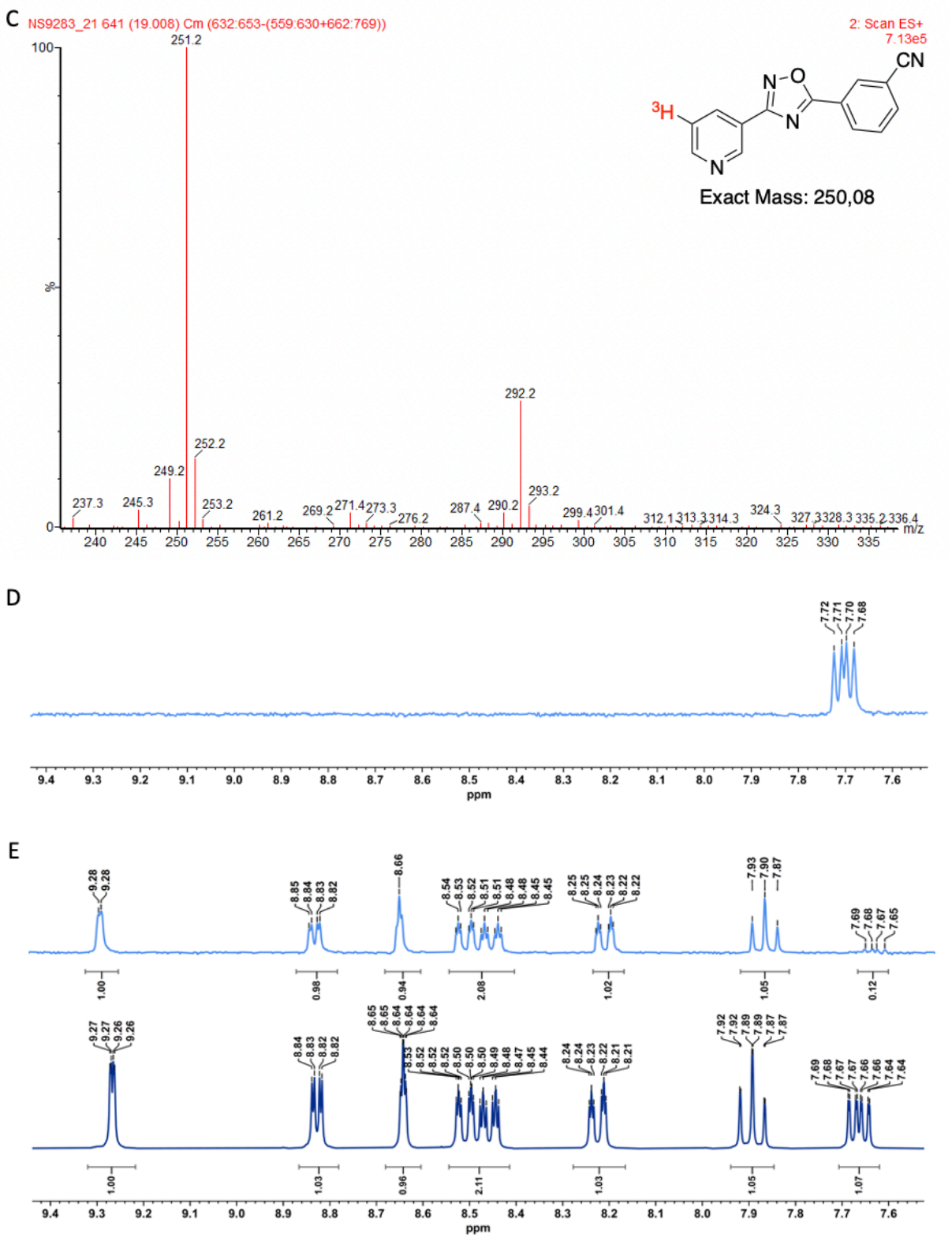

Figure 39. (A) LC-MS chromatograms and spectrum of crude [^{3}H]NS9283; (B) radio HPLC chromatogram of pure [^{3}H]NS9283; (C) LC-MS spectrum of pure [^{3}H]NS9283; (D) ^{3}H-^{1}H NMR [^{3}H]NS9283 in DMSO-d_6; (E) ^{1}H NMR [^{3}H]NS9283 (in light blue) and ^{1}H NMR [^{1}H]NS9283 (in dark blue)in DMSO-d6.

3.6.4. Biology

3.6.4.1. Binding assays

For the binding affinities, we started designing the experiment to calculate the Kd for [^{3}H]NS9283. For this purpose, we used a saturation binding assay using membranes isolated from HEK-293 cells stably transfected with human α4β2 (HEK-α4β2) and [^{3}H]NS9283 at different concentrations. This analysis depends on the assumption that the incubation has reached the equilibrium. As a first attempt, we used a filtration-based assay to determine the reversible binding of [^{3}H]NS9283 to HEK-α4β2 membranes. In this first experiment, we couldn't saturate the α4β2 nAChR with [^{3}H]NS9283, so it was impossible to calculate the Kd (*Figure 40A*). Subsequently, we tried to solve the problem using: 1) centrifugation instead of filtration to separate the bound [^{3}H]NS9283 from the unbound, 2) lower concentration of HEK-α4β2 membranes in order to reduce binding sites, 3) purified LS-α4β2 nAChRs in lipid vesicles instead of membranes to reduce non-specific binding, 4) isotopically diluted [^{3}H]NS9283 with cold NS9283 in order to reduce the specific activity. Unfortunately, none of these attempts gave positive results, so we couldn't calculate the Kd for [^{3}H]NS9283. Furthermore, it was noticed that application of [^{3}H]NS9283 with cold NS9283, increased the radioactivity by more than 10-folds, a phenomenon which does not occur with α4β2 nAChRs agonists such as nicotine and TC2559 which bind to the orthosteric binding site (*Figure 40B*). To investigate this phenomenon, we used two different batched of cold NS9283 (one synthesized in our lab and one purchased from Tocris) in the binding assays towards [^{3}H]CMPI, [^{3}H]Epibatidine and [^{3}H]dFBr and we did not observe any increase nor decrease in the radioactivity. This proves that, cold NS9283 somehow interacts with [^{3}H]NS9283 radioactivity and does not affects the the HEK-α4β2 membrane or the filter (*Figure 40C*).

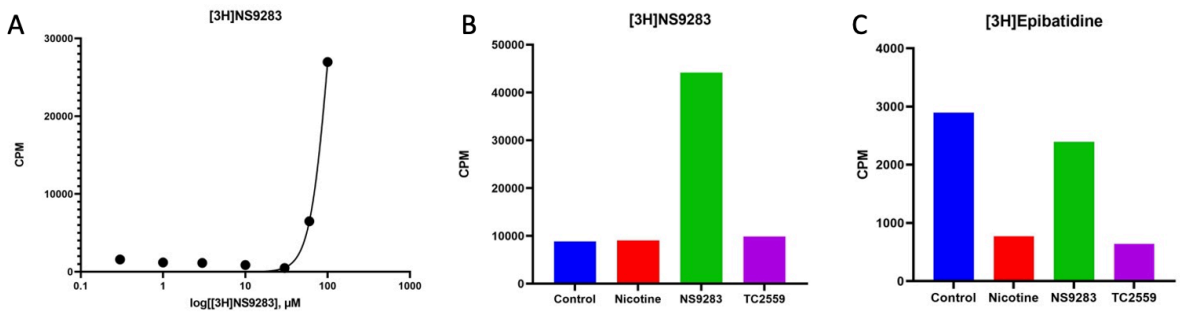

Figure 40. (A) Saturation binding assay for [^{3}H]NS9283, on the X axis [^{3}H]NS9283 concentration in µM, on the Y axis counts per minute; (B); binding assay of cold nicotine, NS9283 and TC2559 (α4β2nAChR partial agonist) towards [^{3}H]NS9283, on the Y axis counts per minute; (C) binding assay of cold nicotine, NS9283 and TC2559 towards [^{3}H]Epibatidine, on the Y axis counts per minute.

Due to the impossibility of performing binding assays, we switched our effort on functional assays. Functional assays were performed in collaboration with prof. Isabel Bermudez from the Department of Biological and Medical Sciences of Oxford Brookes University.

3.6.4.2. Functional assays

Animals

Xenopus laevis toads were housed and cared for following the UK Home Office code of practice guidelines for the species. The collecting of oocytes from *Xenopus* toads was carried out in a regulated room in the Biomedical Services facility at Oxford University, where the toads were housed. Adult female *Xenopus laevis* were purchased from *Xenopus* 1 (MI, USA). *Xenopus* toads were housed in a climate-controlled, light-regulated room. 50 toads were used. Toads were anaesthetized by immersion in 0.5% tricaine until no-responsive to toe pinch. Toads were then decapitated and ovarian lobes were harvested and then incubated in 2 mg/mL collagenase Type IA at room temperature for 2 h to isolate and defolliculate oocytes. The collagenase incubation procedure was carried out in a solution (OR2) containing 82 mM NaCl, 2 mM KCl, 2 mM $MgCl_2$, 5 mM HEPES; pH 7.6. Oocytes were maintained until use at 18 °C in the same solution (minus collagenase), supplemented with 20 mg/mL of neomycin, 100 IU/mL penicillin and 100 mg/mL streptomycin.

Xenopus oocytes: expression of nAChR and two-electrode voltage clamp recordings

Electrophysiological experiments were carried out with human α7, α4β2 or α5α4β2 nicotinic acetylcholine receptors (nAChR) expressed heterologously in *Xenopus* oocytes. Oocytes were injected with α7 or α4 and β2 cDNAs or α5α4β2 cRNA, and recorded using standard procedures, as described previously.[117,118] We expressed the two stoichiometries of the α4β2 nAChR. For the stoichiometry $(\alpha4)_3(\beta2)_2$, a mixture of 10 α4: 1 β2 cDNAs was injected into the nucleus of oocytes, whereas for the $(\alpha4)_2(\beta2)_3$ subtype the cDNA ratio injected was 1 α4: 10 β2. α7 cDNA was co-injected with chaperone NACHO at a ratio of 1 α7: 0.01 NACHO. For expression of α5α4β2 nAChR, cRNA of fully concatenated subunits (α5-β2-α4-β2-α4) was injected into the cytoplasm of the oocytes. Receptor expression was examined at least two days later, as previously described.[117]

Oocytes were impaled with two electrodes filled with 3 M KCl, and their membrane potential was maintained at -60 mV throughout the experiment. All recordings were performed at 18 °C, and cells were perfused with OR2 solution at pH 7.4. Currents were recorded using an automated platform equipped with a standard two-electrode voltage-clamp configuration (HiClamp; Multi Channel Systems, Reutlingen, Germany). This system differs from standard electrophysiology and other automated platforms because, instead of applying the compound in the perfusion, the oocyte is moved into a well from a 96-well microtiter plate containing 230 µl of the desired solution. Experiments were carried out only if the resting potential of the impaled oocytes was greater than -10 mV and the total holding current was less than 0.2 µA. Data were filtered at 10 Hz and captured at 100 Hz using proprietary data acquisition and analysis software running under Matlab (Mathworks Inc., Natick, MA). Ligands were prepared as concentrated stock solutions in DMSO and then diluted in the recording medium to obtain the desired test concentrations. To determine the potentiating efficacy of the ligands tested, a single concentration of ligand (30 µM) was co-applied with an EC_{20} ACh (30 µM for α7 or $(\alpha4)_3(\beta2)_2$ nAChR or 3 µM for $(\alpha4)_2(\beta2)_3$ or α5α4β2 nAChR). For comparison purposes, 30 µM of the compound NS9283 was also tested in the presence of 30 µM ACh. Concentration-Response curves were determined only for ligands that showed potentiating effects on ACh EC_{30} current responses. The potentiating effect was only observed at the $(\alpha4)_3(\beta2)_2$ nAChR; the ligands have no effect on the other nAChR tested. The concentration-response curves

were determined using a protocol of 6-8 concentrations with a reference response (30 µM ACh), The ligand was co-applied with ACh 30 µM. A complete experiment on a single oocyte comprised all initial control applications of 30 µM ACh followed by the full planned concentration-response relationship for the compound + 30 µM tested. Following the initial control applications, the actual concentration-response relationships of the agonists were obtained. The ligand + 30 µM ACh were applied for 5 s and the washing period between applications was 5 min.

Concentration-activation curve data were fitted with the Hill equation:

$$y = I_{max}/[1/(EC_{50}/[agonist])^{nH}],$$

where y is the normalised current amplitude, I_{max} is the maximal response (I_{max}/I_{AChMax}), EC_{50} is the agonist concentration at half-maximal efficacy, [agonist] is the agonist concentration, and nH the Hill coefficient. Curve fitting was carried out using the least squares method in MATLAB or using GraphPad version 5 (GraphPad Software, Inc., San Diego, CA, USA).

Experimental design and statistical analysis of functional data

Final data sets were assembled from a minimum of 5 independent recordings (i.e., n = 5) conducted on oocytes obtained from at least 3 different *Xenopus* donors (i.e., N = 3 The data sets represent full concentration-response relationships obtained from individual oocytes (i.e., incomplete experiments were discarded). The data from each experiment were fitted separately and the estimated EC_{50} values were used to obtain the mean EC_{50} or IC_{50} (95% CI) reported in the Table of EC_{50}. Prior to the ANOVA analysis, the data were tested for normality using the D'Agostino and Pearson normality test in PRISM and were normally distributed. Post hoc tests were run only if F achieved $P < 0.05$ and there was no significant variance in homogeneity. For all the functional data shown here, differences between wild type and tests were considered statistically different if $p < 0.05$.

3.6.5. Results and discussion

Functional assays have shown the following results. None of the compounds was able to potentiate the effects of ACh better than NS9283. However, few compounds resulted to have similar effects to NS9283 in terms of potency (EC_{50}) and relative efficacy of the potentiation.

Regarding the compounds derived from the Shape Similarity Screening, none of them was able to potentiate the currents evoked by 30µM ACh (*Figure 41*). These results suggest that these compounds are not able to bind the α4/α4 interface nor other PAM binding sites. Furthermore, it is possible to assume that the α4/α4 unorthodox binding site is highly restrictive and selective and does not permit the compounds with significantly different structures to bind.

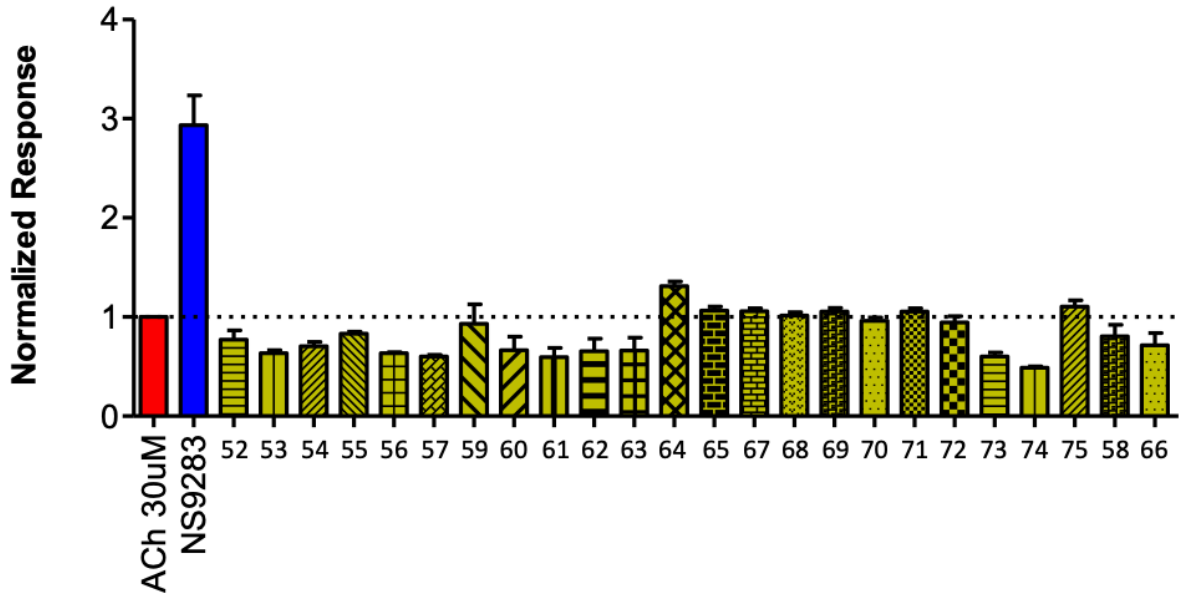

Figure 41. Relative efficacy ligands for potentiating the current responses of submaximal ACh concentrations (EC_{20}, 30 µM) of $(\alpha4)_3(\beta2)_2$ nAChR expressed heterogously in Xenopus oocytes. The relative efficacy of the ligands at a concentration of 30 µM was determined using the equation: maximal response to 30 µM test compound / maximal response to 30 µM ACh. Values are the mean ± SEM of 3-7 independent experiments carried out on oocytes from 5-6 different Xenopus donors. For comparison purposes, the potentiating efficacy of NS9283 is included.

On the other hand, NS9283 structural analogues, designed using FBDD approach and the work of Jin *et al*, have shown interesting profiles which can help to better understand the SAR (*Figure 42*) of the lead compound. The most interesting NS9283 analogues resulted to be **31** and **32,** in which the 3 cyano phenyl residue, was substituted with 3 and 4 nitro phenyl

moieties respectively and **26,** in which the nitrile group of the lead compound was moved on 4 position of the benzene ring. The 3-cyano phenyl group was also replaced with a pyridine residue, leading to compounds **28** and **29** and with N-acetyl and N-formyl piperidine leading to **50** and **51** respectively. From the first screening at a 30µM dose of the selected compound, it is possible to see that, except for NS9283 and its 4 substituted analogue **26**, the compounds substituted at position 4 resulted to have a higher efficacy rather than their *meta*-substituted analogue. This can be attributed to the positioning of the substituent in the hydrophilic pocket on α4(-) face with subsequent interaction with the binding site. The most interesting results are obtained with **50** and **51**, because an action on the potentiation of the currents evoked by the ACh similar to that of NS9283 is associated to a significantly new substructure. Instead of the usual differently substituted aromatic ring, these compounds carry an aliphatic piperidine ring formylated or acetylated on the nitrogen. These results broaden the horizons for further development of new potentiators selective for the unorthodox binding site. For the most promising compounds, the functional assays to study their dose-response curve will be per performed.

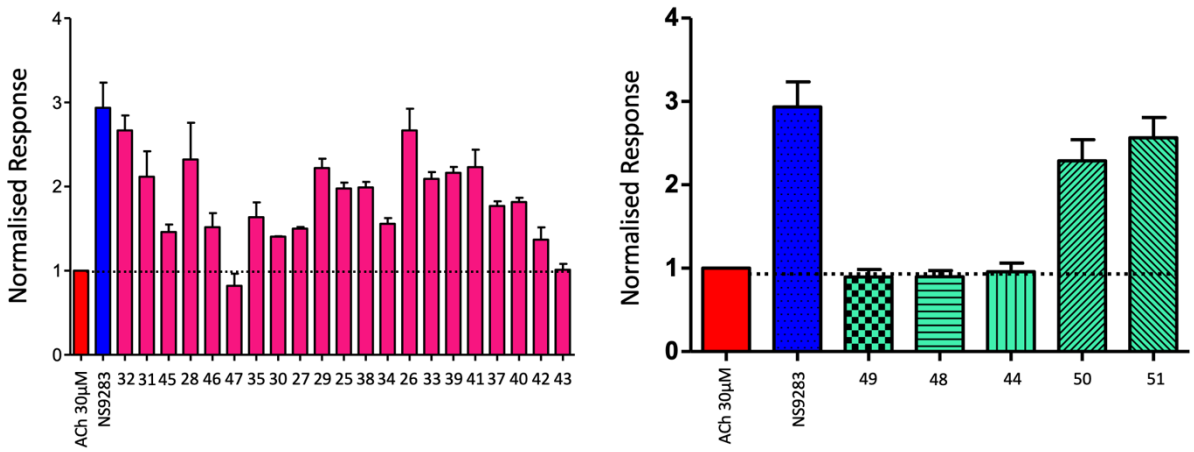

*Figure 42. Relative efficacy ligands for potentiating the current responses of submaximal ACh concentrations (EC_{20}, 30 µM) of $(\alpha4)_3(\beta2)_2$ nAChR expressed heterogously in Xenopus oocytes. The relative efficacy of the ligands at a concentration of 30 µM was determined using the equation: maximal response to 30 µM test compound / maximal response to 30 µM ACh. Values are the mean ± SEM of 3-7 independent experiments carried out on oocytes from 5-6 different Xenopus donors. For comparison purposes, the potentiating efficacy of NS9283 is included. Compound **36** was not included due to its low solubility in buffer solution.*

4. Part 2: Synthesis of photoactivatable α4β2 nAChRs agonist

4.1. State of the art

Biological processes are very complex, and to study their mechanisms, cellular activity needs to be controlled and tuned with the help of orthogonal tools. During the last decade, huge attention was paid to the light as a major orthogonal trigger. It is used in many biological fields such as neuroscience, genetics, and embryology.[119–121] Photoactivation was also used in the development of light-dependent drug release using nanocarriers which permit precise spatial and temporal control of the drug release.[122] This mechanism allows to activate the molecule after its diffusion and to better understand the reaction kinetics. So, *in vivo* uncaging could be a new therapeutic approach. Upon the irradiation, photons provide the energy to cleave the covalent bond between the photoremovable protecting group (PPG) and the drug molecule, which regains its activity, allowing the study of physiological processes in cell culture, intact tissues, and whole animals. This photo-releasing process can be initiated by one-photon excitation (1PE) of UV or near-UV light. Lately, the two-photon excitation (2PE) process was investigated due to its advantages compared to 1PE.

As previously, uncaging consists of the dissociation between PPG and the active molecule, and this reaction requires energy. The photon wavelength needed for this dissociation can be calculated as the average bond energy. C-C and C-O bonds correspond to 320-350 nm light, while C-N bond up to 395 nm UV light.[123] After the irradiation with a UV lamp, the absorption of one UV photon provides the necessary energy to reach the excited state at which photo release can start. Normally, at the excited point, the molecule can emit light and return to its ground state or can undergo the bond cleavage or rearrangement reaction. Despite having been adopted for several biological studies, 1PE has different disadvantages.

In 1929 Maria Göppert-Mayer supposed that an atom could be excited through the absorption of two photons.[124] Lately, in 1961 the 2PE was studied by Kaiser and Garret in CaF_2:Eu2+ crystals.[125] In 1990, Denk, Strickler and Webb observed the fluorogenic indicators in biological samples using a laser-scanning two-photon microscope.[126] In 1994, Denk showed the distribution of ACh-gated ion channels through a highly localized liberation of “caged”

neurotransmitter carbamoylcholine by two-photon absorption-mediated photoactivation in conjunction with recording the induced whole-cell current.[127] The 2PE has a few advantages compared to 1PE:

1. Excitation is localized to small volumes (femtoliter range).
2. Less photodamage to biological tissues.
3. Deeper penetration into the sample.

In 2PE, the excited molecule absorbs not one, but two nonresonant photons of the same wavelength. This absorption permits to generate an electronically excited state with subsequent photolysis as in 1PE but using the light with twice the wavelength required to achieve 1PE, and consequently with half energy (*Figure 43*).[128]

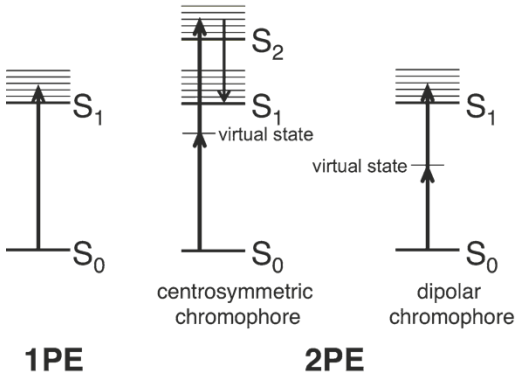

Figure 43. Jablonski diagrams of electronic transitions of a chromophore upon 1PE and 2PE. Adapted from Dore et al.[128]

The 2PE process uses a short-lived virtual excited state that consists of a combination of the ground and excited stats. This state exists only when the chromophore interacts with the first photon. After the absorption of the second photon, the molecule passes from the virtual to electronically excited state following photolysis. In the case of centrosymmetric chromophores, the transition for the excited state is different for 2PE compared to 1PE, leading to a different excited state, called S_2. This results in a different absorption wavelength which is not exactly twice the 1PE absorbance maximum. For dipolar chromophores, there is no difference between 1PE and 2PE excitation, and in this case, the maximum 2PE absorption is twice the maximum 1PE absorption.[128] 2PE can be explained in terms of nonlinear optical phenomena. The irradiation of the chromophore provokes a nonlinear response. Therefore, the excitation can exist only where the light intensity is maximum, called the focal point of the

optical system used, and if the numerical aperture objective is used, the irradiated volume can be as small as a femtoliter (*Figure 44*).

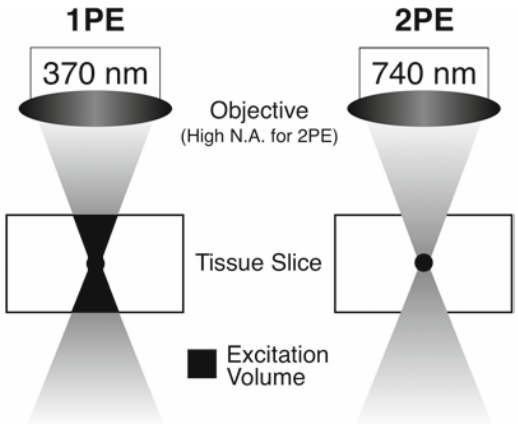

Figure 44. Comparison between the spatial selectivity of excitation with 1PE and 2PE. Adapted from Dore et al.[128]

So, the probability of absorption (P) increases with the square of the light intensity (I), in the relation to the two-photon absorption cross-section (σ_2) of the molecule. On the contrary, 1PE depends linearly on the light intensity.[129]

$$P = \frac{1}{2}\sigma_2 I^2$$

For the generation of large density photons for 2PE it is required a focused and pulsed laser, such as titanium-sapphire laser with tuning ranges of 700-1000 nm, <140 fs pulses, 90 MHz repetition rate and average power of at least 1 W.[128]

To recapitulate, the 2PE process is more advantageous than 1PE because, as described previously:

1. Excitation is localized to the order of femtoliter which is much smaller than a mammalian cell. This allows having the photolysis reaction in a precise area.
2. Used wavelengths are not absorbed by biomolecules in cells and tissues, making this process safer.
3. A longer wavelength of light is not scattered or absorbed by native chromophores as UV wavelengths, allowing deeper penetration into the biological tissue.

Photoremovable protecting groups (PPGs) permit spatial and temporal control over the release of different molecules. PPGs are widely used in synthesis, biochemistry, neurobiology, biomedicine, etc. The molecule protected by a PPG was defined as "caged". Generally, PPG should have absorption wavelengths above 300 nm. Also, the photolysis reaction should occur with a high quantum yield, Φ_{rel}. The quantum yield is equal to the amount of released substrate, n_{rel}/mol, divided by the number of photons at the irradiation wavelength λ, n_p/mol, that were absorbed by the caged compound:[130]

$$\Phi_{rel} = \frac{n_{rel}}{n_p}$$

The efficacy of PPG is measured as the product of the quantum yield and the molar decadic absorption coefficient ε of the PPG, but the sensitive detection of the response depends also on the background level of activity of the caged compound before its irradiation. Thus, the PPG should be stable in the media and has low intrinsic activity. Furthermore, it is not enough for PPG to be stable in the media, but it should also be soluble in order to eventually pass different biological barriers. It is a good thing if the photochemical byproducts are transparent, so they don't compete in the absorption of the excitation wavelengths.[130] Also, a good PPG should have a large two-photon uncaging cross-section, δ_u, which is the product of the two-photon absorbance cross-section δ_a and the uncaging quantum yield Φ_{rel}. It represents the parameter used to quantify the photosensitivity of a cage group to a photolysis induced by 2PE. It is expressed in Göppert-Mayer (GM) where 1 GM is 10^{-50} cm^4s per photon. Preferably, to be relevant for biological studies, δ_u value should exceed 0.1 GM.[131]

Photoremovable protecting groups were developed with the purpose of functional group protection and subsequent selective deprotection using light to achieve better yields.[132] The first studies on caged compounds for *in vitro* light controlled release of ATP and cAMP were performed by Hoffman[133], Schlaeger[134] and co-workers. These studies gave new perspectives on the use of this class of protecting groups. In the past years, different types of PPGs were developed for a selective photo-regulation of functional group, e.g., 2-nitrobenzyl (a), 1-(4,5-dimethoxy-2-nitrophenyl)-ethyl (b), 6-bromo-7-hydroxy-coumarin-4-yl-methyl (c), [7-(diethyl-amino)- coumarin-4-yl]-methyl (e), and 7-nitro-indolinyl (e) (*Figure 45*). They were successfully used to photo-regulate metal ions, neurotransmitters, carboxylic acids, proteins, nucleotides,

peptides, RNAs, and DNAs release. Unfortunately, they have different unfavourable properties such as poor water solubility, high self-fluorescence, and/or lower photolysis sensitivity towards 2PE.

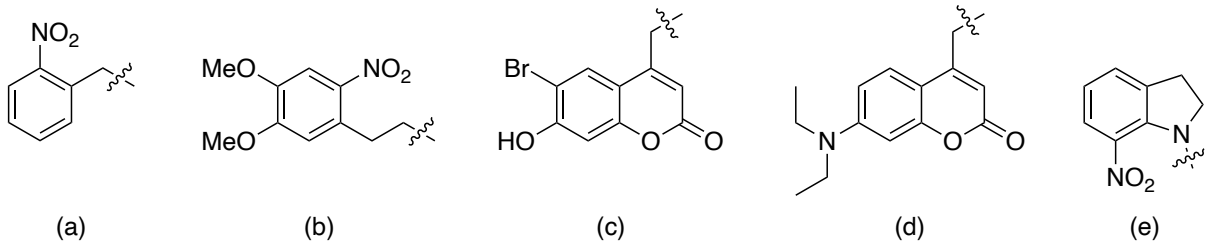

Figure 45. Structure of most common PPGs.

In 2001, Matsuzaki *et al.* have developed a caged-glutamate compound and managed the neurotransmitter's release using 2PE allowing a systematic investigation of glutamate receptors at the synaptic level. For this purpose, they used a 4-methoxy-7-nitroindolinyl cage.[135] The next step was to design new PPGs with better two-photon absorption properties. In 2006, Zhu *et al.* developed an 8-bromo-7-hydroxyquinoline (BHQ) cage that showed δ_u values from 0.40 GM to 0.90 GM based on the nature of the released compound after a 740 nm irradiation.[136] In 2009, Jarrett Davis *et al.* studied different substituents on BHQ structure and their effect on sensitivity towards 1PE and 2PE. This study led to the discovery of 8-cyano-7-hydroxyquinoline (CyHQ) (*Figure 46*). The substitution of bromine with -CN group increases by 3-folds the sensitivity for acetate release due to its high ε value. The quinoline based caging groups provided a new prospective in photoactivation studies. In comparison to previously used PPGs, BHQ and CyHQ have better photochemical and photophysical characteristics such as a larger δ_u, better water solubility, a reduced self-fluorescence and higher uncaging Φ_{rel}. These quinoline-based PPGs are excellent for the study of biological systems. For example, a commercially available 4,5-dimethoxy-2-nitrobenzyl group (DMNB) has poor sensitivity to two-photon excitation (δ_u = 0.03 GM at 740 nm). A variant of this protecting group, 3-(4,5-dimethoxy-2-nitrophenyl)-2-butyl (DMNPB), has a slightly higher but still low cross-section (δ_u = 0.17 GM at 720 nm). 4-methoxy-7-nitroindolinyl PG (MNI) has a cross-section of 0.06 GM at 720 nm. Coumarin- and quinoline-based caging groups have much higher sensitivity to two-photon excitation; values of δ_u for 6-bromo-7-hydroxycoumarin (Bhc) and 8-bromo-7-hydroxyquinoline (BHQ) are 0.72 and 0.59 GM, respectively. [137] BHQ and CyHQ are efficient cage groups in releasing of different types of molecules, carboxylates, primary and secondary

amines, diols and phenols, phosphates, using both UV light (365 nm) and 1PE and near-visible light (740 nm) and 2PE.[138]

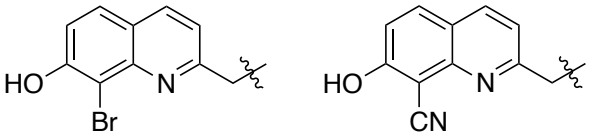

BHQ **CyHQ**

Figure 46. BHQ and CyHQ structures.

Since 2005, different research groups developed photoactivable forms of Tamoxifen, a chemotherapy drug for breast cancer, and its active 4-hydroxylated metabolite for the regulation of gene expression through Cre-recombinase systems through 1PE.[139–141] In 2017, Wong *et al.* developed a series of new 4-hydroxylated tamoxifen probes caged with a coumarin-based caging group and their effective uncaging activity *in vitro* using both 1PE and 2PE. Moreover, promising results were obtained in a preliminary *in vivo* study on mice.[142] Based on these studies, Asad *et al.* decided to design Tamoxifen and 4-OH-Tamoxifen caged with CyHQ as a quaternary ammonium salt. They were able to efficiently release the drug and its metabolite with both 1PE and 2PE. The photoactivable forms of Tamoxifen and 4-OH-Tamoxifen could be used to control gene expression in the Cre-recombinase system. Not only photoactivable Tamoxifen were studied, but also other tertiary amines were linked to CyHQ providing the corresponding quaternary ammonium salts and their release was studied (*Figure 47*). They discovered the pKa of the leaving group is crucial for effective photorelease of the biologically active messenger. Ammonium and alkylammonium ions have pK_a values in the range of 9-11, and quaternary ammonium salt of CyHQ would release a tertiary amine upon exposure to light. A threshold of 10.1 has been established for BHQ and slightly higher for CyHQ. This is because amines with sp2 hybridization did not photolyze, despite being good leaving groups, probably because photophysical decay processes out-competed C−N bond cleavage. CyHQ-protected tertiary anilines underwent a photoaza-Claisen rearrangement instead of photolysis to reveal a tertiary amine.[138]

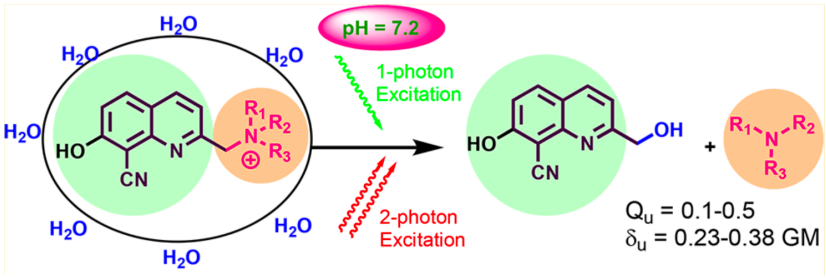

Figure 47. Schematic representation for tertiary amines uncaging upon 1PE and 2PE. Adapted from Asad et al.[138]

In 2020, Asad *et al.* developed photoactivable forms of dopamine (DA) and sulpiride using previously reported CyHQ. Particularly, CyHQ-*O*-DA and CyHQ-sulpiride have shown Φ_{rel} of 0.20 with high sensitivity to 1PE and modest sensitivity to 2PE with δ_u values of 0.24 and 0.26 GM, respectively. *In vitro* studies have shown that CyHQ-*O*-DA activates D1 receptors on breast cancer cell line after exposure to 405 nm light. Furthermore, CyHQ-*O*-DA releases dopamine and activates D2 receptors in brain slices from SNc. On the other hand, CyHQ-sulpiride releases efficiently sulpiride which antagonizes D2 receptors enabling the measurement of agonist off rates and other elements of dopamine synapse physiology.[143]

4.2. Synthesis of photoactivatable α4β2 nAChRs agonist

4.2.1. Introduction and aim

PPGs, initially used only for transient protection of functional groups of intermediates in organic synthesis, were successively developed to cage bioactive compounds. During the years, a wide variety of PPGs were developed. However, the preeminent position is occupied by 8-bromo-7-hydroxy-2-methylquinoline (BHQ) and 8-cyano-7-hydroxy-2-methylquinoline (CyHQ). Recent works published by Asad *et al.*[138,143] have demonstrated that BHQ and CyHQ are effective cage groups in the release of different types of molecules such as tertiary amines and phenols in response to irradiation with 1PE (365 nm) or 2PE (740 nm). In addition, these PPGs show good water solubility, a low self-fluorescence and high uncaging that are extremely important for the study of living cells and tissue cultures.

For this reason, we decided to study this strategy based on the photoremovable-protecting group to control the spatiotemporally the release of α4β2 nAChR full agonist (*S*)-**VI** with light at specific sites of action using quinoline-based PPGs (*Figure 48*).

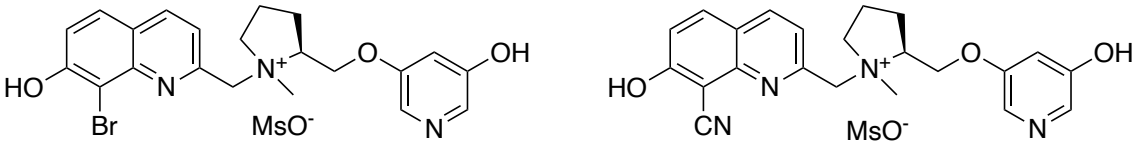

BHQ-(*S*)-VI **CyHQ-(*S*)-VI**

*Figure 48. BHQ- and CyHQ-protected full agonist (S)-**VI**.*

4.2.2. Chemistry

The synthesis of MEM protected (*S*)-**VI 114** is described in the *Scheme 13.* The mesyl ester derivative of *N*-Cbz protected (*S*)-prolinol **111** reacted with 3-hydroxy-5-((2-methoxyethoxy)methoxy)pyridine **112** to give the intermediate **113**, than converted into corresponding *N*-methyl derivative **114** by treatment with $LiAlH_4$.

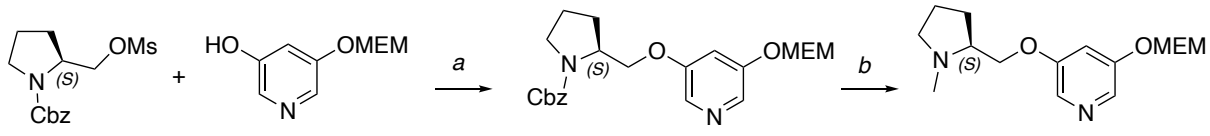

111 **112** **113** **114**

Scheme 13. Reagents and conditions: (a) DMF, NaH, N_2, rt, 4h, 64%; (b) THF, $LiAlH_4$, N_2, rt, 3h, 72%.

(*S*)-*N*-benzyloxycarbonyl-2-methylsulfonyoxymethyl **111** pyrrolidine was synthesized by the reduction of (*S*)-proline with $LiAlH_4$ and subsequent protection with benzyl chloroformate and methanesulfonyl chloride (*Scheme 14*).

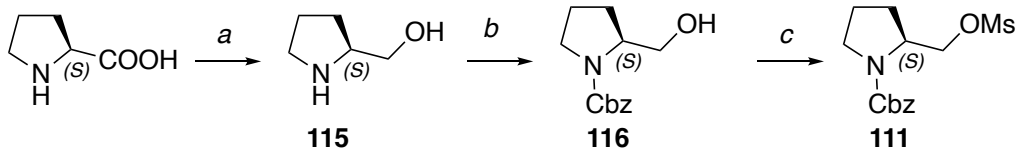

115 **116** **111**

Scheme 14. Reagents and conditions: (a) THF, $LiAlH_4$, N_2, reflux, 2h, 63%; (b) THF, benzyl chloroformate, $NaHCO_3$, rt, 16h, 56%; (c) DCM, TEA, MsCl, rt, 3h, 94%

3-hydroxy-5-((2-methoxyethoxy)methoxy)pyridine **112** is described in the *Scheme 15*. The nucleophilic displacement of one of the two chlorine atoms from commercial available 3,5-dichloropyridine with sodium salt of benzylic alcohol gave 3-benzyloxy-5-chloro pyridine **117**.

Subsequent copper-mediated amination using ammonia provide 3-amino-5-benzyloxypyridine **118** which was converted into 3-benzyloxy-5-hydroxypyridine **119** via diazonium salt. *O*-MEM protection and benzyl removal by hydrogenolysis gave the intermediate **112**.

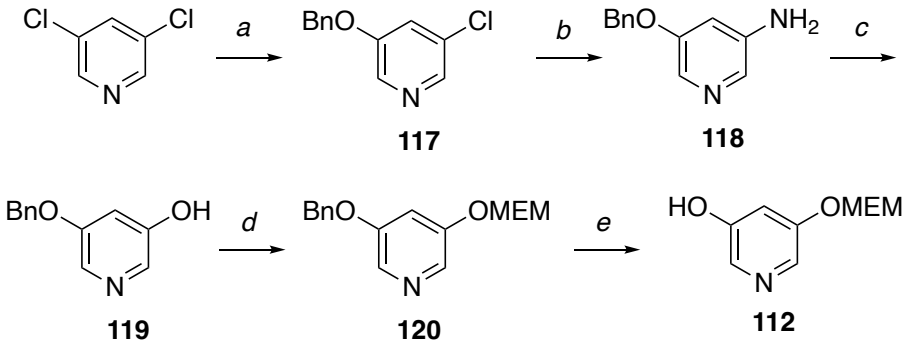

Scheme 15. Reagents and conditions: (a) DMF, BnOH, NaH, N_2, rt, overnight, 81%; (b) NH_3 25% in water, $CuSO_4$, 180°C, overnight, 52%; (c) H_2O, H_2SO_4, $NaNO_2$, rt, 3h, 97%; (d) DCM, MEMCl, DIPEA, N_2, 35°C, 4h, 63%; (e) MeOH, H_2, Pd/C, rt, 3h, 95%;

The synthesis of BHQ-OMs **121** and CyHQ-OMs **122** started from the synthesis of 7-hydroxy-2-methylquinolin-1-ium-4-metylbenzenesulfonate **123** that was obtained through a multistep process. Firstly, a Skraup reaction between the commercially available crotonaldehyde and 3-hydroxyaniline gave 7-hydroxy-2-methyquinoline as intermediated, which was subsequently isolated as para-toluene sulfonic salt (*Scheme 16*).

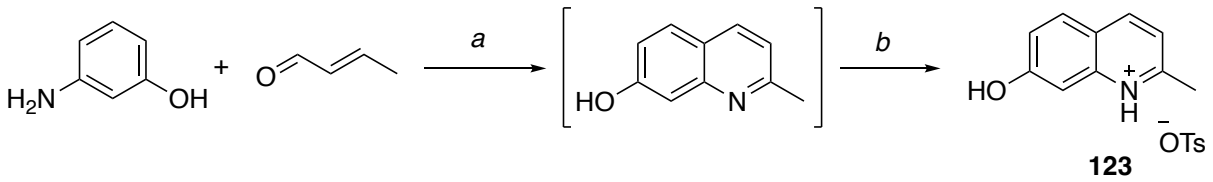

Scheme 16. Reagents and conditions: (a) butanol, 6N HCl, $FeCl_3$, 95°C, 1h; (b) 2-propanol, p-TSA, rt, 2h, 30%.

Treatment of this salt with *N*-bromosuccinimide (NBS) resulted in bromination at C-8 of quinoline to give **124**. The same reaction conducted using *N*-idosuccinimide (NIS) instead of NBS resulted in iodination on C-8 (**125**) (*Scheme 17*).

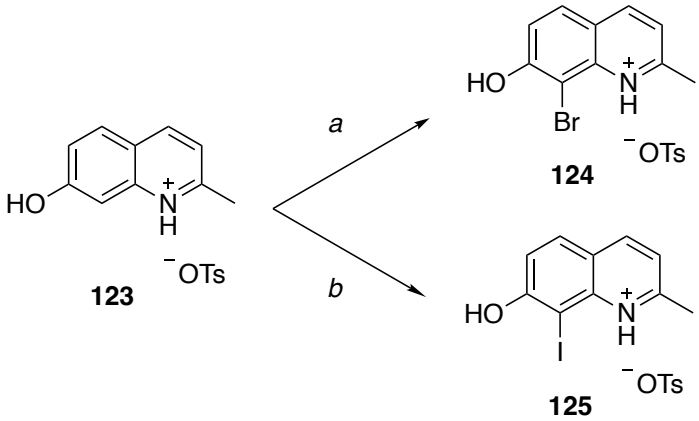

Scheme 17. Reagents and conditions: (a) methanol, NBS, rt, overnight, 66%; (b) methanol, NIS, rt, overnight, 60%.

Iodine was replaced with cyano, after protecting the phenolic function with an acetyl group (**126**), by treatment with CuCN. Hydrolysis of the acetate gave the quinoline **127** (*Scheme 18*).

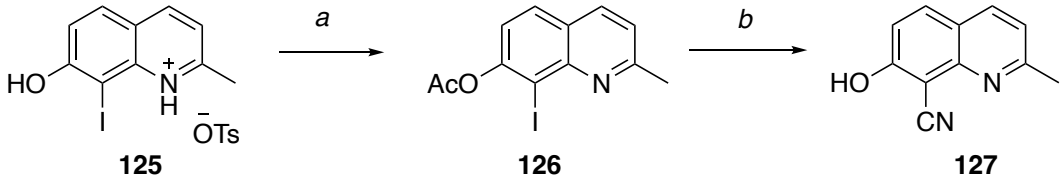

Scheme 18. Reagents and conditions: (a) ACN, TEA, Acetyl Chloride, N_2, 0°C to rt, 30 min, 100%; (c) DMA, CuCN, Pd-Tetrakis, 5h, reflux, 61%.

The intermediates **124** and **127** were then submitted to the same synthetic procedure to give the desired PPGs. In detail, MEM protection of the phenolic function (**128, 129**) followed by methyl oxidation with SeO_2 will provide the aldehydes **130** and **131**. Subsequent reduction with $NaBH_4$ (**132, 133**) followed by treatment with methansulfonyl chloride (MsCl) gave the corresponding MEM-BHQ-OMs **134** and MEM-CyHQ-OMs **135** PPGs which were then MEM deprotected to obtain desired intermediates BHQ-OMs **121** and CyHQ-OMs **122** (*Scheme 19*).

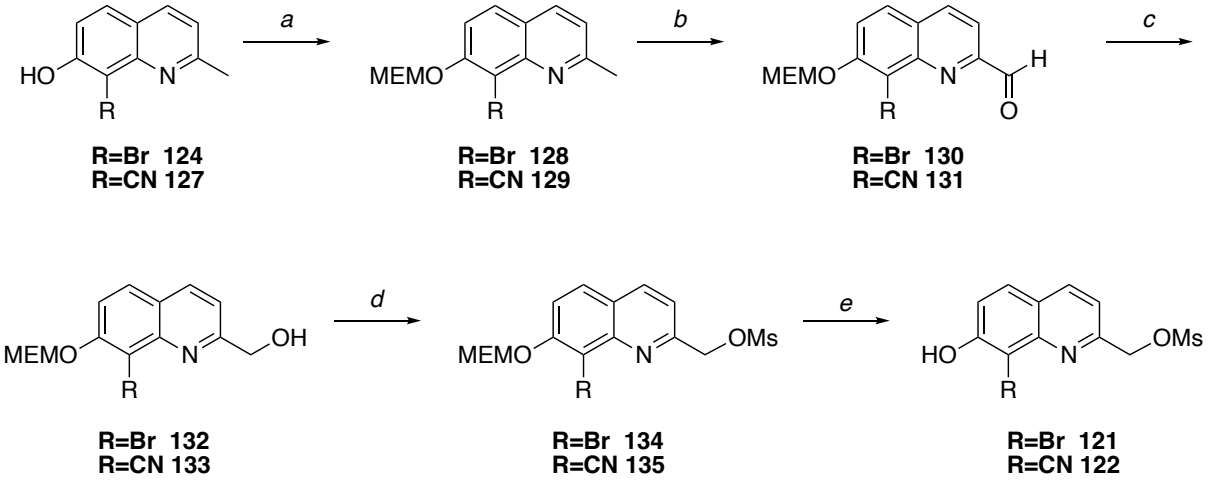

*Scheme 19. Reagents and conditions: (a) acetone, MEMCl, K_2CO_3, N_2, 0°C to rt, overnight, 69% (**128**); 88% (**129**); (b) dioxane, SeO_2, 80°C, 1h, quantitative (**130**); 60°C, 3h, 60% (**131**); (c) ethanol, $NaBH_4$, rt, 1h, quantitative (**132**); 86% (**133**); (d) DCM, MsCl, 0°C, 1h, 57% (**134**); 79% (**135**); (e) DCM, TFA, rt, 8h, 90% (**121**); 72% (**122**).*

The final compounds **BHQ-(*S*)-VI** and **CyHQ-(*S*)-VI** were synthesized with a simple nucleophilic substitution between **114** and **121** or **122** in acetonitrile and subsequent MEM deprotection using TFA (*Scheme 20*).

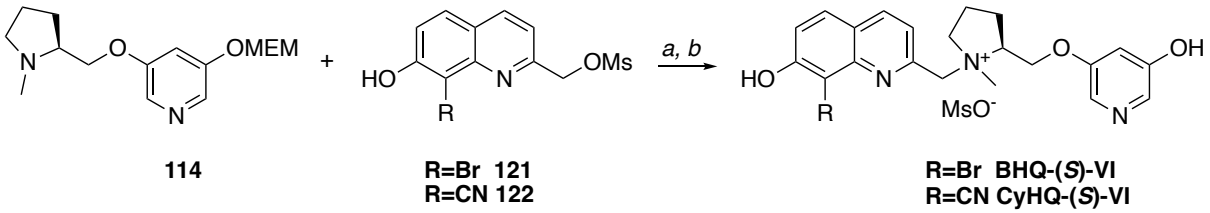

*Scheme 20. Reagents and conditions: (a) acetonitrile, rt, 4h, 55% (**136**), 76% (**137**); (b) DCM, TFA, rt, 5h, 17% (**BHQ-(S)-VI**), 59% (**CyHQ-(S)-VI**).*

4.2.3. Photochemical characterization of uncaging studies

Determination of the solubility of compounds BHQ-(*S*)-VI and CyHQ-(*S*)-VI in aqueous solution

Compounds BHQ-(*S*)-**VI** and CyHQ-(*S*)-**VI** (1 mg) was added to HEPES buffer (500 µL), and the resulting suspension was heated at 65 °C with sonication for 1 h. The solution was allowed to equilibrate at room temperature in the dark for 12 h before being filtered and analysed by HPLC. For each compound, the experiment was performed in triplicate. Quantification of BHQ-(*S*)-**VI** and CyHQ-(*S*)-**VI** was achieved by comparison with a calibration curve obtained from a standard solution in acetonitrile. The final solubility values obtained were 1.33 mg/mL for CyHQ-(*S*)-**VI** and 1.5 mg/mL for BHQ-(*S*)-**VI**.

UV-vis spectra of 138, 139, BHQ-(*S*)-VI, CyHQ-(*S*)-VI and (*S*)-VI

Based on the proposed uncaging mechanisms[138], compounds **138** and **139** were synthesized as a by-product of the uncaging reaction.

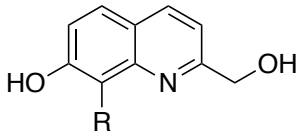

R=Br 138
R=CN 139

Solutions of **138**, **139**, BHQ-(*S*)-**VI**, CyHQ-(*S*)-**VI** and (*S*)-**VI** in HEPES buffer were used to acquire the UV-vis spectrum using a blank solution of HEPES buffer as baseline. Spectra were acquired with an Shimadzu® UV-1900 UV-Vis spectrophotometer in the 600-200nm range.

BHQ-(*S*)-**VI** λ_{max} = 260 nm;

CyHQ-(*S*)-**VI** λ_{max} = 247 nm;

(S)-**VI** λ_{max} = 306 nm.

Determination of the molar extinction coefficient (ε)

Solutions of BHQ-(*S*)-**VI** and CyHQ-(*S*)-**VI** (0.1 mM) in HEPES buffer were used to acquire the UV-vis spectrum using a blank solution of HEPES buffer as baseline. The measurement was repeated in triplicate and the absorbance values averaged. Final ε values at λ=365 nm were obtained from the Beer-Lambert law: $\varepsilon = A(cl)^{-1}$.

BHQ-(*S*)-**VI** ε_{365} = 1800 $M^{-1}cm^{-1}$;

CyHQ-(*S*)-**VI** ε_{365} = 5600 $M^{-1}cm^{-1}$.

Assessment of the stability of compounds BHQ-(*S*)-VI and CyHQ-(*S*)-VI in the dark

Solutions of BHQ-(*S*)-**VI** and CyHQ-(*S*)-**VI** in HEPES buffer were stored in the dark at room temperature and sampled periodically to determine the extent of degradation by HPLC as

described for the photolysis reaction. Less than 1% of BHQ-(*S*)-**VI** and CyHQ-(*S*)-**VI** degraded during a period of one week.

Photolysis reaction with 1-photon excitation of compounds BHQ-(*S*)-VI and CyHQ-(*S*)-VI

Substrates were dissolved in HEPES buffer to a final concentration of 2.73 mM. 1 mL of the resulting solution was irradiated in a quartz cuvette using a LED lamp (Cairn MonoLED) at 365 nm with stirring. Aliquots (50 µL) were sampled at different time intervals and analysed by HPLC, using external standard calibration method to obtain quantitative data for BHQ-(*S*)-**VI** and CyHQ-(*S*)-**VI** cleavage and calibration curve to obtain quantitative data for (*S*)-**VI** release. Each experiment was repeated in triplicate. Chromatographic runs were performed using Hypersil® BDS C18 column (particle size 5µm, 250x4.6 mm dimension), monitoring the AUC at the wavelength of 305 nm (λ_{max} of *(S)*-**VI**). Separations were obtained with a gradient elution (flow rate 1 mL/min) using as mobile phases (A) H2O and (B) CH3CN, both containing 0.1% of TFA; the elution was set as follows (%B): 0 min, 10%; 9 min, 20%; 12 min, 20%; 14 min, 10%; 16 min, 10%. The quantitative data obtained were plotted versus time of photolysis and the $t_{90\%}$ values (time in seconds for 90% of reaction to complete) calculated by fitting the data to a one phase exponential decay curve using the software GraphPad Prism version 8 (GraphPad Software, Inc., CA, USA). The released compound (*S*)-**VI** was monitored during the appearance and plotted as an exponential rise.

4.2.4. Results and discussions

Upon the irradiation of BHQ-(*S*)-**VI** and CyHQ-(*S*)-**VI**, dissolved in the simulated physiological buffer (HEPES pH 7.4) using 365 nm light, the release of the full agonist (*S*)-**VI** was observed. The time course of the photolysis was monitored by HPLC, and the appearance of the (*S*)-**VI** and disappearance of BHQ-(*S*)-**VI** and CyHQ-(*S*)-**VI** were observed by comparison with calibration curves. The irradiation was performed at different times from 1 sec to 120 sec.

Regarding the compounds BHQ-(*S*)-**VI** it is possible to observe that the disappearance of the starting material is complete with the $t_{90\%}$ of 43 sec. However, that the maximum release of the full agonist (*S*)-**VI** is only of 30% circa. This phenomenon is due to the photobleaching of the compound BHQ-(*S*)-**VI** or intramolecular photo-rearrangement or photo-degradation due to the prolonged exposure to a high lamp intensity (*Figure 49*).

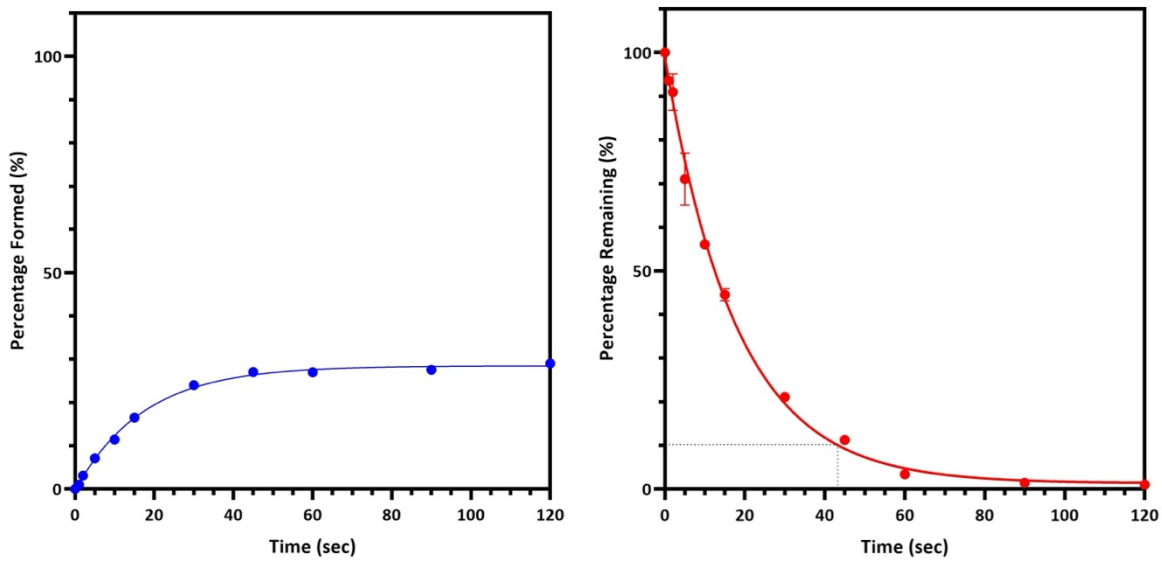

*Figure 49. Time courses for the photolysis reaction of BHQ-(S)-**VI**: percentage of released (S)-**VI** (left) and percentage of remaining BHQ-(S)-**VI** (right). Curves were obtained using GraphPad Prism version 8 using one phase exponential decay curve.*

The same experiment was performed also on CyHQ-(*S*)-**VI**, in order to analyse and compare with the previously obtained results using bromo-substituted PPG. In this case, the photolysis is still efficient with the $t_{90\%}$ of 47 sec. However, the release of the full agonist (*S*)-**VI** from cyano-substituted PPG base compound is much higher than the bromo-substituted one. The release of full agonist (*S*)-**VI** is of 75% (*Figure 50*).

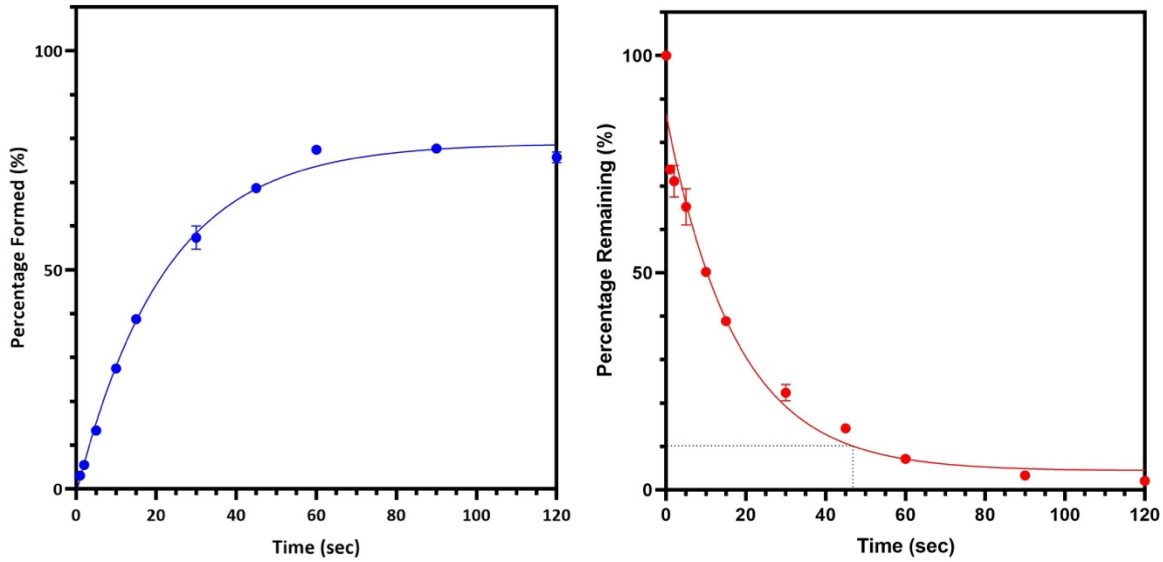

*Figure 50. Time courses for the photolysis reaction of CyHQ-(S)-**VI**: percentage of released (S)-**VI** (left) and percentage of remaining CyHQ-(S)-**VI** (right). Curves were obtained using GraphPad Prism version 8 using one phase exponential decay curve.*

In conclusion, two photoactivatable forms of (*S*)-**VI,** namely BHQ-(*S*)-**VI** and CyHQ-(*S*)-**VI,** were designed, synthesized, and tested for their ability to release the full agonist through 1PE

excitation. The photorelease reactions occur with complete consumption of the caged compounds. However, this process is accompanied by photobleaching. Therefore, a proper HPLC analysis protocol was developed to evaluate the effective release of (*S*)-**VI**. Of the two photoactivatable compounds, CyHQ-(*S*)-**VI** shows better photochemical properties than its brominated analogue, releasing the nicotinic agonist (*S*)-**VI** up to nearly 80%. Such a behaviour highlights the higher photostability of the cyano derivative, CyHQ-(*S*)-**VI,** compared to its brominated analogue BHQ-(*S*)-**VI.**Subsequently, *in vitro* studies will be performed in collaboration with Dr. Nicola Origlia from Instituto di Neuroscienze of CNR of Pisa. The use of a photoactivatable α4β2 nAChR full agonist represents an important tool to deeply investigate the neurophysiology of the entorhinal-hippocampal circuitry, that is essential for cognitive functioning and involved in a variety of neurological disorders and neurodegenerative diseases. Indeed, its spatiotemporal control in a brain slice, by local uncaging, can be used to understand the critical role of α4β2 nAChRs in CNS and how stimulation of such receptors, in different brain circuitries, can subtly influence various aspects of neuronal communication and contribute to the overall efficiency of synaptic connections.

5. General conclusions and future perspectives

In conclusion, it was observed that the mutation of Ser108 amino acid of the small hydrophilic β2 pocket modifies the epibatidine binding. If the hydroxymethyl side chain of Ser108 is replaced with bulkier isopropyl of Leu It abolishes the binding. On contrary, the substitution with less bulky methyl of Ala increases or does not affect the affinity of α4β2 partial agonist.

Based on these results, a series of benzofuran derivatives were synthesized. These compounds have demonstrated that the position of the oxygens of the heterocycle and the decoration of the aromatic ring are crucial. Also, the studies on the two isoforms of the receptor show the involvement of these characteristics with the receptor interaction.

Subsequently, the most promising compounds were tested *in vivo* and it was demonstrated that α4β2 full agonists are involved in attention and spatial memory improvement in a way similar to nicotine. On the other hand, partial agonist *(S,R)*-**IV** when co-applied with nicotine antagonises the rewarding effects. The results of these *in vivo* studies have identified potential new lead molecules for improving learning and memory ((*S*)-**V** and (*S*)-**VI**) or for inducing smoking cessation ((*S*)-**VI**).

Studies on the compounds selective for the α4/α4 interface of the α4β2 nAChR have shown that this unorthodox binding site is highly selective and restrictive. SAR studies broaden the horizons for the further development of new potentiators selective for the unorthodox binding site. The future perspectives are to synthesize other compounds based on NS9283. Two synthetic strategies will be studied. The first one consists of the combination of the most promising modifications of the pyridine and 3-CN substituted phenyl rings. The second approach is based on the further investigation of the piperidine moiety instead of the phenyl ring with the corresponding lengthening of the substituent on the *N* and shrinkage/enlargement of the piperidine ring to pyrrolidine and azepane one.

Regarding the photoactivatable α4β2 full agonist, it was observed that BHQ and CyHQ protecting groups are efficient in the photolysis reaction using a 365 nm lamp. With the BHQ group, the release of the full agonist was only 30% due to photobleaching of the compound, intramolecular rearrangement and photo-degradation. However, the same experiment

performed on CyHQ caged full agonist, the photolysis in more effective with the release of the full agonist of 75%. Further studies will be focused on the investigation of other quinoline-based cage groups substituted with fluorine or trifluoromethyl groups in the 8-position and their coupling with the full agonist (*S*)-**VI**. Also, the use of different cage groups such as BODIPY will be investigated. Another aspect to deepen is the coupling of the PPGs at different positions of the active compounds (pyridine nitrogen, pyrrolidine nitrogen or phenyl oxygen).

6. Experimental section

All chemicals and solvents were used as received from commercial sources or prepared as described in the literature. Flash chromatography purifications were performed using Biotage® Isolera™ flash purification system using KP-Sil 32-63 µm 60 Å cartridges and Merck Silica Gel 60 (0.040-0.063 µm). TLC analyses were performed using 0.25mm silica gel plates on aluminium foil, containing a fluorescent indicator (Macherey-Nagel Alugram® SilG/UV 254). The spots were visualized under UV light (l = 254 or 365 nm). The staining of TLC plates was performed with potassium permanganate, cerium sulfate, ninhydrin and cerium molybdate stain; R_f values are given for guidance. ^{1}H and ^{13}C NMR spectra were recorded at 300 and 75 MHz using Varian Mercury 300 spectrometer and elaborated with Mnova software. Chemical shifts are reported in ppm relative to residual solvent ($CHCl_3$, MeOH or DMSO) as internal standard. Melting points were determined by Buchi Melting Point B-540 apparatus. Optical rotations were determined in a 1 dm cell of 1 mL capacity on Jasco P-1010 Polarimeter. The purity of compounds was assessed by HPLC analysis using HP1050 instrument. All compounds showed a purity ≥95%. Mass Spectra of compounds were acquired on a 4000 QTRAP (ABSciex), operated in both positive and negative electrospray ionization. High Resolution Electrospray Mass Spectra of all the final compounds were acquired on Q-TOF Synapt G2 Si (WATERS). Computation studies were performed using Schrodinger®, BIOVIA Discovery Studio® and BROOD® software. Absorption spectra were recorded using a Shimadzu® UV-1900 UV-Vis spectrophotometer in the 900nm-200nm range using a 1.5 mL quartz cuvette.

6.1. Part 1

General procedure for benzylation of 2-bromo-benzofuranols to give 12 and 13 (A)

A solution of benzofuranol (1.0 eq) in anhydrous THF (4 mL) was added dropwise to a suspension of NaH (1.1 eq) in anhydrous THF (3 mL) at 0 °C under N_2. The resulting suspension was stirred at 0 °C for 10 min. Then, BnBr (2.0 eq) was added rapidly. The mixture was allowed to warm to rt and stirred at rt for 16 h. The mixture was quenched with H_2O (1 mL) and concentrated under reduced pressure. Saturated $NaHCO_3$ (10 mL) was added, and the mixture was extracted with EtOAc (3 x 5 mL). The combined organic layers were dried (Na_2SO_4) and

evaporated under reduced pressure to give the corresponding crude 2-bromo-benzyloxybenzofuran.

General procedure for methylation of 2-bromo-benzofuranols to give 14 and 15 (B)

A solution of benzofuranol (1.0 eq) in anhydrous THF (4 mL) was added dropwise to a suspension of NaH (1.1 eq) in anhydrous THF (3 mL) at 0 °C under N_2. The resulting suspension was stirred at 0 °C for 10 min. Then, MeI (2.0 eq) was added rapidly. The mixture was allowed to warm to rt and stirred at rt for 16 h. The mixture was quenched with H_2O (1 mL) and concentrated under reduced pressure. Saturated $NaHCO_3$ (10 mL) was added, and the mixture was extracted with EtOAc (3 x 5 mL). The combined organic layers were dried (Na_2SO_4) and evaporated under reduced pressure to give the corresponding crude 2-bromo-methoxybenzofuran.

General procedure for Catalytic Lithiation-Negishi Coupling for compounds 16-19,24 (C)

Procedure adapted from literature.[144] *s*-BuLi (2.9 mL of a 1.3 M solution in hexane, 1.3 eq) was added dropwise to a stirred solution of *N*-Boc pyrrolidine (1.0 eq) in anhydrous THF (5 mL) at –30 °C under N_2. The resulting solution was stirred at –30 °C for 5 min. Then, $ZnCl_2$ (1.8 mL of a 1.0 M solution in Et_2O, 0.6 eq) was added dropwise. The resulting solution was stirred at –30 °C for 30 min and allowed to warm to rt and stirred for 30 min. To this stirred solution of the organozinc reagent, the aryl bromide (0.7 eq) was added. Then, $Pd(OAc)_2$ (0.1 eq, 10 mol%) and $^tBu_3PHBF_4$ (0.13 eq, 12.5 mol%) were added in one portion and the resulting solution was stirred at rt for 16 h. 35% $NH_4OH_{(aq)}$ (10 mL) was added and the solution was stirred at rt for 1 h. The solids were removed by filtration through Celite® and washed with Et_2O (20 mL). The filtrate was washed with HCl 1M (20 mL) and brine (20 mL), dried (Na_2SO_4) and evaporated under reduced pressure to give the crude product.

General procedure for the removal of Boc protecting group and N-methylation to give compounds 3, 5, 20 and 21 (D)

Procedure adapted from literature.[98,145] HCl in MeOH (3 mL of a 1.25 M solution) was added to a stirred solution of the *N*-Boc benzofuran (1.0 eq) in MeOH (3 mL) at rt. The resulting solution was stirred at 50 °C for 3 h. Then, the solvent was evaporated under reduced pressure

to give the crude HCl salt as a brown oil. Then, H_2O (5 mL) and saturated $NaHCO_3$ (5 mL) were added, and the mixture was extracted with EtOAc (3 x 5 mL). The combined organic layers were dried (Na_2SO_4) and evaporated under reduced pressure to give the crude product. MeOH (5 mL) and AcOH (80 µL) were added at 0 °C. 37% $HCHO_{(aq)}$ (0.1 mL) was added dropwise to a stirred reaction mixture. Then, pic-BH_3 (1.0 eq) was added, and the resulting solution was stirred at rt for 2 h. The mixture was concentrated under reduced pressure. HCl 1 M (5 mL) was added, and the resulting solution was stirred at rt for 1 h to quench the unreacted 2-picolin-borane. Then, Na_2CO_3 2M was added at 0 °C. The mixture was extracted with EtOAc (3 x 5 mL). The combined organic layers were washed with brine (10 mL), dried (Na_2SO_4) and evaporated under reduced pressure to give the crude product that was purified by flash column chromatography.

General procedure for the removal of benzyl protecting group for compounds 1 and 2 (E)

Procedure adapted from literature.[98] 10% Pd/C (0.5 eq) was added to a solution of benzyloxybenzofuran (1.0 eq) in MeOH (5 mL). The resulting mixture was stirred at rt for 4 h under H_2 (1 atm). Then, the stirred solution was filtered over Celite® and washed with MeOH. The filtrate was evaporated under reduced pressure to give the crude product as an orange oil.

***N*-Boc-pyrrolidine (7)**

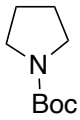

Molecular Weight: 171,24

Procedure adapted from literature.[146] TEA (3.4 mL, 0.02 mmol) and $(Boc)_2O$ (6.88 g, 0.03 mmol) were added to a stirred solution of pyrrolidine (2 mL, 0.02 mol) in DCM (8 mL) at 0 °C and the resulting mixture was stirred at rt overnight. The stirred solution was washed with HCl 1 M (10 mL), brine (10 mL), dried (Na_2SO_4) and evaporated under reduced pressure to give *N*-Boc-pyrrolidine (**7**) (4.06 g, 0.02 mol, 98%) as a colourless oil; $\boldsymbol{R_f}$ (Cyclohexane/EtOAc 8:2) 0.41; **^{1}H NMR** (300 MHz, $CDCl_3$): δ 3.35 – 3.26 (m, 4H), 1.88 – 1.78 (m, 4H), 1.46 (s, 9H).

2-bromo-5-hydroxybenzofuran (11)

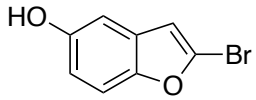

Molecular Weight: 213.03

Procedure adapted from literature.[147] A solution of CBr_4 (9.6 g, 28.96 mmol) in ACN was added dropwise to a suspension of 2,5-dihydroxybenzaldehyde (1.0 g, 7.24 mmol), PPh_3 (7.6 g, 28.96 mmol) and Zn powder (1.89 g, 28.96 mmol) in ACN at rt under N_2. The resulting suspension was stirred at rt for 30 min. Then, NH_4Cl (1.94 g, 36.20 mmol) was added, and the mixture was stirred vigorously until it became a clear solution. K_2CO_3 (5.00 g, 36.20 mmol) and CuI (138 mg, 0.72 mmol, 10 mol%) were added and the suspension was stirred and heated at reflux for 3 h. Then, the suspension was allowed to cool to rt, filtered through Celite® and evaporated under reduced pressure to give the crude product. Purification by flash column chromatography with 9:1 cyclohexane-ethyl acetate as eluent gave 2-bromo-5-hydroxybenzofuran (**11**) (550 mg, 2.58 mmol, 36%) as a pale orange solid, **mp** decomposes at 68 °C; $\boldsymbol{R_f}$ (Cyclohexane/EtOAc 8:2) 0.25; **^{1}H NMR** (300 MHz, $CDCl_3$): δ 7.30 (d, *J* = 8.9 Hz, 1H), 6.91 (d, *J* = 2.6 Hz, 1H), 6.76 (dd, *J* = 8.9, 2.6 Hz, 1H), 6.63 (s, 1H), 4.91 (br s, 1H, exchange with D_2O).

2-bromo-5-benzyloxybenzofuran (13)

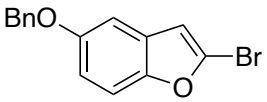

Molecular Weight: 303.16

Using the general procedure **A**, a mixture of 2-bromo-benzofuran-5-ol (**11**) (260 mg, 1.22 mmol), NaH (32 mg, 1.34 mmol) and BnBr (0.29 mL, 2.44 mmol) in anhydrous THF (7 mL) gave the crude product as an orange oil. Purification by flash column chromatography with 9:1 petroleum ether-DCM as eluent gave 2-bromo-5-benzyloxybenzofuran (**13**) (269 mg, 0.89 mmol, 73%) as a colourless oil; $\boldsymbol{R_f}$ (cyclohexane) 0.17; **^{1}H NMR** (300 MHz, $CDCl_3$): δ 7.49 – 7.28 (m, 6H), 7.03 (d, *J* = 2.6 Hz, 1H), 6.94 (dd, *J* = 9.1, 2.6 Hz, 1H), 6.65 (s, 1H), 5.08 (s, 2H).

2-(*N*-*tert*-butoxycarbonyl-2'-pyrrolidinyl)-5-benzyloxybenzofuran (17)

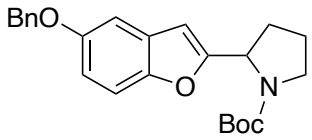

Molecular Weight: 393.48

Using the general procedure **C**, a mixture of *N*-Boc-pyrrolidine (**7**) (280 mg, 1.65 mmol), *s*-BuLi (1.6 mL of a 1.3 M solution in hexane, 2.13 mmol), $ZnCl_2$ (0.98 mL of a 1.0 M solution in Et_2O, 0.98 mmol), $Pd(OAc)_2$ (37 mg, 0.16 mmol), $^tBu_3PHBF_4$ (60 mg, 0.21 mmol) and 2-bromo-5-benzyloxybenzofuran (**13**) (347 mg, 1.15 mmol) in anhydrous THF (10 mL) gave the crude product. Purification by flash column chromatography with 10:0 to 9:1 cyclohexane-ethyl acetate as eluent gave 2-(*N*-*tert*-butoxycarbonyl-2'-pyrrolidinyl)-5-benzyloxybenzofuran (**17**) (130 mg, 0.33 mmol, 20%) as yellow oil; R_f (Cyclohexane/EtOAc 8:2) 0.32; **^{1}H NMR** (300 MHz, $CDCl_3$: δ 7.50 – 7.27 (m, 6H), 7.04 (s, 1H), 6.90 (d, *J* = 7.0 Hz, 1H), 6.38 (br s, 1H), 5.02 (s, 2H), 4.99 – 4.85 (m, 1H), 3.74 – 3.37 (m, 2H), 2.31 – 2.07 (m, 2H), 2.01 – 1.88 (m, 2H), 1.42 (s, 9H).

2-(5-(benzyloxybenzofuran-2-yl)-1-methylpyrrolidine (21)

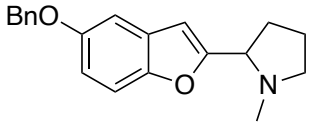

Molecular Weight: 307.39

Using the general procedure **D**, a mixture of HCl in MeOH (5 mL of a 1.25 M solution) and tert-butyl 2-(5-(benzyloxy)benzofuran-2-yl)pyrrolidine-1-carboxylate (**17**) (130 mg, 0.33 mmol) in MeOH (3 mL) gave 2-(5-(benzyloxy)benzofuran-2-yl)pyrrolidine as a brown oil. Then, 2-(5-(benzyloxy)benzofuran-2-yl)pyrrolidine (70 mg, 0.24 mmol), 37% $HCHO_{(aq)}$ (0.1 mL) and pic-BH_3 (25 mg, 0.24 mmol) in MeOH (4 mL) and AcOH (60 µL) gave the crude product. Purification by flash column chromatography with 98:2 DCM-MeOH and 0.5% $NH_{3(22\% \text{ in water})}$ as eluent gave 2-(5-(benzyloxybenzofuran-2-yl)-1-methylpyrrolidine (**21**) (30 mg, 0.10 mmol, 41%) as an orange oil; R_f (DCM/MeOH 9:1 + 0.1% $NH_{3(22\% \text{ in water})}$) 0.48; **^{1}H NMR** (300 MHz, $CDCl_3$): δ 7.51 – 7.29 (m, 6H), 7.06 (d, *J* = 2.6 Hz, 1H), 6.93 (dd, *J* = 8.9, 2.6 Hz, 1H), 6.53 (s, 1H), 5.09 (s, 2H),

3.34 (t, *J* = 8.0 Hz, 1H), 3.25 (ddd, *J* = 9.5, 7.4, 2.3 Hz, 1H), 2.45 – 2.27 (m, 4H), 2.21 – 2.10 (m, 2H), 2.10 – 1.97 (m, 1H), 1.94 – 1.76 (m, 1H).

2-(5-hydroxybenzofuran-2-yl)-1-methylpyrrolidine (1)

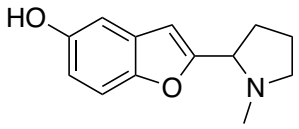

Molecular Weight: 217.27

Using the general procedure **E**, a mixture of 2-(5-(benzyloxy)benzofuran-2-yl)-1-methylpyrrolidine (**21**) (90 mg, 0.29 mmol) and 10% Pd/C (15 mg) in MeOH (9 mL) gave the crude product. Purification by flash column chromatography with 9:1 DCM-MeOH and 0.1% $NH_{3(22\%\ in\ water)}$ as eluent gave 2-(5-hydroxybenzofuran-2-yl)-1-methylpyrrolidine (**1**) (42 mg, 0.19 mmol, 66%) as a light yellow oil; R_f (DCM/MeOH 9:1 + 0.1% $NH_{3(22\%\ in\ water)}$) 0.41; **^{1}H NMR** (300 MHz, CD_3OD): δ 7.23 (d, *J* = 8.8 Hz, 1H), 6.89 (d, *J* = 2.5 Hz, 1H), 6.72 (dd, *J* = 8.8, 2.5 Hz, 1H), 6.57 (s, 1H), 3.44 (t, *J* = 8.4 Hz, 1H), 3.16 (ddd, *J* = 9.5, 7.4, 2.7 Hz, 1H), 2.41 (dd, *J* = 9.5, 8.4, 1H), 2.32 (s, 3H), 2.29 – 2.10 (m, 2H), 2.09 – 1.81 (m, 2H); **^{13}C NMR** (75 MHz, CD_3OD): δ 157.55, 152.90, 149.53, 128.97, 112.34, 110.62, 105.08, 103.99, 63.89, 56.14, 39.33, 29.80, 21.95.

2-bromo-6-hydroxybenzofuran (10)

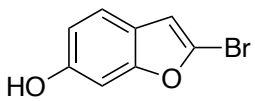

Molecular Weight: 213,03

Procedure adapted from literature.[147] A solution of CBr_4 (9.60 g, 28.96 mmol) in ACN was added dropwise to a suspension of 2,4-dihydroxybenzaldehyde (1.00 g, 7.24 mmol), PPh_3 (7.6 g, 28.96 mmol) and Zn powder (1.89 g, 28.96 mmol) in ACN at rt under N_2. The resulting suspension was stirred at rt for 30 min. Then, NH_4Cl (1.94 g, 36.20 mmol) was added, and the mixture was stirred vigorously until it became a clear solution. Cs_2CO_3 (11.79 g, 36.10 mmol) and CuI (138 mg, 0.72 mmol, 10 mol%) were added and the suspension was stirred and heated

at reflux for 3 h. Then, the suspension was allowed to cool to rt, filtered through Celite® and evaporated under reduced pressure to give the crude product. Purification by flash column chromatography with 9:1 cyclohexane-ethyl acetate as eluent gave 2-bromo-6-hydroxybenzofuran (**10**) (655 mg, 3.08 mmol, 43%) as a white solid, **mp** decomposes at 50 °C; R_f (Cyclohexane/EtOAc 7:3) 0.46; **^{1}H NMR** (300 MHz, $CDCl_3$): δ 7.33 (d, *J* = 8.4 Hz, 1H), 6.95 (d, *J* = 2.2 Hz, 1H), 6.77 (dd, *J* = 8.4, 2.2 Hz, 1H), 6.64 (s, 1H), 4.81 (br s, 1H, exchange with D_2O).

2-bromo-6-benzyloxybenzofuran (12)

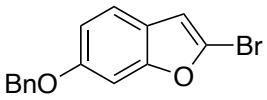

Molecular Weight: 303.16

Using the general procedure **A**, a mixture of 2-bromo-benzofuran-6-ol (**10**) (580 mg, 2.72 mmol), NaH (72 mg, 2.99 mmol) and BnBr (0.65 mL, 5.45 mmol) in anhydrous THF (7 mL) gave the crude product as an orange oil. Purification by flash column chromatography with cyclohexane as eluent gave 2-bromo-6-benzyloxybenzofuran (**12**) (690 mg, 2.28 mmol, 84%) as a colourless oil; R_f (cyclohexane) 0.20; **^{1}H NMR** (300 MHz, $CDCl_3$): δ 7.48 – 7.30 (m, 6H), 7.05 (d, *J* = 2.3 Hz, 1H), 6.94 (dd, *J* = 8.6, 2.3 Hz, 1H), 6.64 (s, 1H), 5.09 (s, 2H).

2-(*N*-*tert*-butoxycarbonyl-2'-pyrrolidinyl)-6-benzyloxybenzofuran (16)

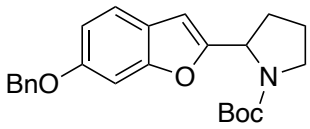

Molecular Weight: 393.48

Using the general procedure **C**, a mixture of *N*-Boc-pyrrolidine (**7**) (500 mg, 2.92 mmol), *s*-BuLi (2.9 mL of a 1.3 M solution in hexane, 3.8 mmol), $ZnCl_2$ (1.8 mL of a 1.0 M solution in Et_2O, 1.75 mmol), $Pd(OAc)_2$ (65 mg, 0.29 mmol), $^tBu_3PHBF_4$ (106 mg, 0.37 mmol) and 2-bromo-6-benzyloxybenzofuran (**12**) (620 mg, 2.04 mmol) in anhydrous THF (10 mL) gave the crude product. Purification by flash column chromatography with 10:0 to 9:1 cyclohexane-ethyl acetate as eluent gave 2-(*N*-*tert*-butoxycarbonyl-2'-pyrrolidinyl)-6-benzyloxybenzofuran (**16**)

(180 mg, 0.46 mmol, 16%) as a yellow oil; R_f (Cyclohexane/EtOAc 8:2) 0.45; **^{1}H NMR** (300 MHz, $CDCl_3$): δ 7.54 – 7.29 (m, 6H), 7.03 (d, *J* = 2.2 Hz, 1H), 6.91 (d, *J* = 8.3 Hz, 1H), 6.45 (br s, 1H), 5.09 (s, 2H), 5.08 – 4.83 (m, 1H), 3.67 – 3.35 (m, 2H), 2.30 – 1.98 (m, 2H), 1.98 – 1.88 (m, 2H), 1.46 (s, 9H).

2-(6-(benzyloxybenzofuran-2-yl)-1-methylpyrrolidine (20)

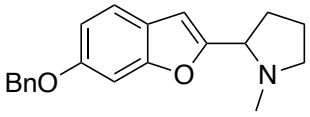

Molecular Weight: 307.39

Using the general procedure **D**, a mixture of HCl in MeOH (3 mL of a 1.25 M solution) and tert-butyl 2-(6-(benzyloxy)benzofuran-2-yl)pyrrolidine-1-carboxylate (**16**) (63 mg, 0.16 mmol) in MeOH (3 mL) gave 2-(6-(benzyloxy)benzofuran-2-yl)pyrrolidine as a brown oil. Then, 2-(6-(benzyloxy)benzofuran-2-yl)pyrrolidine (32 mg, 0.11 mmol), 37% $HCHO_{(aq)}$ (0.1 mL) and pic-BH_3 (12 mg, 0.11 mmol) in MeOH (2 mL) and AcOH (60 µL) gave the crude product. Purification by flash column chromatography with 1:1 cyclohexane-ethyl acetate and 0.5% TEA as eluent gave 2-(6-(benzyloxybenzofuran-2-yl)-1-methylpyrrolidine (**20**) (20 mg, 0.07 mmol, 60%) as orange oil; R_f (Cyclohexane/EtOAc 1:1 + 0.5% TEA) 0.18; **^{1}H NMR** (300 MHz, $CDCl_3$): δ 7.54 – 7.29 (m, 6H), 7.07 (d, *J* = 2.2 Hz, 1H), 6.91 (dd, *J* = 8.4, 2.2 Hz, 1H), 6.50 (s, 1H), 5.09 (s, 2H), 3.36 – 3.18 (m, 2H), 2.54 – 2.39 (m, 1H), 2.40 – 2.25 (m, 4H), 2.15 (dd, *J* = 8.1, 7.4 Hz, 2H), 2.09 – 1.95 (m, 1H).

2-(6-hydroxybenzofuran-2-yl)-1-methylpyrrolidine (2)

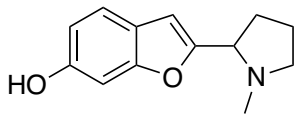

Molecular Weight: 217.27

Using the general procedure **E**, a mixture of 2-(6-(benzyloxy)benzofuran-2-yl)-1-methylpyrrolidine (**20**) (60 mg, 0.20 mmol) and 10% Pd/C (15 mg) in MeOH (9 mL) gave the crude product. Purification by flash column chromatography with 9:1 DCM-MeOH and 0.1%

$NH_{3(22\% \text{ in water})}$ as eluent gave 2-(6-hydroxybenzofuran-2-yl)-1-methylpyrrolidine (**2**) (33 mg, 0.15 mmol, 78%) as a light yellow oil; R_f (DCM/MeOH 9:1 + 0.1% $NH_{3(22\% \text{ in water})}$) 0.42; **^{1}H NMR** (300 MHz, CD_3OD): δ 7.31 (d, *J* = 8.4 1H), 6.85 (d, *J* = 2.2, 1H), 6.71 (dd, *J* = 8.4, 2.2 Hz, 1H), 6.60 (s, 1H), 3.47 (t, *J* = 8.3 Hz, 1H), 3.23 – 3.12 (m, 1H), 2.51 – 2.36 (m, 1H), 2.33 (s, 3H), 2.25 – 2.14 (m, 2H), 2.07 – 1.87 (m, 2H); **^{13}C NMR** (75 MHz, CD_3OD): δ 156.14, 155.22, 154.75, 120.49, 111.57, 104.25, 104.19, 97.09, 63.90, 56.06, 39.20, 29.54, 21.86.

2-bromo-5-methoxybenzofuran (15)

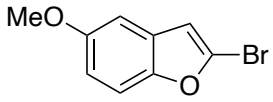

Molecular Weight: 227.06

Using the general procedure **B**, a mixture of 2-bromo-benzofuran-5-ol (**11**) (870 mg, 4.08 mmol), NaH (108 mg, 4.49 mmol) and MeI (0.51 mL, 8.17 mmol) in anhydrous THF (15 mL) gave the crude product as an orange oil. Purification by flash column chromatography with 9:1 petroleum ether-DCM as eluent gave 2-bromo-5-methoxybenzofuran (**15**) (800 mg, 3.52 mmol, 86%) as a pale-yellow oil; R_f (petroleum ether) 0.23; **^{1}H NMR** (300 MHz, $CDCl_3$): δ 7.33 (d, *J* = 9.0 Hz, 1H), 6.96 (d, *J* = 2.6 Hz, 1H), 6.85 (dd, *J* = 9.0, 2.6 Hz, 1H), 6.66 (s, 1H), 3.83 (s, 3H).

2-(*N*-*tert*-butoxycarbonyl-2'-pyrrolidinyl)-5-methoxybenzofuran (18)

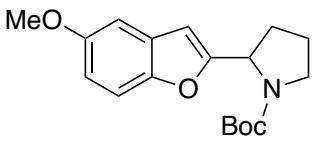

Molecular Weight: 317.39

Using the general procedure **C**, a mixture of *N*-Boc-pyrrolidine (**7**) (310 mg, 1.81 mmol), *s*-BuLi (1.8 mL of a 1.3 M solution in hexane, 2.35 mmol), $ZnCl_2$ (1.1 mL of a 1.0 M solution in Et_2O, 1.09 mmol), $Pd(OAc)_2$ (41 mg, 0.18 mmol), $^tBu_3PHBF_4$ (66 mg, 0.23 mmol) and 2-bromo-5-methoxybenzofuran (**15**) (288 mg, 1.27 mmol) in anhydrous THF (10 mL) gave the crude product. Purification by flash column chromatography with 10:0 to 9:1 cyclohexane-ethyl

acetate as eluent gave 2-(*N*-*tert*-butoxycarbonyl-2'-pyrrolidinyl)-5-methoxybenzofuran (**18**) (100 mg, 0.32 mmol, 17%) as a yellow oil; R_f (Cyclohexane/EtOAc 8:2) 0.38; **^{1}H NMR** (300 MHz, $CDCl_3$): δ 7.34 – 7.24 (m, 1H), 7.00 – 6.93 (m, 1H), 6.88 – 6.76 (m, 1H), 6.39 (br s, 1H), 5.05 – 4.90 (m, 1H), 3.83 (s, 3H), 3.67 – 3.39 (m, 2H), 2.28 – 2.02 (m, 2.45H), 2.01 – 1.86 (m, 2H), 1.46 (s, 9H).

2-(5-methoxybenzofuran-2-yl)-1-methylpyrrolidine (3)

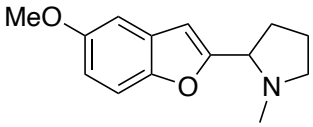

Molecular Weight: 231.30

Using the general procedure **D**, a mixture of HCl in MeOH (6 mL of a 1.25 M solution) and tert-butyl 2-(5-methoxybenzofuran-2-yl)pyrrolidine-1-carboxylate (**18**) (84 mg, 0.27 mmol) in MeOH (3 mL) gave 2-(5-(benzyloxy)benzofuran-2-yl)pyrrolidine as a light yellow oil. Then, 2-(5-methoxybenzofuran-2-yl)pyrrolidine (57 mg, 0.27 mmol), 37% $HCHO_{(aq)}$ (0.2 mL) and pic-BH_3 (28 mg, 0.27 mmol) in MeOH (8 mL) and AcOH (120 µL) gave the crude product. Purification by flash column chromatography with 98:2 DCM-MeOH and 0.5% $NH_{3(22\% \text{ in water})}$ as eluent gave 2-(5-methoxybenzofuran-2-yl)-1-methylpyrrolidine (**3**) (22 mg, 0.1 mmol, 37%) as pale-yellow oil; R_f (DCM/MeOH 9:1 + 0.1% $NH_{3(22\% \text{ in water})}$) 0.33; **^{1}H NMR** (300 MHz, $CDCl_3$): δ 7.34 (d, *J* = 8.9 Hz, 1H), 6.98 (d, *J* = 2.6 Hz, 1H), 6.84 (dd, *J* = 8.9, 2.6 Hz, 1H), 6.53 (s, 1H), 3.83 (s, 3H), 3.35 (t, *J* = 8.0 Hz, 1H), 3.28 – 3.20 (m, 1H), 2.43 – 2.28 (m, 4H), 2.16 (qd, *J* = 8.0, 2.4 Hz, 2H), 2.09 – 1.96 (m, 1H), 1.93 – 1.80 (m, 1H); **^{13}C NMR** (75 MHz, $CDCl_3$): δ 159.19, 155.78, 150.02, 128.87, 112.20, 111.66, 103.95, 103.24, 64.22, 56.78, 55.92, 40.50, 30.98, 22.70.

2-bromo-6-methoxybenzofuran (14)

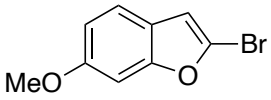

Molecular Weight: 227.06

Using the general procedure **B**, a mixture of 2-bromo-benzofuran-6-ol (**10**) (400 mg, 1.88 mmol), NaH (50 mg, 2.06 mmol) and MeI (0.23 mL, 3.76 mmol) in anhydrous THF (7 mL) gave the crude product as an orange oil. Purification by flash column chromatography with 9:1 cyclohexane-ethyl acetate as eluent gave 2-bromo-6-methoxybenzofuran (**14**) (300 mg, 1.32 mmol, 70%) as a colourless oil; $\boldsymbol{R_f}$ (petroleum ether) 0.23; **^{1}H NMR** (300 MHz, $CDCl_3$): δ 7.36 (d, *J* = 8.6 Hz, 1H), 6.99 (d, *J* = 2.2 Hz, 1H), 6.86 (dd, *J* = 8.6, 2.2 Hz, 1H), 6.64 (s, 1H), 3.84 (s, 3H).

2-(*N*-*tert*-butoxycarbonyl-2'-pyrrolidinyl)-6-methoxybenzofuran (19)

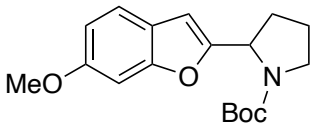

Molecular Weight: 317.39

Using the general procedure **C**, a mixture of *N*-Boc-pyrrolidine (**7**) (365 mg, 2.13 mmol), *s*-BuLi (2.1 mL of a 1.3 M solution in hexane, 2.77 mmol), $ZnCl_2$ (1.3 mL of a 1.0 M solution in Et_2O, 1.28 mmol), $Pd(OAc)_2$ (24 mg, 0.11 mmol), $^tBu_3PHBF_4$ (39 mg, 0.13 mmol) and 2-bromo-6-methoxybenzofuran (**14**) (339 mg, 1.49 mmol) in anhydrous THF (10 mL) gave the crude product. Purification by flash column chromatography with 10:0 to 9:1 cyclohexane-ethyl acetate as eluent gave tert-butyl 2-(*N*-*tert*-butoxycarbonyl-2'-pyrrolidinyl)-6-methoxybenzofuran (**19**) (70 mg, 0.22 mmol, 10%) as a yellow oil; $\boldsymbol{R_f}$ (Cyclohexane/EtOAc 8:2) 0.38; **^{1}H NMR** (300 MHz, $CDCl_3$): δ 7.40 – 7.29 (m, 1H), 7.02 – 6.93 (m, 1H), 6.88 – 6.74 (m, 1H), 6.38 (br s, 1H), 5.03 – 4.80 (m, 1H), 3.82 (s, 3H), 3.69 – 3.36 (m, 2H), 2.31 – 1.98 (m, 2H), 1.97 – 1.88 (m, 2H), 1.52 – 1.38 (m, 9H).

2-(6-methoxybenzofuran-2-yl)-1-methylpyrrolidine (4)

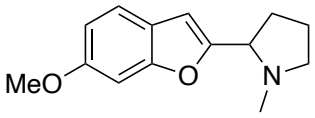

Molecular Weight: 231.30

$LiAlH_4$ (107 mg, 2.84 mmol) was added to a solution of 2-(6-methoxybenzofuran-2-yl)-1-methypyrrolidine (**19**) (300 mg, 0.95 mmol) in anhydrous THF (5 mL) at 0 °C and the resulting solution was stirred for 20 min. Then, the reaction mixture was stirred and heated at reflux for 3 h. MeOH (5 mL) and H_2O (5 mL) were added dropwise to the solution at 0 °C. The two layers were separated, and the aqueous layer was extracted with EtOAc (3 × 5 mL). The combined organic layers were dried (Na_2SO_4) and concentrated under reduced pressure to give the crude product as a brown oil. Purification by flash column chromatography with 9:1 cyclohexane-acetone as eluent gave 2-(6-methoxybenzofuran-2-yl)-1-methylpyrrolidine (**4**) (30 mg, 0.13 mmol, 14%) as an light yellow oil; $\boldsymbol{R_f}$ (DCM/MeOH 9:1 + 0.1% $NH_{3(22\% \text{ in water})}$) 0.33; **^{1}H NMR** (300 MHz, $CDCl_3$): δ 7.36 (d, *J* = 8.4 Hz, 1H), 7.02 (d, *J* = 2.3 Hz, 1H), 6.83 (dd, *J* = 8.4, 2.3 Hz, 1H), 6.51 (s, 1H), 3.82 (s, 3H), 3.32 (t, *J* = 8.1 Hz, 1H), 3.28 – 3.17 (m, 1H), 2.44 – 2.23 (m, 4H), 2.22 – 2.08 (m, 2H), 2.07 – 1.96 (m, 1H), 1.95 – 1.76 (m, 1H); **^{13}C NMR** (75 MHz, $CDCl_3$): δ 157.59, 157.07, 156.01, 121.58, 120.56, 111.35, 103.72, 96.19, 64.16, 56.73, 55.68, 40.43, 30.80, 22.63.

2-(benzofuran-2-yl)pyrrolidine (22)

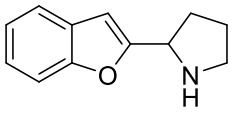

Molecular Weight: 187.24

Procedure adapted from literature.[148] n-BuLi (1.7 mL of a 2.5 M solution in hexanes, 4.24 mmol) was added dropwise to a stirred solution of the 1-benzofuran (500 mg, 4.24 mmol) in anhydrous THF (6 mL) at –78 °C under N_2. The resulting mixture was stirred at –78 °C for 30 min, to give the corresponding lithiated benzofuran solution. n-BuLi (1.1 mL of a 2.5 M solution in hexanes, 2.83 mmol) was added dropwise to a stirred solution of pyrrolidine (201 mg, 2.83

mmol) in anhydrous Et_2O (5 mL) at –78 °C under N_2. The resulting solution was stirred at –78 °C for 10 min. To this solution was then added via cannula a solution of benzophenone (618 mg, 3.39 mmol) in anhydrous Et_2O (5 mL). The resulting mixture was stirred at –78 °C for 10 min and added to the stirred solution of the organometallic nucleophile (4.24 mmol) in one portion, followed immediately by the addition of $BF_3{\cdot}Et_2O$ (3.4 mL of a 1 M solution in THF, 3.39 mmol). Subsequently, the reaction vessel was taken out of the low temperature bath and stirred at rt for 2 h. The reaction mixture was then cooled to 0 °C and quenched with MeOH (1 mL). The resulting mixture was diluted with Et_2O (20 mL) and washed with NaOH 1 M (20 mL). The aqueous layer was extracted with Et_2O (3 x 20 mL) and the combined organic layers were washed with brine (30 mL), dried (Na_2SO_4), and evaporated under reduced pressure to give the crude product. Purification by flash column chromatography with 95:5 DCM-MeOH and 0.1% $NH_{3(22\%\ in\ water)}$ as eluent gave 2-(benzofuran-2-yl)-1-pyrrolidine (**22**) (38 mg, 0.20 mmol, 7%) as an pale-yellow oil; $\boldsymbol{R_f}$ (DCM/MeOH 95:5 + 0.1% $NH_{3\ (22\%\ in\ water)}$) 0.21; **^{1}H NMR** (300 MHz, $CDCl_3$): δ 7.52 – 7.47 (m, 1H), 7.45 – 7.40 (m, 1H), 7.29 – 7.12 (m, 2H), 6.53 (s, 1H), 4.36 (t, *J* = 6.7 Hz, 1H), 3.21 – 3.11 (m, 1H), 3.03 (ddd, *J* = 10.0, 7.7, 5.8 Hz, 1H), 2.36 – 2.11 (m, 1H), 2.08 – 1.79 (m, 3H).[148]

2-(benzofuran-2-yl)-1-methylpyrrolidine (5)

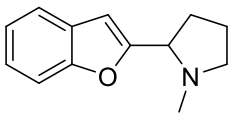

Molecular Weight: 201.27

Using the general procedure **D**, a mixture of 2-(benzofuran-2-yl)pyrrolidine (**22**) (137 mg, 0.73 mmol), 37% $HCHO_{(aq)}$ (0.1 mL) and pic-BH_3 (78 mg, 0.73 mmol) in MeOH (5 mL) and AcOH (172 µL) gave the crude product. Purification by flash column chromatography with 95:5 DCM-MeOH and 0.1% $NH_{3(22\%\ in\ water)}$ as eluent gave 2-(benzofuran-2-yl)-1-methylpyrrolidine (**5**) (91 mg, 0.45 mmol, 62%) as an pale-yellow oil; $\boldsymbol{R_f}$ (Cyclohexane/EtOAc 8:2 + 0.1% $NH_{3\ (22\%\ in\ water)}$) 0.25; **^{1}H NMR** (300 MHz, $CDCl_3$): δ 7.54 – 7.43 (m, 2H), 7.27 – 7.15 (m, 2H), 6.58 (s, 1H), 3.37 (t, *J* = 8.1 Hz, 1H), 3.25 (ddd, *J* = 9.9, 7.7, 2.5 Hz, 1H), 2.41 – 2.30 (m, 4H), 2.23 – 2.13 (m, 2H),

2.12 – 1.97 (m, 1H), 1.93 – 1.77 (m, 1H); **^{13}C NMR** (75 MHz, $CDCl_3$): δ 158.32, 155.06, 128.36, 123.68, 122.50, 120.54, 111.31, 103.82, 64.19, 56.81, 40.53, 31.00, 22.70.

3-bromo-benzofuran (23)

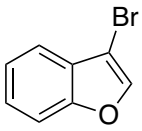

Molecular Weight: 197.03

Procedure adapted from literature.[149] A solution of Br_2 (1.1 ml, 21.2 mmol) in DCM (5 mL) was added dropwise to a stirred solution of benzofuran (2.21 g, 20.0 mmol) in DCM (20 mL) at –10 °C and the resulting mixture was stirred at rt for 1 h. Then, NaOH 1 M (1 mL) was added. The solution was washed with H_2O (5 mL) and $Na_2S_2O_3$ (5 mL), and the combined aqueous layers were extracted with DCM (3 x 5 mL). The combined organic layers were dried (Na_2SO_4) and evaporated under reduced pressure, the crude was dissolved in EtOH (20 mL) and the saturated solution of KOH in EtOH (20 mL) was added dropwise at 0 °C. The mixture was stirred at reflux for 2h. Then, the solution was allowed to cool to rt, H_2O (10 mL) was added, EtOH was concentrated under reduced pressure and the mixture was extracted with EtOAc (3 x 5 mL). The combined organic layers were washed with brine (10 mL), dried (Na_2SO_4) and evaporated under reduced pressure to give 3-bromo-benzofuran (**23**) (2.19 g, 11.2 mmol, 56%) as a yellow oil; R_f (petroleum ether) 0.75; **^{1}H NMR** (300 MHz, $CDCl_3$): δ 7.66 (s, 1H), 7.59 – 7.54 (m, 1H), 7.53 – 7.47 (m, 1H), 7.40 – 7.28 (m, 2H).

3-(*N*-*tert*-butoxycarbonyl-2'-pyrrolidinyl)benzofuran (24)

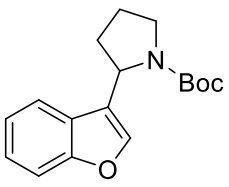

Molecular Weight: 287.36

Using the general procedure **C**, a mixture of *N*-Boc-pyrrolidine (**7**) (500 mg, 2.92 mmol), *s*-BuLi (2.9 mL of a 1.3 M solution in hexane, 3.80 mmol), $ZnCl_2$ (1.8 mL of a 1.0 M solution in Et_2O,

1.75 mmol), $Pd(OAc)_2$ (65 mg, 0.29 mmol), $^tBu_3PHBF_4$ (106 mg, 0.37 mmol) and 3-bromo-benzofuran (**23**) (402 mg, 2.04 mmol) in anhydrous THF (10 mL) gave the crude product. Purification by flash column chromatography with 10:0 to 9:1 cyclohexane-ethyl acetate as eluent gave 3-(*N*-*tert*-butoxycarbonyl-2'-pyrrolidinyl)benzofuran (**24**) (180 mg, 0.46 mmol, 16%) as a light yellow oil; R_f (Cyclohexane/EtOAc 8:2) 0.32; **^{1}H NMR** (300 MHz, $CDCl_3$): δ 7.55 – 7.49 (m, 1H), 7.48 – 7.42 (m, 1H), 7.38 (s, 1H), 7.32 – 7.14 (m, 2H), 5.18 – 4.98 (m, 1H), 3.67 – 3.41 (m, 2H), 2.00 – 1.72 (m, 4H), 1.45 (m, 9H).

2-(benzofuran-3-yl)-1-methylpyrrolidine (6)

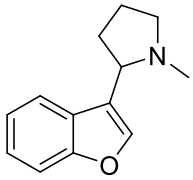

Molecular Weight: 201.27

Using the general procedure **D**, a mixture of HCl in MeOH (5 mL of a 1.25 M solution) and tert-butyl 2-(benzofuran-3-yl)pyrrolidine-1-carboxylate (**24**) (185 mg, 0.64 mmol) in MeOH (3 mL) gave 2-(benzofuran-3-yl)pyrrolidine as a brown oil. Then, 2-(benzofuran-3-yl)pyrrolidine (40 mg, 0.21 mmol), 37% $HCHO_{(aq)}$ (0.1 mL) and pic-BH_3 (23 mg, 0.21 mmol) in MeOH (3 mL) and AcOH (80 µL) gave the crude product. Purification by flash column chromatography with 98:2 DCM-MeOH and 0.1% $NH_{3(22\% \text{ in water})}$ as eluent gave 2-(benzofuran-3-yl)-1-methylpyrrolidine (**6**) (11 mg, 0.06 mmol, 26%) as an light yellow oil; R_f (DCM/MeOH 9:1 + 0.1% $NH_{3\ (22\% \text{ in water})}$) 0.41; **^{1}H NMR** (300 MHz, $CDCl_3$): δ 7.70 (dd, *J* = 7.4, 1.6 Hz, 1H), 7.57 (s, 1H), 7.53 – 7.42 (m, 1H), 7.34 – 7.15 (m, 2H), 3.37 (t, *J* = 8.0 Hz, 1H), 3.33 – 3.20 (m, 1H), 2.40 – 2.16 (m, 5H), 2.11 – 1.95 (m, 2H), 1.95 – 1.74 (m, 1H); **^{13}C NMR** (75 MHz, $CDCl_3$): δ 155.77, 141.95, 126.99, 124.17, 122.28, 121.69, 120.62, 111.48, 62.16, 57.02, 40.67, 32.33, 22.54.

6.2. Part 2

General procedure for amidoximes 76 and 103-106 synthesis (F)

Procedure adapted form literature.[150] Hydroxylamine hydrochloride (2.0 eq) and $NaHCO_3$ (1.0 eq) were dissolved in H_2O (20 mL) and the mixture was stirred until no effervescence occurred.

Then, nitrile (1.3 eq) dissolved in EtOH (20 mL) was added. The resulting solution was stirred and heated at reflux for 3 h. Then, the solution was allowed to cool to rt, and ethanol was concentrated under reduce pressure. The aqueous residue was extracted with EtOAc (3 x 20 mL). The combined organics were dried (Na_2SO_4) and evaporated under reduced pressure to give the crude product used for the next reaction without further purification.

General procedure for acyl chloride 77-98 and 107 synthesis (G)

Procedure adapted form literature.[151] Carboxylic acid (1.0 eq) was dissolved in $SOCl_2$ (20 mL), and the mixture was stirred and heated at reflux for 2 h. Then, the solution was allowed to cool to rt and evaporated under reduced pressure to give the crude acyl chloride used for the next reaction without further purification.

General procedure for the condensation for compounds 25-42 and 44-51 (H)

Procedure adapted form literature.[112] Acyl chloride (1.2 eq) dissolved in toluene or pyridine (20 mL) was slowly added to a suspension of amidoxime (1.0 eq) in toluene or pyridine (80 mL). The resulting mixture was stirred and heated at reflux overnight. Then, the solution was allowed to cool to rt, concentrated under reduce pressure and washed with HCl 1M (2 x 10 mL), saturated $NaHCO_3$ solution (2 x 10 mL) and brine (2 x 10 mL). The combined organics were dried (Na_2SO_4) and evaporated under reduced pressure to give the crude product.

***N*-hydroxynicotinimidamide (76)**

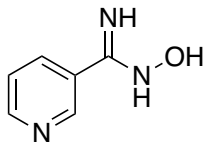

Molecular Weight: 137.14

Using the general procedure **F**, a mixture of $NH_2OH{\cdot}HCl$ (3.48 g, 50.00 mmol), $NaHCO_3$ (2.65 g, 25.00 mmol), 3-cyanopyridine (3.4 g, 33.00 mmol) in H_2O (20 mL) and EtOH (20 mL) gave the crude product. Purification by crystallization in DCM (10 mL) gave *N*-hydroxynicotinimidamide (**76**) (2.5 g, 18.3 mmol, 55%) as a white solid, **mp** 131.5-132.9 °C (lit., [152]133.0-134.0 °C); R_f (DCM/MeOH 9:1) 0.40; **^{1}H NMR** (300 MHz, DMSO-*d6*): δ 9.80 (bs, 1H, exchange with D_2O),

8.84 (dd, *J* = 2.3, 0.9 Hz, 1H), 8.54 (dd, *J* = 4.8, 1.7 Hz, 1H), 7.99 (ddd, *J* = 8.0, 2.3, 1.7 Hz, 1H), 7.38 (ddd, *J* = 8.0, 4.8, 0.9 Hz, 1H), 5.94 (bs, 2H, exchange with D_2O).[150]

Benzoyl chloride (77)

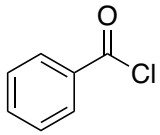

Molecular Weight: 140.57

Using the general procedure **G**, a mixture of benzoic acid (300 mg, 2.46 mmol) in $SOCl_2$ (7 mL) gave benzoyl chloride (**77**) (345 mg, 2.45 mmol, 100%) as a clear oil used for the next reaction without further purification.

5-phenyl-3-(pyridin-3-yl)-1,2,4-oxadiazole (25)

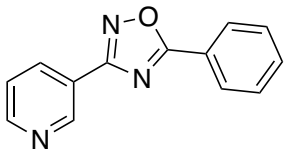

Molecular Weight: 223.24

Using the general procedure **H**, a mixture of benzoyl chloride (**77**) (362 mg, 2.64 mmol), *N*-hydroxynicotinimidamide (**76**) (460 mg, 3.27 mmol) in pyridine (30 mL) gave the crude product. Purification by flash column chromatography with 8:2 petroluem ether-ethyl acetate as eluent gave 5-phenyl-3-(pyridin-3-yl)-1,2,4-oxadiazole (**25**) (380 mg, 1.70 mmol, 52%) as a white solid, **mp** 138.6-141.0 °C (lit., [153]138.1-138.3 °C); $\boldsymbol{R_f}$ (Cyclohexane/EtOAc 8:2) 0.21; **^{1}H NMR** (300 MHz, $CDCl_3$): δ 9.41 (dd, *J* = 2.2, 0.9 Hz, 1H), 8.77 (dd, *J* = 4.9, 1.7 Hz, 1H), 8.45 (ddd, *J* = 8.0, 2.2, 1.7 Hz, 1H), 8.29 – 8.12 (m, 2H), 7.68 – 7.52 (m, 4H), 7.46 (ddd, *J* = 8.0, 4.9, 0.9 Hz, 1H); **^{13}C NMR** (75 MHz, $CDCl_3$): δ 176.13, 167.00, 151.99, 148.70, 134.73, 133.00, 129.16, 128.20, 123.92, 123.62, 123.25.[153]; **MS (ESI$^+$)** *m/z* calcd for $C_{13}H_9N_3O$ $(M+H)^+$ 224.08, found 224.1

4-cyanbenzoyl chloride (78)

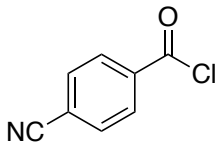

Molecular Weight: 165.58

Using the general procedure **G**, a mixture of 4-cyanobenzoic acid (300 mg, 2.04 mmol) in $SOCl_2$ (5 mL) gave 4-cyanobenzoyl chloride (**78**) (337 mg, 2.04 mmol, 100%) as a white solid used for the next reaction without further purification.

5-(4-cyanophenyl)-3-(pyridin-3-yl)-1,2,4-oxadiazole (26)

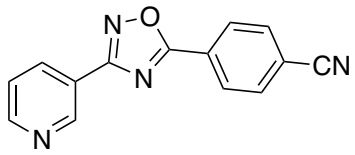

Molecular Weight: 248.25

Using the general procedure **H**, a mixture of 4-cyanobenzoyl chloride (**78**) (360 mg, 2.17 mmol), *N*-hydroxynicotinimidamide (**76**) (239 mg, 1.74 mmol) in pyridine (25 mL) gave the crude product. Purification by crystallization in *i*PrOH gave 5-(4-cyanophenyl)-3-(pyridin-3-yl)-1,2,4-oxadiazole (**26**) (276 mg, 1.11 mmol, 51%) as a white solid, **mp** 179.9-180.8 °C; R_f (Cyclohexane/EtOAc 7:3) 0.21; **^{1}H NMR** (300 MHz, $CDCl_3$): δ 9.41 (s, 1H), 8.85 – 8.73 (m, 1H), 8.45 (d, *J* = 6.5 Hz, 1H), 8.41 – 8.31 (m, 2H), 7.94 – 7.83 (m, 2H), 7.49 (t, *J* = 6.5 Hz, 1H); **^{13}C NMR** (75 MHz, $CDCl_3$): 174.38, 167.44, 152.37, 148.72, 134.75, 132.96, 128.72, 127.59, 123.76, 122.74, 117.64, 116.50; **MS (ESI$^+$)** *m/z* calcd for $C_{14}H_8N_4O$ $(M+H)^+$ 249.08, found 249.1.

Picolinoyl chloride (79)

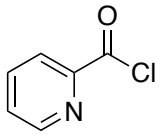

Molecular Weight: 141.55

Using the general procedure **G**, a mixture of picolinic acid (300 mg, 2.44 mmol) in $SOCl_2$ (6 mL) gave picolinoyl chloride (**79**) (345 mg, 2.44 mmol, 100%) as a brown solid used for the next reaction without further purification.

5-(pyridin-2-yl)-3-(pyridin-3-yl)-1,2,4-oxadiazole (27)

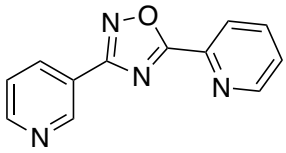

Molecular Weight: 224.22

Using the general procedure **H**, a mixture of picolinoyl chloride (**79**) (340 mg, 2.40 mmol), *N*-hydroxynicotinimidamide (**76**) (264 mg, 1.92 mmol) in pyridine (30 mL) gave the crude product. Purification by flash column chromatography with 7:3 to 6:4 DCM-ethyl acetate as eluent gave 5-(pyridin-2-yl)-3-(pyridin-3-yl)-1,2,4-oxadiazole (**27**) (174 mg, 0.78 mmol, 32%) as a white solid, **mp** 131.7-133.3 °C; R_f (DCM/MeOH 95:5) 0.37; **^{1}H NMR** (300 MHz, $CDCl_3$): δ 9.43 (dd, *J* = 2.2, 0.8 Hz, 1H), 8.87 (ddd, *J* = 4.8, 1.8, 0.8 Hz, 1H), 8.76 (dd, *J* = 4.9, 1.8 Hz, 1H), 8.53 – 8.43 (m, 1H), 8.30 (dd, *J* = 7.9, 1.1 Hz, 1H), 7.95 (td, *J* = 7.9, 1.8 Hz, 1H), 7.60 – 7.48 (m, 1H), 7.45 (ddd, *J* = 7.9, 4.9, 0.8 Hz, 1H); **^{13}C NMR** (75 MHz, $CDCl_3$): δ 174.81, 167.32, 152.13, 150.82, 148.73, 143.35, 137.44, 134.95, 126.93, 124.35, 123.69, 122.96; **MS (ESI$^+$)** *m/z* calcd for $C_{12}H_8N_4O$ $(M+H)^+$ 225.08, found 225.2.

Nicotinoyl chloride (80)

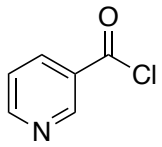

Molecular Weight: 141.55

Using the general procedure **G**, a mixture of nicotinic acid (1.00 g, 8.12 mmol) in $SOCl_2$ (20 mL) gave nicotinoyl chloride (**80**) (1.15 g, 8.12 mmol, 100%) as a white solid used for the next reaction without further purification.

3,5-di(pyridin-3-yl)-1,2,4-oxadiazole (28)

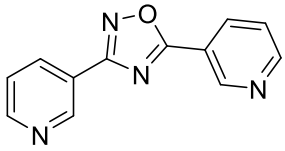

Molecular Weight: 224.22

Using the general procedure **H**, a mixture of nicotinoyl chloride (**80**) (997 mg, 7.04 mmol), *N*-hydroxynicotinimidamide (**76**) (779 mg, 5.68 mmol) in toluene (100 mL) gave the crude product. Purification by flash column chromatography with 8:2 cyclohexane-ethyl acetate as eluent gave 3,5-di(pyridin-3-yl)-1,2,4-oxadiazole (**28**) (600 mg, 2.68 mmol, 47%) as a white solid, **mp** 126.3-127.4 °C (lit., [154]125.0-127.0 °C); R_f (Cyclohexane/EtOAc 1:1) 0.31; **^{1}H NMR** (300 MHz, DMSO-*d6*): δ 9.35 (d, *J* = 1.8 Hz, 1H), 9.26 (d, *J* = 1.8 Hz, 1H), 8.90 (dd, *J* = 4.8, 1.5 Hz, 1H), 8.81 (dd, *J* = 4.8, 1.5 Hz, 1H), 8.56 (dt, *J* = 8.0, 1.8 Hz, 1H), 8.45 (dt, *J* = 8.0, 1.8 Hz, 1H), 7.71 (dd, *J* = 8.0, 4.9 Hz, 1H), 7.65 (dd, *J* = 8.0, 4.9 Hz, 1H); **^{13}C NMR** (75 MHz DMSO-*d6)*: δ 174.60, 167.05, 154.25, 152.99, 148.98, 148.27, 136.07, 135.19, 124.95, 124.83, 122.66, 120.28.[155]; **MS (ESI$^+$)** *m/z* calcd for $C_{12}H_8N_4O$ $(M+H)^+$ 225.08, found 225.0.

Isonicotinoyl chloride (81)

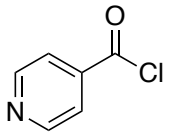

Molecular Weight: 141.55

Using the general procedure **G**, a mixture of isonicotinic acid (300 mg, 2.44 mmol) in $SOCl_2$ (7 mL) gave isonicotinoyl chloride (**81**) (345 mg, 2.44 mmol, 100%) as a white solid used for the next reaction without further purification.

3-(pyridin-3-yl)-5-(pyridin-4-yl)-1,2,4-oxadiazole (29)

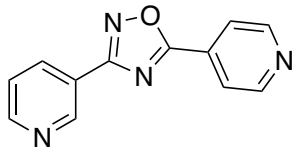

Molecular Weight: 224.22

Using the general procedure **H**, a mixture of isonicotinoyl chloride (**81**) (460 mg, 3.25 mmol), *N*-hydroxynicotinimidamide (**76**) (357 mg, 2.60 mmol) in pyridine (25 mL) gave the crude product. Purification by crystallization in *i*PrOH gave 3-(pyridin-3-yl)-5-(pyridin-4-yl)-1,2,4-oxadiazole (**29**) (296 mg, 1.32 mmol, 41%) as a white solid, **mp** 123.4-125.7 °C; $\boldsymbol{R_f}$ (DCM/MeOH 98:2) 0.44; **^{1}H NMR** (300 MHz, CD_3OD): δ 9.32 (d, *J* = 2.2 Hz, 1H), 8.92 – 8.84 (m, 2H), 8.76 (dd, *J* = 4.9, 1.7 Hz, 1H), 8.58 (dt, *J* = 8.0, 2.0 Hz, 1H), 8.25 – 8.17 (m, 2H), 7.71 – 7.61 (m, 1H); **^{13}C NMR** (75 MHz, CD_3OD): δ 174.34, 167.05, 151.42, 150.37, 147.33, 135.45, 131.41, 124.37, 123.24, 121.60; **MS (ESI$^+$)** *m/z* calcd for $C_{12}H_8N_4O$ $(M+H)^+$ 225.08, found 225.1.

2-nitrobenzoyl chloride (82)

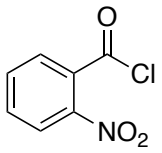

Molecular Weight: 185.56

Using the general procedure **G**, a mixture of 2-nitrobenzoic acid (1.0 g, 5.98 mmol) in $SOCl_2$ (20 mL) gave 3-nitrobenzoyl chloride (**82**) (1.11 g, 5.98 mmol, 100%) as a clear oil used for the next reaction without further purification.

5-(2-nitrophenyl)-3-(pyridin-3-yl)-1,2,4-oxadiazole (30)

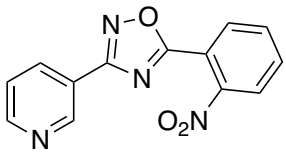

Molecular Weight: 268.23

Using the general procedure **H**, a mixture of 2-nitrobenzoyl chloride (**81**) (617 mg, 3.23 mmol), *N*-hydroxynicotinimidamide (**76**) (400 mg, 9.92 mmol) in pyridine (20 mL) gave the crude product. Purification by crystallization in EtOAc and Et_2O gave 5-(2-nitrophenyl)-3-(pyridin-3-yl)-1,2,4-oxadiazole (**30**) (231 mg, 0.86 mmol, 30%) as a white solid, **mp** 105.2-106.2 °C (lit., [156]104-105 °C); R_f(Cyclohexane/EtOAc 1:1) 0.26; **^{1}H NMR** (300 MHz, $CDCl_3$): δ 9.37 (s, 1H), 8.78 (d, *J* = 4.7 Hz, 1H), 8.41 (dt, *J* = 8.1, 1.8 Hz, 1H), 8.12 – 7.96 (m, 2H), 7.88 – 7.76 (m, 2H), 7.47 (dd, *J* = 8.1, 4.7 Hz, 1H); **^{13}C NMR** (75 MHz, $CDCl_3$): δ 173.00, 167.10, 152.22, 148.77, 148.66, 134.97, 133.28, 133.02, 131.41, 124.76, 123.78, 122.73, 118.83; **MS (ESI$^+$)** *m/z* calcd for $C_{13}H_8N_4O$ $(M+H)^+$ 268.06, found 269.0.

3-nitrobenzoyl chloride (83)

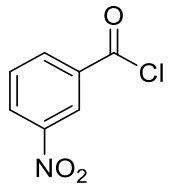

Molecular Weight: 185.56

Using the general procedure **G**, a mixture of 3-nitrobenzoic acid (1.0 g, 5.98 mmol) in $SOCl_2$ (20 mL) gave 3-nitrobenzoyl chloride (**83**) (1.11 g, 5.98 mmol, 100%) as a white solid used for the next reaction without further purification.

5-(3-nitrophenyl)-3-(pyridin-3-yl)-1,2,4-oxadiazole (31)

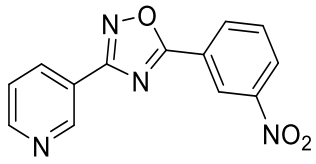

Molecular Weight 268.23

Using the general procedure **H**, a mixture of 3-nitrobenzoyl chloride (**83**) (983 mg, 5.30 mmol), *N*-hydroxynicotinimidamide (**76**) (586 mg, 4.27 mmol) in pyridine (30 mL) gave the crude product. Purification by crystallization in EtOAc gave 5-(3-nitrophenyl)-3-(pyridin-3-yl)-1,2,4-oxadiazole (**31**) (685 mg, 2.55 mmol, 59%) as a light yellow solid, **mp** 137.7-138.6 °C (lit., [157]142.0-144.0 °C); R_f (Cyclohexane/EtOAc 1:1) 0.52; **^{1}H NMR** (300 MHz, $CDCl_3$): δ 9.42 (d, *J* = 1.5 Hz, 1H), 9.09 (s, 1H), 8.80 (dd, *J* = 4.8, 1.5 Hz, 1H), 8.56 (d, *J* = 8.0 Hz, 1H) 8.52 – 8.40 (m, 2H), 7.81 (t, *J* = 8.0 Hz, 1H), 7.48 (dd, *J* = 8.0, 4.8 Hz, 1H)[158]; **^{13}C NMR** (75 MHz, $CDCl_3$): δ 174.03, 167.43, 152.40, 148.76, 134.79, 133.59, 130.58, 127.32, 125.53, 123.73, 123.25, 122.70; **MS (ESI$^+$)** *m/z* calcd for $C_{13}H_8N_4O$ $(M+H)^+$ 268.06, found 269.0.

4-nitrobenzoyl chloride (84)

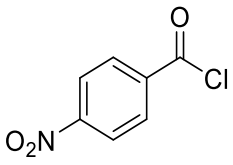

Molecular Weight: 185.56

Using the general procedure **G**, a mixture of 4-nitrobenzoic acid (1.0 g, 5.98 mmol) in $SOCl_2$ (20 mL) gave 4-nitrobenzoyl chloride (**84**) (1.11 g, 5.98 mmol, 100%) as a white solid used for the next reaction without further purification.

5-(4-nitrophenyl)-3-(pyridin-3-yl)-1,2,4-oxadiazole (32)

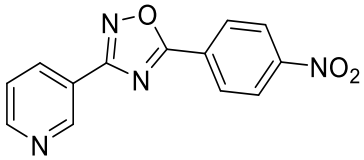

Molecular Weight 268.23

Using the general procedure **H**, a mixture of 4-nitrobenzoyl chloride (**84**) (1.20 g, 6.46 mmol), *N*-hydroxynicotinimidamide (**76**) (715 mg, 5.21 mmol) in toluene (100 mL) gave the crude product. Purification by flash column chromatography with 7:3 cyclohexane-ethyl acetate as eluent gave 5-(4-nitrophenyl)-3-(pyridin-3-yl)-1,2,4-oxadiazole (**32**) (838 mg, 3.13 mmol, 60%) as light-yellow solid, **mp** 178.2-178.5 °C (lit., [159]179.0-181.0 °C); $\boldsymbol{R_f}$ (Cyclohexane/EtOAc 1:1) 0.40; **^{1}H NMR** (300 MHz, $CDCl_3$): δ 9.41 (d, *J* = 1.6 Hz, 1H), 8.80 (dd, *J* = 4.8, 1.6 Hz, 1H), 8.51 – 8.37 (m, 5H), 7.48 (dd, *J* = 8.0, 4.8 Hz, 1H); **^{13}C NMR** (75 MHz, $CDCl_3$): δ 174.12, 167.52, 152.41, 150.38, 148.75, 134.75, 129.30, 129.16, 124.42, 123.72, 122.67; **MS (ESI$^+$)** *m/z* calcd for $C_{13}H_8N_4O$ $(M+H)^+$ 268.06, found 269.1.

3-fluorobenzoyl chloride (85)

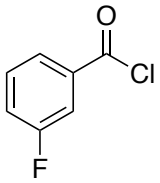

Molecular Weight: 158.56

Using the general procedure **G**, a mixture of 3-fluorobenzoic acid (400 mg, 2.86 mmol) in $SOCl_2$ (7 mL) gave 3-fluorobenzoyl chloride (**85**) (453 mg, 2.86 mmol, 100%) as a clear oil used for the next reaction without further purification.

5-(3-fluorophenyl)-3-(pyridin-3-yl)-1,2,4-oxadiazole (33)

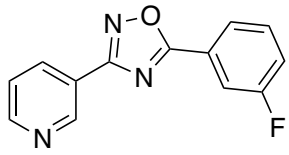

Molecular Weight: 241.23

Using the general procedure **H**, a mixture of 3-fluorobenzoyl chloride (**85**) (455 mg, 2.87 mmol), *N*-hydroxynicotinimidamide (**76**) (394 mg, 2.87 mmol) in pyridine (20 mL) gave the crude product. Purification by flash column chromatography with 7:3 petroleum ether-ethyl acetate gave 5-(3-fluorophenyl)-3-(pyridin-3-yl)-1,2,4-oxadiazole (**33**) (186 mg, 0.77 mmol, 26%) as a light yellow solid, **mp** 112.4-113.3 °C (lit., [160]112-113 °C); $\boldsymbol{R_f}$ (Cyclohexane/EtOAc 7:3) 0.47; 1H NMR (300 MHz, CDCl3): δ 9.38 (d, *J* = 2.1 Hz, 1H), 8.76 (dd, *J* = 4.9, 1.7 Hz, 1H), 8.42 (dt, *J* = 8.0, 2.1 Hz, 1H), 8.01 (dt, *J* = 7.8, 1.2 Hz, 1H), 7.91 (ddd, *J* = 9.0, 2.7, 1.7 Hz, 1H), 7.55 (ddd, *J* = 8.4, 7.8, 5.5 Hz, 1H), 7.45 (dd, *J* = 8.0, 4.9 Hz, 1H), 7.32 (td, *J* = 8.4, 2.7 Hz, 1H); **^{13}C NMR** (75 MHz, $CDCl_3$): δ 175.08, 167.14, 162.81 (d, *J* = 246.8 Hz), 152.12, 148.68, 131.07 (d, *J* = 8.3 Hz), 125.73 (d, *J* = 9.0 Hz), 124.02, 123.69, 123.04, 120.15 (d, *J* = 21.0 Hz), 115.23 (d, *J* = 24.09 Hz); **MS (ESI$^+$)** *m/z* calcd for $C_{13}H_8FN_3O$ $(M+H)^+$ 242.08, found 242.1

4-fluorobenzoyl chloride (86)

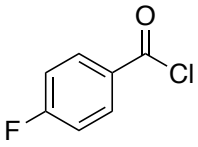

Molecular Weight: 158.56

Using the general procedure **G**, a mixture of 4-fluorobenzoic acid (300 mg, 2.14 mmol) in $SOCl_2$ (6 mL) gave 4-fluorobenzoyl chloride (**86**) (340 mg, 2.14 mmol, 100%) as a clear oil used for the next reaction without further purification.

5-(4-fluorophenyl)-3-(pyridin-3-yl)-1,2,4-oxadiazole (34)

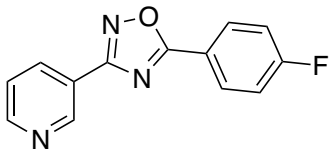

Molecular Weight: 241.23

Using the general procedure **H**, a mixture of 4-fluorobenzoyl chloride (**86**) (340 mg, 2.14 mmol), *N*-hydroxynicotinimidamide (**76**) (294 mg, 2.14 mmol) in pyridine (20 mL) gave the crude product. Purification by flash column chromatography with 7:3 petroleum ether-ethyl acetate gave 5-(4-fluorophenyl)-3-(pyridin-3-yl)-1,2,4-oxadiazole (**34**) (121 mg, 0.50 mmol, 23%) as a white solid, **mp** 144.6-156.4 °C; $\boldsymbol{R_f}$(Cyclohexane/EtOAc 7:3) 0.47; **^{1}H NMR** (300 MHz, CDCl3): δ 9.40 (s, 1H), 8.82 – 8.74 (m, 1H), 8.45 (dt, *J* = 8.2, 1.9 Hz, 1H), 8.30 – 8.21 (m, 2H), 7.48 (ddd, *J* = 8.2, 4.8, 0.9 Hz, 1H), 7.32 – 7.21 (m, 2H).; **^{13}C NMR** (75 MHz, $CDCl_3$): δ 175.29, 166.98, 165.64 (d, *J* = 253.5 Hz), 151.80, 148.46, 134.99, 130.72 (d, *J* = 9.0 Hz), 123.79, 123.30, 120.30 (d, *J* = 3.0 Hz), 116.62 (d, *J* = 21.8 Hz); **MS (ESI$^+$)** *m/z* calcd for $C_{13}H_8FN_3O$ $(M+H)^+$ 242.08, found 242.2.

3,4-difluorobenzoyl chloride (87)

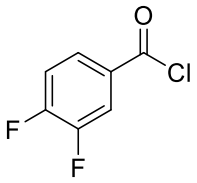

Molecular Weight: 176.55

Using the general procedure **G**, a mixture of 3,4-difluorobenzoic acid (1.00 g, 6.32 mmol) in $SOCl_2$ (20 mL) gave 3,4-difluorobenzoyl chloride (**87**) (1.12 g, 6.32 mmol, 100%) as a white solid used for the next reaction without further purification.

5-(3,4-difluorophenyl)-3-(pyridin-3-yl)-1,2,4-oxadiazole (35)

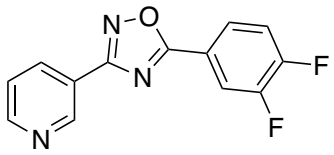

Molecular Weight: 259.22

Using the general procedure **H**, a mixture of 3,4-difluorobenzoyl chloride (**87**) (1.00 g, 5.66 mmol), *N*-hydroxynicotinimidamide (**76**) (626 mg, 4.57 mmol) in pyridine (30 mL) gave the crude product. Purification by flash column chromatography with 1:1 cyclohexane-ethyl acetate as eluent gave 5-(3,4-difluorophenyl)-3-(pyridin-3-yl)-1,2,4-oxadiazole (**35**) (1.10 g, 4.24 mmol, 93%) as an orange solid, **mp** 121.4-122.7 °C (lit., [161]123.0-124.0°C); R_f (Cyclohexane/EtOAc 4:6) 0.58; **^{1}H NMR** (300 MHz, $CDCl_3$): δ 9.39 (s, 1H), 8.78 (dd, *J* = 4.8, 1.6 Hz, 1H), 8.42 (dt, *J* = 8.0, 1.6 Hz, 1H), 8.13 – 7.97 (m, 2H), 7.46 (dd, *J* = 8.0, 4.8 Hz, 1H), 7.43 – 7.30 (m, 1H); **^{13}C NMR** (75 MHz, $CDCl_3$): δ 174.26, 167.17, 153.5 (dd, *J* = 257.6, 12.5 Hz), 152.17, 150.65 (dd, *J* = 251.5, 13.4 Hz), 148.66, 134.77, 125.19 (dd, *J* = 7.5, 4.0 Hz), 123.69, 122.92, 120.88 (dd, *J* = 6.8, 4.1 Hz), 118.55 (d, *J* = 18.4 Hz), 117.69 (dd, *J* = 19.6, 1.2 Hz); **MS (ESI$^+$)** *m/z* calcd for $C_{13}H_7F_2N_3O$ $(M+H)^+$ 259.06, found 259.9.

2,3,4-trifluorobenzoyl chloride (88)

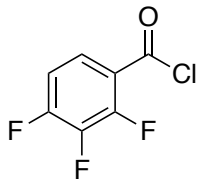

Molecular Weight: 194.54

Using the general procedure **G**, a mixture of 2,3,4-trifluorobenzoic acid (500 mg, 2.84 mmol) in $SOCl_2$ (7 mL) gave 2,3,4-trifluorobenzoyl chloride (**88**) (552 mg, 2.84 mmol, 100%) as a clear oil used for the next reaction without further purification.

3-(pyridin-3-yl)-5-(2,3,4-trifluorophenyl)-1,2,4-oxadiazole (36)

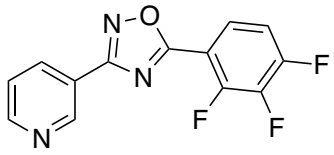

Molecular Weight: 277.21

Using the general procedure **H**, a mixture of 2,3,4-trifluorobenzoyl chloride (**88**) (552 mg, 2.84 mmol), *N*-hydroxynicotinimidamide (**76**) (389 mg, 2.84 mmol) in pyridine (32 mL) gave the crude product. Purification by flash column chromatography with 8:2 cyclohexane-ethyl acetate as eluent gave 3-(pyridin-3-yl)-5-(2,3,4-trifluorophenyl)-1,2,4-oxadiazole (**36**) (80 mg, 0.29 mmol, 10%) as a white solid, **mp** 146.5-147.8 °C; R_f (Cyclohexane/EtOAc 7:3) 0.34; **^{1}H NMR** (300 MHz, $CDCl_3$): δ 9.39 (d, *J* = 2.1 Hz, 1H), 8.78 (dd, *J* = 4.9, 1.7 Hz, 1H), 8.43 (dt, *J* = 8.0, 2.1 Hz, 1H), 8.08 – 7.93 (m, 1H), 7.46 (dd, *J* = 8.0, 4.9 Hz, 1H), 7.25 – 7.15 (m, 1H); **^{13}C NMR** (75 MHz, $CDCl_3$): δ 171.56, 166.94, 155.97, 155.93, 155.84, 155.80, 152.49, 152.33, 152.30, 148.77, 148.74, 142.67, 142.48, 139.30, 139.10, 134.81, 125.01, 124.95, 129.90, 124.83, 123.71, 122.73, 113.52, 113.28, 110.48, 110.43, 110.37, 110.32; **MS (ESI$^+$)** *m/z* calcd for $C_{13}H_6F_3N_3O$ $(M+H)^+$ 278.06, found 278.2.

3,4,5-trifluorobenzoyl chloride (89)

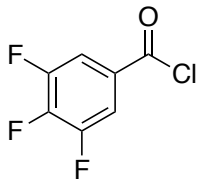

Molecular Weight: 194.54

Using the general procedure **G**, a mixture of 3,4,5-trifluorobenzoic acid (400 mg, 2.27 mmol) in $SOCl_2$ (6 mL) gave 3,4,5-trifluorobenzoyl chloride (**89**) (442 mg, 2.27 mmol, 100%) as a clear oil used for the next reaction without further purification.

3-(pyridin-3-yl)-5-(3,4,5-trifluorophenyl)-1,2,4-oxadiazole (37)

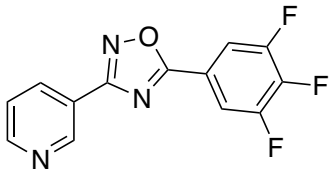

Molecular Weight: 277.21

Using the general procedure **H**, a mixture of 3,4,5-trifluorobenzoyl chloride (**87**) (440 mg, 2.26 mmol), *N*-hydroxynicotinimidamide (**76**) (250 mg, 1.83 mmol) in toluene (45 mL) gave the crude product. Purification by flash column chromatography with 8:2 cyclohexane-ethyl acetate as eluent gave 3-(pyridin-3-yl)-5-(3,4,5-trifluorophenyl)-1,2,4-oxadiazole (**37**) (85 mg, 0.31 mmol, 14%) as a white solid, **mp** 152.0-153.2 °C; R_f (Cyclohexane/EtOAc 7:3) 0.49; **^{1}H NMR** (300 MHz, $CDCl_3$): δ 9.38 (d, *J* = 1.4 Hz, 1H), 8.79 (dd, *J* = 4.9, 1.8 Hz, 1H), 8.42 (dt, *J* = 8.0, 1.8 Hz, 1H), 7.97 – 7.82 (m, 2H), 7.48 (ddd, *J* = 8.0, 4.9, 0.9 Hz, 1H); **^{13}C NMR** (75 MHz, $CDCl_3$): δ 167.37, 153.44, 153.27, 152.37, 152.27, 150.37, 146.63, 148.70, 148.64, 134.85, 134.81, 123.76, 123.73, 122.70, 113.18, 113.07, 112.97, 112.86, 112.68; **MS (ESI$^+$)** *m/z* calcd for $C_{13}H_6F_3N_3O$ $(M+H)^+$ 278.06, found 278.2

2,3,4,5-tetrafluorobenzoyl chloride (90)

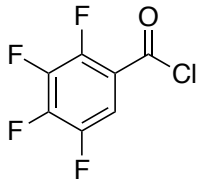

Molecular Weight: 212.53

Using the general procedure **G**, a mixture of 2,3,4,5-tetrafluorobenzoic acid (400 mg, 2.06 mmol) in $SOCl_2$ (6 mL) gave 2,3,4,5-tetrafluorobenzoyl chloride (**90**) (438 mg, 2.06 mmol, 100%) as a yellow solid used for the next reaction without further purification.

3-(pyridin-3-yl)-5-(2,3,4,5-tetrafluorophenyl)-1,2,4-oxadiazole (38)

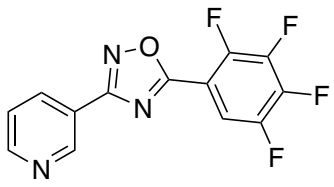

Molecular Weight: 295.20

Using the general procedure **H**, a mixture of 2,3,4,5-tetrafluorobenzoyl chloride (**90**) (438 mg, 2.06 mmol), *N*-hydroxynicotinimidamide (**76**) (228 mg, 1.66 mmol) in toluene (40 mL) gave the crude product. Purification by flash column chromatography with 8:2 cyclohexane-ethyl acetate as eluent gave 3-(pyridin-3-yl)-5-(2,3,4,5-tetrafluorophenyl)-1,2,4-oxadiazole (**38**) (85 mg, 0.28 mmol, 14%) as a white solid, **mp** 112.1-113.0 °C; $\boldsymbol{R_f}$(Cyclohexane/EtOAc 7:3) 0.37; **^{1}H NMR** (300 MHz, $CDCl_3$): δ 9.40 (dd, *J* = 2.3, 0.9 Hz, 1H), 8.80 (dd, *J* = 4.9, 1.7 Hz, 1H), 8.44 (ddd, *J* = 8.0, 2.3, 1.7 Hz, 1H), 7.98 – 7.84 (m, 1H), 7.48 (ddd, *J* = 8.0, 4.9, 0.9 Hz, 1H); **^{13}C NMR** (75 MHz, $CDCl_3$): δ 170.80, 167.00, 152.50, 152.31, 149.04, 149.01, 148.99, 148.96, 148.90, 148.87, 148.85, 148.82, 148.72, 148.61, 145.72, 145.69, 145.67, 145.64, 145.56, 145.53, 145.50, 145.40, 145.36, 145.31, 145.23, 145.20, 145.18, 145.15, 145.06, 145.04, 145.01, 143.59, 143.54, 143.43, 143.38, 143.33, 143.22, 143.17, 142.08, 142.04, 141.92, 141.88, 141.82, 141.69, 141.66, 140.20, 140.15, 140.03, 139.99, 139.94, 139.82, 139.77, 134.84, 134.72, 134.67, 123.78, 123.74, 123.66, 122.44, 112.05, 112.00, 111.95, 111.76, 111.72,

111.67, 108.85, 108.77, 108.66, 108.61; **MS (ESI$^+$)** *m/z* calcd for $C_{13}H_5F_4N_3O$ $(M+H)^+$ 296.05, found 296.2.

3-fluoro-4-nitrobenzoyl chloride (91)

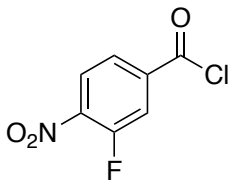

Molecular Weight: 203.55

Using the general procedure **G**, a mixture of 3-fluoro-4-nitrobenzoic acid (400 mg, 2.16 mmol) in $SOCl_2$ (6 mL) gave 3-fluoro-4-nitrobenzoyl chloride (**91**) (440 mg, 2.16 mmol, 100%) as a clear oil used for the next reaction without further purification.

5-(3-fluoro-4-nitrophenyl)-3-(pyridin-3-yl)-1,2,4-oxadiazole (39)

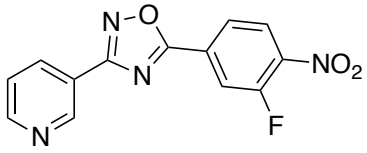

Molecular Weight: 286.22

Using the general procedure **H**, a mixture of 3-fluoro-4-nitrobenzoyl chloride (**91**) (440 mg, 2.16 mmol), *N*-hydroxynicotinimidamide (**76**) (297 mg, 2.16 mmol) in toluene (20 mL) gave the crude product. Purification by flash column chromatography with 7:3 to 8:2 petroleum ether-ethyl acetate as eluent gave 5-(3-fluoro-4-nitrophenyl)-3-(pyridin-3-yl)-1,2,4-oxadiazole (**39**) (100 mg, 0.35 mmol, 16%) as a white solid, **mp** 176.1-177.3 °C; $\boldsymbol{R_f}$ (Cyclohexane/EtOAc 7:3) 0.33; **^{1}H NMR** (300 MHz, $CDCl_3$): 9.40 (d, *J* = 1.6 Hz, 1H), 8.81 (dd, *J* = 4.9, 1.6 Hz, 1H), 8.51 – 8.40 (m, 1H), 8.34 – 8.10 (m, 2H), 7.50 (dd, *J* = 8.0, 4.9 Hz, 1H); **^{13}C NMR** (75 MHz, $CDCl_3$): δ 174.00, 173.08, 167.58, 155.55 (d, *J* = 265.5 Hz), 152.32, 148.55, 135.00, 130.03 (d, *J* = 9.0 Hz), 127.28 (d, *J* = 2.25 Hz), 124.22, 124.02 (d, *J* = 20.3 Hz), 122.57, 118.38 (d, *J* = 23.3 Hz); **MS (ESI$^+$)** *m/z* calcd for $C_{13}H_7FN_4O_3$ $(M+H)^+$ 287.06, found 287.2.

4-fluoro-3-nitrobenzoyl chloride (92)

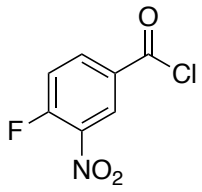

Molecular Weight: 203.55

Using the general procedure **G**, a mixture of 4-fluoro-3-nitrobenzoic acid (500 mg, 2.70 mmol) in $SOCl_2$ (8 mL) gave 3-fluoro-4-nitrobenzoyl chloride (**92**) (550 mg, 2.70 mmol, 100%) as a yellow oil used for the next reaction without further purification.

5-(4-fluoro-3-nitrophenyl)-3-(pyridin-3-yl)-1,2,4-oxadiazole (40)

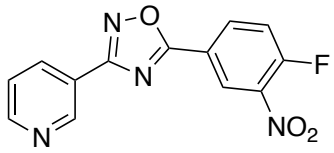

Molecular Weight: 286.22

Using the general procedure **H**, a mixture of 4-fluoro-3-nitrobenzoyl chloride (**92**) (550 mg, 2.70 mmol), *N*-hydroxynicotinimidamide (**76**) (371 mg, 2.70 mmol) in toluene (25 mL) gave the crude product. Purification by flash column chromatography with 8:2 petroleum ether-ethyl acetate as eluent gave 5-(4-fluoro-3-nitrophenyl)-3-(pyridin-3-yl)-1,2,4-oxadiazole (**40**) (103 mg, 0.36 mmol, 13%) as a light yellow solid, **mp** 149.9-151.9 °C; $\boldsymbol{R_f}$ (Cyclohexane/EtOAc 7:3) 0.34; **^{1}H NMR** (300 MHz, $CDCl_3$): δ 9.38 (d, *J* = 2.3 Hz, 1H), 8.93 (dd, *J* = 7.0, 2.3 Hz, 1H), 8.78 (dd, *J* = 4.9, 1.8 Hz, 1H), 8.49 (ddd, *J* = 8.7, 4.1, 2.2 Hz, 1H), 8.43 (dt, *J* = 8.0, 1.9 Hz, 1H), 7.60 – 7.40 (m, 2H); **^{13}C NMR** (75 MHz, $CDCl_3$): δ 173.16, 173.13, 167.42, 157.89 (d, *J* = 271.5 Hz), 152.39, 148.66, 134.86 (d, *J* = 9.8 Hz), 134.79, 126.41 (d, *J* = 2.3 Hz), 123.79, 122.60, 121.10 (d, *J* = 4.5 Hz), 119.98 (d, *J* = 21.75 Hz); **MS (ESI$^+$)** *m/z* calcd for $C_{13}H_7FN_4O_3$ $(M+H)^+$ 287.06, found 287.3.

6-fluoronicotinoyl chloride (93)

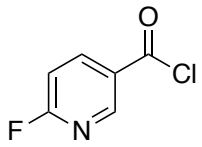

Molecular Weight: 159.54

Using the general procedure **G**, a mixture of 6-fluoronicotinic acid (400 mg, 2.83 mmol) in $SOCl_2$ (8 mL) gave 6-fluoronicotinoyl chloride (**93**) (452 mg, 2.83 mmol, 100%) as a clear oil used for the next reaction without further purification.

5-(2-fluoropyridin-4-yl)-3-(pyridin-3-yl)-1,2,4-oxadiazole (41)

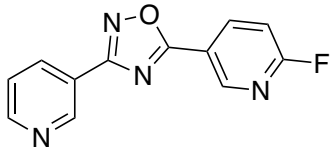

Molecular Weight: 242.21

Using the general procedure **H**, a mixture of 6-fluoronicotinoyl chloride (**93**) (452 mg, 2.83 mmol), *N*-hydroxynicotinimidamide (**76**) (389 mg, 2.83 mmol) in pyridine (20 mL) gave the crude product. Purification by flash column chromatography with 7:3 to 8:2 petroleum ether-ethyl acetate as eluent gave 5-(2-fluoropyridin-4-yl)-3-(pyridin-3-yl)-1,2,4-oxadiazole (**41**) (83 mg, 0.34 mmol, 12%) as a white solid, **mp** 161.7-162.5 °C; $\boldsymbol{R_f}$(Cyclohexane/EtOAc 7:3) 0.21; **^{1}H NMR** (300 MHz, $CDCl_3$): δ 9.40 (dd, *J* = 2.2, 0.9 Hz, 1H), 9.12 (dt, *J* = 2.5, 0.9 Hz, 1H), 8.79 (dd, *J* = 4.9, 1.8 Hz, 1H), 8.61 (m, 1H), 8.44 (ddd, *J* = 8.0, 2.2, 1.8 Hz, 1H), 7.48 (ddd, *J* = 8.0, 4.9, 0.9 Hz, 1H), 7.17 (ddd, *J* = 8.6, 3.0, 0.9 Hz, 1H); **^{13}C NMR** (75 MHz, $CDCl_3$): δ 173.20, 167.37, 165.65 (d, *J* = 235.5 Hz), 152.35, 148.73, 148.46, 144.68, 140.84 (d, *J* = 9.0 Hz), 134.84, 123.76, 122.37, 110.61 (d, *J* = 37.5Hz); **MS (ESI$^+$)** *m/z* calcd for $C_{12}H_7FN_4O$ $(M+H)^+$ 243.22, found 243.3.

3-cyanobenzoyl chloride (107)

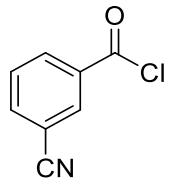

Molecular weight: 165.58

Using the general procedure **G**, a mixture of 3-cianobenzoic acid (1 g, 6.80 mmol) in $SOCl_2$ (30 mL) gave 3-cyanibenzoyl chloride (**107**) (1.13 g, 6.80 mmol, 100%) as a white solid used for the next reaction without further purification.

3-[(hydroxyamino)(imino)methyl]benzoic acid (106)

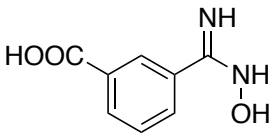

Molecular Weight: 180.16

Using the general procedure **F**, a mixture of $NH_2OH{\cdot}HCl$ (3.54 g, 50.97 mmol), K_2CO_3 (7.05 g, 50.97 mmol), 3-cyanobenzoic acid (1.50 g, 10.20 mmol) in H_2O (15 mL) and EtOH (30 mL) gave 3-[(hydroxyamino)(imino)methyl] benzoic acid (**106**) (1.80 g, 9.99 mmol, 98%) as a white solid, **mp** decomposes at 235°C; $\boldsymbol{R_f}$ (DCM/MeOH 9:1) 0.32; **^{1}H NMR** (300 MHz, DMSO-*d6*): δ 9.47 (bs, 1H, exchange with D_2O), 8.20 (s, 1H), 7.91 (d, *J* = 7.7 Hz, 1H), 7.83 (d, *J* = 7.7 Hz, 1H), 7.44 (t, *J* = 7.7 Hz, 1H), 6.38 (s, 1H), 5.66 (bs, 1H, exchange with D_2O), 5.14 (bs, 1H, exchange with D_2O).[162]

3-(5-(3-cyanophenyl)-1,2,4-oxadiazol-3-yl)-benzoic acid (42)

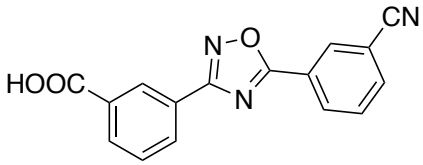

Molecular Weight: 291.27

Using the general procedure **H**, a mixture of 3-cyanobenzoyl chloride (**107**) (1.50 g, 9.06 mmol), 3-[(hydroxyamino)(imino)methyl]benzoic acid (**106**) (1.63 g, 9.06 mmol) in pyridine (15 mL) gave the crude product. Purification by crystallization in MeOH (5 mL) gave 3-(5-(3-cyanophenyl)-1,2,4-oxadiazol-3-yl)benzoic acid (**42**) (1.33 g, 4.57 mmol, 50%) as a light yellow solid, **mp** 270-272 °C; $\boldsymbol{R_f}$ (DCM/MeOH 9:1) 0.38; **^{1}H NMR** (300 MHz, DMSO-*d6*): δ 13.33 (s, 1H), 8.65 – 8.55 (m, 2H), 8.48 (d, *J* = 7.9 Hz, 1H), 8.30 (d, *J* = 7.9 Hz, 1H), 8.21 – 8.11 (m, 2H), 7.85 (t, *J* = 7.9 Hz, 1H), 7.72 (t, *J* = 7.9 Hz, 1H); **^{13}C NMR** (75 MHz, DMSO-*d6*) δ 174.57, 168.27, 166.91, 137.13, 132.88, 132.80, 132.28, 131.96, 131.54, 131.31, 130.32, 128.26, 126.70, 124.91, 118.06, 113.29; **MS (ESI$^+$)** *m/z* calcd for $C_{16}H_9N_3O_3$ $(M-H)^-$ 291.06, found 290.0.

3-(pyridine-3-yl)-1,2,4-oxadiazole (108)

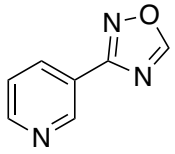

Molecular Weight: 147.14

Procedure adapted form literature.[150] To a solution of *N*-hydroxypyridine-3-carboximidamide (**76**) (500 mg, 3.65 mmol) in trimethyl orthoformate (10 mL) was added a catalytic amount of TFA (0.8 mL). The mixture was stirred for 5 min and then heated up to 60 °C and stirred for additional 30 min. Then, the mixture was allowed to cool to rt and concentrated under reduced pressure. The crude was diluted with $NaHCO_3$ (30 mL) and extracted with EtOAc (3 x 15 mL). The combined organics were washed with brine (10 mL), dried (Na_2SO_4) and evaporated under reduced pressure to give 3-(1,2,4-oxadiazol-3-yl)pyridine (**108**) (340 mg, 2.31 mmol, 63%) as a white solid, **mp** 89.9-92.1 °C; $\boldsymbol{R_f}$ (Cyclohexane/EtOAc 6:4) 0.26; **^{1}H NMR**

(300 MHz, $CDCl_3$): δ 9.36 (s, 1H), 8.85 (s, 1H), 8.77 (d, *J* = 4.9, 1H), 8.39 (d, *J* = 8.0, 1H), 7.50 (dd, *J* = 8.0, 4.9 Hz, 1H).

Methyl 3-iodobenzoate (109)

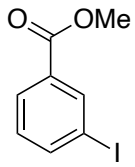

Molecular Weight: 262.05

Procedure adapted from literature.[163] To a solution of 3-iodobenzoic acid (2.00 g, 8.06 mmol) in MeOH (50 mL) was assed dropwise concentrated H_2SO_4 (5 mL). The resulting solution was stirred and heated at reflux for 3 h. Then, the solution was allowed to cool to rt, diluted with Et_2O (100 mL) and washed with H_2O (2 × 10 mL), saturated $NaHCO_3$ (100 mL) and brine (100 mL). The organic layer was dried (Na_2SO_4) and evaporated under reduced pressure to give methyl 3-iodobenzoate (**109**) (1.96 g, 7.46 mmol, 93%) as a white solid, **mp** 53.0-54.5 °C (lit., [164]54-56°C); ***R*$_f$** (Cyclohexane/EtOAc 7:3) 0.72; **^{1}H NMR** (300 MHz, $CDCl_3$): δ 8.38 (s, 1H), 8.00 (d, *J* = 7.9 Hz, 1H), 7.88 (d, *J* = 7.9 Hz, 1H), 7.18 (t, *J* = 7.9 Hz, 1H), 3.92 (s, 3H).[164]

Methyl 3-(3-(pyridin-3-yl)-1,2,4-oxadiazol-5-yl)benzoate (110)

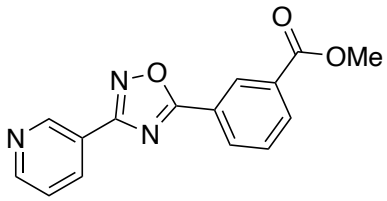

Molecular Weight: 281.27

Procedure adapted from literature.[150] A mixture of 3-(1,2,4-oxadiazol-3-yl)pyridine (**108**) (170 mg, 1.12 mmol), 3-iodobenzoate (**109**) (590 mg, 2.24 mmol), $Pd(OAc)_2$ (25 mg, 0.11 mmol), PPh_3 (60 mg, 0.22 mmol) and AgOAc (506 mg, 3.36 mmol) in toluene (27 mL) was stirred and heated at reflux overnight. Then, the suspension was allowed to cool to rt, and the solids were removed by filtration through Celite® and washed with EtOAc (3 x 25 mL). The combined organics were washed with brine (15 mL), dried (Na_2SO_4) and evaporated under reduced

pressure to give the crude product. Purification by flash column chromatography on silica with 8:2 cyclohexane-ethyl acetate as eluent gave methyl 3-(3-(pyridin-3-yl)-1,2,4-oxadiazol-5-yl)benzoate (**110**) (170 mg, 0.60 mmol, 54%) as a white solid, **mp** 123.2-125.2 °C; R_f (Cyclohexane/EtOAc 8:2) 0.23; **^{1}H NMR** (300 MHz, $CDCl_3$): δ 9.42 (d, *J* = 1.2 Hz, 1H), 8.90 (s, 1H), 8.79 (dd, *J* = 4.8, 1.2 Hz, 1H), 8.55 – 8.38 (m, 2H), 8.31 (d, *J* = 7.9 Hz, 1H), 7.68 (t, *J* = 7.9 Hz, 1H), 7.47 (dd, *J* = 7.9, 5.2 Hz, 1H), 4.01 (s, 3H).

3-(3-(pyridin-3-yl)-1,2,4-oxadiazol-5-yl)sodium benzoate (43)

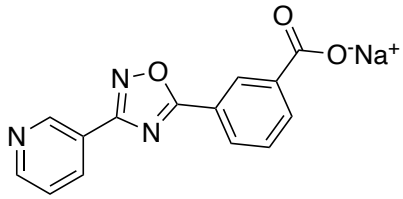

Molecular Weight: 289.23

NaOH 1M (4 mL) was added to a solution of methyl 3-(3-(pyridin-3-yl)-1,2,4-oxadiazol-5-yl)benzoate (**110**) (150 mg, 0.53 mmol) in MeOH (5 mL). The solution was stirred at rt for 2 h and then concentrated under reduced pressure. The residue was diluted with H_2O (20 mL) and extracted with EtOAc (3 x 10 mL). The combined organics were dried (Na_2SO_4) and evaporated under reduced pressure to give 3-(3-(pyridin-3-yl)-1,2,4-oxadiazol-5-yl)sodium benzoate (**43**) (120 mg, 0.41 mmol, 78%) as a white solid, **mp** decomposes at 290°C ; R_f (DCM/MeOH 9:1) 0.21; **^{1}H NMR** (300 MHz, DMSO-*d6*): δ 9.25 (s, 1H), 8.79 (d, *J* = 4.9 Hz, 1H), 8.68 (s, 1H), 8.45 (d, *J* = 7.9 Hz, 1H), 8.18 (d, *J* = 7.7 Hz, 1H), 8.12 (d, *J* = 7.7 Hz, 1H), 7.68 – 7.51 (m, 2H); **^{13}C NMR** (75 MHz, DMSO-*d6*) δ 176.68, 168.12, 166.98, 152.79, 148.23, 142.39, 135.22, 134.36, 129.07, 129.04, 128.48, 124.81, 123.03, 122.61; **MS (ESI$^+$)** *m/z* calcd for $C_{14}H_8N_3O_3$ $(M\text{-}Na)^-$ 289.05, found 289.9.

Cyclohex-1-ene-1-carbonyl chloride (98)

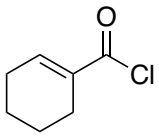

Molecular Weight: 144.60

Using the general procedure **G**, a mixture of cyclohex-l-ene-1-carboxylic acid (500mg, 3.96 mmol) in $SOCl_2$ (12 mL) gave cyclohex-1-ene-1-carbonyl chloride (**98**) (550 mg, 3.80 mmol, 96%) as a yellow liquid used for the next reaction without further purification.

5-(cyclohex-1-en-1-yl)-3-(pyridin-3-yl)-1,2,4-oxadiazole (44)

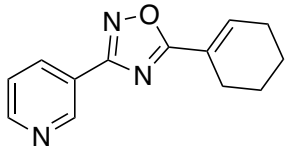

Molecular Weight: 227.27

Using the general procedure **H**, a mixture of cyclohex-1-ene-1-carbonyl chloride (**98**) (556 mg, 3.84 mmol), *N*-hydroxynicotinimidamide (**76**) (425 mg, 3.10 mmol) in pyridine (30 mL) gave the crude product. Purification by flash column chromatography with 8:2 cyclohexane-ethyl acetate as eluent gave 5-(cyclohex-1-en-1-yl)-3-(pyridin-3-yl)-1,2,4-oxadiazole (**44**) (210 mg, 0.92 mmol, 30%) as a light-yellow solid, **mp** 79.6-81.1 °C; $\boldsymbol{R_f}$ (Cyclohexane/EtOAc 8:2) 0.32; **^{1}H NMR** (300 MHz, $CDCl_3$): δ 9.31 (dd, *J* = 2.1, 0.9 Hz, 1H), 8.72 (dd, *J* = 4.9, 1.9 Hz, 1H), 8.36 (dt, *J* = 8.0, 1.9 Hz, 1H), 7.41 (ddd, *J* = 8.0, 4.9, 0.9 Hz, 1H), 7.22 – 7.15 (m, 1H), 2.60 – 2.49 (m, 2H), 2.40 – 2.26 (m, 2H), 1.86 – 1.65 (m, 4H); **^{13}C NMR** (75 MHz, $CDCl_3$): δ 176.97, 166.41, 151.71, 148.56, 139.04, 134.72, 123.96, 123.58, 123.54, 25.86, 24.54, 21.74, 21.29; **MS (ESI$^+$)** *m/z* calcd for $C_{13}H_{13}N_3O$ $(M+H)^+$ 227.11, found 228.1.

_N_-hydroxyfuran-3-carboximidamide (103)

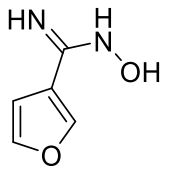

Molecular weight: 126.12

Using the general procedure **F**, a mixture of $NH_2OH{\cdot}HCl$ (3.48 g, 50.00 mmol), $NaHCO_3$ (2.65 g, 25.00 mmol), 3-furonitrile (3.07 g, 33.00 mmol) in H_2O (20 mL) and EtOH (20 mL) gave *N*-hydroxyfuran-3-carboximidamide (**103**) (2.21 g, 17.52 mmol, 53%) as yellow oil; $\boldsymbol{R_f}$ (Cyclohexane/EtOAc 1:1) 0.40; **^{1}H NMR** (300 MHz, DMSO-*d6*): δ 9.58 (bs, 1H, exchange with D_2O), 7.65 (dd, *J* = 1.8, 0.8 Hz, 1H), 6.73 (dd, *J* = 3.4, 0.8 Hz, 1H), 6.50 (dd, *J* = 3.4, 1.8 Hz, 1H), 5.67 (bs, 2H, exchange with D_2O).[165]

3-(3-(furan-3-yl)-1,2,4-oxadiazol-5-yl)-benzonitrile (45)

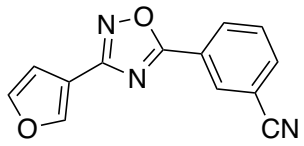

Molecular weight: 237.22

Using the general procedure **H**, a mixture of 3-cyanobenzoyl chloride (**107**) (1.0 g, 6.04 mmol), *N*-hydroxyfuran-3-carboximidamide (**103**) (614 mg, 4.87 mmol) in pyridine (30 mL) gave the crude product. Purification by flash column chromatography with 8:2 cyclohexane-ethyl acetate as eluent gave 3-(3-(furan-3-yl)-1,2,4-oxadiazol-5-yl)-benzonitrile (**45**) (525 mg, 2.21 mmol, 45%) as a light pink solid, **mp** 124.0-124.4 °C; $\boldsymbol{R_f}$ (Cyclohexane/EtOAc 1:1) 0.67; **^{1}H NMR** (300 MHz, $CDCl_3$): δ 8.52 (s, 1H), 8.44 (dt, *J* = 7.9, 1.4 Hz, 1H), 7.90 (dt, *J* = 7.9, 1.4 Hz, 1H), 7.71 (t, *J* = 7.9 Hz, 1H), 7.68 - 7.65 (m, 1H), 7.24 (d, *J* = 3.5 Hz, 1H), 6.62 (dd, *J* = 3.5, 1.8 Hz, 1H); **^{13}C NMR** (75 MHz, $CDCl_3$): δ 173.61, 162.08, 145.55, 141.85, 135.88, 131.99, 131.69, 130.21, 125.20, 117.35, 114.37, 113.92, 112.01; **MS (ESI$^+$)** *m/z* calcd for $C_{13}H_7N_3O_2$ $(M+H)^+$ 237.05, found 238.1.

_N_-hydroxycyclohexanecarboximidamide (104)

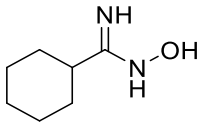

Molecular weight: 142.20

Using the general procedure **F**, a mixture of $NH_2OH{\cdot}HCl$ (3.48 g, 50.00 mmol), $NaHCO_3$ (2.65 g, 25.00 mmol), cyclohexanecarbonitrile (3.60 g, 33.00 mmol) in H_2O (20 mL) and EtOH (20 mL) gave *N*-hydroxycyclohexanecarboximidamide (**104**) (2.18 g, 15.30 mmol, 46%) as a white solid, **mp** 90.4-92.7 °C; R_f (Cyclohexane/EtOAc 1:1) 0.17; **^{1}H NMR** (300 MHz, DMSO-*d6*): δ 8.64 (s, 1H), 5.18 (s, 2H), 1.93 (tt, *J* = 11.9, 3.0 Hz, 1H), 1.81 – 1.53 (m, 5H), 1.40 – 1.02 (m, 5H).

3-(3-cyclohexyl-1,2,4-oxadiazol-5-yl)benzonitrile (46)

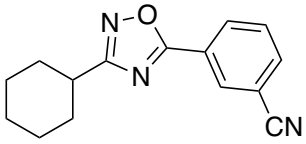

Molecular weight: 253.31

Using the general procedure **H**, a mixture of 3-cyanobenzoyl chloride (**107**) (1.00 g, 6.04 mmol), *N*-hydroxycyclohexanecarboximidamide (**104**) (693 mg, 4.87 mmol) in pyridine (30 mL) gave the crude product. Purification by flash column chromatography with 8:2 cyclohexane-ethyl acetate as eluent gave 3-(3-cyclohexyl-1,2,4-oxadiazol-5-yl)benzonitrile (**46**) (530 mg, 2.09 mmol, 43%) as a white solid, **mp** 62.0-62.6 °C; R_f (Cyclohexane/EtOAc 9:1) 0.36; **^{1}H NMR** (300 MHz, $CDCl_3$): δ 8.42 (s, 1H), 8.34 (d, *J* = 7.9 Hz, 1H), 7.85 (d, *J* = 7.9 Hz, 1H), 7.66 (t, *J* = 7.9 Hz, 1H), 2.88 (tt, *J* = 11.4, 3.6 Hz, 1H), 2.14 – 2.01 (m, 2H), 1.93 – 1.55 (m, 5H), 1.51 – 1.24 (m, 3H); **^{13}C NMR** (75 MHz, $CDCl_3$): δ 175.00, 172.97, 135.41, 131.77, 131.41, 130.07, 125.76, 117.43, 113.66, 35.84, 30.55, 25.69, 25.60; **MS (ESI$^+$)** *m/z* calcd for $C_{15}H_{15}N_3O$ $(M+H)^+$ 253.12, found 254.2.

_N_-hydroxypiperidine-1-carboximidamide (105)

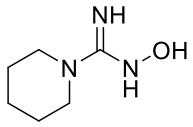

Molecular weight: 143.19

Using the general procedure **F**, a mixture of $NH_2OH{\cdot}HCl$ (1.74 g, 25.00 mmol), $NaHCO_3$ (1.33 g, 12.50 mmol), piperidine-1-carbonitrile (1.82 g, 16.50 mmol) in H_2O (20 mL) and EtOH (20 mL) gave *N*-hydroxypiperidine-1-carboximidamide (**105**) (939 mg, 6.56 mmol, 53%) as a yellow oil; R_f (Cyclohexane/EtOAc 4:6) 0.33; **^{1}H NMR** (300 MHz, $CDCl_3$): δ 4.82 (s, 1H), 4.70 - 4.20 (s, 2H), 3.32 (m, 4H), 3.03 (m, 6H).

3-(3-(piperidin-1-yl)-1,2,4-oxadiazol-5-yl)benzonitrile (47)

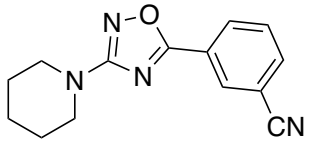

Molecular weight: 254.29

Using the general procedure **H**, a mixture of 3-cyanobenzoyl chloride (**107**) (1.00 g, 6.04 mmol), *N*-hydroxypiperidine-1-carboximidamide (**105**) (697 mg, 4.87 mmol) in pyridine (30 mL) gave the crude product. Purification by flash column chromatography with 8:2 cyclohexane-ethyl acetate as eluent gave 3-(3-(piperidin-1-yl)-1,2,4-oxadiazol-5-yl)benzonitrile (**47**) (672 mg, 2.64 mmol, 54%) as a white solid, **mp** 87.8°C; R_f (Cyclohexane/EtOAc 8:2) 0.43; **^{1}H NMR** (300 MHz, $CDCl_3$): δ 8.37 (s, 1H), 8.28 (d, *J* = 7.9 Hz, 1H), 7.83 (d, *J* = 7.9 Hz, 1H), 7.63 (t, *J* = 7.9 Hz, 1H), 3.49 (m, 4H), 1.71 – 1.63 (m, 6H); **^{13}C NMR** (75 MHz, $CDCl_3$): δ 171.91, 170.75, 135.18, 131.63, 131.32, 129.91, 126.13, 117.60, 113.52, 47.00, 24.99, 24.10; **MS (ESI$^+$)** *m/z* calcd for $C_{14}H_{14}N_4O$ $(M+H)^+$ 254.12, found 255.3.

1-acetylpiperidine-3-carboxylic acid (99)

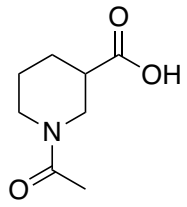

Molecular Weight: 171.19

Procedure adapted from literature.[166] Nipecotic acid (500 mg, 3.87 mmol) was added to the solution of DCM (9 mL) and acetic anhydride (0.37 mL, 3.87 mmol). The rection mixture was stirred at rt overnight. Then, the solution was concentrated under reduced pressure to give the crude compound. Purification by ion-exchange resin (Dowex 50WX4-400) in water gave 1-acetylpiperidine-3-carboxylic acid (**99**) (530 mg, 3.10 mmol, 80%) as a clear oil; $\boldsymbol{R_f}$(DCM/MeOH 8:2) 0.43; **^{1}H NMR** (300 MHz, $CDCl_3$) (50:50 mixture of rotamers): δ 11.67 (bs, 1H), 4.06 (dd, *J* = 13.1, 3.9 Hz, 0.5H), 3.90 (dt, *J* = 13.1, 4.9 Hz, 0.5H), 3.72 (dd, *J* = 13.1, 3.9 Hz, 0.5H), 3.59 – 3.39 (m, 1H), 3.33 (dd, *J* = 13.1, 8.5 Hz, 0.5H), 3.23 (ddd, *J* = 13.0, 9.4, 3.3 Hz, 0.5H), 3.12 (ddd, *J* = 13.0, 9.4, 3.3 Hz, 0.5H), 2.52 – 2.34 (m, 1H), 2.12 (s, 1.5H), 2.06 (s, 1.5H), 2.02 – 1.90 (m, 1H), 1.89 – 1.70 (m, 1.5H), 1.70 – 1.58 (m, 0.5H), 1.56 – 1.38 (m, 1H).

1-acetylpiperidine-3-carbonyl chloride (94)

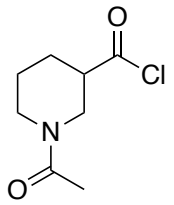

Molecular Weight: 189.64

Using the general procedure **G**, a mixture of 1-acetylpiperidine-3-carboxylic acid (**99**) (530 mg, 3.10 mmol) in $SOCl_2$ (15 mL) gave 1-acetylpiperidine-3-carbonyl chloride (**94**) (585 mg, 3.10 mmol, 100%) as a brown oil used for the next reaction without further purification.

1-(3-(3-(pyridin-3-yl)-1,2,4-oxadiazol-5-yl)piperidin-1-yl)ethan-1-one (48)

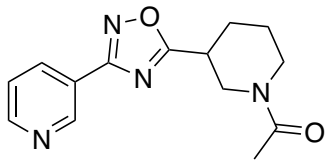

Molecular Weight: 272.31

Using the general procedure **H**, 1-acetylpiperidine-3-carbonyl chloride (**94**) (585 mg, 3.08 mmol), *N*-hydroxynicotinimidamide (**76**) (341 mg, 2.49 mmol) in pyridine (30 mL) gave the crude product. The obtained solid was dissolved in DCM (20 mL) washed with NaOH 20% (2 x 10 mL) gave the crude product. Purification by flash column chromatography with 8:2 to 9:1 ethyl acetate-petroleum ether as eluent gave 1-(3-(3-(pyridin-3-yl)-1,2,4-oxadiazol-5-yl)piperidin-1-yl)ethan-1-one (**48**) (50 mg, 0.19 mmol, 12%) as a light yellow oil; R_f (EtOAc/petroleum ether 8:2) 0.38; **^{1}H NMR** (300 MHz, $CDCl_3$) (50:50 mixture of rotamers): δ 9.25 (s, 1H), 8.71 (s, 1H), 8.37 – 8.25 (m, 1H), 7.41 (dd, *J* = 8.0, 4.8 Hz, 1H), 4.84 – 4.70 (m, 0.5H), 4.03 – 3.87 (m, 1H), 3.83 – 3.69 (m, 1H), 3.32 – 3.00 (m, 2.5H), 2.38 – 2.18 (m, 1H), 2.15 (s, 1.5H), 2.09 (s, 1.5H), 2.13 – 1.98 (m, 0.5H), 1.99– 1.84 (m, 1H), 1.79 – 1.51 (m, 1.5H); **^{13}C NMR** (75 MHz, $CDCl_3$): δ 180.18, 179.91, 169.12, 166.29, 166.13, 151.81, 151.51, 148.27, 148.16, 135.07, 134.91, 123.81, 123.26, 48.64, 46.57, 43.97, 41.60, 35.11, 34.53, 28.50, 28.07, 24.75, 23.26, 21.48, 21.43; **MS (ESI$^+$)** *m/z* calcd for $C_{14}H_{16}N_4O_2$ $(M+H)^+$ 273.13, found 273.1.

1-formylpiperidine-3-carboxylic acid (101)

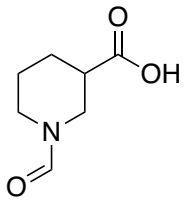

Molecular weight: 157.17

Procedure adapted from literature.[167] A solution of formic acid (4.5 mL) and acetic anhydride (11 mL) was heated at 60 °C for 1 h and then cooled to 0 °C. Nipecotic acid (500 mg, 3.87

mmol) was added to the solution portion-wise. The mixture was allowed to warm to rt and stirred for 16 h. Then, the pH was adjusted to 7 using NaOH, concentrated under reduced pressure, diluted with DCM (5 mL) and filtered. The filtrate was concentrated under reduced pressure to give the crude product. Purification by crystallization in *i*PrOH (5 mL) gave 1-formyllpiperidine-3-carboxylic acid (**9**) (460 mg, 2.93 mmol, 76%) as a white solid, **mp** 110.9 111.4 °C (lit., [167]110.0-112.0°C); R_f (DCM/MeOH 8:2) 0.46; **^{1}H NMR** (300 MHz, $CDCl_3$) (50:50 mixture of rotamers): δ 11.13 (s, 1H), 8.09 (s, 1H), 4.58 (dd, *J* = 13.3, 4.2 Hz, 0.5H), 3.86 (ddd, *J* = 13.3, 5.8, 4.2 Hz, 0.5H), 3.78 – 3.64 (m, 1H), 3.53 (dd, *J* = 13.8, 8.2 Hz, 0.5H), 3.22 (ddd, *J* = 13.3, 9.1, 3.4 Hz, 0.5H), 3.10 (ddd, *J* = 13.8, 11.2, 3.4 Hz, 0.5H), 2.92 (dd, *J* = 13.3, 10.4 Hz, 0.5H), 2.61 – 2.39 (m, 1H), 2.06 – 1.92 (m, 1H), 1.92 – 1.77 (m, 1H), 1.76 – 1.60 (m, 1H), 1.60 – 1.40 (m, 1H).

1-formylpiperidine-3-carbonyl chloride (95)

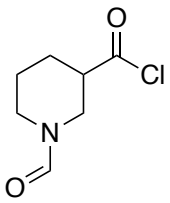

Molecular Weight: 175.61

Using the general procedure **G**, a mixture of 1-formylpiperidine-3-carboxylic acid (**101**) in $SOCl_2$ (15mL) gave 1-formylpiperidine-3-carbonyl chloride (**95**) (510 mg, 2.90 mmol, 99.2%) as a yellow solid used for the next reaction without further purification.

3-(3-(pyridin-3-yl)-1,2,4-oxadiazol-5-yl)piperidine-1-carbaldehyde (49)

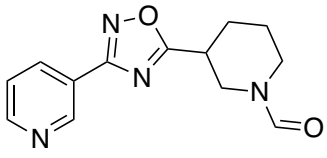

Molecular Weight: 258.28

Using the general procedure **H**, a mixture of 1-formylpiperidine-3-carbonyl chloride (**95**) (508 mg, 2.90 mmol), *N*-hydroxynicotinimidamide (**76**) (341 mg, 2.49 mmol) in pyridine (30 mL)

gave the crude product. Purification by flash column chromatography with 8:2 ethyl acetate-petroleum ether + 1% TEA as eluent gave 3-(3-(pyridin-3-yl)-1,2,4-oxadiazol-5-yl)piperidine-1-carbaldehyde (**49**) (47 mg, 0.19 mmol, 8%) as a yellow oil; R_f (EtOAc/petroleum ether 8:2) 0.33; **^{1}H NMR** (300 MHz, $CDCl_3$) (50:50 mixture of rotamers): δ 9.27 (bs, 1H), 8.72 (bs, 1H), 8.32 (ddt, *J* = 8.0, 2.7, 1.8 Hz, 1H),), 8.10 (s, 0.5H), 8.07 (s, 0.5H), 7.42 (dd, *J* = 8.0, 4.8 Hz, 1H), 4.64 – 4.55 (m, 0.5H), 3.97 – 3.83 (m, 1H), 3.74 – 3.57 (m, 1H), 3.22 – 3.12 (m, 2.5H), 2.42 – 2.24 (m, 1H), 2.19 – 1.86 (m, 1.5H), 1.85 – 1.48 (m, 1.5H); **^{13}C NMR** (75 MHz, $CDCl_3$) δ 179.77, 179.50, 166.34, 166.26, 161.13, 160.99, 151.90, 151.73, 148.36, 148.31, 134.97, 134.90, 123.79, 48.12, 45.77, 42.09, 39.88, 35.15, 34.23, 28.75, 28.41, 24.85, 23.01; **MS (ESI$^+$)** *m/z* calcd for $C_{13}H_{14}N_4O_2$ $(M+H)^+$ 259.11, found 259.7.

1-acetylpiperidine-4-carboxylic acid (100)

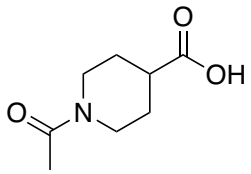

Molecular Weight: 171.20

Procedure adapted from literature.[166] Isonipecotic acid (500 mg, 3.87 mmol) was added to the solution of DCM (9 mL) and acetic anhydride (0.37 mL, 3.87 mmol). The rection mixture was stirred at rt overnight. Then, the solution was concentrated under reduced pressure to give the crude compound. Purification by ion-exchange resin (Dowex 50WX4-400) in water gave 1-acetylpiperidine-4-carboxylic acid (**100**) (648 mg, 3.79 mmol, 98%) as a pale yellow oil; R_f (DCM/MeOH 8:2) 0.45; **^{1}H NMR** (300 MHz, $CDCl_3$): δ 9.88 (s, 1H), 4.48 – 4.37 (m, 1H), 3.88 – 3.77 (m, 1H), 3.16 (t, *J* = 12.5 Hz, 1H), 2.85 (t, *J* = 12.5 Hz, 1H), 2.76 – 2.56 (m, 1H), 2.10 (s, 3H), 2.05 – 1.94 (m, 2H), 1.82 – 1.58 (m, 2H)[168].

1-acetylpiperidine-4-carbonyl chloride (96)

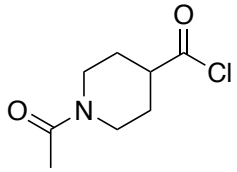

Molecular Weight: 189.64

Using the general procedure **G**, a mixture of 1-acetylpiperidine-4-carboxylic acid (**100**) (800 mg, 4.67) in $SOCl_2$ (5 mL) gave the 1-acetylpiperidine-4-carbonyl chloride (**96**) (343 mg, 1.81 mmol, 39%) as pink solid used for the next reaction without further purification.

1-(4-(3-(pyridin-3-yl)-1,2,4-oxadiazol-5-yl)piperidin-1-yl)ethan-1-one (50)

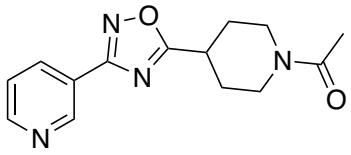

Molecular Weight: 272.31

Using the general procedure **H**, a mixture of 1-acetylpiperidine-4-carbonyl chloride (**96**) (342.90 mg, 1.81 mmol), *N*-hydroxynicotinimidamide (**76**) (200 mg, 1.46 mmol) in pyridine (30 mL) gave the crude product. Purification by flash column chromatography with 8:2 DCM-acetone as eluent gave 1-(4-(3-(pyridin-3-yl)-1,2,4-oxadiazol-5-yl)piperidin-1-yl)ethan-1-one (**50**) (80 mg, 0.29 mmol, 20%) as a yellow solid, **mp** 105.3-106.3 °C; $\boldsymbol{R_f}$ (DCM/Acetone 8:2) 0.14; **^{1}H NMR** (300 MHz, $CDCl_3$): δ 9.26 (dd, *J* = 2.0, 0.9 Hz, 1H), 8.71 (dd, *J* = 4.8, 1.9 Hz, 1H), 8.31 (dt, *J* = 8.0, 1.9 Hz, 1H), 7.40 (ddd, *J* = 8.0, 4.8, 0.9 Hz, 1H), 4.50 (dtd, *J* = 13.7, 4.2, 1.4 Hz, 1H), 3.89 (dtd, *J* = 13.7, 4.2, 1.4 Hz, 1H), 3.33 – 3.18 (m, 2H), 2.94 (ddd, *J* = 13.7, 11.1, 3.2 Hz, 1H), 2.24 – 2.13 (m, 2H), 2.11 (s, 3H), 2.02 – 1.78 (m, 2H); **^{13}C NMR** (75 MHz, $CDCl_3$): δ 181.39, 168.92, 166.37, 152.05, 148.59, 134.65, 123.65, 123.00, 45.42, 40.52, 34.30, 29.53, 28.89, 21.41; **MS (ESI$^+$)** *m/z* calcd for $C_{14}H_{16}N_4O_2$ $(M+H)^+$ 272.13, found 273.2.

1-formylpiperidine-4-carboxylic acid (102)

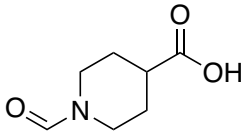

Molecular Weight: 157.17

Procedure adapted from literature.[167]Formic acid (0.99 mL, 23.22 mmol) was added to acetic anhydride (2.2 mL, 23.22 mmol). The resulting solution was stirred and heated at 60 °C for 1 h. Then, the reaction mixture was gradually cooled to 5 °C, and isonipecotic acid (500 mg, 3.87 mmol) was added. The resulting mixture was stirred at rt for 16 h. Then, the mixture was concentrated under reduced pressure and 2-propanol (2 mL) was added. The suspension was filtered under cooled condition (6 °C) to obtained 1-formylpiperidine-4-carboxylic acid (**102**) (574 mg, 3.65, 94%) as a white solid, **mp** 136-138 °C; R_f (DCM/Acetone 8:2) 0.38; **^{1}H NMR** (300 MHz, $CDCl_3$): δ 8.04 (s, 1H), 4.32 – 4.14 (m, 1H), 3.73 – 3.56 (m, 1H), 3.25 – 3.11 (m, 1H), 3.00 – 2.87 (m, 1H), 2.78 – 2.58 (m, 1H), 2.08 – 1.94 (m, 2H), 1.80 – 1.60 (m, 2H).

1-formylpiperidine-4-carbonyl chloride (97)

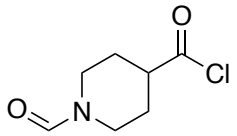

Molecular Weight: 175.61

Using the general procedure **G**, a mixture of 1-formylpiperidine-4-carboxylic acid (**102**) in $SOCl_2$ (3 mL) gave 1-formylpiperidine-4-carbonyl chloride (**97**) (876 mg, 4.99 mmol, 100%) as light oil used for the next reaction without further purification.

4-(3-(pyridin-3-yl)-1,2,4-oxadiazol-5-yl)piperidin-1-carbaldehyde (51)

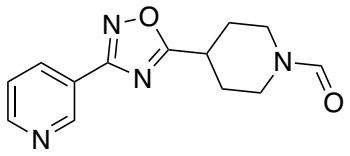

Molecular Weight: 258.28

Using the general procedure **H**, a mixture of 1-formylpiperidine-4-carbonyl chloride (**97**) (873 mg, 4.97 mmol), *N*-hydroxynicotinimidamide (**76**) (550 mg, 4.01 mmol) in pyridine (30 mL) gave the crude product. Then, the solution was allowed to cool to rt and concentrated under reduce pressure. The obtained solid was dissolved in DCM (20 mL) washed with NaOH 20% (2 x 10 mL) gave the crude product. Purification by flash column chromatography with 2:8 petroleum ether-ethyl acetate + 1% TEA as eluent gave 4-(3-(pyridin-3-yl)-1,2,4-oxadiazol-5-yl)piperidin-1-carbaldehyde (**51**) (54 mg, 0.21 mmol, 18%) as a light yellow solid, **mp** 103.9-105.5 °C; $\boldsymbol{R_f}$ (Petroleum ether/EtOAc + 1% TEA) 0.18; **^{1}H NMR** (300 MHz, $CDCl_3$): δ 9.28 (s, 1H), 8.73 (dd, *J* = 4.9, 1.9 Hz, 1H), 8.32 (dt, *J* = 8.0, 1.9 Hz, 1H), 8.07 (s, 1H), 7.41 (dd, *J* = 8.0, 4.9 Hz, 1H), 4.32 (dtd, *J* = 13.5, 4.2, 1.3 Hz, 1H), 3.74 (dtd, *J* = 13.5, 4.2, 1.3 Hz, 1H), 3.41 – 3.21 (m, 2H), 3.11 – 2.94 (m, 1H), 2.31 – 2.12 (m, 2H), 2.04 – 1.80 (m, 2H); **^{13}C NMR** (75 MHz, $CDCl_3$): δ 181.05, 166.40, 160.79, 152.03, 148.55, 134.75, 123.69, 123.00, 44.70, 38.64, 34.54, 29.70, 28.44; **MS (ESI$^+$)** *m/z* calcd for $C_{13}H_{14}N_4O_2$ $(M+H)^+$ 258.11, found 259.2.

6.3. Part 3

(*S*)-prolinol (115)

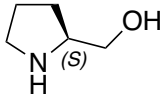

Molecular Weight: 101.15

Procedure adapted from literature.[96] To a suspension of $LiAlH_4$ (1.05 g, 27.80 mmol) in anhydrous THF (20 mL) was added very slowly (*S*)-proline (2.00 g, 17.37 mmol) at 0 °C under N_2. The mixture was stirred at reflux for 2 h. A solution of KOH 20% (10 mL) was added very

slowly, and the precipitate was removed by filtration. The solvent was concentrated under reduced pressure to give (*S*)-prolinol (**115**) (1.10 g, 10.91 mmol, 63%) as a pale-yellow oil; R_f (DCM/MeOH 9:1 stained with $KMnO_4$) 0.77; **[α]D^{25}** = +31.70° (*c*1, $CHCl_3$) (lit., [169]**[α]D^{25}** = +35.6° (*c*1, $CHCl_3$)); **^{1}H NMR** (300 MHz, $CDCl_3$): δ 3.53 – 3.46 (m, 1H), 3.43 – 3.16 (m, 2H), 3.01 – 2.78 (m, 2H), 1.93 – 1.58 (m, 3H), 1.46 – 1.36 (m, 1H).

(*S*)-*N*-benzyloxycarbonylprolinol (116)

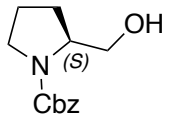

Molecular Weight: 235.28

Procedure adapted from literature.[170] Saturated $NaHCO_3$ (30 mL) was added to a solution of (*S*)-prolinol (**115**) (2.72 g, 26.92 mmol) in THF (20 mL) and the solution was cooled to 0 °C. Benzyl chloroformate (5.1 mL, 35.81 mmol) was added dropwise and the obtained mixture was stirred at 0 °C for 1 h, and then at rt for 16 h. The resulting mixture was diluted with H_2O (10 mL) and extracted with EtOAc (3 x 20 mL). The combined organic layers were washed with brine (30 mL), dried (Na_2SO_4), and evaporated under reduced pressure to give the crude product. Purification by flash column chromatography with 8:2 to 7:3 petroleum ether-ethyl acetate as eluent gave (*S*)-*N*-benzyloxycarbonylprolinol (**116**) (3.54 g, 15.02 mmol, 56%) as colourless oil; R_f (Cyclohexane/EtOAc 7:3) 0.19; **[α]D^{20}** = -41.86° (*c*1, $CHCl_3$) (lit., [170]**[α]D^{20}** = -40.2° (*c*1, $CHCl_3$)); **^{1}H NMR** (300 MHz, $CDCl_3$): δ 7.30 – 7.39 (m, 5H), 5.18 (s, 2H), 4.06 – 3.90 (m, 1H), 3.70 – 3.30 (m, 4H), 3.15 – 3.00 (br s, 1H, exchange with D_2O), 2.05 – 1.55 (m, 4H).

(*S*)-*N*-benzyloxycarbonyl-2-methylsulfonyoxymethylpyrrolidine (111)

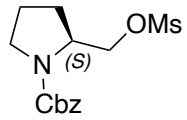

Molecular Weight: 313.37

Procedure adapted from literature.[96] TEA (1.7 mL, 12.17 mmol) was added to a stirred solution of (*S*)-*N*-benzyloxycarbonylprolinol (**116**) (2.60 g, 11.05 mmol) in DCM (10 mL) at -10 °C. The resulting mixture was stirred for 10 min. Then, MsCl (0.94 mL, 12.17 mmol) was added dropwise and the solution was stirred at rt for 3 h. The stirred solution was washed with HCl 1 M (10 mL) and the organic layer was dried (Na_2SO_4) and evaporated under reduced pressure to give the crude product. Purification by flash column chromatography with 7:3 petroleum ether-ethyl acetate as eluent gave (*S*)-*N*-benzyloxycarbonyl-2-methylsulfonyoxymethylpyrrolidine (**111**) (3.24 g, 10.34 mmol, 94%) as a light yellow solid, **mp** 43.7 – 44.1 °C (lit.,[96]43.7°C); $\boldsymbol{R_f}$ (Cyclohexane/EtOAc 6:4 stained with $KMnO_4$) 0.26; **[α]D^{25}** = -51.00° (*c*1, $CHCl_3$) (lit.,[96]**[α]D^{25}** = -51.00° (*c*1, $CHCl_3$)) ; **^{1}H NMR** (300 MHz, $CDCl_3$): δ 7.30 – 7.38 (m, 5H), 5.13 (s, 2H), 4.32 – 4.05 (m, 3H), 3.48 – 3.43 (m, 2H), 2.95 – 2.83 (m, 3H), 2.17 – 1.85 (m, 4H).

3-benzyloxy-5-chloropyridine (117)

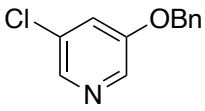

Molecular Weight: 219.67

Procedure adapted from literature.[171] A solution of benzyl alcohol (3.5 mL, 33.79 mmol) in anhydrous DMF (5 mL) was added dropwise to a suspension of NaH (1.05 g, 43.92 mmol) in anhydrous DMF (10 mL) at -10 °C under N_2. The resulting suspension was stirred at 0 °C for 30 min. Then, a solution of 3,5-dichloropyridine (5.00 g, 33.79 mmol) in anhydrous DMF (10 mL) was added dropwise. The mixture was stirred at rt overnight. The mixture was quenched with H_2O (10 mL) and extracted with EtOAc (3 x 10 mL). The combined organic layers were dried

(Na_2SO_4) and evaporated under reduced pressure to give the crude product. Purification by flash column chromatography with 9:1 petroleum ether-ethyl acetate as eluent gave 3-benzyloxy-5-chloropyridine (**117**) (5.99 g, 27.28 mmol, 81%) as a white solid, **mp** 46.4-47.3°C; R_f (Petroleum ether/EtOAc 9:1) 0.34; **^{1}H NMR** (300 MHz, $CDCl_3$): δ 8.28 (d, *J* = 2.6 Hz, 1H), 8.28 (d, *J* = 1.9 Hz, 1H), 7.47 – 7.30 (m, 5H), 7.27 (dd, *J* = 2.6, 1.9 Hz,1H), 5.10 (s, 2H).

3-amino-5-benzyloxypyridine (118)

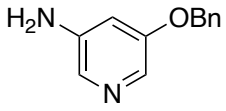

Molecular Weight: 200.24

In a pressure vessel, 3-benzyloxy-5-chloropyridine (**117**) (970 mg, 3.67 mmol), $CuSO_4$ (1.84 g, 1.84 mmol) and $NH_{3\,(25\%\,in\,water)}$ (15 mL) were added and stirred at 180 °C overnight. The mixture was allowed to warm at rt and when cooled to 0 °C. The product was filtered off, washed with saturated K_2CO_3 (2 x 10 mL) and suspended in EtOAc (15 mL). Undissolved material was filtered off and the filtrate was dried (Na_2SO_4) and concentrated under reduced pressure to give 3-amino-5-benzyloxypyridine (**118**) (380 g, 1.90 mmol, 52%) as a light yellow solid, **mp** 100.5-101.3°C; R_f (DCM/MeOH 95:5) 0.31; **^{1}H NMR** (300 MHz, $CDCl_3$): δ 7.82 (s, 1H), 7.75 (s, 1H), 7.47 – 7.27 (m, 5H), 6.58 (t, *J* = 2.3 Hz, 1H), 5.06 (s, 2H), 3.55 (br s, 2H).

3-benzyloxy-5-hydroxypyridine (119)

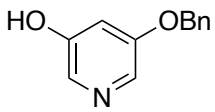

Molecular Weight: 201.23

3-amino-5-benzyloxypyridine (**118**) (666 mg, 3.33 mmol) was stirred into concentrated H_2SO_4 (3 mL), H_2O (3 mL) and ice. The mixture was heated until the solution became homogenous and when allowed to stir at rt for 10 min. Then, the suspension was cooled to 0 °C and a solution of $NaNO_2$ (230 mg, 3.33 mmol) in H_2O (5 mL) was added. The mixture was allowed to stir for 10 min at 0 °C and then for 10 min at rt. A boiling solution of concentrated H_2SO_4 (1

mL) was added. The mixture was stirred at rt for 3 h. Then, the pH was adjusted to 10 with 10% NaOH solution (10 mL) and the mixture was extracted with EtOAc (3 x 10 mL). The combined organic layers were dried (Na_2SO_4) and evaporated under reduced pressure to give 3-benzyloxy-5-hydroxypyridine (**119**) (525 mg, 2.61 mmol, 97%) as a red solid, **mp** 128.1-130.2°C; R_f (EtOAc) 0.63; **^{1}H NMR** (300 MHz, $CDCl_3$): δ 7.93 – 7.87 (m, 2H), 7.48 – 7.26 (m, 5H), 6.91 (t, *J* = 2.1 Hz, 1H), 5.08 (s, 2H).

3-(benzyloxy)-5-((2-methoxyethoxy)methoxy)pyridine (120)

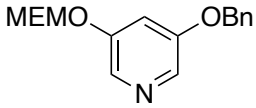

Molecular Weight: 289.33

MEMCl (0.15 mL, 1.31 mmol) was added dropwise to a solution of 3-benzyloxy-5-hydroxypyridine (**119**) (188 mg, 0.94 mmol) and DIPEA (0.29 mL, 1.66 mmol) in DCM (5 mL) at 0 °C under N_2. The mixture was stirred and heated at 35 °C for 4 h. Then, the mixture was quenched with saturated aqueous NH_4Cl at 0 °C. The aqueous layer was extracted with EtOAc (3 x 10 mL). The combined organic layers were dried (Na_2SO_4) and evaporated under reduced pressure to give the crude product. Purification by flash column chromatography with 6:4 cyclohexane-ethyl acetate as eluent gave 3-(benzyloxy)-5-((2-methoxyethoxy)methoxy)pyridine (**120**) (171 mg, 0.60 mmol, 63%) as a yellow oil; R_f (Cyclohexane/EtOAc 6:4) 0.31; **^{1}H NMR** (300 MHz, $CDCl_3$): δ 8.07 (t, *J* = 2.4 Hz, 2H), 7.47 – 7.30 (m, 5H), 7.04 (t, *J* = 2.4 Hz, 1H), 5.27 (s, 2H), 5.09 (s, 2H), 3.87 – 3.78 (m, 2H), 3.58 – 3.52 (m, 2H), 3.38 (s, 3H).

3-hydroxy-5-((2-methoxyethoxy)methoxy)pyridine (112)

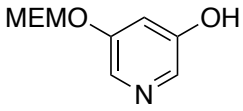

Molecular Weight: 199.20

10% Pd/C (40 mg) was added to a solution of 3-(benzyloxy)-5-((2-methoxyethoxy)methoxy)pyridine (**120**) (229 mg, 0.79 mmol) in MeOH (5 mL). The resulting mixture was stirred at rt for 3 h under H_2. Then, the stirred solution was filtered over Celite® and washed with MeOH. The filtrate was evaporated under reduced pressure to give the crude product. Purification by flash column chromatography with 3:7 petroleum ether-ethyl acetate as eluent gave 3-hydroxy-5-((2-methoxyethoxy)methoxy)pyridine (**112**) (150 mg, 0.75 mmol, 95%) as a yellow oil; R_f (Petroleum ether/EtOAc 3:7) 0.38; **^{1}H NMR** (300 MHz, $CDCl_3$): δ 7.99 (d, *J* = 2.3 Hz, 1H), 7.93 (d, *J* = 2.3 Hz, 1H), 7.10 (t, *J* = 2.3 Hz, 1H), 5.27 (s, 2H), 3.88 – 3.79 (m, 2H), 3.63 – 3.54 (m, 2H), 3.39 (s, 3H).

(*S*)-*N*-Cbz-2-(((5-((2-methoxyethoxy)methoxy)pyridine-3-yl)oxy)methyl)pyrrolidine (113)

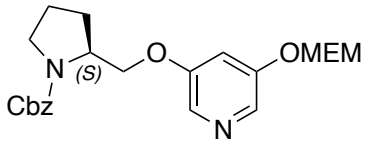

Molecular Weight: 416.47

A solution of 3-hydroxy-5-((2-methoxyethoxy)methoxy)pyridine (**112**) (160 mg, 0.80 mmol) in anhydrous DMF (5 mL) was added dropwise to a suspension of NaH (19 mg, 0.80 mmol) in anhydrous DMF (5 mL) at -10 °C under N_2. The resulting suspension was stirred at -10 °C for 10 min. Then, a solution of (*S*)-*N*-Cbz-2-(((methylsulfonyl)oxy)methyl)pyrrolidine (**111**) (252 mg, 0.80 mmol) in anhydrous DMF (5 mL) was added dropwise. The mixture was stirred at 80 °C for 4 h. The reaction was cooled to rt, DMF was evaporated and the residue was treated with H_2O (15 mL) and extracted with EtOAc (3 x 10 mL). The combined organic layers were dried (Na_2SO_4) and evaporated under reduced pressure to give the crude product. Purification by flash column chromatography with 1:1 petroleum ether-ethyl acetate + 1% TEA as eluent

gave (*S*)-*N*-Cbz-2-(((5-((2-methoxyethoxy)methoxy)pyridine-3-yl)oxy)methyl)pyrrolidine (**113**) (213 mg, 0.51 mmol, 64%) as a yellow oil; R_f (Petroleum ether/EtOAc + 1% TEA 8:2) 0.36; **[α]D^{25}** = -40.50° (*c*0.5, $CHCl_3$); **^{1}H NMR** (300 MHz, $CDCl_3$): δ 8.03 (m, 2H), 7.42 – 7.31 (m, 5H), 7.04 (s, 1H), 5.27 (s, 2H), 5.17 – 5.10 (m, 2H), 4.24 – 4.18 (m, 2H), 3.92 – 3.77 (m, 3H), 3.61 – 3.51 (m, 2H), 3.51 – 3.45 (m, 2H), 3.37 (s, 3H), 2.09 – 1.81 (m, 4H).

(*S*)-3-((2-methoxyethoxy)methoxy)-5-((1-methylpyrrolidin-2-yl)methoxy)pyridine (114)

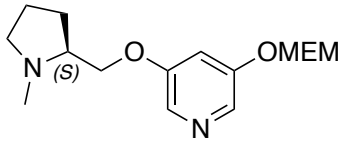

Molecular Weight: 296.37

A solution of (*S*)-*N*-Cbz-2-(((methylsulfonyl)oxy)methyl)pyrrolidine (**113**) (204 mg, 0.49 mmol) in anhydrous THF (3 mL) was added dropwise to a suspension of $LiAlH_4$ (74 mg, 1.96 mmol) in anhydrous THF (5 mL) at 0 °C under N_2. The reaction was stirred at rt for 3 h. Then, H_2O (15 mL) was added to quench $LiAlH_4$. HCl 1M (10 mL) was added and the mixture was extracted with DCM (3 x 10 mL). The aqueous layer was basified at pH 10 with NaOH 1M (11 mL) and extracted with DCM (3 x 15 mL). The combined organic layers were dried (Na_2SO_4) and evaporated under reduced pressure to give (*S*)-3-((2-methoxyethoxy)methoxy)-5-((1-methylpyrrolidin-2-yl)methoxy)pyridine (**114**) (104 mg, 0.35 mmol, 72%) as light yellow oil; R_f (DCM/MeOH 93:7 + 1% $NH_{3\ (22\%\ in\ water)}$) 0.18; **[α]D^{25}** = -0.656° (*c*0.5, MeOH); **^{1}H NMR** (300 MHz, $CDCl_3$): δ 8.10 – 7.94 (m, 2H), 6.97 (t, *J* = 2.4 Hz, 1H), 5.27 (s, 2H), 4.11 – 4.00 (m, 1H), 3.99 – 3.88 (m, 1H), 3.87 – 3.78 (m, 2H), 3.60 – 3.51 (m, 2H), 3.37 (s, 3H), 3.22 – 3.11 (m, 1H), 2.75 – 2.69 (m, 1H), 2.51 (s, 3H), 2.43 – 2.28 (m, 1H), 2.14 – 1.97 (m, 2H), 1.86 – 1.68 (m, 2H).

7-hydroxy-2-methylquinolin-1-ium-4-metylbenzenesulfonate (123)

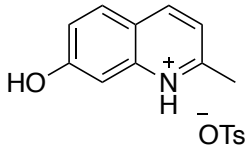

Molecular Weight: 331.39

Procedure adapted from literature.[138] 3-aminophenol (10.00 g, 91.63 mmol) was added to a solution of $FeCl_3$ (14.86 g, 91.63 mmol) in 6N HCl (40 mL). Then butanol (25 mL) was added and the resulting mixture was stirred and heated to 95 °C. At the desired temperature, crotonaldehyde (9 mL, 108.63 mmol) in butanol (12 mL) was added dropwise over 45 min and the resulting suspension was stirred at the reflux for 1 h. Then the mixture was allowed to cool first to room temperature and subsequently to <10 °C on an ice bath. The pH was adjusted to 7.5 using $NH_{3\ (22\%\ in\ water)}$. The temperature was not allowed to go above 40 °C during the neutralization. Then, butanol (20 mL) was added and the resulting biphasic mixture was filtered over Celite® and washed with butanol (10 mL) and H_2O (10 mL). The layers were separated and the aqueous layer extracted with THF (3 x 20 mL). The combined organic layers were dried (Na_2SO_4) and filtered over Celite® and washed with THF (10 mL). The filtrate was concentrated under reduced pressure and then diluted with 2-propanol (20 mL). Undissolved material was filtered off and the resulting cake was washed with 2-propanol (15 mL). Para-toluene sulfonic acid monohydrate (17.43 g, 91.63 mmol) was added to the organic filtrate and the mixture was stirred at rt for 2 h. The product was filtered off, washed with 2-propanol (2 x 5 mL) and left to dry under vacuum to give 7-hydroxy-2-methylquinolin-1-ium-4-metylbenzenesulfonate (**123**) (9.20 g, 27.70 mmol, 30%) as a light brown solid, **mp** 236-237 °C; $\boldsymbol{R_f}$ (Cyclohexane/EtOAc 3:7 + 1% TEA) 0.31; **^{1}H NMR** (300 MHz, DMSO-*d6*): δ 15.40 (s, 1H), 11.55 (s, 1H), 8.85 (d, *J* = 8.3 Hz, 1H), 8.14 (d, *J* = 8.9 Hz, 1H), 7.65 (d, *J* = 8.3 Hz, 1H), 7.46 (d, *J* = 7.9 Hz, 2H), 7.41 – 7.34 (m, 2H), 7.10 (d, *J* = 7.9 Hz, 2H), 2.84 (s, 3H), 2.27 (s, 3H).[138]

8-Bromo-7-hydroxy-2-methylquinolin-1-ium-4-metylbenzenesulfonate (124)

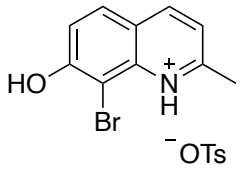

Molecular Weight: 410.28

7-hydroxy-2-methylquinolin-1-ium-4-metylbenzenesulfonate (**123**) (9.19 g, 27.73 mmol) was dissolved in MeOH (25 mL) and the mixture was stirred at rt for 10 min. *N*-bromosuccinimide (9.87 g, 55.45 mmol) was added in portions to the stirred solution and the resulting suspension was stirred at rt overnight. Then, the resulting mixture was concentrated under reduced pressure to dryness to give the crude compound. Acetonitrile (20 mL) was added and the formed slurry was stirred at rt for 1 h. Undissolved material was filtered off, washed with acetonitrile (2 x 5 mL) and left to dry under vacuum to give 8-Bromo-7-hydroxy-2-methylquinolin-1-ium-4-metylbenzenesulfonate (**124**) (7.50 g, 18.28 mmol, 66%) as a yellow-orange powder, **mp** 218-220 °C; **^{1}H NMR** (300 MHz, DMSO-d6,): δ 8.44 (d, *J* = 8.2 Hz, 1H), 7.91 (d, J = 9.1 Hz, 1H), 7.54 – 7.39 (m, 3H). 7.37 (d, *J* = 9.1 Hz, 1H), 7.10 (d, *J* = 8.2 Hz, 2H), 2.75 (s, 3H), 2.28 (s, 3H).[138]

8-Bromo-7-((2-methoxyethoxy)methoxy)-2-methylquinoline (128)

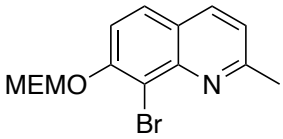

Molecular Weight: 326.19

Procedure adapted from literature.[172] A mixture of previously released 8-Bromo-7-Hydroxy-2-metylquinoline from **124** (2.62 g, 11.00 mmol) and K_2CO_3 (1.52 g, 11.00 mmol) in acetone (20 mL) was stirred at rt for 30 min under N_2. Then, the mixture was cooled to 0 °C and a solution of MEMCl (1.3 mL, 11.00 mmol) in acetone (10 mL) was added dropwise over 20 min and the resulting mixture was stirred at rt overnight. EtOAc (20 mL) was added to the mixture, acetone was evaporated under reduced pressure and then the reaction mixture was

quenched with NaOH 1M. The layers were separated and the aqueous phase was extracted with EtOAc (3 x 10 mL). The combined organic layers were dried (Na_2SO_4) and concentrated under reduced pressure to dryness to give a brownish oil. Purification by flash column chromatography with 8:2 cyclohexane-ethyl acetate as eluent gave 8-Bromo-7-((2-methoxyethoxy)methoxy)-2-methylquinoline (**128**) (2.50 g, 7.66 mmol, 69%) as a colourless oil; R_f (Cyclohexane-Acetone 7:3) 0.46; **^{1}H NMR** (300 MHz, $CDCl_3$): δ 7.98 (d, *J* = 8.3 Hz, 1H), 7.70 (d, *J* = 9.0 Hz, 1H), 7.48 (d, *J* = 9.0 Hz, 1H), 7.23 (d, *J* = 8.3 Hz, 1H), 5.48 (s, 2H), 4.01 – 3.87 (m, 2H), 3.63 – 3.52 (m, 2H), 3.36 (s, 3H), 2.80 (s, 3H).

8-Bromo-7-((2-methoxyethoxy)methoxy)-quinoline-2-carbaldehyde (130)

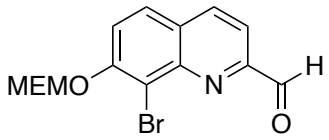

Molecular Weight: 340.17

Procedure adapted from literature.[173] Selenium dioxide (780 mg, 7.03 mmol) was added to a solution of 8-Bromo-7-(2-(methoxyetoxy)methoxy)-2-methylquinoline (**128**) (1.95 g, 5.98 mmol) in dioxane (15 mL) and the mixture was heated at 80 °C for 1 h. Then, the mixture was filtered and the filtrate was concentrated under reduced pressure to give 8-Bromo-7-((2-methoxyethoxy)methoxy)-quinoline-2-carbaldehyde (**130**) (2.04 g, 5.98 mmol, 100%) as a dark red solid, **mp** 80-83 °C; R_f (Cyclohexane-Acetone 7:3) 0.41; ^{1}H NMR (300 MHz, $CDCl_3$): δ 10.30 (s, 1H), 8.28 (d, *J* = 8.3 Hz, 1H), 7.99 (d, *J* = 8.3 Hz, 1H), 7.85 (d, *J* = 9.1 Hz, 1H), 7.71 (d, *J* = 9.1 Hz, 1H), 5.54 (s, 2H), 4.05 – 3.88 (m, 2H), 3.65 – 3.50 (m, 2H), 3.36 (s, 3H).

8-Bromo-7-((2-methoxyethoxy)methoxy)quinolin-2-yl)methanol (132)

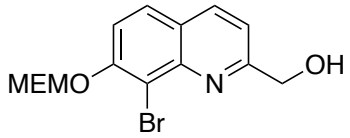

Molecular Weight: 342.15

Procedure adapted from literature.[173] $NaBH_4$ (226 mg, 5.98 mmol) was added portionwise to a suspension of 8-Bromo-7-((2-methoxyethoxy)methoxy)-quinolin-2-carbaldehyde (**130**) (2.03 g, 5.98 mmol) in ethanol (20 mL) and the resulting solution was stirred at rt for 1 h. EtOAc (15 mL) was added and the organic phase washed with H_2O (10 mL). The two layers were separated and the aqueous layer was extracted with EtOAc (3 × 7 mL). The combined organic layers were dried (Na_2SO_4) and concentrated under reduced pressure to give 8-Bromo-7-((2-methoxyethoxy)methoxy)quinolin-2-yl)methanol (**132**) (2.05 g, 5.98 mmol, 100%) as a brown-orange solid, **mp** 78-81 °C; R_f (Cyclohexane-Acetone 7:3) 0.27; **^{1}H NMR** (300 MHz, $CDCl_3$): δ 8.09 (d, *J* = 8.3 Hz, 1H), 7.76 (d, *J* = 9.1 Hz, 1H), 7.55 (d, *J* = 9.1 Hz, 1H), 7.22 (d, *J* = 8.3 Hz, 1H), 5.51 (s, 2H), 4.94 (s, 2H), 3.99 – 3.89 (m, 2H), 3.62 – 3.53 (m, 2H), 3.36 (s, 3H).

(8-Bromo-7-((2-methoxyethoxy)methoxy)quinolin-2-yl)methyl methansulfonate (134)

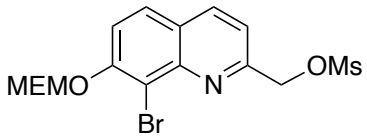

Molecular Weight: 420.27

Procedure adapted from literature.[138] TEA (2.6 mL, 18.43 mmol) was added to a solution of 8-Bromo-7-((2-methoxyethoxy)methoxy)quinolin-2-yl)methanol (**132**) (2.05 g, 5.98 mmol) in DCM (20 mL) and the resulting solution was stirred for 5 min. Then, the mixture was cooled to 5 °C and methanesulfonyl chloride (0.94 mL, 12.16 mmol) was slowly added. The resulting solution was stirred at 5 °C for 1 h. Upon completion, the reaction was quenched with H_2O (7 mL) and the layers were separated. The organic layer was dried (Na_2SO_4) and concentrated under reduced pressure to give the crude product. Purification by flash column chromatography with 7:3 cyclohexane-ethyl acetate as eluent gave (8-Bromo-7-((2-

methoxyethoxy)methoxy)quinolin-2-yl)methyl methansulfonate (**134**) (1.45 g, 3.45 mmol, 57%) as a white solid; R_f (Cyclohexane/EtOAc 7:3) 0.12; **^{1}H NMR** (300 MHz, $CDCl_3$): δ 8.19 (d, *J* = 8.3 Hz, 1H), 7.79 (d, *J* = 9.1 Hz, 1H), 7.60 (d, *J* = 9.1 Hz, 1H), 7.52 (d, *J* = 8.3, 2H), 5.56 (s, 2H), 5.51 (s, 2H), 4.00 – 3.91 (m, 2H), 3.63 – 3.51 (m, 2H), 3.36 (s, 3H), 3.22 (s, 3H).

(8-Bromo-7-hydroxyquinolin-2-yl)methyl methansulfonate (121)

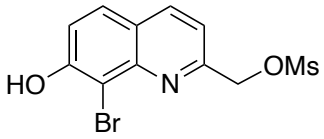

Molecular Weight: 332.17

Procedure adapted from literature.[138] Trifluoroacetic acid (2.6 mL, 34.50 mmol) was added to a solution of (8-Bromo-7-((2-methoxyethoxy)methoxy)quinolin-2-yl)methyl methansulfonate (**134**) (1.45 g, 3.45 mmol) in DCM (15 mL) and the resulting solution was stirred at rt for 8 h. Then, the solution was washed with H_2O (5 mL) and the layers were separated. The aqueous layer was extracted with EtOAc (2 x 7 mL). The combined organic layers were dried (Na_2SO_4) and concentrated under reduced pressure to give the crude product. Purification by flash column chromatography with 10:0 to 7:3 Cyclohexane-Acetone as eluent gave (8-Bromo-7-hydroxyquinolin-2-yl)methyl methansulfonate (**121**) (1.03 g, 3.10 mmol, 90%) as an orange-brown solid, **mp** 132-134 °C; R_f (Cyclohexane-Acetone 7:3) 0.17; **^{1}H NMR** (300 MHz, $CDCl_3$): δ 8.18 (d, *J* = 8.4 Hz, 1H), 7.74 (d, *J* = 8.8 Hz, 1H), 7.50 (d, *J* = 8.4 Hz, 1H), 7.37 (d, *J* = 8.8 Hz, 1H), 5.55 (s, 2H), 3.20 (s, 3H).

(2*S*)-1-((8-bromo-7-hydroxyquinolin-2-yl)methyl)-2-(((5-((2-methoxyethoxy)methoxy)pyridin-3-yl)oxy)methyl)-1-methylpyrrolidin-1-ium methanesulfonate (136)

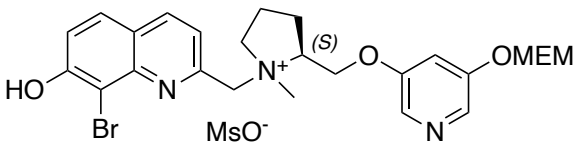

Molecular Weight: 628.54

Procedure adapted from literature.[138] (8-bromo-7-hydroxyquinolin-2-yl)methylmethansulfonate (**121**) (85 mg, 0.26 mmol) and (*S*)-3-((2-methoxyethoxy)methoxy)-5-((1-methylpyrrolidin-2-yl)methoxy)pyridine (**114**) (95 mg, 0.32 mmol) were dissolved in acetonitrile (5 mL). The mixture was stirred at rt for 4 h. Then, the solvent was concentrated under reduced pressure to give the crude product as a brown oil. Purification by flash column chromatography with 8:2 DCM/MeOH as eluent gave ((2*S*)-1-((8-bromo-7-hydroxyquinolin-2-yl)methyl)-2-(((5-((2-methoxyethoxy)methoxy)pyridin-3-yl)oxy)methyl)-1-methylpyrrolidin-1-ium methanesulfonate (**136**) (110 mg, 0.18 mmol, 55%) as a light yellow oil; ***Rf*** (DCM/MeOH 8:2) 0.15; **^{1}H NMR** (300 MHz, CD_3OD): δ 8.35 (dd, *J* = 8.3, 6.2 Hz, 1H), 8.04 – 7.94 (m, 2H), 7.84 (dd, *J* = 8.9, 5.0 Hz, 1H), 7.54 (dd, *J* = 8.3, 6.2 Hz, 1H), 7.35 (dd, *J* = 8.9, 4.1 Hz, 1H), 7.25 (dt, *J* = 8.7, 2.4 Hz, 1H), 5.32 (d, *J* = 5.1 Hz, 2H), 5.22 (d, *J* = 14.1 Hz, 1H), 4.99 (d, *J* = 14.1 Hz, 1H), 4.81 – 4.61 (m, 2H), 4.27 (dd, *J*= 12.0, 7.1 Hz, 1H), 4.03 – 3.93 (m, 1H), 3.86 – 3.77 (m, 2H), 3.60 – 3.49 (m, 3H), 3.38 (s, 3H), 3.29 (s, 3H), 2.85 (s, 3H), 2.55 – 2.22 (m, 4H).

(2*S*)-1-((8-bromo-7-hydroxyquinolin-2-yl)methyl)-2-(((5-hydroxypyridin-3-yl)oxy)methyl)-1-methylpyrrolidin-1-ium methanesulfonate (BHQ-(*S*)-VI)

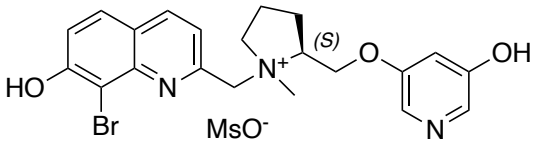

Molecular Weight: 540.43

Procedure adapted from literatrure.[138] Trifluoroacetic acid (0.13 mL, 1.75 mmol) was added to a solution of ((2*S*)-1-((8-bromo-7-hydroxyquinolin-2-yl)methyl)-2-(((5-((2-

methoxyethoxy)methoxy)pyridin -3-yl)oxy)methyl)-1-methylpyrrolidin-1-ium methanesulfonate (**136**) (110 mg, 0.18 mmol) in DCM (5 mL). The mixture was stirred at rt for 3 h. Then, the solvent was concentrated under reduced pressure to give the crude product as a brown oil. Crystallization with DCM (2 mL) gave (*S*)-1-((8-bromo-7- hydroxyquinolin-2-yl)methyl)-2-(((5-hydroxypyridin-3-yl)oxy)methyl)-1-methylpyrrolidin-1-ium (BHQ-(*S*)-**VI**) (10.4 mg, 0.02 mmol, 17%) as a light yellow oil; ***Rf*** (DCM/MeOH 8:2) 0.48; **[α]**= -15.04° (*c*0.5, MeOH); **^{1}H NMR** (300 MHz, CD_3OD) (50:50 mixture of rotamers): δ 8.33 (dd, *J* = 8.3, 6.2 Hz, 1H), 8.10 – 8.04 (m, 1H), 7.99 – 7.88 (m, 1H), 7.82 (dd, *J* = 9.0, 4.5 Hz, 1H), 7.54 (dd, *J* = 8.3, 5.9 Hz, 1H), 7.43 (d, *J* = 16.1 Hz, 1H), 7.34 (dd, *J* = 8.9, 3.9 Hz, 1H), 5.20 (d, *J* = 14.1 Hz, 0.5H), 4.98 (d, *J* = 14.2 Hz, 0.5H), 4.93 – 4.82 (m, 1H), 4.81 – 4.65 (m, 3H), 4.35 – 4.15 (m, 1H), 4.03 – 3.91 (m, 0.5H), 3.83 – 3.68 (m, 0.5H), 3.51 (s, 1,5H), 3.39 (s, 1.5H), 2.70 (s, 3H), 2.55 – 2.20 (m, 4H); **^{13}C NMR** (75 MHz, CD_3OD): δ 161.74, 161.27, 156.71, 150.96, 146.07, 146.05, 138.05, 127.99, 127.97, 125.29, 123.46, 123.31, 120.57, 120.25, 119.84, 119.76, 115.07, 106.23, 106.13, 74.72, 72.81, 67.17, 66.40, 65.77, 65.55, 64.82, 60.53, 50.18, 44.36, 38.19, 38.16, 33.97, 23.93, 23.51, 19.48, 19.19; **HRMS (ESI^{+})** *m/z* calcd for $C_{21}H_{23}N_3O_3Br$ $(M+H)^{+}$ 444.0923, found 444.0923.

8-Iodio-7-hydroxy-2-methylquinolin-1-ium-4-metylbenzenesulfonate (125)

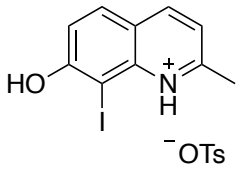

Molecular Weight: 457.28

7-hydroxy-2-methylquinolin-1-ium-4-metylbenzenesulfonate (**123**) (2.19 g, 6.61 mmol) was dissolved in MeOH (20 mL) and the mixture was stirred at rt for 10 min. *N*-iodosuccinimide (2.98 g, 13.22 mmol) was added in portions to the stirred solution and the resulting suspension was stirred at rt overnight. Then, the resulting mixture was concentrated under reduced pressure to dryness to give the crude compound. Acetonitrile (20 mL) was added and the formed slurry was stirred at rt for 1 h. Undissolved material was filtered off, washed with acetonitrile (2 x 5 mL) and left to dry under vacuum to give 8-Iodio-7-hydroxy-2-methylquinolin-1-ium-4-metylbenzenesulfonate (**125**) (1.81 g, 3.97 mmol, 60%) as a dark

orange powder; **mp** 218-220°C; **^{1}H NMR** (300 MHz, DMSO-*d6*): δ 8.11 (d, *J* = 7.9 Hz, 1H), 7.76 (d, *J* = 8.7 Hz, 1H), 7.45 (d, *J* = 8.1 Hz, 2H), 7.29 – 7.17 (m, 2H), 7.12 – 7.02 (m, 2H), 2.65 (s, 3H), 2.27 (s, 3H).

8-Iodio-2-methylquinolin-7-yl acetate (126)

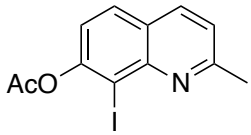

Molecular Weight: 327.12

Procedure adapted from literature.[138] TEA (1.4 mL, 9.83 mmol) was added to a suspension of 8-Iodio-7-hydroxy-2-methylquinolin-1-ium-4-metylbenzenesulfonate (**125**) (1.81 g, 3.97 mmol) in acetonitrile under a N_2 and the resulting solution was cooled to 5 °C. Acetyl chloride (0.34 mL, 4.75 mmol) in acetonitrile (2.5 mL) was added dropwise to the cold solution over 20 min. The mixture was allowed to warm to rt and then it was concentrated under reduced pressure to dryness. EtOAc (5 mL) and H_2O (5 mL) were added to the crude and the layers were separated. The organic layer was washed with saturated $NaHCO_3$ solution (2.5 mL) and H_2O (2 x 2.5 mL), dried (Na_2SO_4) and concentrated under reduced pressure to give 8-Iodio-2-methylquinolin-7-yl acetate (**126**) (1.30 g, 3.97 mmol, 100%) as a brownish solid, **mp** 88-93 °C; ***R*$_f$** (Cyclohexane/EtOAc 7:3) 0.51; **^{1}H NMR** (300 MHz, $CDCl_3$): δ 7.99 (d, *J* = 8.2, 1H), 7.76 (d, *J* = 8.7, 1H), 7.31 (d, *J* = 8.2, 1H), 7.24 (d, *J* = 8.7, 1H), 2.81 (s, 3H), 2.45 (s, 3H).

8-Cyano-7-Hydroxy-2-methylquinolin (127)

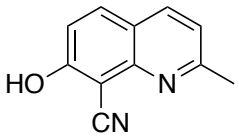

Molecular Weight: 184.20

Procedure adapted from literature.[138] A solution of 8-Iodio-2-methylquinolin-7-yl acetate (**126**) (1.30 g, 3.97 mmol) in *N,N*-dimethylacetamide (5 mL) was added dropwise over 1 h to a refluxing solution of CuCN (0.71 g, 7.95 mmol) in *N,N*-dimethylacetamide. After the

completion of the addition, Pd-Tetrakis (0.23 mg, 0.20 mmol) was added. The resulting mixture was stirred at reflux for 5 h. Then, the suspension was cooled to rt. H_2O (10 mL) was slowly added and a precipitate was formed. The suspension was filtered and the solid material was dissolved in $NH_4OH_{(aq)}$ and the resulting solution was adjusted to pH=3 using HCl 37%. The aqueous solution was extracted with 2-butanol, dried (Na_2SO_4) and concentrated under reduced pressure to give the crude product. DCM (10 mL) and Et_2O (10 mL) were added to the crude and the precipitate was filtered. The organic layer was concentrated under reduced pressure and then acetonitrile (20 mL) was added. The mixture was filtered, and the organic layer was evaporated to give the crude product. Purification by flash column chromatography with 9:1 to 7:3 Cyclohexane-Acetone as eluent gave 8-Cyano-7-Hydroxy-2-methylquinolin (**127**) (460 mg, 2.49 mmol, 61%) as a yellow solid, **mp** 81-85 °C; $\boldsymbol{R_f}$ (Cyclohexane/EtOAc 4:6) 0.51; **^{1}H NMR** (300 MHz, CD_3OD): δ 8.20 (d, *J* = 8.5 Hz, 1H), 8.02 (d, *J* = 9.1 Hz, 1H), 7.33 (d, *J* = 8.5 Hz, 1H), 7.25 (d, *J* = 9.1 Hz, 1H), 2.78 (s, 3H).[138]

8-Cyano-7-((2-methoxyethoxy)methoxy)-2-methylquinoline (129)

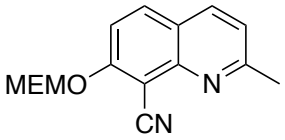

Molecular Weight: 272.304

Procedure adapted from literature.[172] A mixture of 8-Cyano-7-Hydroxy-2-methylquinoline (**127**) (460 g, 2.49 mmol) and K_2CO_3 (690 mg, 4.99 mmol) in acetone (10 mL) was stirred at rt for 30 min under N_2. Then, the mixture was cooled to 0 °C and a solution of MEMCl (0.28 mL, 2.49 mmol) in acetone (5 mL) was added dropwise over 20 min and the resulting mixture was stirred at rt overnight. EtOAc (15 mL) was added to the mixture, acetone was evaporated under reduced pressure and then the reaction mixture was quenched with NaOH 1M. The layers were separated and the aqueous phase was extracted with EtOAc (3 x 10 mL). The combined organic layers were dried (Na_2SO_4) and concentrated under reduced pressure to dryness to give a brownish oil. Purification by flash column chromatography with 8:2 cyclohexane-ethyl acetate as eluent gave 8-Cyano-7-((2-methoxyethoxy)methoxy)-2-methylquinoline (**129**) (600 mg, 2.20 mmol, 88%) as a light yellow oil; $\boldsymbol{R_f}$ (Cyclohexane/EtOAc

7:3) 0.17; **^{1}H NMR** (300 MHz, $CDCl_3$): δ 8.00 (d, *J* = 8.5 Hz, 1H), 7.91 (d, *J* = 9.1 Hz, 1H), 7.51 (d, *J* = 9.1 Hz, 1H), 7.27 (d, *J* = 8,5 Hz, 1H), 5.53 (s, 2H), 4.00 – 3.89 (m, 2H), 3.58 – 3.51 (m, 2H), 3.36 (s, 3H), 2.78 (s, 3H).

8-Cyano-7-((2-methoxyethoxy)methoxy)-quinoline-2-carbaldehyde (131)

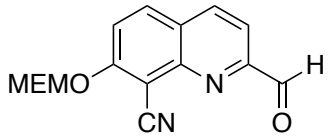

Molecular Weight: 286.29

Selenium dioxide (286 mg, 1.17 mmol) was added to a solution of 8-Cyano-7-((2-methoxyethoxy)methoxy)-2-methylquinoline (**129**) (600 mg, 2.20 mmol) in dioxane (15 mL) and the mixture was heated at 60 °C for 3 h. Then, the mixture was filtered and the filtrate was concentrated under reduced pressure to give the crude product. Purification by flash column chromatography with 7:3 to 1:1 petroleum ether-ethyl acetate as eluent gave 8-Cyano-7-((2-methoxyethoxy)methoxy)-quinoline-2-carbaldehyde (**131**) (380 mg, 1.33 mmol, 60%) as yellow solid, **mp** 73-75; ***R$_f$*** (Cyclohexane/EtOAc 6:4) 0.18; **^{1}H NMR** (300 MHz, $CDCl_3$): δ 10.29 (s, 1H), 8.32 (d, *J* = 8.3 Hz, 1H), 8.08 (d, *J* = 8.3 Hz, 1H), 8.03 (d, *J* = 9.1 Hz, 1H), 7.76 (d, *J* = 9.1 Hz, 1H), 5.58 (s, 2H), 4.03 – 3.90 (m, 2H), 3.62 – 3.53 (m, 2H), 3.35 (s, 3H).

8-Cyano-7-((2-methoxyethoxy)methoxy)quinolin-2-yl)methanol (133)

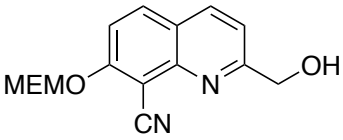

Molecular Weight: 288.30

Procedure adapted from literature.[138] $NaBH_4$ (50 mg, 1.33 mmol) was added portionwise to a suspension of 8-Cyano-7-((2-methoxyethoxy)methoxy)-quinoline-2-carbaldehyde (**131**) (380 mg, 1.33 mmol) in ethanol (5 mL) and the resulting solution was stirred at rt for 1 h. EtOAc (10 mL) was added and the organic phase washed with H_2O (7 mL) . The two layers were separated and the aqueous layer was extracted with EtOAc (3 x 5 mL). The combined organic layers were

dried (Na_2SO_4) and concentrated under reduced pressure to give 8-Cyano-7-((2-methoxyethoxy)methoxy)quinolin-2-yl)methanol (**133**) (329 mg, 1.14 mmol, 86% yield) as a dark yellow oil; R_f (Cyclohexane/EtOAc 4:6) 0.27; **^{1}H NMR** (300 MHz, $CDCl_3$): δ 8.13 (d, *J* = 8.5 Hz, 1H), 7.99 (d, *J* = 9.1 Hz, 1H), 7.59 (d, *J* = 9.1 Hz, 1H), 7.30 (d, *J* = 8.5 Hz, 1H), 5.55 (s, 2H), 4.96 (s, 2H), 3.99 – 3.91 (m, 2H), 3.60 – 3.54 (m, 2H), 3.38 (s, 3H).

(8-Cyano-7-((2-methoxyethoxy)methoxy)quinolin-2-yl)methyl methansulfonate (135)

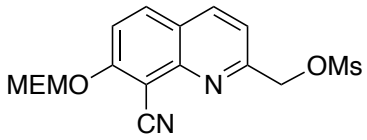

Molecular Weight: 366.39

Procedure adapted from literature.[138] TEA (0.32 mL, 2.28 mmol) was added to a solution of 8-Cyano-7-((2-methoxyethoxy)methoxy)quinolin-2-yl)methanol (**133**) (329 mg, 1.14 mmol) in DCM (5 mL) and the resulting solution was stirred for 5 min. Then, the mixture was cooled to 5°C and methanesulfonyl chloride (0.18 mL, 2.28 mmol) was slowly added. The resulting solution was stirred at 5 °C for 1h. Upon completion, the reaction was quenched with H_2O (4 mL) and the layers were separated. The organic layer was dried (Na_2SO_4) and concentrated under reduced pressure to give the crude product. Purification by flash column chromatography with 1:1 to 4:6 cyclohexane-ethyl acetate as eluent gave (8-Cyano-7-((2-methoxyethoxy)methoxy)quinolin-2-yl)methyl methansulfonate (**135**) (330 mg, 0.90 mmol, 79%) as a white solid, **mp** 93-96 °C; R_f (Cyclohexane/EtOAc 4:6) 0.24; **^{1}H NMR** (300 MHz, $CDCl_3$): δ 8.22 (d, *J* = 8.5 Hz, 1H), 8.01 (d, *J* = 9,1 Hz, 1H), 7.63 (d, *J* = 9,1 Hz, 1H), 7.56 (d, *J* = 8,5, 1H), 5.55 (s, 4H), 4.06 – 3.83 (m, 2H), 3.62 – 3.46 (m, 2H), 3.36 (s, 3H), 3.27 (s, 3H).

(8-Cyano-7-hydroxyquinolin-2-yl)methyl methansulfonate (122)

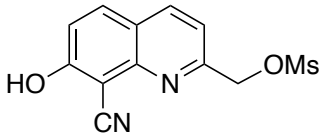

Molecular Weight: 278.28

Procedure adapted from literature.[138] Trifluoroacetic acid (0.69 mL, 9.00 mmol) was added to a solution of (8-Cyano-7-((2-methoxyethoxy)methoxy)quinolin-2-yl)methyl methansulfonate (**135**) (330 mg, 0.90 mmol) in DCM (5 mL) and the resulting solution was stirred at rt for 8 h. Then, the solution was washed with H_2O (5 mL) and the layers were separated. The aqueous layer was extracted with EtOAc (2 x 7 mL). The combined organic layers were dried (Na_2SO_4) and concentrated under reduced pressure to give the crude compound. Titration with DCM gave (8-Cyano-7-hydroxyquinolin-2-yl)methyl methansulfonate (**122**) (180 mg, 0.65 mmol, 72%) as a white solid; R_f (Cyclohexane/EtOAc 4:6) 0.17; **^{1}H NMR** (300 MHz, MeOD): δ 8.29 (d, *J* = 8.5 Hz, 1H), 7.99 (d, *J* = 9.1 Hz, 1H), 7.51 (d, *J* = 8.5 Hz, 1H), 7.22 (d, *J* = 9.1 Hz, 1H), 5.52 (s, 2H), 3.28 (s, 3H).

(2*S*)-1-((8-cyano-7-hydroxyquinolin-2-yl)methyl)-2-(((5-((2-methoxyethoxy)methoxy)pyridin-3-yl)oxy)methyl)-1-methylpyrrolidin-1-ium methanesulfonate (137)

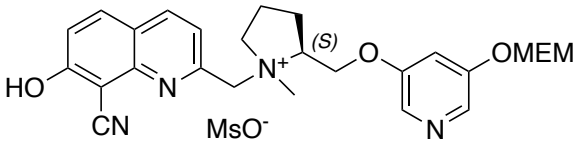

Molecular Weight: 574.65

Procedure adapted from literature.[138] (8-cyano-7-hydroxyquinolin-2-yl)methylmethansulfonate (**122**) (48 mg, 0.17 mmol) and (*S*)-3-((2-methoxyethoxy)methoxy)-5-((1-methylpyrrolidin-2-yl)methoxy)pyridine (**114**) (41 mg, 0.14 mmol) were dissolved in acetonitrile (4 mL). The mixture was stirred at rt for 4h. Then, the solvent was concentrated under reduced pressure to give the crude product as a yellow wax. Purification by flash column chromatography with 9:1 DCM/MeOH + 1% $NH_{3(22\% \text{ in water})}$ as eluent gave (2*S*)-1-((8-cyano-7-

hydroxyquinolin-2-yl)methyl)-2-(((5-((2-methoxyethoxy)methoxy)pyridin-3-yl)oxy)methyl)-1-methylpyrrolidin-1-ium methanesulfonate (**137**) (75 mg, 0.13 mmol, 76%) as a light yellow oil; ***R_f*** (DCM/MeOH 8:2) 0.22; **^{1}H NMR** (300 MHz, CD_3OD): δ 8.12 – 7.98 (m, 3H), 7.68 (dd, *J* = 9.3, 2.0 Hz, 1H), 7.28 (dt, *J* = 3.6, 2.3 Hz, 1H), 7.23 (dd, *J* = 8.0, 2.0 Hz, 1H), 6.96 (dd, *J* = 9.3, 2.0 Hz, 1H), 5.34 (s, 2H), 5.05 (d, *J* = 13.7 Hz, 1H), 4.90 – 4.80 (m, 1H), 4.78 – 4.65 (m, 2H), 4.65 – 4.55 (m, 2H), 4.39 – 4.19 (m, 1H), 3.90 – 3.76 (m, 2H), 3.59 – 3.43 (m, 2H), 3.40 (s, 3H), 3.28 (s, 3H), 2.86 (s, 3H), 2.51 – 2.19 (m, 4H).

(2*S*)-1-((8-cyano-7-hydroxyquinolin-2-yl)methyl)-2-(((5-hydroxypyridin-3-yl)oxy)methyl)-1-methylpyrrolidin-1-ium 2,2,2-trifluoroacetate (CyHQ-(*S*)-VI)

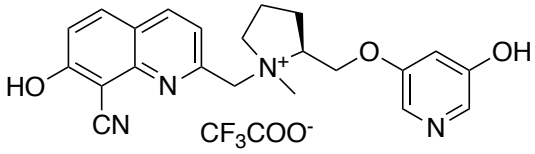

Molecular Weight: 504.47

Procedure adapted from literatrure.[138] TFA (0.1 mL, 1.32 mmol) was added to a solution of (2*S*)-1-((8-cyano-7-hydroxyquinolin-2-yl)methyl)-2-(((5-((2-methoxyethoxy)methoxy)pyridin-3-yl)oxy)methyl)-1-methylpyrrolidin-1-ium methanesulfonate (**137**) (76 mg, 0.13 mmol) in DCM (5 mL). The mixture was stirred at rt for 5 h. Then, the solvent was concentrated under reduced pressure to give the crude product as a brown oil. Crystallization with 2:1 diethyl ether and MeOH gave (2*S*)-1-((8-cyano-7-hydroxyquinolin-2-yl)methyl)-2-(((5-hydroxypyridin-3-yl)oxy)methyl)-1-methylpyrrolidin-1-ium 2,2,2-trifluoroacetate (CyHQ-(*S*)-**VI**) (38 mg, 0.08 mmol, 59%) as a white solid, **mp** 139.8-141.1 °C; ***Rf*** (DCM/MeOH 8:2) 0.23; **[α]**= –8.47° (*c*0.5, MeOH); **^{1}H NMR** (300 MHz, CD_3OD) (55:45 mixture of rotamers): δ 8.41 (dd, *J* = 8.3, 4.8 Hz, 1H), 8.09 (dd, *J* = 9.2, 3.5 Hz, 1H), 7.89 – 7.71 (m, 2H), 7.60 (dd, *J* = 8.3, 2.5 Hz, 1H), 7.35 (dd, *J* = 9.2, 3.5 Hz, 1H), 6.95 (dt, *J* = 10.8, 2.5 Hz, 1H), 5.21 (d, *J* = 14.2 Hz, 0.55H), 4.98 (d, *J* = 14.2 Hz, 0.45H), 4.91 (s, 1H), 4.78 – 4.51 (m, 3H), 4.30 – 4.15 (m, 1H), 3.99 – 3.86 (m, 0.55H), 3.78 – 3.63 (m, 0.45H), 3.46 (s, 1.25H), 3.34 (s, 1.75H), 2.69 – 2.21 (m, 4H); **^{13}C NMR** (75 MHz, CD_3OD): δ 164.91, 155.40, 155.22, 152.10, 152.03, 148.99, 148.83, 138.30, 133.90, 130.54, 130.50, 127.73, 127.63, 121.99, 121.91, 121.52, 119.54, 114.94, 114.88,

109.28, 109.12, 75.36, 73.03, 67.10, 65.83, 64.65, 60.45, 24.02, 23.44, 19.50, 19.39; **HRMS (ESI$^+$)** *m/z* calcd for $C_{22}H_{23}N_4O_3$ $(M+H)^+$ 391.1764.

7. Bibliography

1. Alexander SP, Christopoulos A, Davenport AP, et al. The Concise Guide to PHARMACOLOGY 2017/18: G protein-coupled receptors. *Br J Pharmacol*. 2017;174:17-129. doi:10.1111/bph.13878/full
2. Alexander SP, Kelly E, Marrion N v, et al. The Concise Guide to PHARMACOLOGY 2017/18: Other ion channels. *Br J Pharmacol*. 2017;174:195-207. doi:10.1111/bph.13881/full
3. Albuquerque EX, Pereira EFR, Alkondon M, Rogers SW. Mammalian nicotinic acetylcholine receptors: From structure to function. *Physiol Rev*. 2009;89(1):73-120. doi:10.1152/physrev.00015.2008
4. Jensen AA, Frølund B, Liljefors T, Krogsgaard-Larsen P. Neuronal nicotinic acetylcholine receptors: Structural revelations, target identifications, and therapeutic inspirations. *J Med Chem*. 2005;48(15):4705-4745. doi:10.1021/jm040219e
5. Zoli M, Pucci S, Vilella A, Gotti C. Neuronal and Extraneuronal Nicotinic Acetylcholine Receptors. *Curr Neuropharmacol*. 2018;16(4):338-349. doi:10.2174/1570159x15666170912110450
6. Gotti C, Moretti M, Gaimarri A, Zanardi A, Clementi F, Zoli M. Heterogeneity and complexity of native brain nicotinic receptors. *Biochem Pharmacol*. 2007;74(8):1102-1111. doi:10.1016/j.bcp.2007.05.023
7. Clementi F, Fumagalli Guido, Chiamulera Cristiano. *Farmacologia Generale e Molecolare : Il Meccanismo d'azione Dei Farmaci*. UTET scienze mediche; 2012.
8. Zoli M, Pistillo F, Gotti C. Diversity of native nicotinic receptor subtypes in mammalian brain. *Neuropharmacology*. 2015;96(PB):302-311. doi:10.1016/j.neuropharm.2014.11.003
9. Gotti C, Clementi F. Neuronal nicotinic receptors: From structure to pathology. *Prog Neurobiol*. 2004;74(6):363-396. doi:10.1016/j.pneurobio.2004.09.006
10. Dani JA. Neuronal Nicotinic Acetylcholine Receptor Structure and Function and Response to Nicotine. *Int Rev Neurobiol*. 2015;124:3-19. doi:10.1016/bs.irn.2015.07.001.Neuronal

11. Corradi J, Bouzat C. Understanding the bases of function and modulation of a7 nicotinic receptors: implications for drug discovery. *Mol Pharmacol*. 2016;90(3):288-299. doi:10.1124/mol.116.104240
12. BARLOW RB, ING HR. Curare-like action of polymethylene bis-quaternary ammonium salts. *Br J Pharmacol Chemother*. 1948;3(4):298-304. doi:10.1111/j.1476-5381.1948.tb00390.x
13. Paton WDM, Zaimis EJ. The pharmacological actions of polymethylene bistrimethylammonium salts. *Br J Pharmacol*. 1997;120(4 SUPPL.):60-79. doi:10.1111/j.1476-5381.1997.tb06777.x
14. S Clarke PB, Schwartz RD, Paul SM, Pert CB, Pert A. *Copyrrght 0 Socfety for Neuroscience Nicotinic Binding in Rat*. Vol 5.; 1985.
15. KATZ B, THESLEFF S. A study of the desensitization produced by acetylcholine at the motor end-plate. *J Physiol*. 1957;138(1):63-80. doi:10.1113/jphysiol.1957.sp005838
16. Changeux JP, Devillers-Thiéry A, Chemouilli P. Acetylcholine receptor: An allosteric protein. *Science (1979)*. 1984;225(4668):1335-1345. doi:10.1126/science.6382611
17. Quick MW, Lester RAJ. Desensitization of neuronal nicotinic receptors. *J Neurobiol*. 2002;53(4):457-478. doi:10.1002/neu.10109
18. Mazzaferro S, Benallegue N, Carbone A, et al. Additional Acetylcholine (ACh) binding site at α4/α4 interface of (α4β2) 2α4 nicotinic receptor influences agonist sensitivity. *Journal of Biological Chemistry*. 2011;286(35):31043-31054. doi:10.1074/jbc.M111.262014
19. Mazzaferro S, Bermudez I, Sine SM. Potentiation of a neuronal nicotinic receptor via pseudo-agonist site. *Cellular and Molecular Life Sciences*. 2019;76(6):1151-1167. doi:10.1007/s00018-018-2993-7
20. Wang J, Lindstrom J. Orthosteric and allosteric potentiation of heteromeric neuronal nicotinic acetylcholine receptors Correspondence Jon Lindstrom, Department of Neuroscience, 130 A LINKED ARTICLES. *Br J Pharmacol*. 2018;175:1805. doi:10.1111/bph.v175.11/issuetoc
21. Marotta CB, Rreza I, Lester HA, Dougherty DA. Selective ligand behaviors provide new insights into agonist activation of nicotinic acetylcholine receptors. *ACS Chem Biol*. 2014;9(5):1153-1159. doi:10.1021/cb400937d

22. Harpsøe K, Ahring PK, Christensen JK, Jensen ML, Peters D, Balle T. Unraveling the high- and low-sensitivity agonist responses of nicotinic acetylcholine receptors. *Journal of Neuroscience*. 2011;31(30):10759-10766. doi:10.1523/JNEUROSCI.1509-11.2011
23. Benallegue N, Mazzaferro S, Alcaino C, Bermudez I. The additional ACh binding site at the α4(+)/α4(-) interface of the (α4β2)2α4 nicotinic ACh receptor contributes to desensitization. *Br J Pharmacol*. 2013;170(2):304-316. doi:10.1111/bph.12268
24. Wang J, Kuryatov A, Sriram A, et al. An accessory agonist binding site promotes activation of α4β2∗ nicotinic acetylcholine receptors. *Journal of Biological Chemistry*. 2015;290(22):13907-13918. doi:10.1074/jbc.M115.646786
25. Nelson ME, Kuryatov A, Choi CH, Zhou Y, Lindstrom J. *Alternate Stoichiometries of 42 Nicotinic Acetylcholine Receptors*.; 2003. http://molpharm.aspetjournals.org
26. Walsh RM, Roh SH, Gharpure A, Morales-Perez CL, Teng J, Hibbs RE. Structural principles of distinct assemblies of the human α4β2 nicotinic receptor. *Nature*. 2018;557(7704):261-265. doi:10.1038/s41586-018-0081-7
27. Moroni M, Zwart R, Sher E, Cassels BK, Bermudez I. α4β2 nicotinic receptors with high and low acetylcholine sensitivity: Pharmacology, stoichiometry, and sensitivity to long-term exposure to nicotine. *Mol Pharmacol*. 2006;70(2):755-768. doi:10.1124/mol.106.023044
28. Millar NS, Gotti C. Diversity of vertebrate nicotinic acetylcholine receptors. *Neuropharmacology*. 2009;56(1):237-246. doi:10.1016/j.neuropharm.2008.07.041
29. Brisson A, Unwin PNT. Tubular crystals of acetylcholine receptor. *Journal of Cell Biology*. 1984;99(4 I):1202-1211. doi:10.1083/jcb.99.4.1202
30. Unwin N. Nicotinic Acetylcholine Receptor at 9 A Resolution. Published online 1993:1101-1124.
31. Miyazawa A, Fujiyoshi Y, Stowell M, Unwin N. Nicotinic acetylcholine receptor at 4.6 Å resolution: Transverse tunnels in the channel wall. *J Mol Biol*. 1999;288(4):765-786. doi:10.1006/jmbi.1999.2721
32. Brejc K, Van Dijk WJ, Klaassen R V., et al. Crystal structure of an ACh-binding protein reveals the ligand-binding domain of nicotinic receptors. *Nature*. 2001;411(6835):269-276. doi:10.1038/35077011

33. Smit AB, Celie PHN, Kasheverov IE, et al. Acetylcholine-binding proteins: Functional and structural homologs of nicotinic acetylcholine receptors. *Journal of Molecular Neuroscience*. 2006;30(1-2):9-10. doi:10.1385/JMN:30:1:9

34. Miller PS, Aricescu AR. Crystal structure of a human GABAA receptor. *Nature*. 2014;512(7514):270-275. doi:10.1038/nature13293

35. Hassaine G, Deluz C, Grasso L, et al. X-ray structure of the mouse serotonin 5-HT3 receptor. *Nature*. 2014;512(7514):276-281. doi:10.1038/nature13552

36. Huang X, Shaffer PL, Ayube S, et al. Crystal structures of human glycine receptor α3 bound to a novel class of analgesic potentiators. *Nat Struct Mol Biol*. 2017;24(2):108-113. doi:10.1038/nsmb.3329

37. Du J, Lü W, Wu S, Cheng Y, Gouaux E. Glycine receptor mechanism elucidated by electron cryo-microscopy. *Nature*. 2015;526(7572):224-229. doi:10.1038/nature14853

38. Hibbs RE, Gouaux E. Principles of activation and permeation in an anion-selective Cys-loop receptor. *Nature*. 2011;474(7349):54-60. doi:10.1038/nature10139

39. Hilf RJC, Dutzler R. X-ray structure of a prokaryotic pentameric ligand-gated ion channel. *Nature*. 2008;452(7185):375-379. doi:10.1038/nature06717

40. Bocquet N, Nury H, Baaden M, et al. X-ray structure of a pentameric ligand-gated ion channel in an apparently open conformation. *Nature*. 2009;457(7225):111-114. doi:10.1038/nature07462

41. Morales-Perez CL, Noviello CM, Hibbs RE. X-ray structure of the human α4β2 nicotinic receptor. *Nature*. 2016;538(7625):411-415. doi:10.1038/nature19785

42. Nemecz Á, Prevost MS, Menny A, Corringer PJ. Emerging Molecular Mechanisms of Signal Transduction in Pentameric Ligand-Gated Ion Channels. *Neuron*. 2016;90(3):452-470. doi:10.1016/j.neuron.2016.03.032

43. Dougherty DA. The cation-π interaction. *Acc Chem Res*. 2013;46(4):885-893. doi:10.1021/ar300265y

44. Feduccia AA, Chatterjee S, Bartlett SE. Neuronal nicotinic acetylcholine receptors: Neuroplastic changes underlying alcohol and nicotine addictions. *Front Mol Neurosci*. 2012;5(AUG 2012):1-18. doi:10.3389/fnmol.2012.00083

45. Wang Y, Zhang S, Li F, et al. Therapeutic target database 2020: Enriched resource for facilitating research and early development of targeted therapeutics. *Nucleic Acids Res*. 2020;48(D1):D1031-D1041. doi:10.1093/nar/gkz981

46. Dani JA, Bertrand D. Nicotinic acetylcholine receptors and nicotinic cholinergic mechanisms of the central nervous system. *Annu Rev Pharmacol Toxicol*. 2007;47:699-729. doi:10.1146/annurev.pharmtox.47.120505.105214

47. Utkin YN. Aging Affects Nicotinic Acetylcholine Receptors in Brain. *Cent Nerv Syst Agents Med Chem*. 2019;19(2):119-124. doi:10.2174/1871524919666190320102834

48. Besson M, Granon S, Mameli-Engvall M, et al. Long-term effects of chronic nicotine exposure on brain nicotinic receptors. *Proc Natl Acad Sci U S A*. 2007;104(19):8155-8160. doi:10.1073/pnas.0702698104

49. El Sayed KA, Sylvester PW. Biocatalytic and semisynthetic studies of the anticancer tobacco cembranoids. *Expert Opin Investig Drugs*. 2007;16(6):877-887. doi:10.1517/13543784.16.6.877

50. NIDA. Tobacco , Nicotine , and E-Cigarettes Research Report. 2020;(January):59.

51. Hecht SS. Cigarette smoking: Cancer risks, carcinogens, and mechanisms. *Langenbecks Arch Surg*. 2006;391(6):603-613. doi:10.1007/s00423-006-0111-z

52. Cardinale A, Nastrucci C, Cesario A, Russo P. Nicotine: Specific role in angiogenesis, proliferation and apoptosis. *Crit Rev Toxicol*. 2012;42(1):68-89. doi:10.3109/10408444.2011.623150

53. Grando SA. Connections of nicotine to cancer. *Nat Rev Cancer*. 2014;14(6):419-429. doi:10.1038/nrc3725

54. Sanner T, Grimsrud TK. Nicotine: Carcinogenicity and effects on response to cancer treatment - a review. *Front Oncol*. 2015;5(Aug):1-10. doi:10.3389/fonc.2015.00196

55. Benowitz NL, Porchet H, Jacob P. Nicotine dependence and tolerance in man: Pharmacokinetic and pharmacodynamic investigations. *Prog Brain Res*. 1989;79(C):279-287. doi:10.1016/S0079-6123(08)62487-5

56. Laviolette SR, Van Der Kooy D. The neurobiology of nicotine addiction: Bridging the gap from molecules to behaviour. *Nat Rev Neurosci*. 2004;5(1):55-65. doi:10.1038/nrn1298

57. Markou A. Neurobiology of nicotine dependence. *Philosophical Transactions of the Royal Society B: Biological Sciences*. 2008;363(1507):3159-3168. doi:10.1098/rstb.2008.0095

58. dos Santos Picanco LC, Ozela PF, de Fatima de Brito Brito M, et al. Alzheimer's Disease: A Review from the Pathophysiology to Diagnosis, New Perspectives for Pharmacological Treatment. *Curr Med Chem*. 2018;25(26):3141-3159. doi:10.2174/0929867323666161213101126

59. Sabri O, Meyer PM, Gräf S, et al. Cognitive correlates of α4β2 nicotinic acetylcholine receptors in mild Alzheimer's dementia. *Brain*. 2018;141(6):1840-1854. doi:10.1093/brain/awy099

60. H. Ferreira-Vieira T, M. Guimaraes I, R. Silva F, M. Ribeiro F. Alzheimer's disease: Targeting the Cholinergic System. *Curr Neuropharmacol*. 2016;14(1):101-115. doi:10.2174/1570159x13666150716165726

61. Weller J, Budson A. Current understanding of Alzheimer's disease diagnosis and treatment. *F1000Res*. 2018;7(0):1-9. doi:10.12688/f1000research.14506.1

62. Perez-Lloret S, Barrantes FJ. Deficits in cholinergic neurotransmission and their clinical correlates in Parkinson's disease. *NPJ Parkinsons Dis*. 2016;2(1). doi:10.1038/npjparkd.2016.1

63. Wenthur CJ, Gentry PR, Mathews TP, Lindsley CW. Drugs for allosteric sites on receptors. *Annu Rev Pharmacol Toxicol*. 2014;54:165-184. doi:10.1146/annurev-pharmtox-010611-134525

64. Oosawa H, Fujii T, Kawashima K. Nerve growth factor increases the synthesis and release of acetylcholine and the expression of vesicular acetylcholine transporter in primary cultured rat embryonic septal cells. *J Neurosci Res*. 1999;57(3):381-387. doi:10.1002/(SICI)1097-4547(19990801)57:3<381::AID-JNR10>3.0.CO;2-C

65. Lew MJ. Extended concentration-response curves used to reflect full agonist efficacies and receptor occupancy-response coupling ranges. *Br J Pharmacol*. 1995;115(5):745-752. doi:10.1111/j.1476-5381.1995.tb14996.x

66. Picciotto MR, Higley MJ, Mineur YS. Acetylcholine as a Neuromodulator: Cholinergic Signaling Shapes Nervous System Function and Behavior. *Neuron*. 2012;76(1):116-129. doi:10.1016/j.neuron.2012.08.036

67. Kishioka S, Kiguchi N, Kobayashi Y, Saika F. Nicotine effects and the endogenous opioid system. *J Pharmacol Sci*. 2014;125(2):117-124. doi:10.1254/jphs.14R03CP

68. Calhoun BC. *Tobacco Cessation and Substance Abuse Treatment in Women's Healthcare*.; 2016. doi:10.1007/978-3-319-26710-4

69. Traynor JR. Epibatidine and pain. *Br J Anaesth*. 1998;81(1):69-76. doi:10.1093/bja/81.1.69

70. Fitch RW, Spande TF, Garraffo HM, Yeh HJC, Daly JW. Phantasmidine: An epibatidine congener from the ecuadorian poison frog epipedobates anthonyi. *J Nat Prod*. 2010;73(3):331-337. doi:10.1021/np900727e

71. Tonder J, Olesen P. Agonists at the a4b2 Nicotinic Acetylcholine Receptors Relationships and Molecular Modelling. *Curr Med Chem*. 2012;8(6):651-674. doi:10.2174/0929867013373165

72. Rose JE, Levin ED. Concurrent agonist-antagonist administration for the analysis and treatment of drug dependence. *Pharmacol Biochem Behav*. 1992;41(1):219-226. doi:10.1016/0091-3057(92)90086-U

73. Rollema H, Hurst RS. The contribution of agonist and antagonist activities of α4β2* nAChR ligands to smoking cessation efficacy: a quantitative analysis of literature data. *Psychopharmacology (Berl)*. 2018;235(9):2479-2505. doi:10.1007/s00213-018-4921-9

74. Etter JF. Cytisine for Smoking Cessation. *Arch Intern Med*. 2006;166(15):1553. doi:10.1001/archinte.166.15.1553

75. Etter JF, Lukas RJ, Benowitz NL, West R, Dresler CM. Cytisine for smoking cessation: A research agenda. *Drug Alcohol Depend*. 2008;92(1-3):3-8. doi:10.1016/j.drugalcdep.2007.06.017

76. Da Silva Tavares X, Blum AP, Nakamura DT, et al. Variations in Binding Among Several Agonists at Two Stoichiometries of the Neuronal, α4β2 Nicotinic Receptor. *J Am Chem Soc*. 2012;134(28):11474-11480. doi:10.1021/ja3011379

77. Coe JW, Brooks PR, Vetelino MG, et al. Varenicline: An alpha;4β2 nicotinic receptor partial agonist for smoking cessation. *J Med Chem*. 2005;48(10):3474-3477. doi:10.1021/jm050069n

78. Zwart R, Carbone AL, Moroni M, et al. Sazetidine-A is a potent and selective agonist at native and recombinant α4β2 nicotinic acetylcholine receptors. *Mol Pharmacol*. 2008;73(6):1838-1843. doi:10.1124/mol.108.045104

79. Xiao Y, Fan H, Musachio JL, et al. Sazetidine-A, a novel ligand that desensitizes α4β2 nicotinic acetylcholine receptors without activating them. *Mol Pharmacol*. 2006;70(4):1454-1460. doi:10.1124/mol.106.027318

80. Nicke A, Wonnacott S, Lewis RJ. α-Conotoxins as tools for the elucidation of structure and function of neuronal nicotinic acetylcholine receptor subtypes. *Eur J Biochem*. 2004;271(12):2305-2319. doi:10.1111/j.1432-1033.2004.04145.x

81. Bacher I, Wu B, Shytle DR, George TP. Mecamylamine a nicotinic acetylcholine receptor antagonist with potential for the treatment of neuropsychiatric disorders. *Expert Opin Pharmacother*. 2009;10(16):2709-2721. doi:10.1517/14656560903329102

82. Pandya AA, Yakel JL. Effects of neuronal nicotinic acetylcholine receptor allosteric modulators in animal behavior studies. *Biochem Pharmacol*. 2013;86(8):1054-1062. doi:10.1016/j.bcp.2013.05.018

83. Grupe M, Grunnet M, Bastlund JF, Jensen AA. Targeting α4β2 nicotinic acetylcholine receptors in central nervous system disorders: Perspectives on positive allosteric modulation as a therapeutic approach. *Basic Clin Pharmacol Toxicol*. 2015;116(3):187-200. doi:10.1111/bcpt.12361

84. Wilkerson JL, Deba F, Crowley ML, Hamouda AK, McMahon LR. Advances in the In vitro and In vivo pharmacology of Alpha4beta2 nicotinic receptor positive allosteric modulators. *Neuropharmacology*. 2020;168(September 2019):108008. doi:10.1016/j.neuropharm.2020.108008

85. Deba F, Ali HI, Tairu A, Ramos K, Ali J, Hamouda AK. LY2087101 and dFBr share transmembrane binding sites in the (α4)3(β2)2 Nicotinic Acetylcholine Receptor. *Sci Rep*. 2018;8(1). doi:10.1038/s41598-018-19790-4

86. Broad LM, Zwart R, Pearson KH, et al. Identification and pharmacological profile of a new class of selective nicotinic acetylcholine receptor potentiators. *Journal of Pharmacology and Experimental Therapeutics*. 2006;318(3):1108-1117. doi:10.1124/jpet.106.104505

87. Grupe M, Jensen AA, Ahring PK, Christensen JK, Grunnet M. Unravelling the mechanism of action of NS9283, a positive allosteric modulator of (α4)3(β2)2 nicotinic ACh receptors. *Br J Pharmacol*. 2013;168(8):2000-2010. doi:10.1111/bph.12095

88. Maurer JJ, Sandager-Nielsen K, Schmidt HD. Attenuation of nicotine taking and seeking in rats by the stoichiometry-selective alpha4beta2 nicotinic acetylcholine receptor positive allosteric modulator NS9283. *Psychopharmacology (Berl)*. 2017;234(3):475-484. doi:10.1007/s00213-016-4475-7

89. Lee CH, Zhu C, Malysz J, et al. α4β2 neuronal nicotinic receptor positive allosteric modulation: An approach for improving the therapeutic index of α4β2 nAChR agonists in pain. In: *Biochemical Pharmacology*. Vol 82. ; 2011:959-966. doi:10.1016/j.bcp.2011.06.044

90. Timmermann DB, Sandager-Nielsen K, Dyhring T, et al. Augmentation of cognitive function by NS9283, a stoichiometry-dependent positive allosteric modulator of α2- and α4-containing nicotinic acetylcholine receptors. *Br J Pharmacol*. 2012;167(1):164-182. doi:10.1111/j.1476-5381.2012.01989.x

91. Abreo MA, Lin N horng, Garvey DS, et al. Nicotinic Acetylcholine Receptors. *J Med Chem*. 1996;39:817-825.

92. Elliott RL, Kopecka H, Gunn DE, et al. 2-(aryloxymethyl) azacyclic analogues as novel nicotinic acetylcholine receptor (nAChR) ligands. *Bioorg Med Chem Lett*. 1996;6(19):2283-2288. doi:10.1016/0960-894X(96)00416-7

93. Pallavicini M, Moroni B, Bolchi C, et al. Synthesis and α4β2 nicotinic affinity of unichiral 5-(2-pyrrolidinyl)oxazolidinones and 2-(2-pyrrolidinyl)benzodioxanes. *Bioorg Med Chem Lett*. 2006;16(21):5610-5615. doi:10.1016/j.bmcl.2006.08.020

94. Pallavicini M, Bolchi C, Binda M, et al. 5-(2-Pyrrolidinyl)oxazolidinones and 2-(2-pyrrolidinyl)benzodioxanes: Synthesis of all the stereoisomers and α4β2 nicotinic affinity. *Bioorg Med Chem Lett*. 2009;19(3):854-859. doi:10.1016/j.bmcl.2008.12.002

95. Bolchi C, Gotti C, Binda M, et al. Unichiral 2-(2'-pyrrolidinyl)-1,4-benzodioxanes: The 2 R,2' S diastereomer of the N -methyl-7-hydroxy analogue is a potent α4β2- and α6β2-nicotinic acetylcholine receptor partial agonist. *J Med Chem*. 2011;54(21):7588-7601. doi:10.1021/jm200937t

96. Bolchi C, Valoti E, Gotti C, et al. Chemistry and Pharmacology of a Series of Unichiral Analogues of 2-(2-Pyrrolidinyl)-1,4-benzodioxane, Prolinol Phenyl Ether, and Prolinol 3-Pyridyl Ether Designed as α4β2-Nicotinic Acetylcholine Receptor Agonists. *J Med Chem*. 2015;58(16):6665-6677. doi:10.1021/acs.jmedchem.5b00904

97. Bavo F, Pallavicini M, Appiani R, Bolchi C. Determinants for α4β2 vs. α3β4 subtype selectivity of pyrrolidine-based nachrs ligands: A computational perspective with focus on recent cryo-em receptor structures. *Molecules*. 2021;26(12). doi:10.3390/molecules26123603

98. Bavo F, Pallavicini M, Gotti C, et al. Modifications at C(5) of 2-(2-Pyrrolidinyl)-Substituted 1,4-Benzodioxane Elicit Potent α4β2 Nicotinic Acetylcholine Receptor Partial Agonism with High Selectivity over the α3β4 Subtype. *J Med Chem*. 2020;63(24):15668-15692. doi:10.1021/acs.jmedchem.0c01150

99. Bolchi C, Bavo F, Gotti C, et al. From pyrrolidinyl-benzodioxane to pyrrolidinyl-pyridodioxanes, or from unselective antagonism to selective partial agonism at α4β2 nicotinic acetylcholine receptor. *Eur J Med Chem*. 2017;125:1132-1144. doi:10.1016/j.ejmech.2016.10.048

100. Olsen JA, Ahring PK, Kastrup JS, Gajhede M, Balle T. Structural and functional studies of the modulator NS9283 reveal agonist-like mechanism of action at α4β2 nicotinic acetylcholine receptors. *Journal of Biological Chemistry*. 2014;289(36):24911-24921. doi:10.1074/jbc.M114.568097

101. Wang ZJ, Deba F, Mohamed TS, Chiara DC, Ramos K, Hamouda AK. Unraveling amino acid residues critical for allosteric potentiation of (α4)3(β2)2-type nicotinic acetylcholine receptor responses. *Journal of Biological Chemistry*. 2017;292(24):9988-10001. doi:10.1074/jbc.M116.771246

102. Hamouda AK, Sanghvi M, Chiara DC, Cohen JB, Blanton MP. Identifying the lipid-protein interface of the α4β2 neuronal nicotinic acetylcholine receptor: Hydrophobic photolabeling studies with 3-(trifluoromethyl)-3-(m-[125i]iodophenyl)diazirine. *Biochemistry*. 2007;46(48):13837-13846. doi:10.1021/bi701705r

103. Pinheiro NM, Banzato R, Tibério I, et al. Acute lung injury in cholinergic-deficient mice supports anti-inflammatory role of α7 nicotinic acetylcholine receptor. *Int J Mol Sci*. 2021;22(14). doi:10.3390/ijms22147552

104. Wang J, Blasio A, Chapman HL, et al. Promoting activity of (α4)3(β2)2 nicotinic cholinergic receptors reduces ethanol consumption. *Neuropsychopharmacology*. 2020;45(2):301-308. doi:10.1038/s41386-019-0475-8

105. Bavo F, Pallavicini M, Gotti C, et al. Modifications at C(5) of 2-(2-Pyrrolidinyl)-Substituted 1,4-Benzodioxane Elicit Potent α4β2 Nicotinic Acetylcholine Receptor Partial Agonism with High Selectivity over the α3β4 Subtype. *J Med Chem*. 2020;63(24):15668-15692. doi:10.1021/acs.jmedchem.0c01150

106. Braida D, Ponzoni L, Moretti M, et al. Behavioural and pharmacological profiles of zebrafish administrated pyrrolidinyl benzodioxanes and prolinol aryl ethers with high affinity for heteromeric nicotinic acetylcholine receptors. *Psychopharmacology (Berl)*. 2020;237(8):2317-2326. doi:10.1007/s00213-020-05536-6

107. Itou J, Kawakami H, Burgoyne T, Kawakami Y. Life-long preservation of the regenerative capacity in the fin and heart in zebrafish. *Biol Open*. 2012;1(8):739-746. doi:10.1242/bio.20121057

108. Sison M, Gerlai R. Associative learning in zebrafish (Danio rerio) in the plus maze. *Behavioural Brain Research*. 2010;207(1):99-104. doi:10.1016/j.bbr.2009.09.043

109. Braida D, Ponzoni L, Martucci R, Sparatore F, Gotti C, Sala M. Role of neuronal nicotinic acetylcholine receptors (nAChRs) on learning and memory in zebrafish. *Psychopharmacology (Berl)*. 2014;231(9):1975-1985. doi:10.1007/s00213-013-3340-1

110. Braida D, Ponzoni L, Martucci R, Sala M. A new model to study visual attention in zebrafish. *Prog Neuropsychopharmacol Biol Psychiatry*. 2014;55:80-86. doi:10.1016/j.pnpbp.2014.03.010

111. Ponzoni L, Braida D, Pucci L, et al. The cytisine derivatives, CC4 and CC26, reduce nicotine-induced conditioned place preference in zebrafish by acting on heteromeric neuronal nicotinic acetylcholine receptors. *Psychopharmacology (Berl)*. 2014;231(24):4681-4693. doi:10.1007/s00213-014-3619-x

112. Jin Z, Khan P, Shin Y, et al. Synthesis and activity of substituted heteroaromatics as positive allosteric modulators for α4β2α5 nicotinic acetylcholine receptors. *Bioorg Med Chem Lett*. 2014;24(2):674-678. doi:10.1016/j.bmcl.2013.11.049

113. BROOD 3.1.7.1: OpenEye Scientific Software, Santa Fe, NM. Accessed August 24, 2022. http://www.eyesopen.com

114. Schrödinger Release 2019-4: Maestro, Schrödinger, LLC, New York, NY, 2021.
115. Schrödinger Release 2019-4: Canvas, Schrödinger, LLC, New York, NY, 2021.
116. Duan J, Dixon SL, Lowrie JF, Sherman W. Analysis and comparison of 2D fingerprints: Insights into database screening performance using eight fingerprint methods. *J Mol Graph Model*. 2010;29(2):157-170. doi:10.1016/j.jmgm.2010.05.008
117. Rego Campello H, del Villar SG, Honraedt A, et al. Unlocking Nicotinic Selectivity via Direct C–H Functionalization of (−)-Cytisine. *Chem*. 2018;4(7):1710-1725. doi:10.1016/j.chempr.2018.05.007
118. Moroni M, Vijayan R, Carbone A, Zwart R, Biggin PC, Bermudez I. Non-agonist-binding subunit interfaces confer distinct functional signatures to the alternate stoichiometries of the α4β2 nicotinic receptor: An α4-α4 interface is required for Zn2+ potentiation. *Journal of Neuroscience*. 2008;28(27):6884-6894. doi:10.1523/JNEUROSCI.1228-08.2008
119. Brieke C, Rohrbach F, Gottschalk A, Mayer G, Heckel A. Light-controlled tools. *Angewandte Chemie - International Edition*. 2012;51(34):8446-8476. doi:10.1002/anie.201202134
120. Bort G, Gallavardin T, Ogden D, Dalko PI. From one-photon to two-photon probes: "caged" compounds, actuators, and photoswitches. *Angewandte Chemie - International Edition*. 2013;52(17):4526-4537. doi:10.1002/anie.201204203
121. Gautier A, Gauron C, Volovitch M, Bensimon D, Jullien L, Vriz S. How to control proteins with light in living systems. *Nat Chem Biol*. 2014;10(7):533-541. doi:10.1038/nchembio.1534
122. Zhao Y. Light-responsive block copolymer micelles. *Macromolecules*. 2012;45(9):3647-3657. doi:10.1021/ma300094t
123. Vorobev AY, Moskalensky AE. Long-wavelength photoremovable protecting groups: On the way to in vivo application. *Comput Struct Biotechnol J*. 2020;18(November):27-34. doi:10.1016/j.csbj.2019.11.007
124. Göppert-Mayer M. Über die Wahrscheinlichkeit des Zusammenwirkens zweier Lichtquanten in einem Elementarakt. *Naturwissenschaften*. Published online 1929:932.
125. Kaiser W, Garrett CGB. Two-photon excitation in CaF2: Eu2+. *Phys Rev Lett*. 1961;7(6):229-231. doi:10.1103/PhysRevLett.7.229

126. Denk, W.; Strickler, J. H.; Webb WW. Two-Photon Laser Scanning Fluorescence Microscopy. *Science (1979)*. 1990;248(4951)(April):73-76.

127. Denk W. Two-photon scanning photochemical microscopy : Mapping ligand-gated ion channel distributions. 1994;91(July):6629-6633.

128. Dore TM, Wilson HC. *Chromophores for the Delivery of Bioactive Molecules with Two-Photon Excitation*. Vol 55.; 2011. doi:10.1007/978-1-61779-031-7_4

129. Piant S, Bolze F, Specht A. Two-photon uncaging, from neuroscience to materials. *Opt Mater Express*. 2016;6(5):1679. doi:10.1364/ome.6.001679

130. Klán P, Šolomek T, Bochet CG, et al. Photoremovable protecting groups in chemistry and biology: Reaction mechanisms and efficacy. *Chem Rev*. 2013;113(1):119-191. doi:10.1021/cr300177k

131. Furuta T, Wang SSH, Dantzker JL, et al. Brominated 7-hydroxycoumarin-4-ylmethyls: Photolabile protecting groups with biologically useful cross-sections for two photon photolysis. *Proc Natl Acad Sci U S A*. 1999;96(4):1193-1200. doi:10.1073/pnas.96.4.1193

132. Pillai VNR. Photoremovable Protecting Groups in Organic Synthesis. *Synthesis (Stuttg)*. Published online 1980:1-26.

133. Kaplan JH, Forbush B, Hoffman JF. Rapid Photolytic Release of Adenosine 5'-Triphosphate from a Protected Analogue: Utilization by the Na:K Pump of Human Red Blood Cell Ghosts. *Biochemistry*. 1976;17(10):1929-1935.

134. Engels J, Schlaeger EJ. Synthesis, Structure, and Reactivity of Adenosine Cyclic 3',5'-Phosphate Benzyl Trieste. *J Med Chem*. 1977;20(7):907-911. https://pubs.acs.org/sharingguidelines

135. Matsuzaki M, Ellis-Davies GCR, Nemoto T, Miyashita Y, Iino M, Kasai H. Dendritic spine geometry is critical for AMPA receptor expression in hippocampal CA1 pyramidal neurons. *Nat Neurosci*. 2001;4(11):1086-1092. doi:10.1038/nn736

136. Zhu Y, Pavlos CM, Toscano JP, Dore TM. 8-Bromo-7-hydroxyquinoline as a photoremovable protecting group for physiological use: Mechanism and scope. *J Am Chem Soc*. 2006;128(13):4267-4276. doi:10.1021/ja0555320

137. Jarrett Davis M, Kragor CH, Reddie KG, Wilson HC, Zhu Y, Dore TM. Substituent effects on the sensitivity of a quinoline photoremovable protecting group to one- And two-

photon excitation. *Journal of Organic Chemistry*. 2009;74(4):1721-1729. doi:10.1021/jo802658a

138. Asad N, Deodato D, Lan X, et al. Photochemical Activation of Tertiary Amines for Applications in Studying Cell Physiology. *J Am Chem Soc*. 2017;139(36):12591-12600. doi:10.1021/jacs.7b06363
139. Link KH, Shi Y, Koh JT. Light activated recombination. *J Am Chem Soc*. 2005;127(38):13088-13089. doi:10.1021/ja0531226
140. Inlay MA, Choe V, Bharathi S, et al. Synthesis of a photocaged tamoxifen for light-dependent activation of Cre-ER recombinase-driven gene modification. *Chemical Communications*. 2013;49(43):4971-4973. doi:10.1039/c3cc42179a
141. Faal T, Wong PT, Tang S, et al. 4-Hydroxytamoxifen probes for light-dependent spatiotemporal control of Cre-ER mediated reporter gene expression. *Mol Biosyst*. 2015;11(3):783-790. doi:10.1039/c4mb00581c
142. Wong PT, Roberts EW, Tang S, et al. Control of an Unusual Photo-Claisen Rearrangement in Coumarin Caged Tamoxifen through an Extended Spacer. *ACS Chem Biol*. 2017;12(4):1001-1010. doi:10.1021/acschembio.6b00999
143. Asad N, Mclain DE, Condon AF, et al. Photoactivatable Dopamine and Sulpiride to Explore the Function of Dopaminergic Neurons and Circuits. *ACS Chem Neurosci*. 2020;11(6):939-951. doi:10.1021/acschemneuro.9b00675
144. Barker G, Obrien P, Campos KR. Diamine-free lithiation-trapping of N-Boc heterocycles using s-BuLi in THF. *Org Lett*. 2010;12(18):4176-4179. doi:10.1021/ol1017799
145. Bolchi C, Bavo F, Fumagalli L, et al. Novel 5-substituted 3-hydroxyphenyl and 3-nitrophenyl ethers of S-prolinol as α4β2-nicotinic acetylcholine receptor ligands. *Bioorg Med Chem Lett*. 2016;26(23):5613-5617. doi:10.1016/j.bmcl.2016.10.078
146. NOVARTIS AG. HETEROCYCLIC COMPOUNDS AND METHODS FOR THEIR USE US 2017/0145032 A1. Published online 2017:119.
147. Sivaraman A, Harmalkar DS, Kang J, Choi Y, Lee K. A protecting group-free divergent synthesis of natural benzofurans via one-pot synthesis of 2-bromo-6-hydroxybenzofurans. *Org Biomol Chem*. 2019;17(8):2153-2161. doi:10.1039/C8OB03102A

148. Paul A, Seidel D. α-Functionalization of Cyclic Secondary Amines: Lewis Acid Promoted Addition of Organometallics to Transient Imines. *J Am Chem Soc*. 2019;141(22):8778-8782. doi:10.1021/jacs.9b04325

149. Fredrich S, Bonasera A, Valderrey V, Hecht S. Sensitive Assays by Nucleophile-Induced Rearrangement of Photoactivated Diarylethenes. *J Am Chem Soc*. 2018;140(20):6432-6440. doi:10.1021/jacs.8b02982

150. Li S, Wan P, Ai J, Sheng R, Hu Y, Hu Y. Palladium-Catalyzed, Silver-Assisted Direct C-5–H Arylation of 3-Substituted 1,2,4-Oxadiazoles under Microwave Irradiation. *Adv Synth Catal*. 2017;359(5):772-778. doi:10.1002/adsc.201600913

151. Narayanan V V., Gopalan RS, Chakrabarty D, Mobin SM, Mathur P. Crystal structure and energy optimization of dichlorobis(ethylanthranilatonicotinamide)zinc(II). *J Chem Crystallogr*. 2011;41(6):801-805. doi:10.1007/s10870-010-9981-6

152. Cai J, Wei H, Hong KH, et al. Discovery and preliminary evaluation of 2-aminobenzamide and hydroxamate derivatives containing 1,2,4-oxadiazole moiety as potent histone deacetylase inhibitors. *Eur J Med Chem*. 2015;96:1-13. doi:10.1016/j.ejmech.2015.04.002

153. Zhang Y, Wu C, Wan X, Wang C. Direct synthesis of 3,5-diaryl-1,2,4-oxadiazoles using 1-(2-oxo-2-arylethyl)pyridin-1-iums with benzamidines. *J Heterocycl Chem*. 2021;58(12):2287-2297. doi:10.1002/jhet.4354

154. Pibiri I, Pace A, Buscemi S, Causin V, Rastrelli F, Saielli G. Oxadiazolyl-pyridines and perfluoroalkyl-carboxylic acids as building blocks for protic ionic liquids: Crossing the thin line between ionic and hydrogen bonded materials. *Physical Chemistry Chemical Physics*. 2012;14(41):14306-14314. doi:10.1039/c2cp42467c

155. Outirite M, Lebrini M, Lagrenée M, Bentiss F. New one step synthesis of 3,5-disubstituted 1,2,4-oxadiazoles. *J Heterocycl Chem*. 2007;44(6):1529-1531. doi:10.1002/jhet.5570440647

156. WO2006114400A1

157. Cunha FS, Nogueira JMR, de Aguiar AP. Synthesis and antibacterial evaluation of 3,5-Diaryl-1,2,4-oxadiazole derivatives. *J Braz Chem Soc*. 2018;29(11):2405-2416. doi:10.21577/0103-5053.20180118

158. WO2009148452A1

159. WO2008028903A2
160. WO2006114400A1
161. Xu LL, Wu YF, Wang L, et al. Structure-activity and structure-property relationships of novel Nrf2 activators with a 1,2,4-oxadiazole core and their therapeutic effects on acetaminophen (APAP)-induced acute liver injury. *Eur J Med Chem*. 2018;157:1376-1394. doi:10.1016/j.ejmech.2018.08.071
162. Girnys EA, Porter VR, Mosberg HI. Conformationally restricted analogs of the direct thrombin inhibitor FM 19. *Bioorg Med Chem*. 2011;19(24):7425-7434. doi:10.1016/j.bmc.2011.10.045
163. Offermann DA, McKendrick JE, Sejberg JJP, et al. Synthesis and incorporation into cyclic peptides of tolan amino acids and their hydrogenated congeners: Construction of an array of A-B-loop mimetics of the Cε3 domain of human IgE. *Journal of Organic Chemistry*. 2012;77(7):3197-3214. doi:10.1021/jo202604q
164. Hou F, Wang XC, Quan ZJ. Efficient synthesis of esters through oxone-catalyzed dehydrogenation of carboxylic acids and alcohols. *Org Biomol Chem*. 2018;16(48):9472-9476. doi:10.1039/c8ob02539h
165. US2004127521A1
166. US5891872A
167. Shah UH, Gaitonde SA, Moreno JL, Glennon RA, Dukat M, González-Maeso J. Revised Pharmacophore Model for 5-HT2A Receptor Antagonists Derived from the Atypical Antipsychotic Agent Risperidone. *ACS Chem Neurosci*. 2019;10(5):2318-2331. doi:10.1021/acschemneuro.8b00637
168. Kang SM, Jin C, Kim DH, Lee Y, Lee BJ. Structural and Functional Study of the Klebsiella pneumoniae VapBC Toxin-Antitoxin System, including the Development of an Inhibitor That Activates VapC. *J Med Chem*. 2020;63(22):13669-13679. doi:10.1021/acs.jmedchem.0c01118
169. He ZJ, Wang YM, Tang CC. Studies on chiral thiophosphoric acids and their derivatives 16. - The asymmetric cyclization of L-(+)-prolinol with (thio)phosphoro(-no)dichloridates. *Phosphorus, Sulfur and Silicon and Related Elements*. 1997;127:59-66. doi:10.1080/10426509708040496

170. Dei S, Bellucci C, Buccioni M, et al. Synthesis and cholinergic affinity of diastereomeric and enantiomeric isomers of 1-methyl-2-(2-methyl-1,3-dioxolan-4-yl)- pyrrolidine, 1-methyl-2-(2-methyl-1,3-oxathiolan-5-yl)pyrrolidine and of Their iodomethylates. *Bioorg Med Chem*. 2003;11(14):3153-3164. doi:10.1016/S0968-0896(03)00236-0

171. Kudo N, Perseghini M, Fu GC. A versatile method for suzuki cross-coupling reactions of nitrogen heterocycles. *Angewandte Chemie - International Edition*. 2006;45(8):1282-1284. doi:10.1002/anie.200503479

172. Li YM, Shi J, Cai R, Chen XY, Guo QX, Liu L. Development of new quinoline-based photo-labile groups for photo-regulation of bioactive molecules. *Tetrahedron Lett*. 2010;51(12):1609-1612. doi:10.1016/j.tetlet.2010.01.071

173. Ma J, Rea AC, An H, et al. Unraveling the mechanism of the photodeprotection reaction of 8-bromo- and 8-chloro-7-hydroxyquinoline caged acetates. *Chemistry - A European Journal*. 2012;18(22):6854-6865. doi:10.1002/chem.201200366

8. Supporting information

2-(6-hydroxybenzofuran2-yl)-1-methylpyrrolidine (**1**)

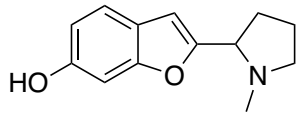

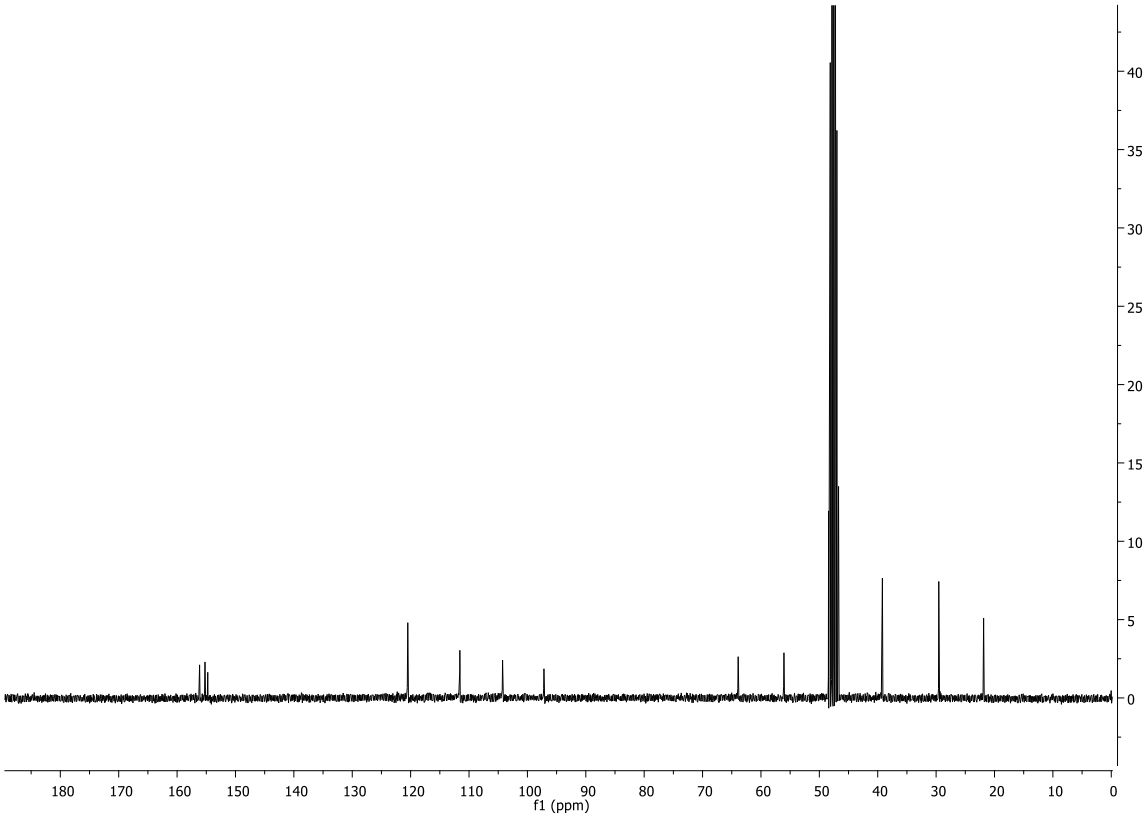

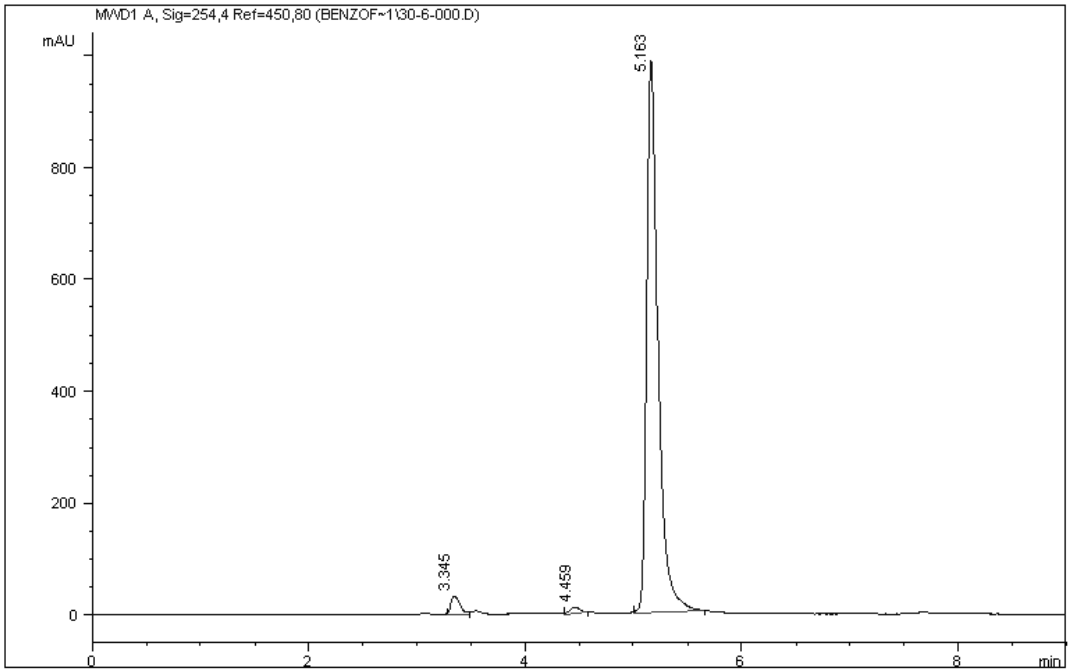

Signal 1: MWD1 A, Sig=254,4 Ref=450,80

Peak #	Area %	Area	RT [min]
1	2.588	194.297	3.345
2	1.021	76.607	4.459
3	96.391	7.235e3	5.163

Column: Supelcosil LC-SI (250x4.6 mm 5 µm)

Flow: 1 mL/min

Inj volume: 10 µL

Mobile Phase: AcOEt/MeOH 97.5/2.5 + 0.5% $NH_{3\ aq}$

λ: 254 nm

Rt/10 min: 5.2 min

Purity: 96.39%

2-(5-hydroxybenzofuran2-yl)-1-methylpyrrolidine (**2**)

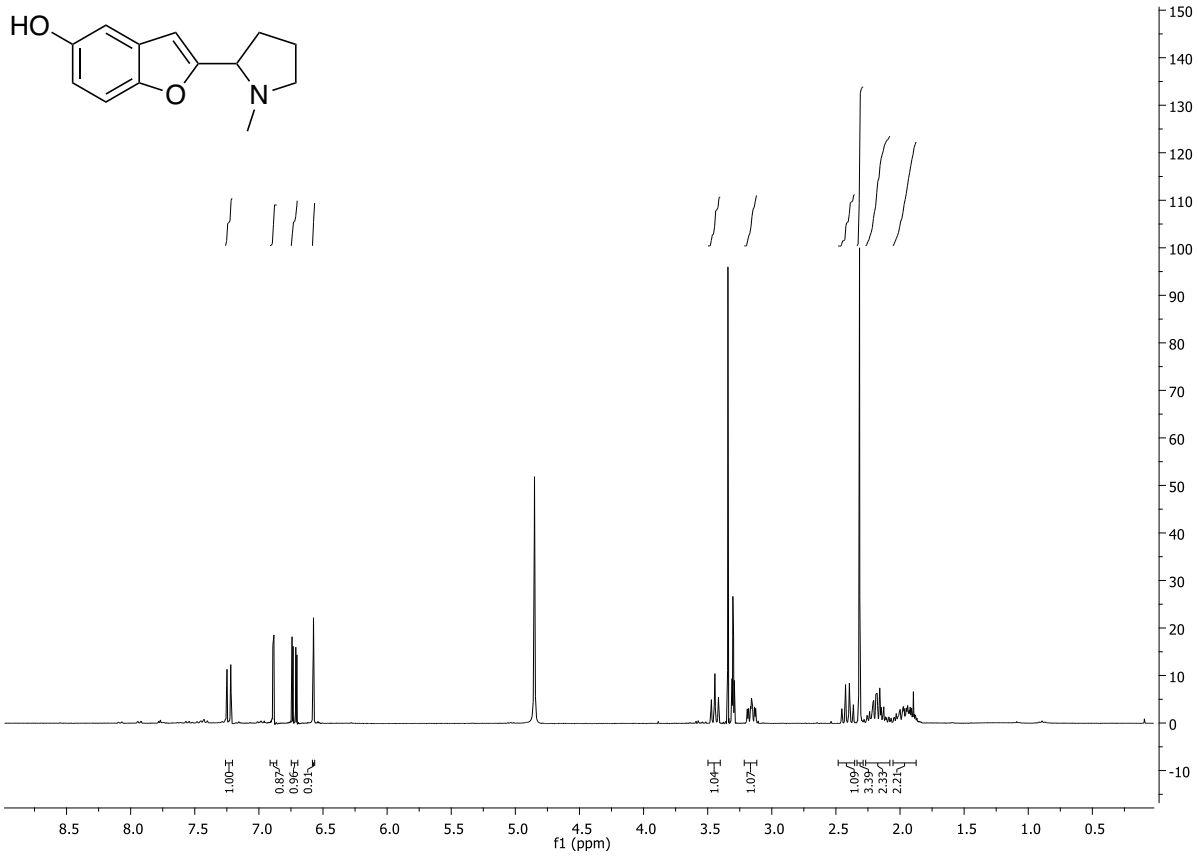

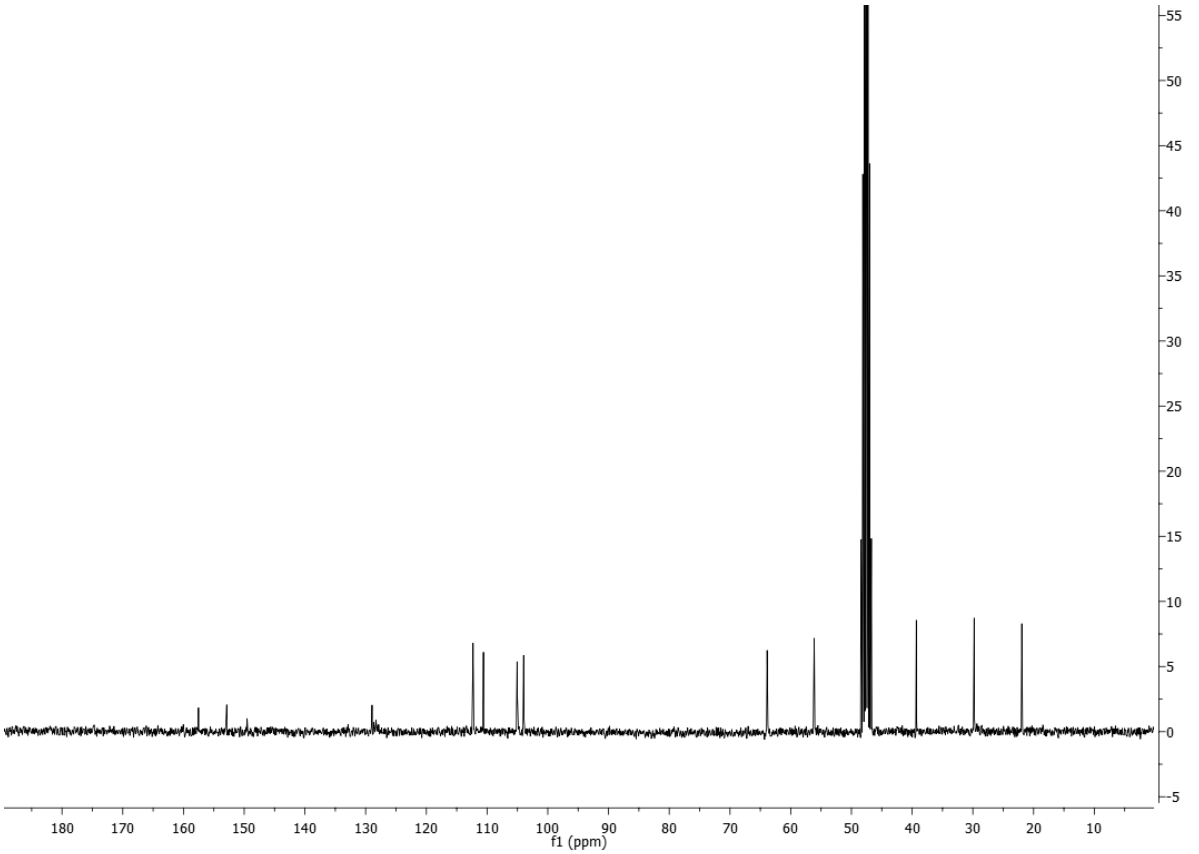

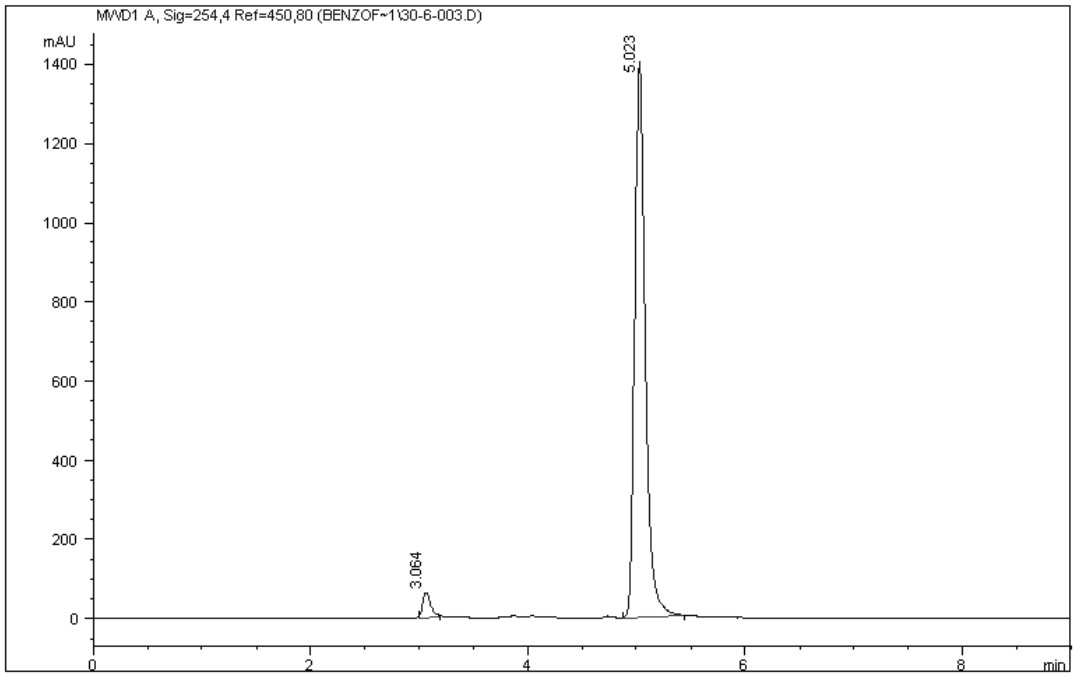

Signal 1: MWD1 A, Sig=254,4 Ref=450,80

Peak #	Area %	Area	RT [min]
1	3.332	314.477	3.064
2	96.668	9.124e3	5.023

Column: Supelcosil LC-SI (250x4.6 mm 5 µm)

Flow: 1 mL/min

Inj volume: 10 µL

Mobile Phase: AcOEt/MeOH 97.5/2.5 + 0.5% $NH_{3\ aq}$

λ: 254 nm

Rt/10 min: 5.0 min

Purity: 96.67%

2-(5-methoxybenzofuran-2-yl)-1-methylpyrrolidine (**3**)

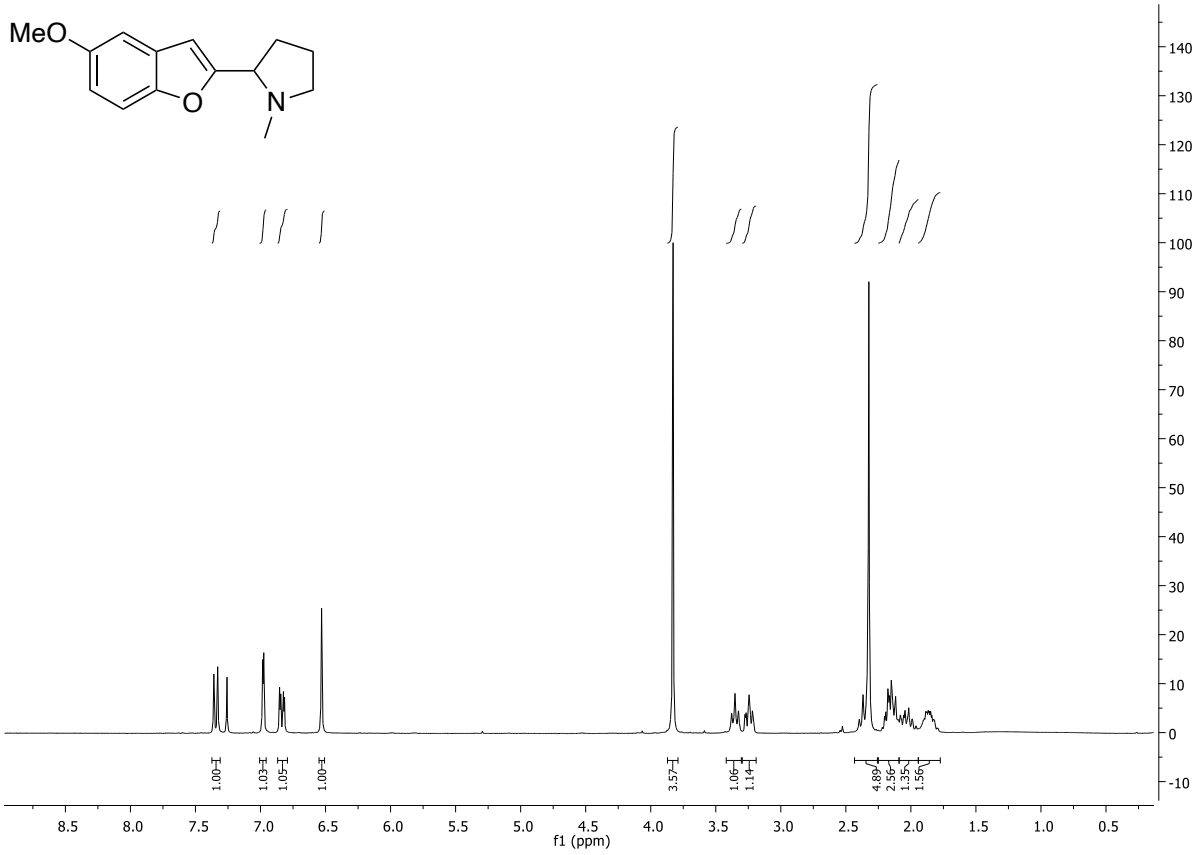

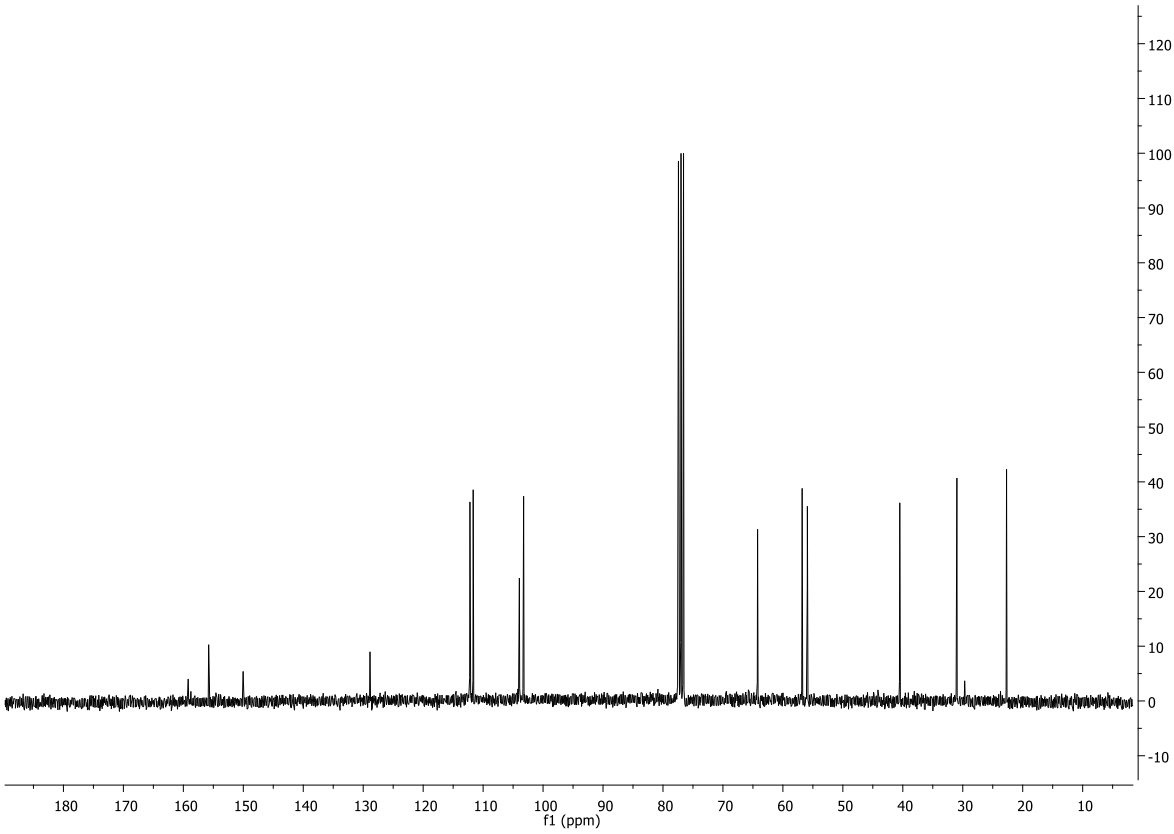

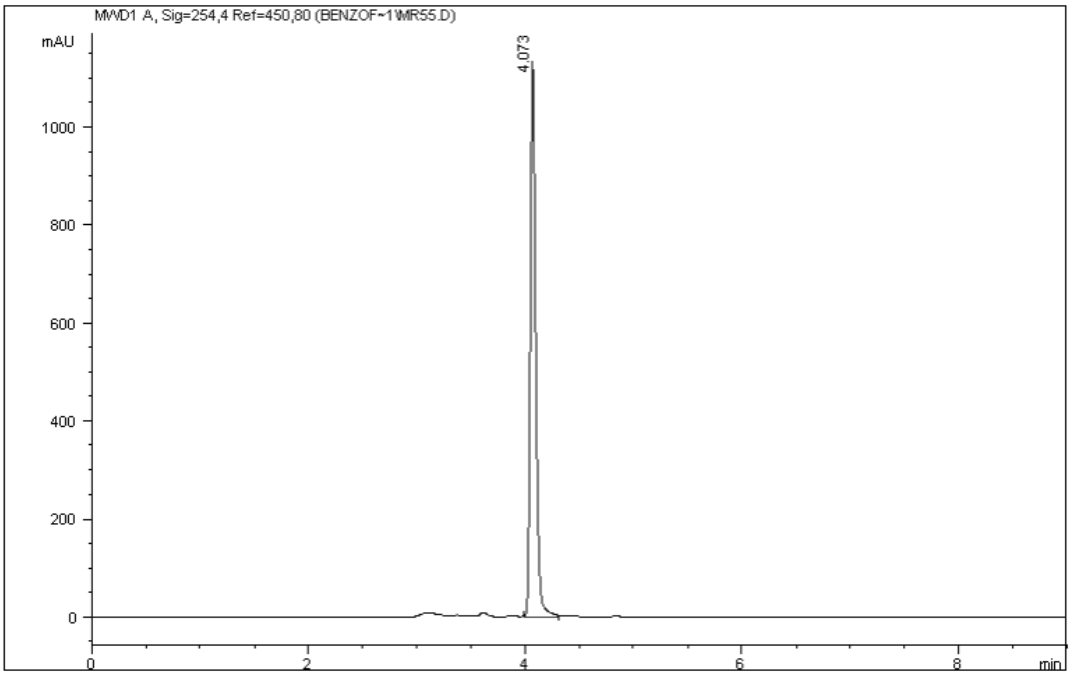

Signal 1: MWD1 A, Sig=254,4 Ref=450,80

Peak #	Area %	Area	RT [min]
1	100.000	4.046e3	4.073

Column: Supelcosil LC-SI (250x4.6 mm 5 µm)

Flow: 1 mL/min

Inj volume: 10 µL

Mobile Phase: AcOEt/MeOH 97.5/2.5 + 0.5% $NH_{3\ aq}$

λ: 254 nm

Rt/10 min: 4.1 min

Purity: 100%

2-(6-methoxybenzofuran-2-yl)-1-methylpyrrolidine (**4**)

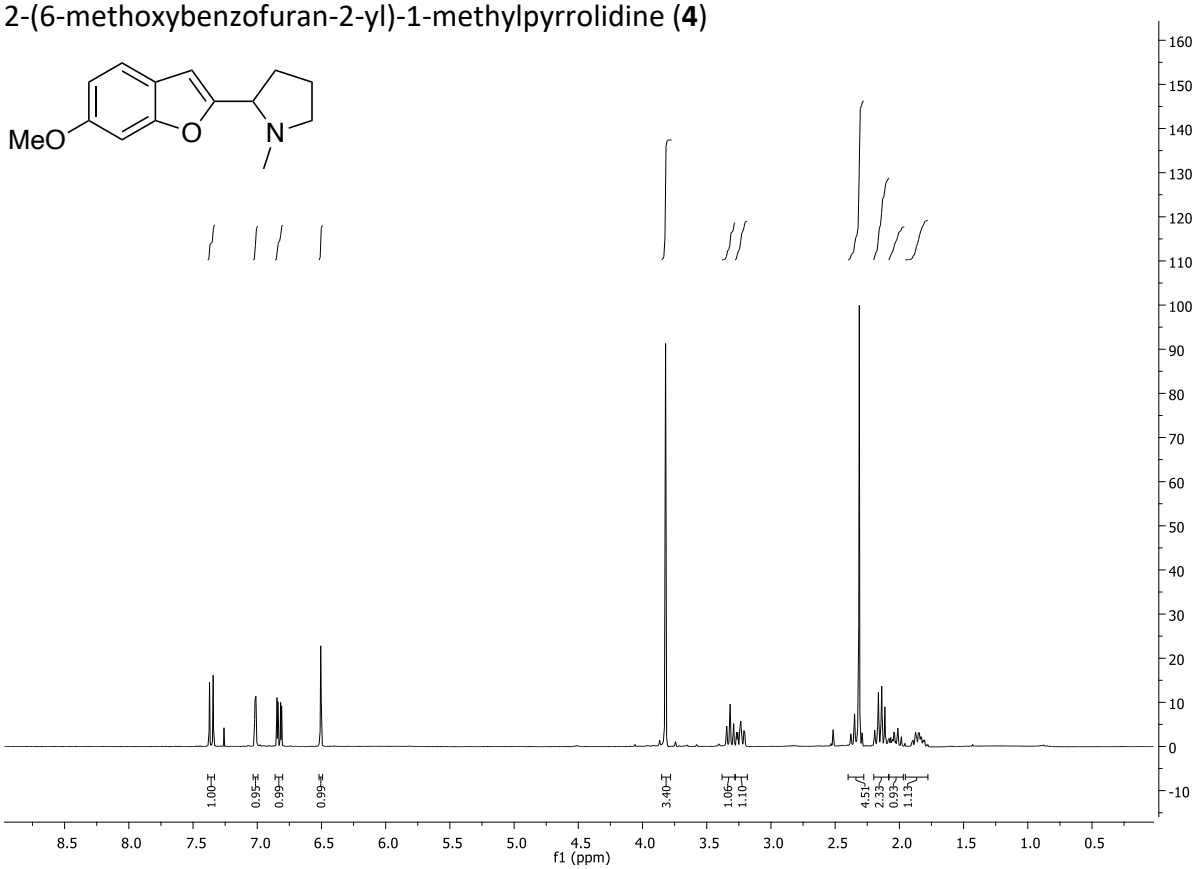

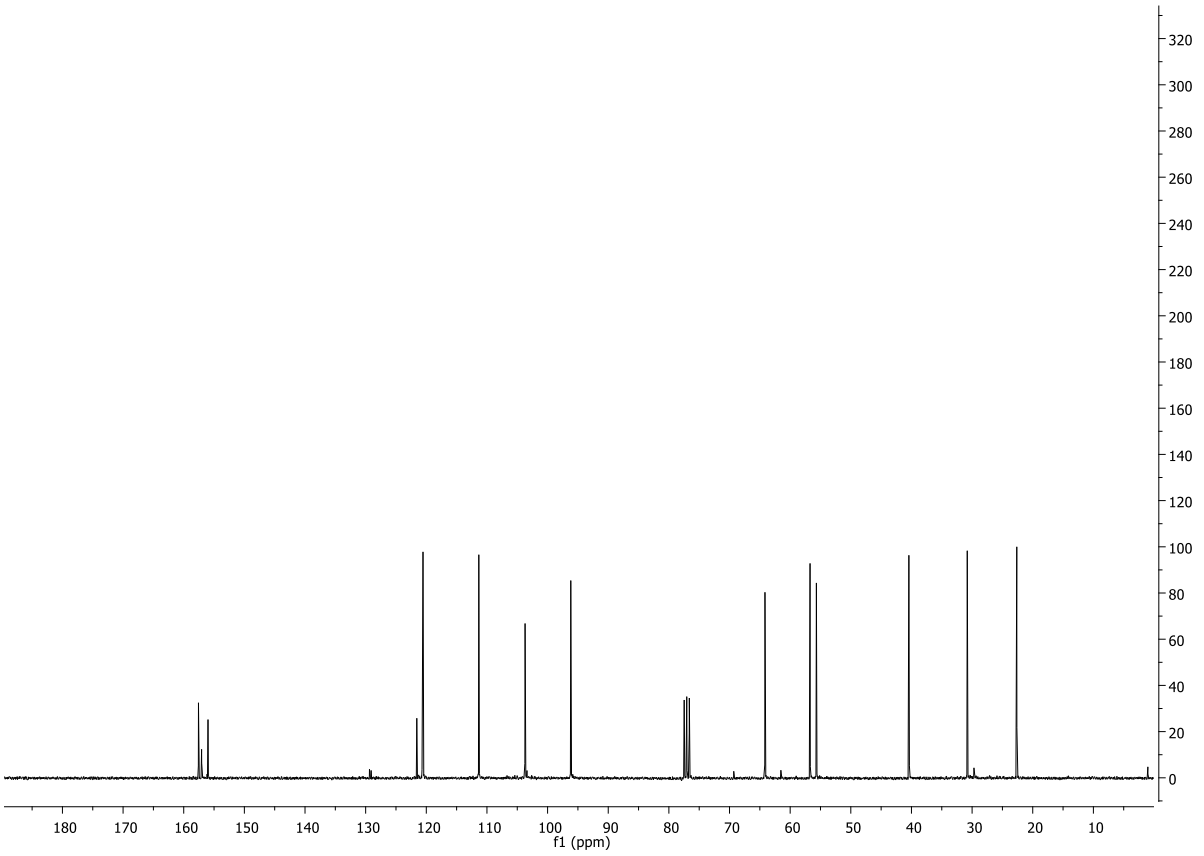

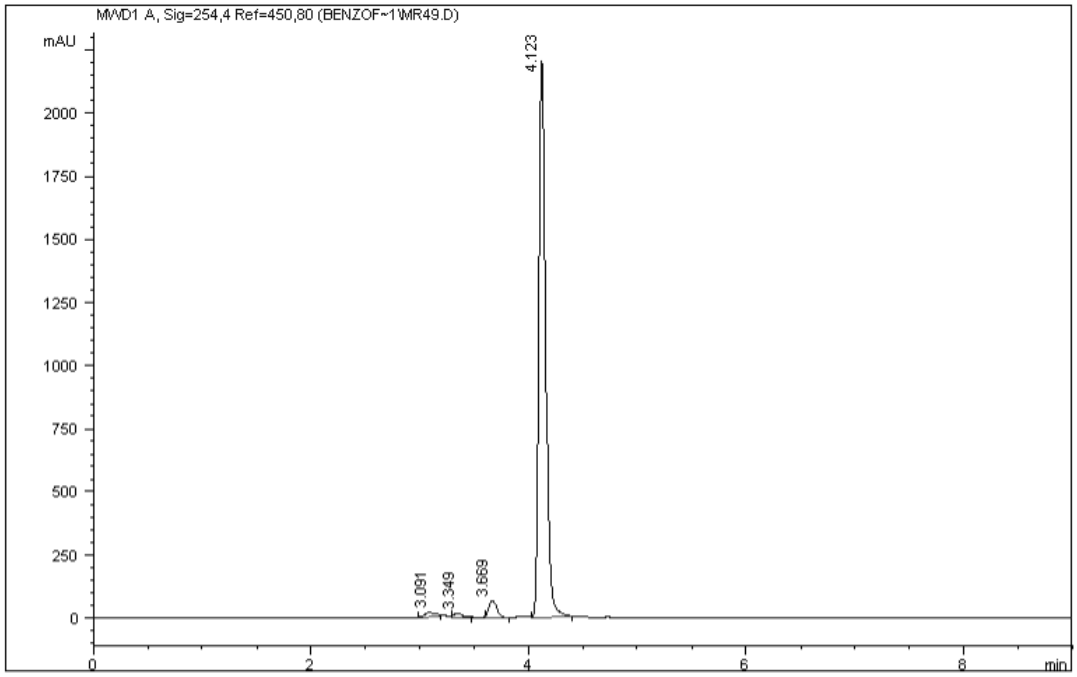

Signal 1: MWD1 A, Sig=254,4 Ref=450,80

Peak #	Area %	Area	RT [min]
1	1.103	112.720	3.091
2	0.793	80.963	3.349
3	3.060	312.553	3.669
4	95.044	9.709e3	4.123

Column: Supelcosil LC-SI (250x4.6 mm 5 µm)

Flow: 1 mL/min

Inj volume: 10 µL

Mobile Phase: AcOEt/MeOH 97.5/2.5 + 0.5% $NH_{3\ aq}$

λ: 254 nm

Rt/10 min: 4.1 min

Purity: 95.04%

2-(benzofuran-2-yl)-1-methylpyrrolidine (**5**)

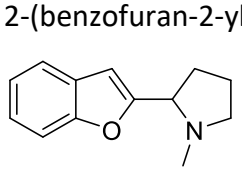

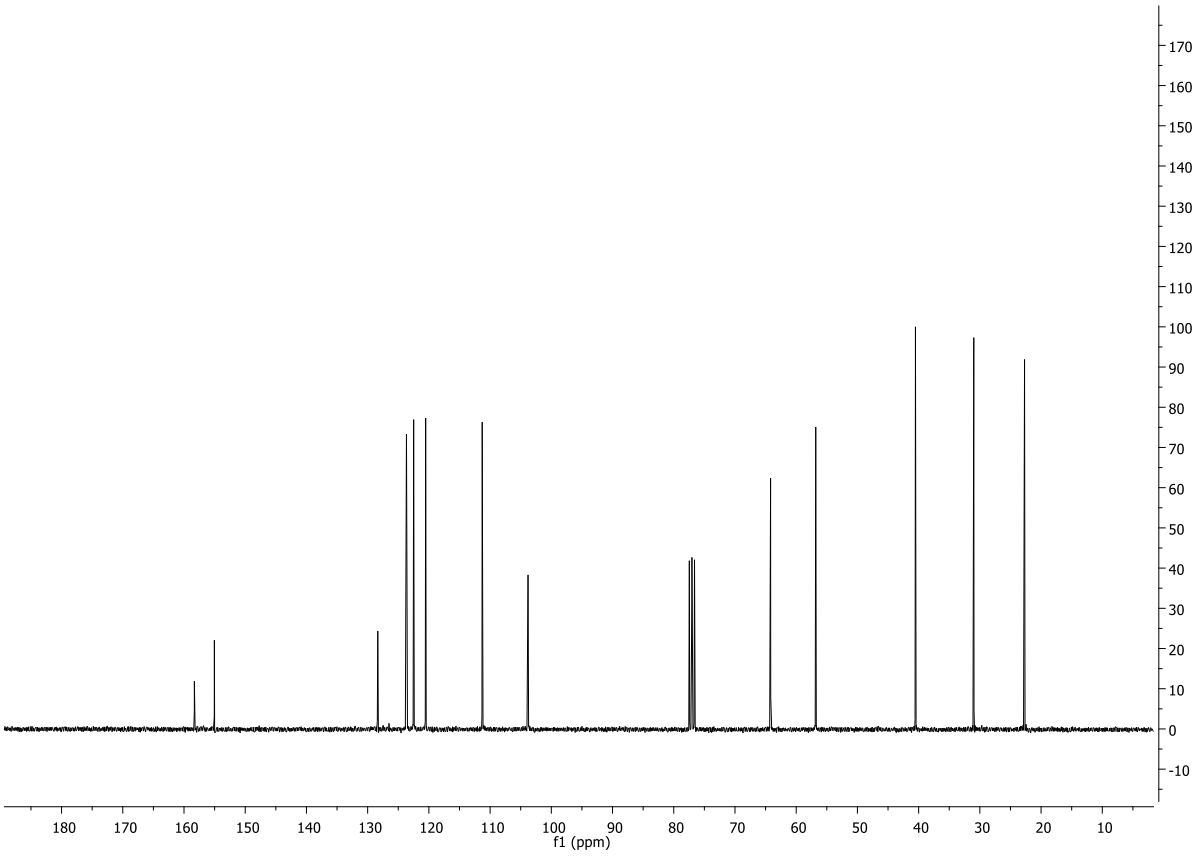

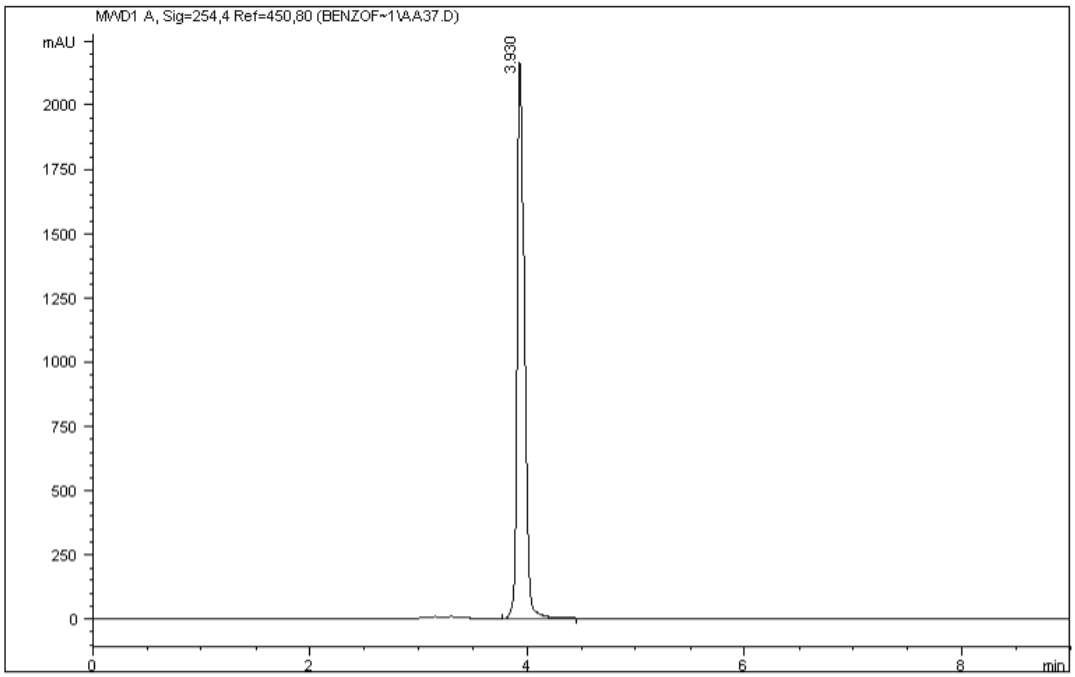

Signal 1: MWD1 A, Sig=254,4 Ref=450,80

Peak #	Area %	Area	RT [min]
1	100.000	9.986e3	3.930

Column: Supelcosil LC-SI (250x4.6 mm 5 µm)

Flow: 1 mL/min

Inj volume: 10 µL

Mobile Phase: AcOEt/MeOH 97.5/2.5 + 0.5% $NH_{3\ aq}$

λ: 254 nm

Rt/10 min: 3.9 min

Purity: 100%

2-(benzofuran-3-yl)-1-methylpyrrolidine (**6**)

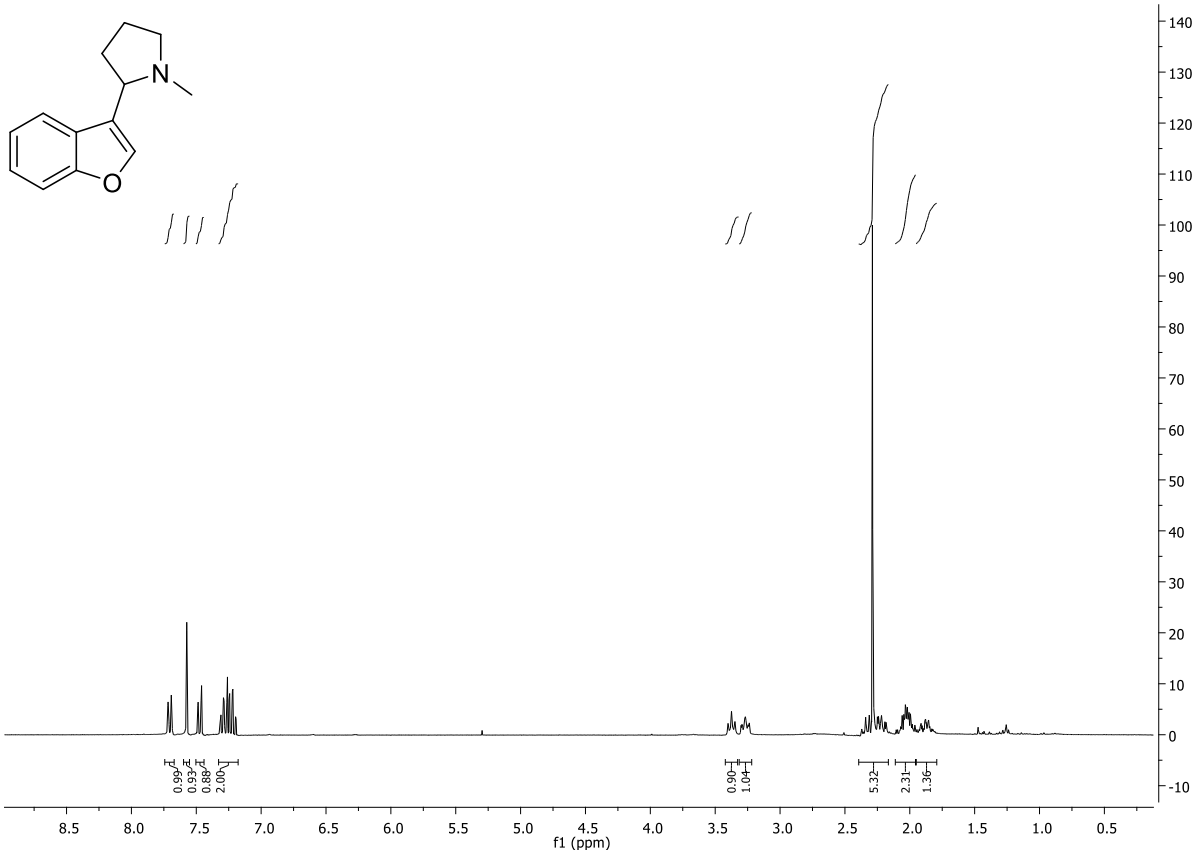

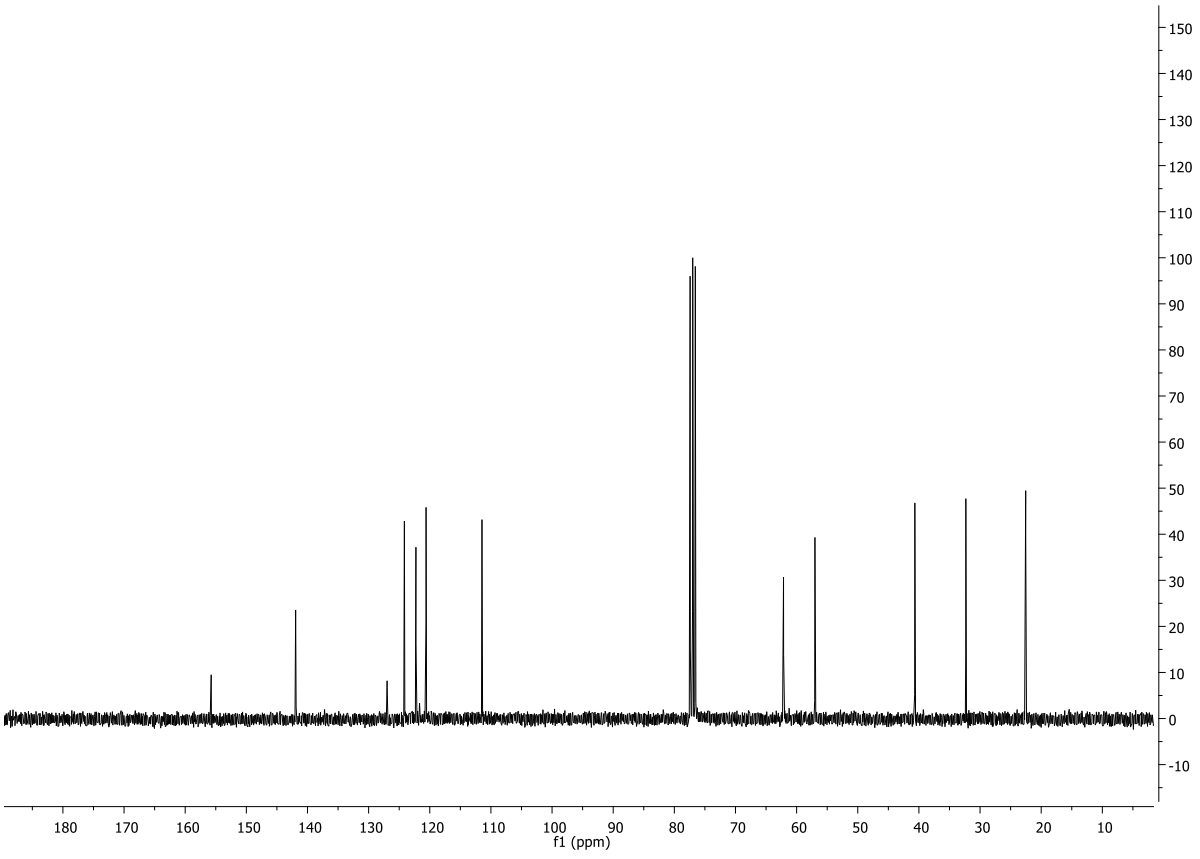

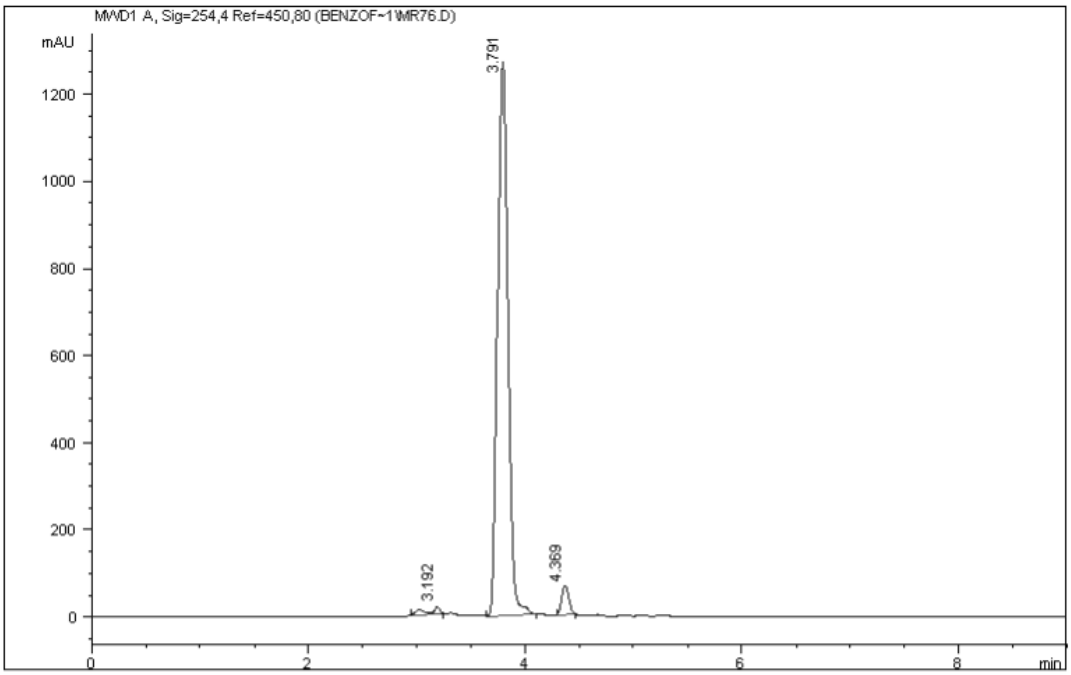

Signal 1: MWD1 A, Sig=254,4 Ref=450,80

Peak #	Area %	Area	RT [min]
1	1.323	118.555	3.192
2	95.458	8.556e3	3.791
3	3.220	288.589	4.369

Column: Supelcosil LC-SI (250x4.6 mm 5 µm)

Flow: 1 mL/min

Inj volume: 10 µL

Mobile Phase: AcOEt/MeOH 97.5/2.5 + 0.5% $NH_{3\ aq}$

λ: 254 nm

Rt/10 min: 3.8 min

Purity: 95.46%

5-phenyl-3-(pyridin-3-yl)-1,2,4-oxadiazole (**25**)

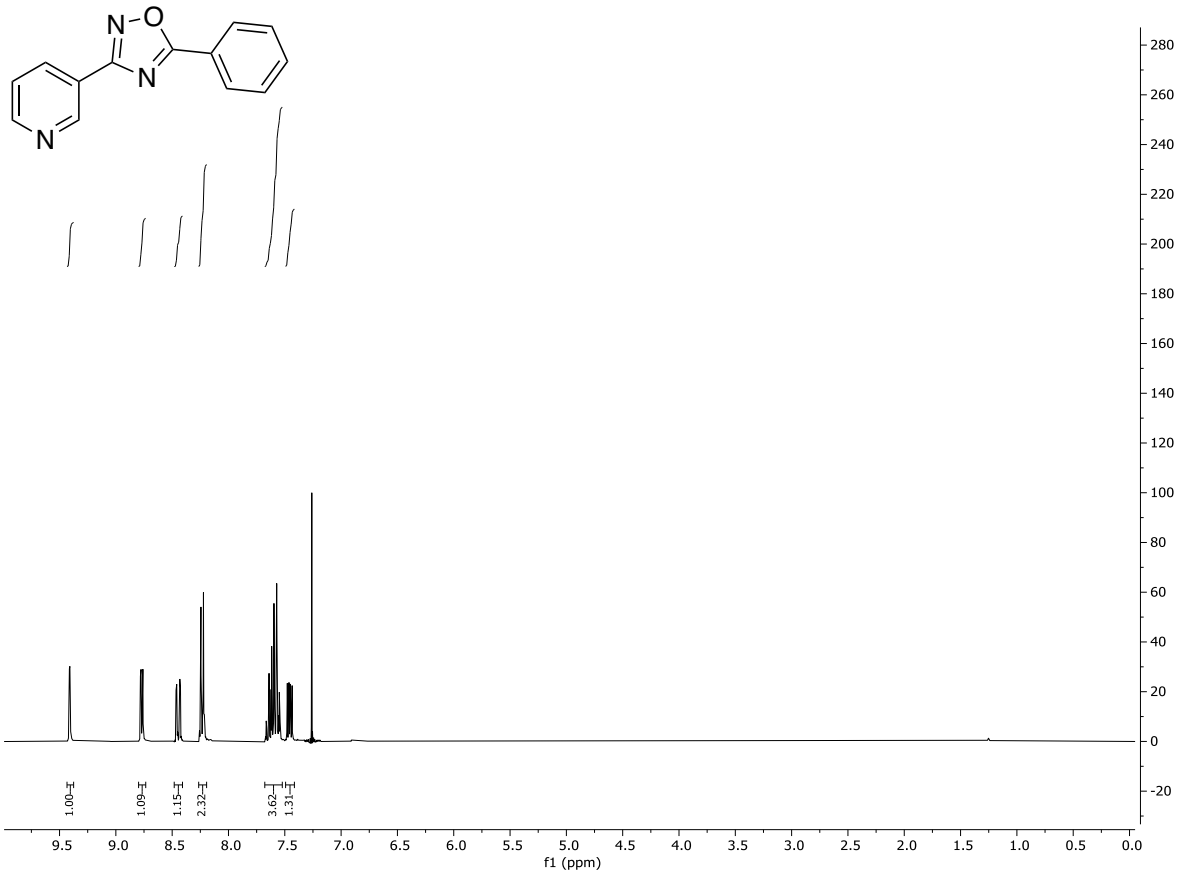

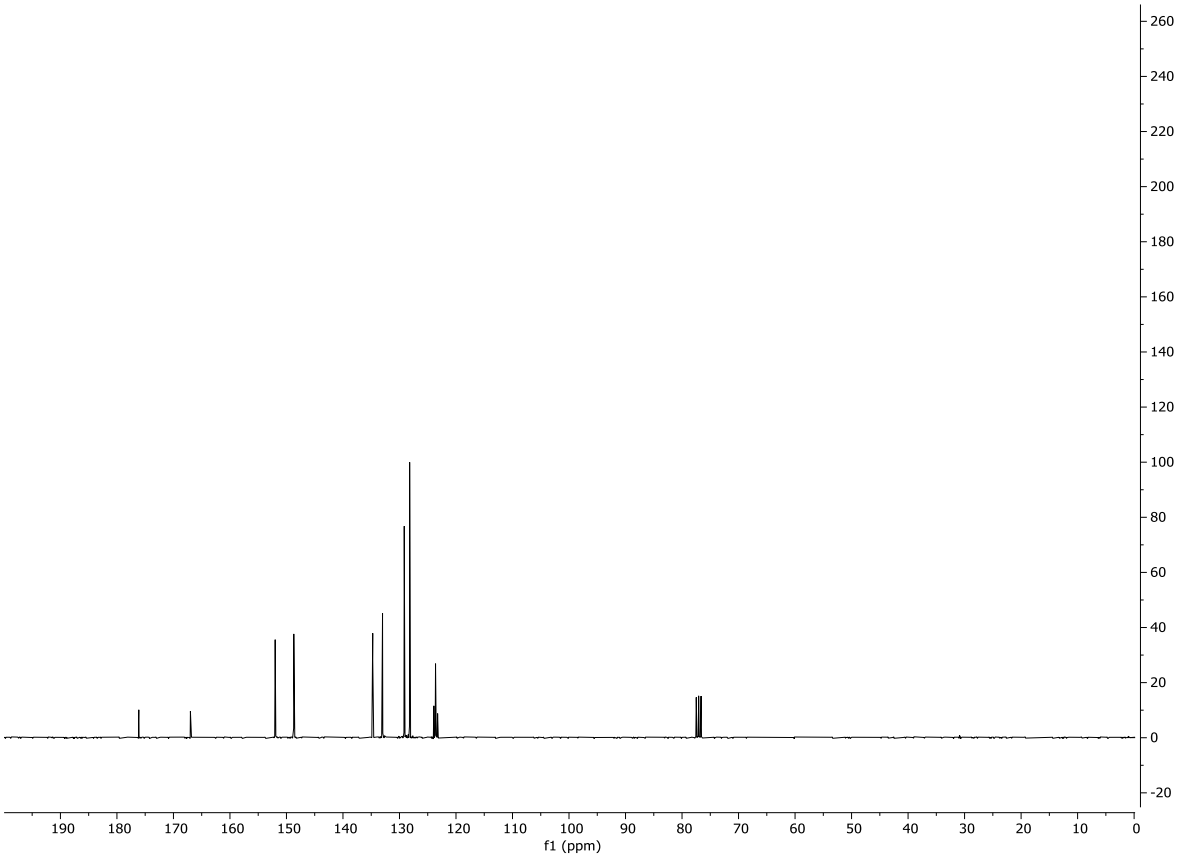

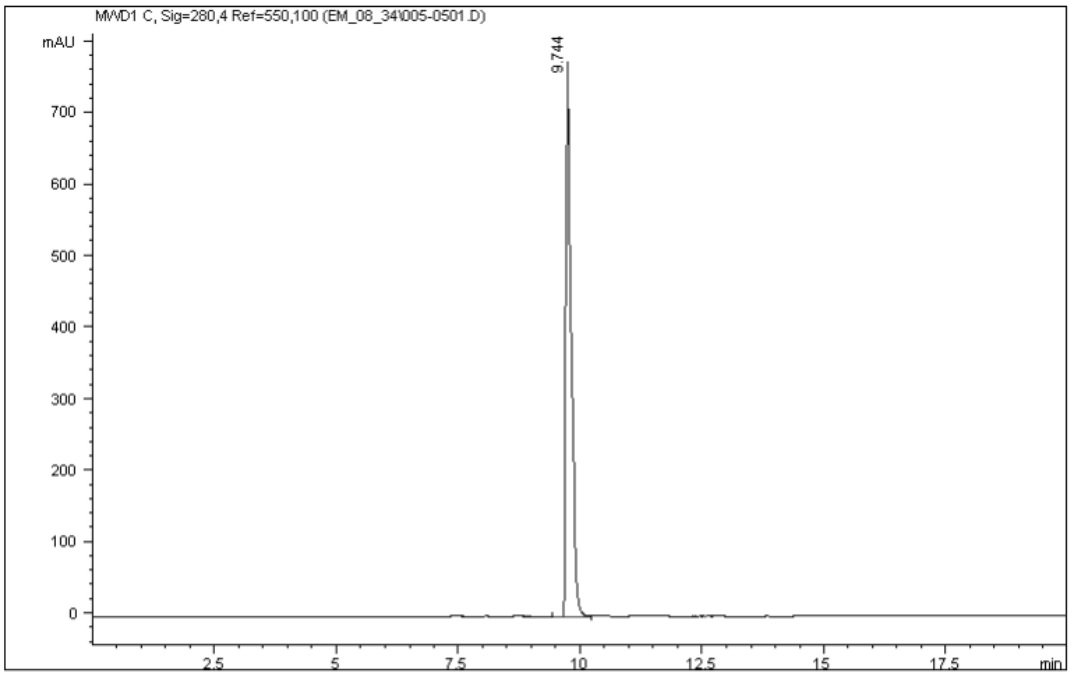

Signal 1: MWD1 C, Sig=280,4 Ref=550,100

Peak #	Area %	Area	RT [min]
1	100.000	5.695e3	9.744

Column: Hypersil BDS C18 (250x4.6 mm 5 µm)

Flow: 1.5 mL/min

Inj volume: 10 µL

Mobile Phase: H_2O/MeOH 70/30-95/5

λ: 280 nm

Rt/20 min: 9.7 min

Purity: 100%

5-(4-cyanophenyl)-3-(pyridin-3-yl)-1,2,4-oxadiazole (**26**)

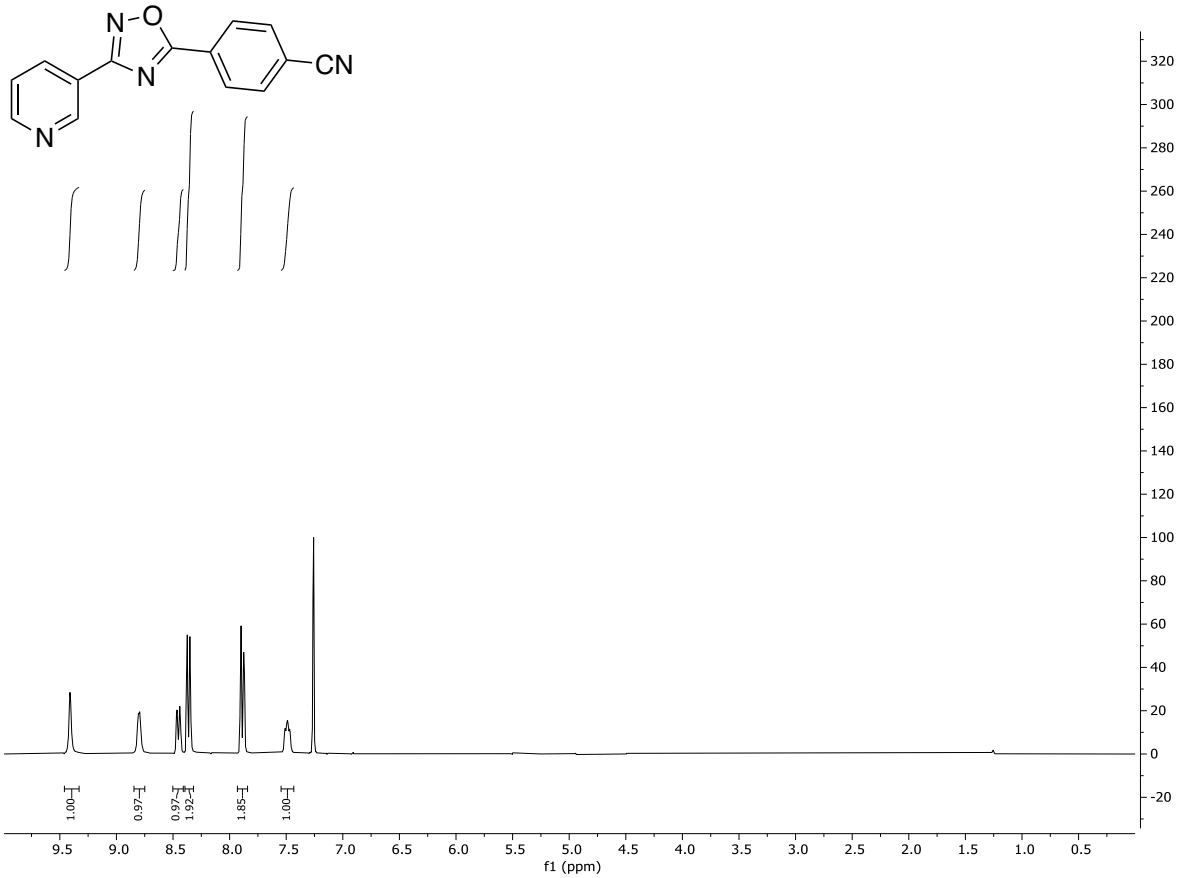

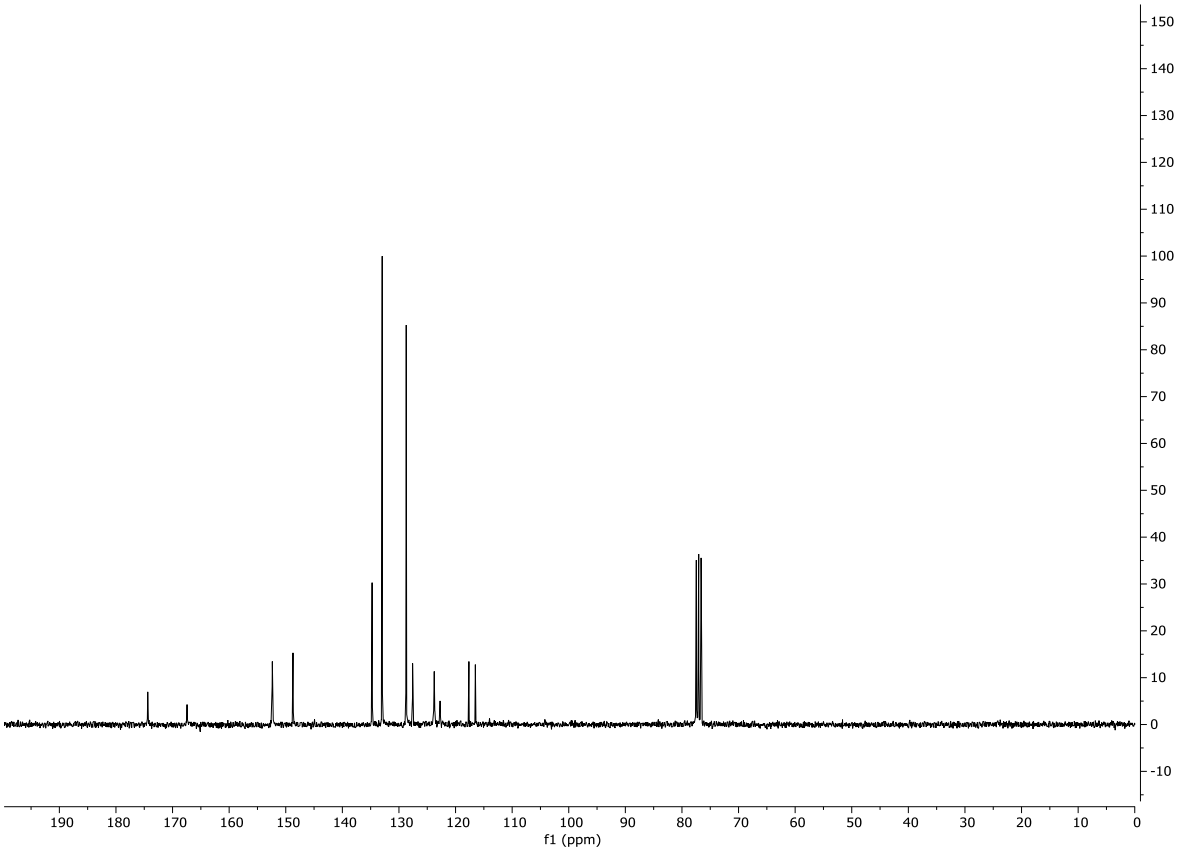

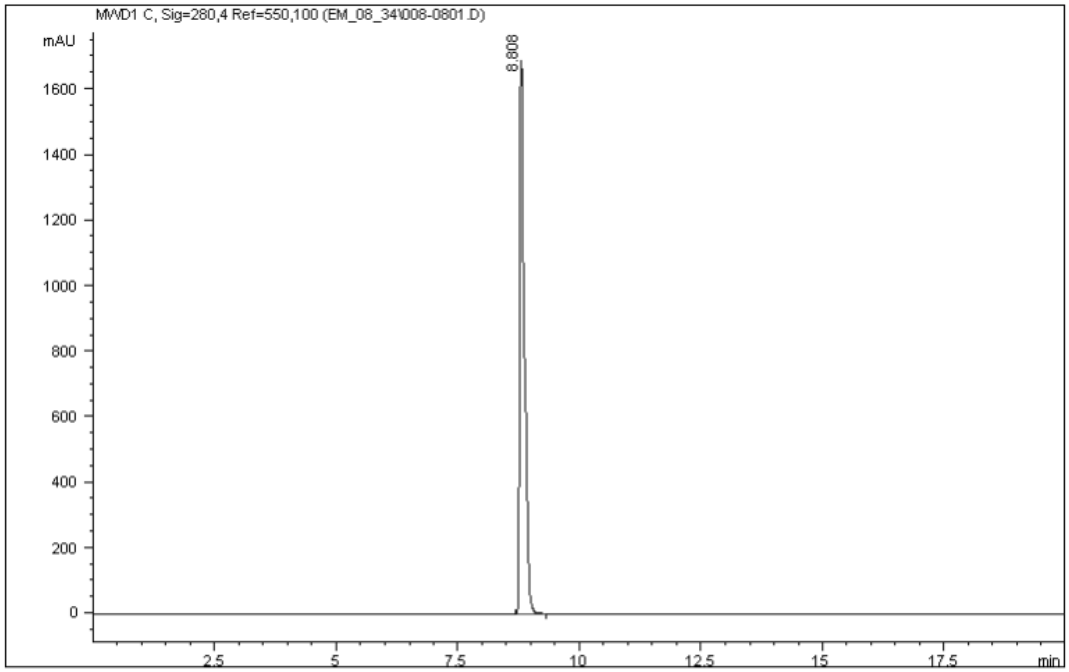

Signal 1: MWD1 C, Sig=280,4 Ref=550,100

Peak #	Area %	Area	RT [min]
1	100.000	1.069e4	8.808

Column: Hypersil BDS C18 (250x4.6 mm 5 µm)

Flow: 1.5 mL/min

Inj volume: 10 µL

Mobile Phase: H_2O/MeOH 70/30-95/5

λ: 280 nm

Rt/20 min: 8.81 min

Purity: 100%

5-(pyridin-2-yl)-3-(pyridin-3-yl)-1,2,4-oxadiazole (**27**)

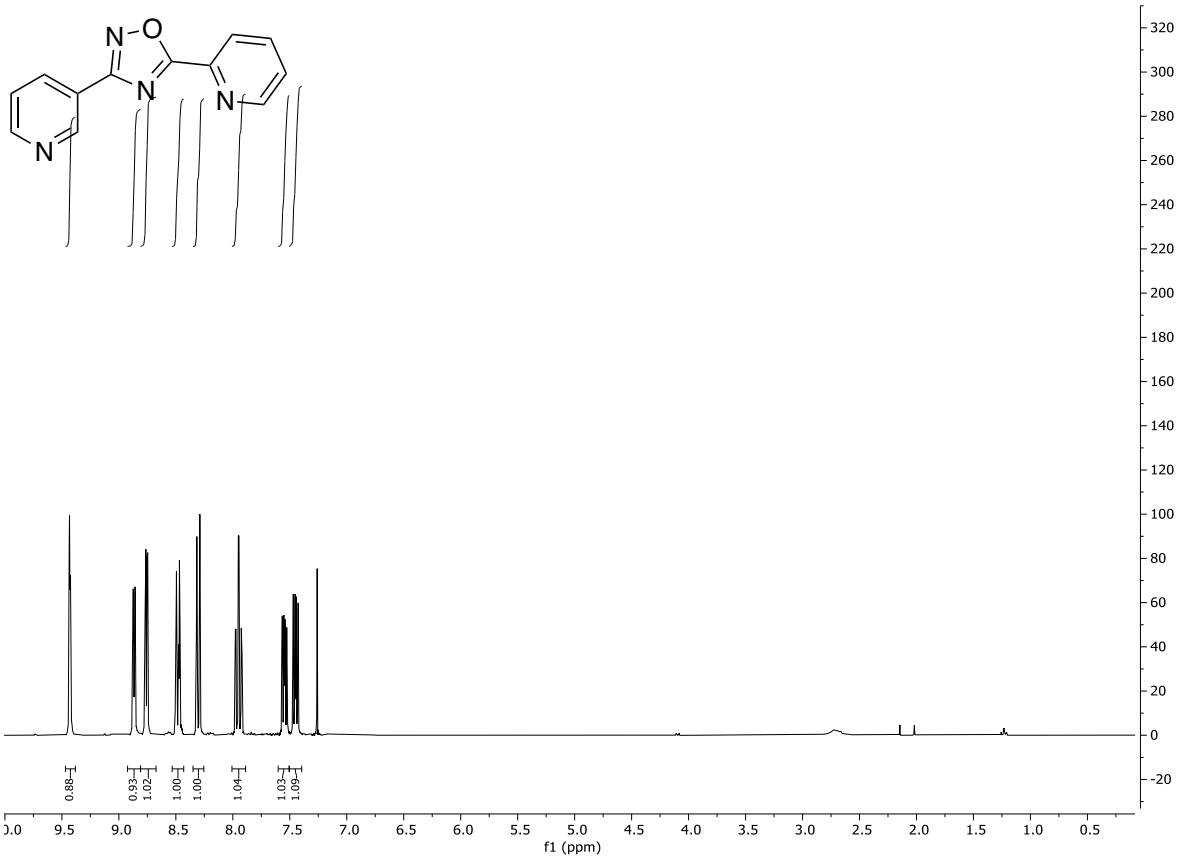

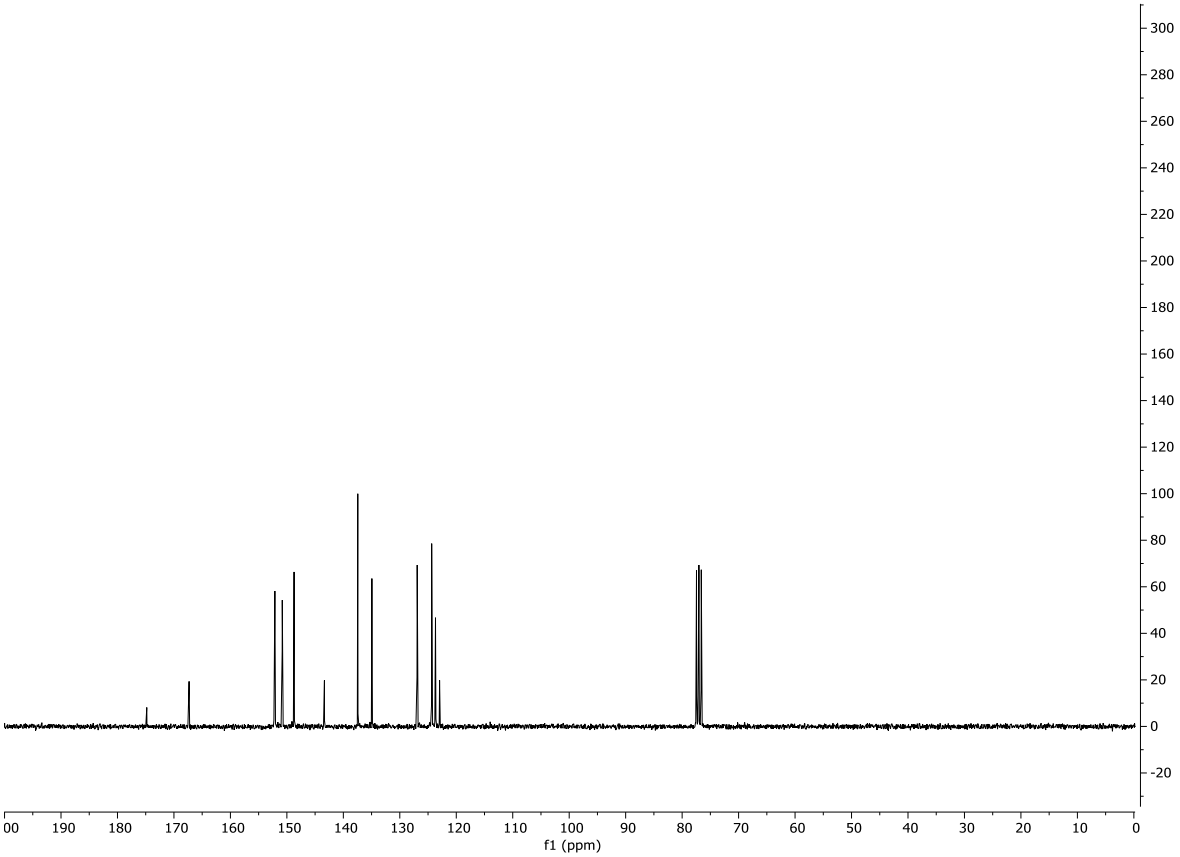

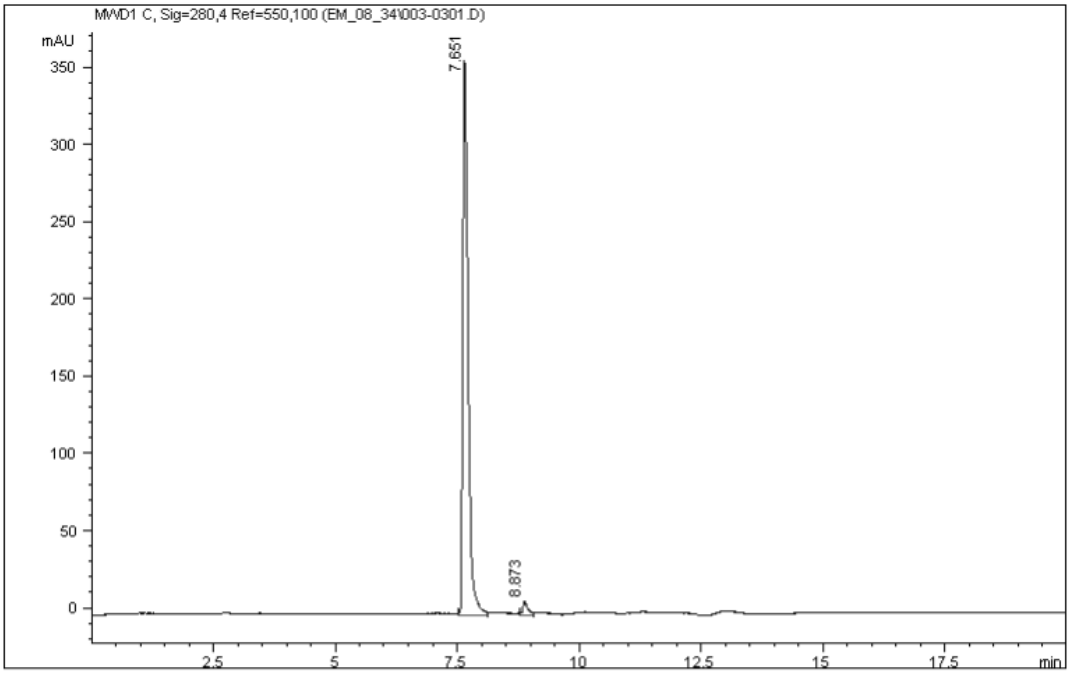

Signal 1: MWD1 C, Sig=280,4 Ref=550,100

Peak #	Area %	Area	RT [min]
1	97.439	2.767e3	7.651
2	2.561	72.734	8.873

Column: Hypersil BDS C18 (250x4.6 mm 5 µm)

Flow: 1.5 mL/min

Inj volume: 10 µL

Mobile Phase: H_2O/MeOH 70/30-95/5

λ: 280 nm

Rt/20 min: 7.65 min

Purity: 97.44%

3,5-di(pyridin-3-yl)-1,2,4-oxadiazole (**28**)

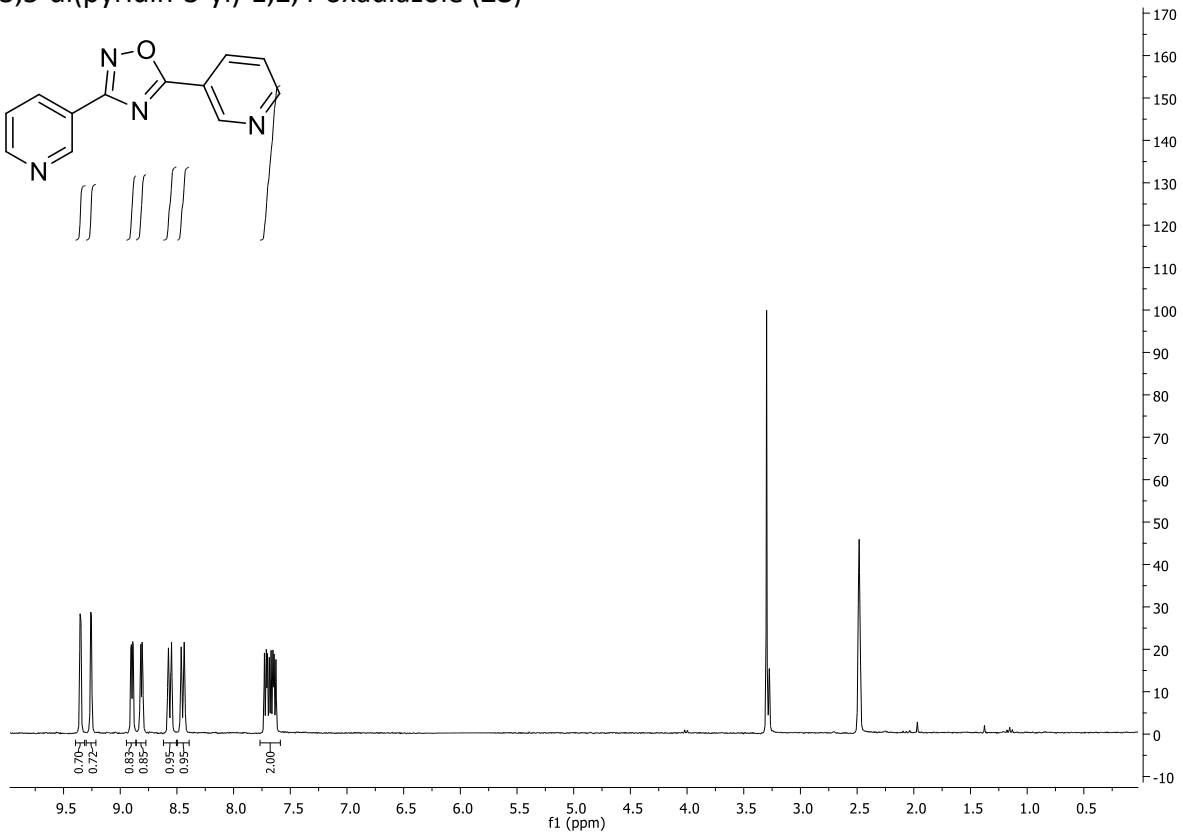

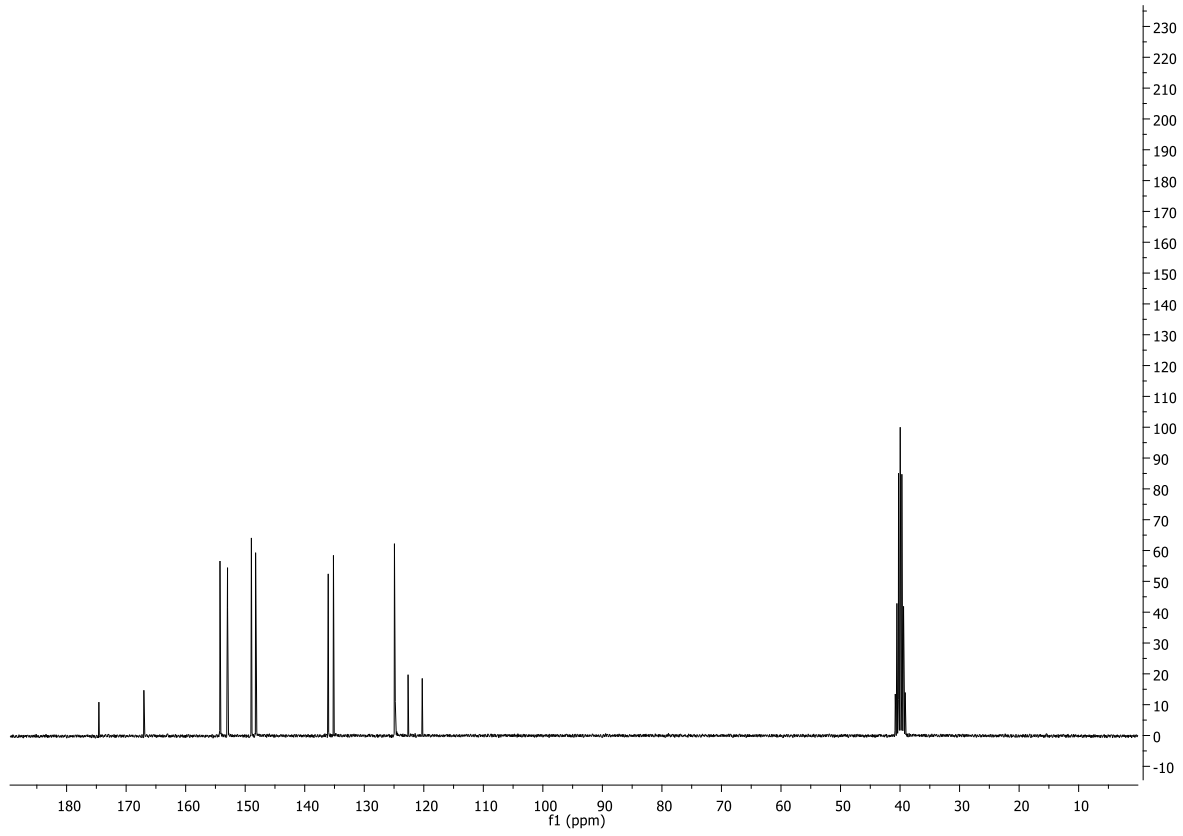

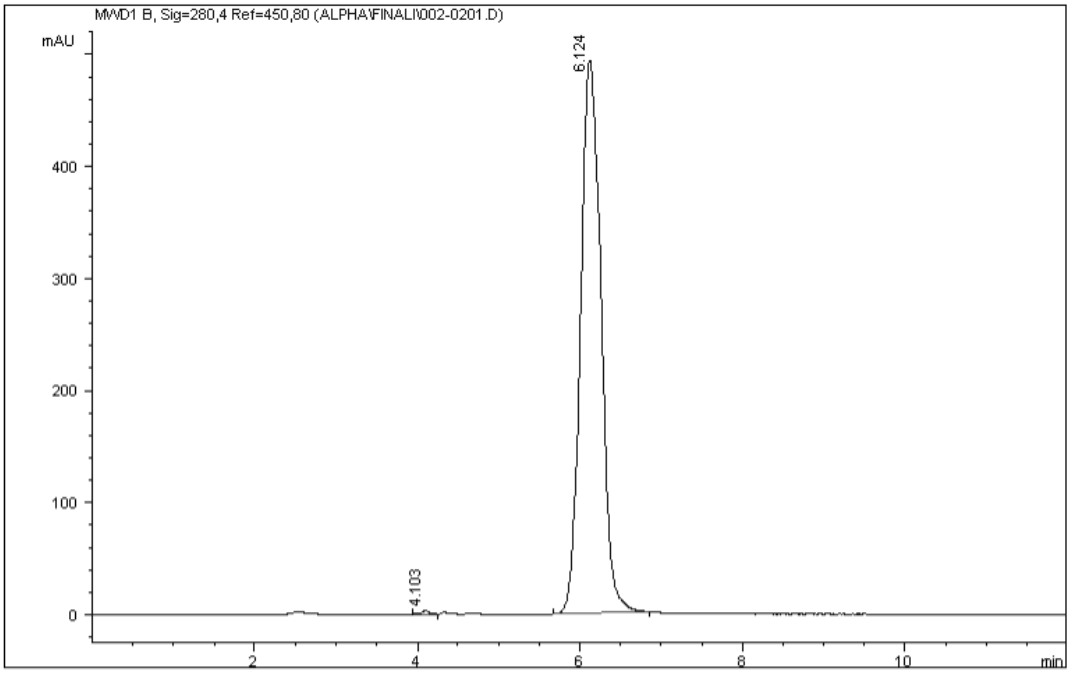

Signal 1: MWD1 B, Sig=280,4 Ref=450,80

Peak #	Area %	Area	RT [min]
1	0.357	30.825	4.103
2	99.643	8.610e3	6.124

Column: Supelcosil LC-SI (250x4.6 mm 5 µm)

Flow: 0.75 mL/min

Inj volume: 10 µL

Mobile Phase: EtOAc

λ: 280 nm

Rt/12 min: 6.1 min

Purity: 99.64%

3-(pyridin-3-yl)-5-(pyridin-4-yl)-1,2,4-oxadiazole (**29**)

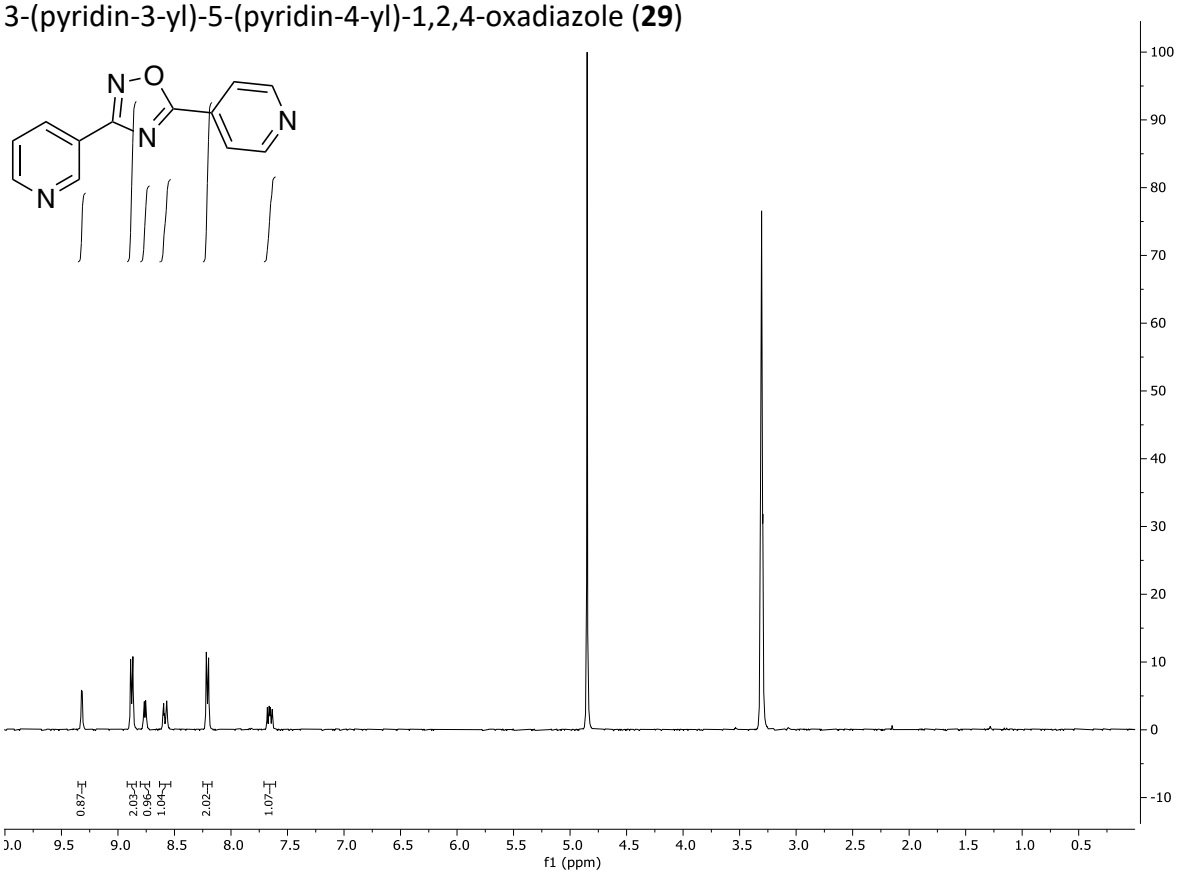

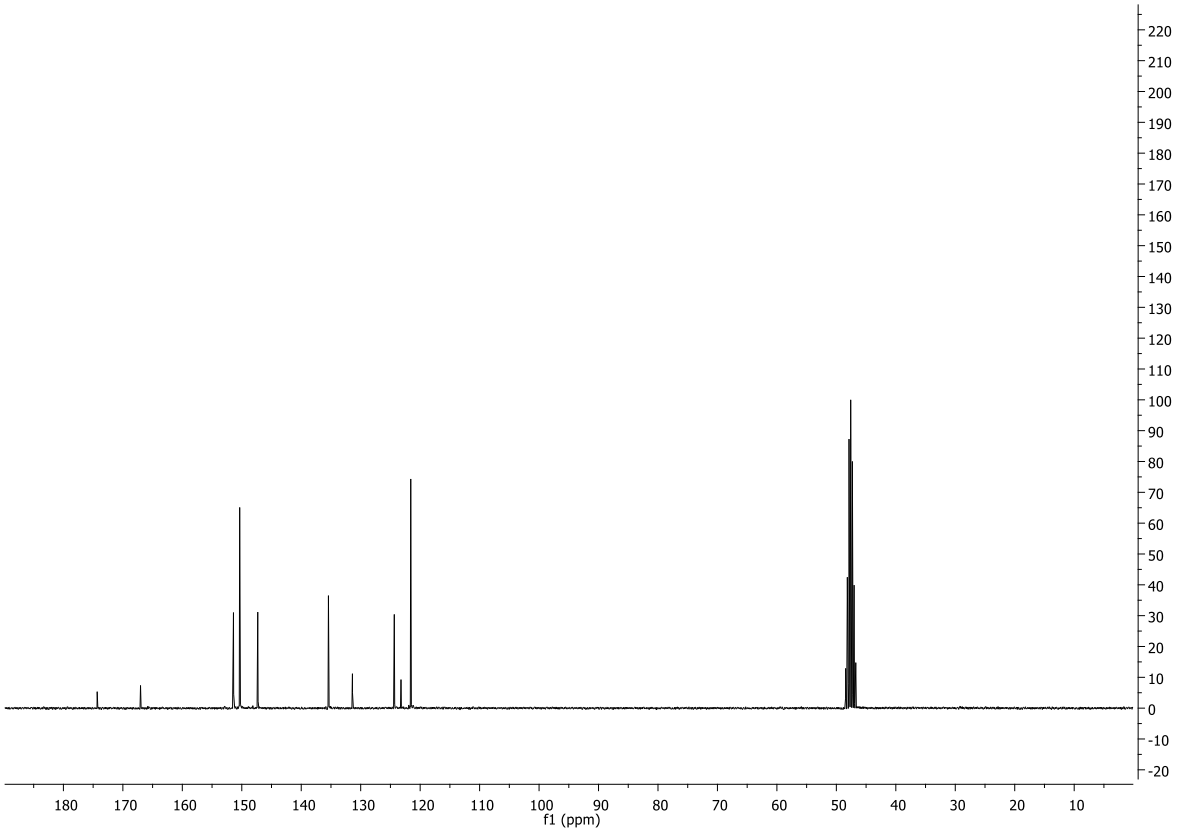

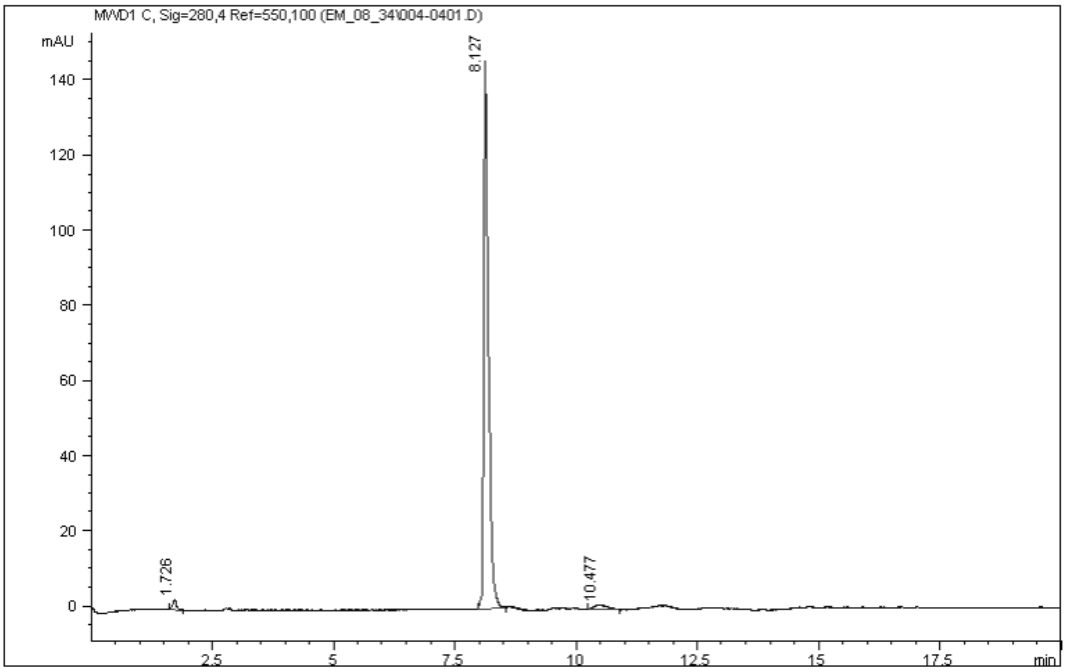

Signal 1: MWD1 C, Sig=280,4 Ref=550,100

Peak #	Area %	Area	RT [min]
1	1.442	15.055	1.726
2	96.457	1.007e3	8.127
3	2.100	21.926	10.477

Column: Hypersil BDS C18 (250x4.6 mm 5 µm)

Flow: 1.5 mL/min

Inj volume: 10 µL

Mobile Phase: H_2O/MeOH 70/30-95/5

λ: 280 nm

Rt/20 min: 8.1 min

Purity: 96.46%

5-(2-nitrophenyl)-3-(pyridin-3-yl)-1,2,4-oxadiazole (**30**)

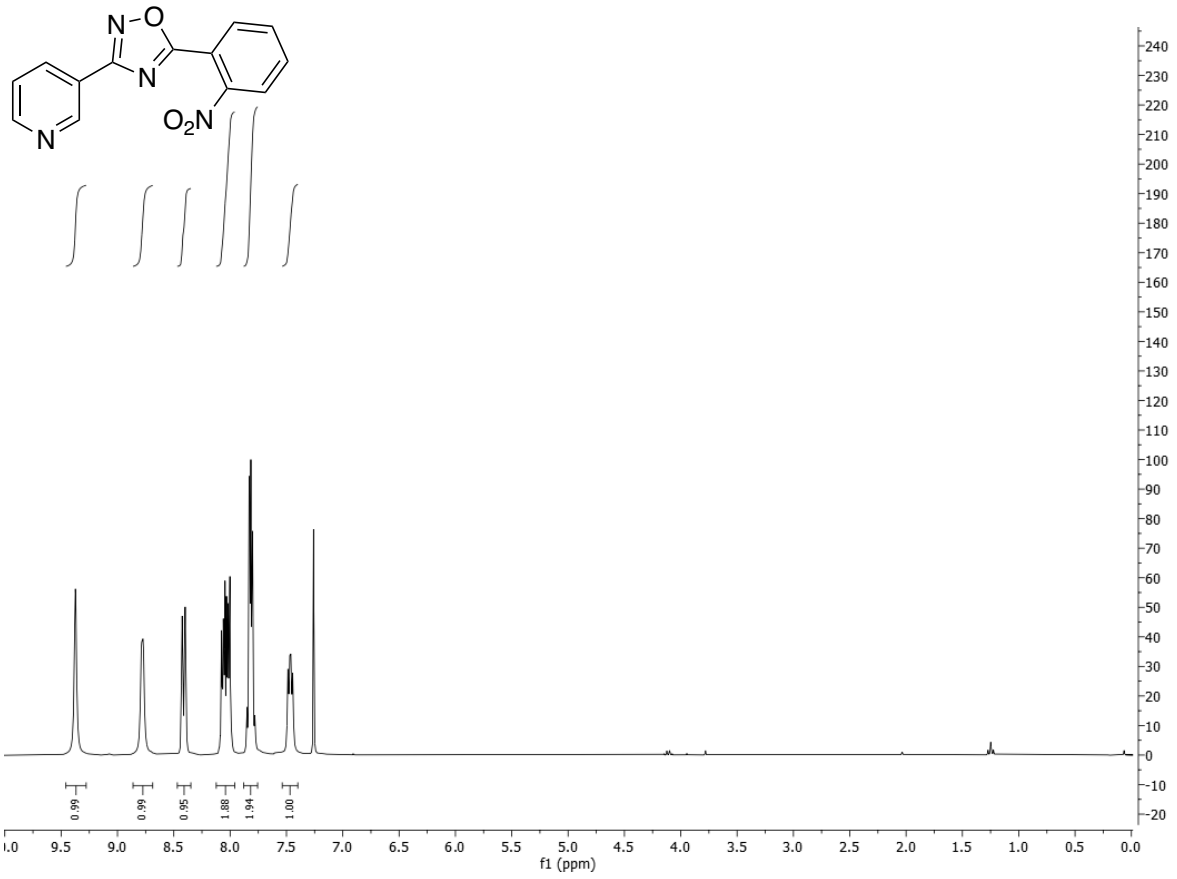

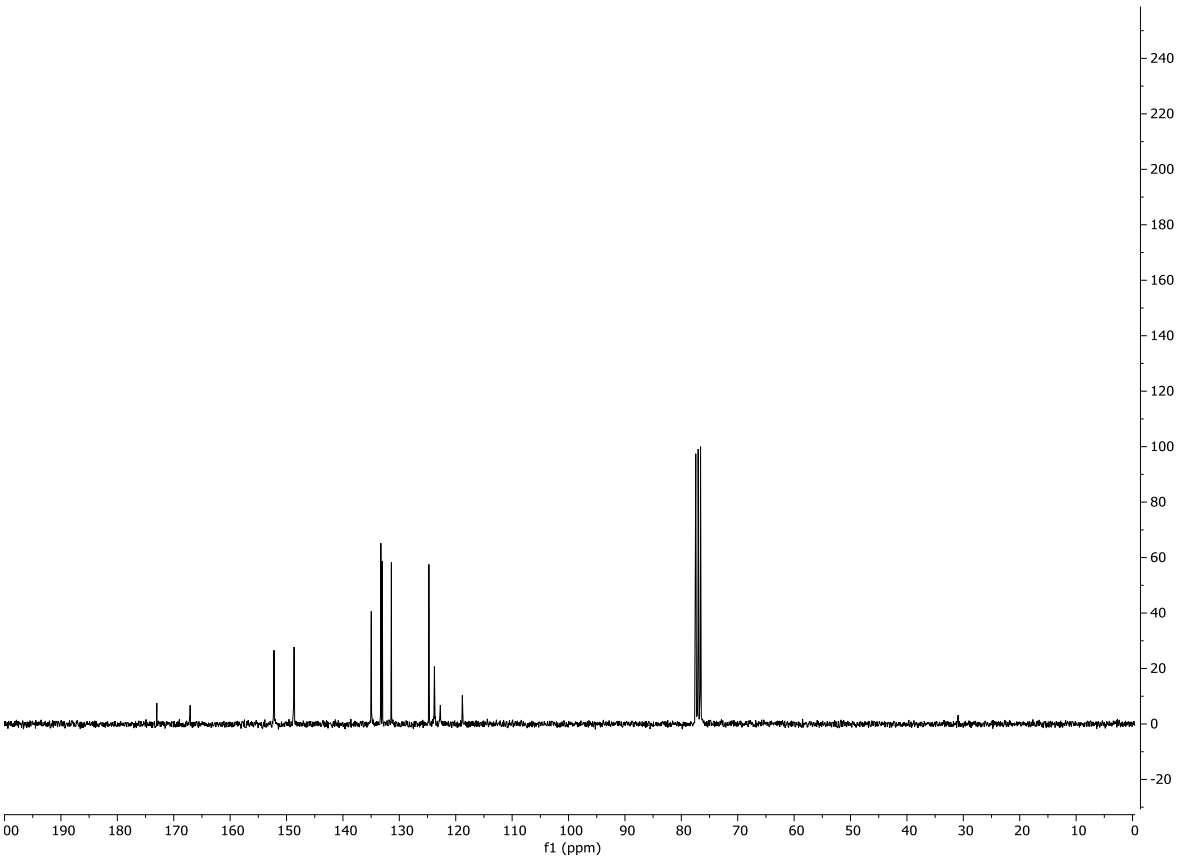

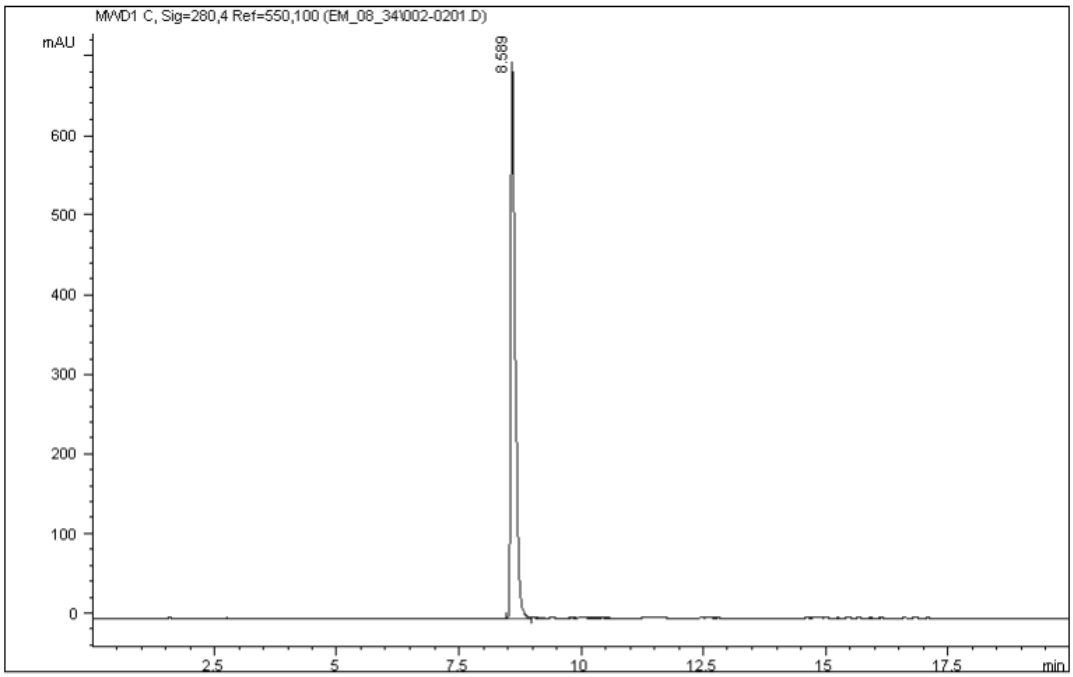

Signal 1: MWD1 C, Sig=280,4 Ref=550,100

Peak #	Area %	Area	RT [min]
1	100.000	4.535e3	8.589

Column: Hypersil BDS C18 (250x4.6 mm 5 µm)

Flow: 1.5 mL/min

Inj volume: 10 µL

Mobile Phase: H_2O/MeOH 70/30-95/5

λ: 280 nm

Rt/20 min: 8.6 min

Purity: 100%

5-(3-nitrophenyl)-3-(pyridin-3-yl)-1,2,4-oxadiazole (**31**)

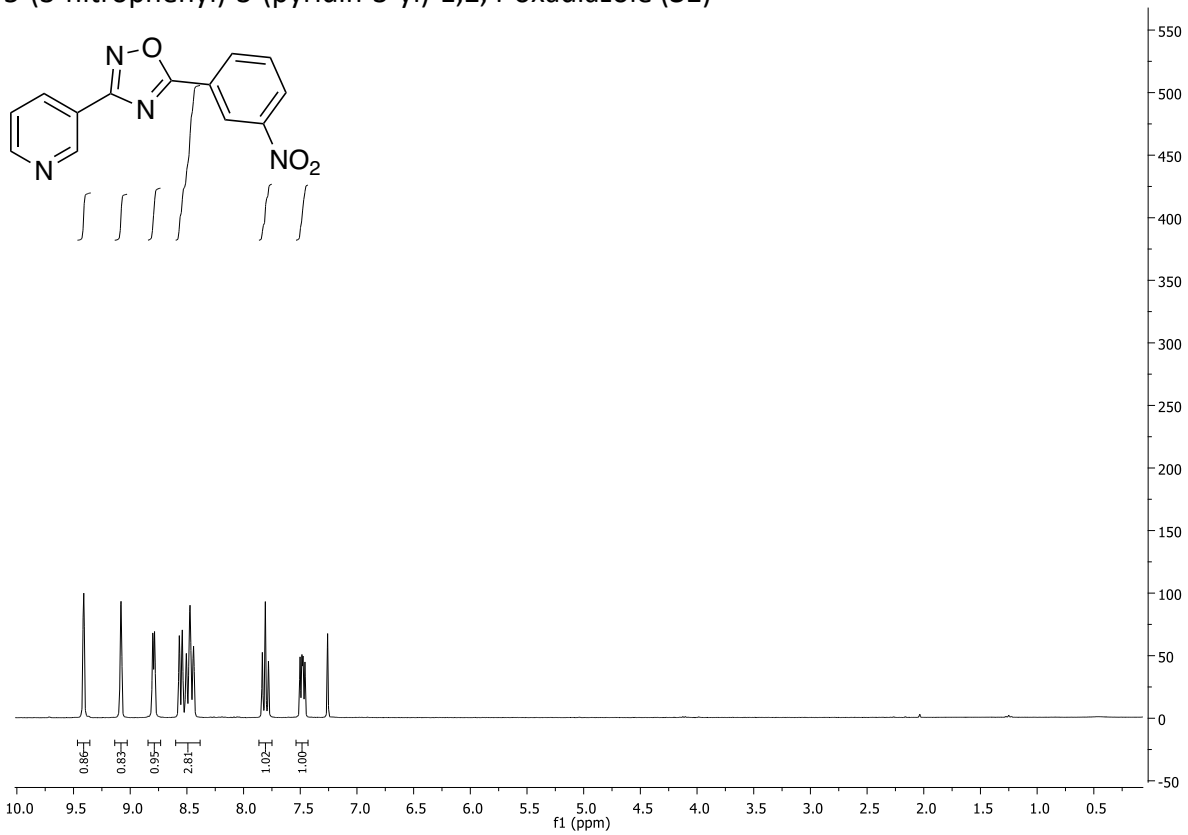

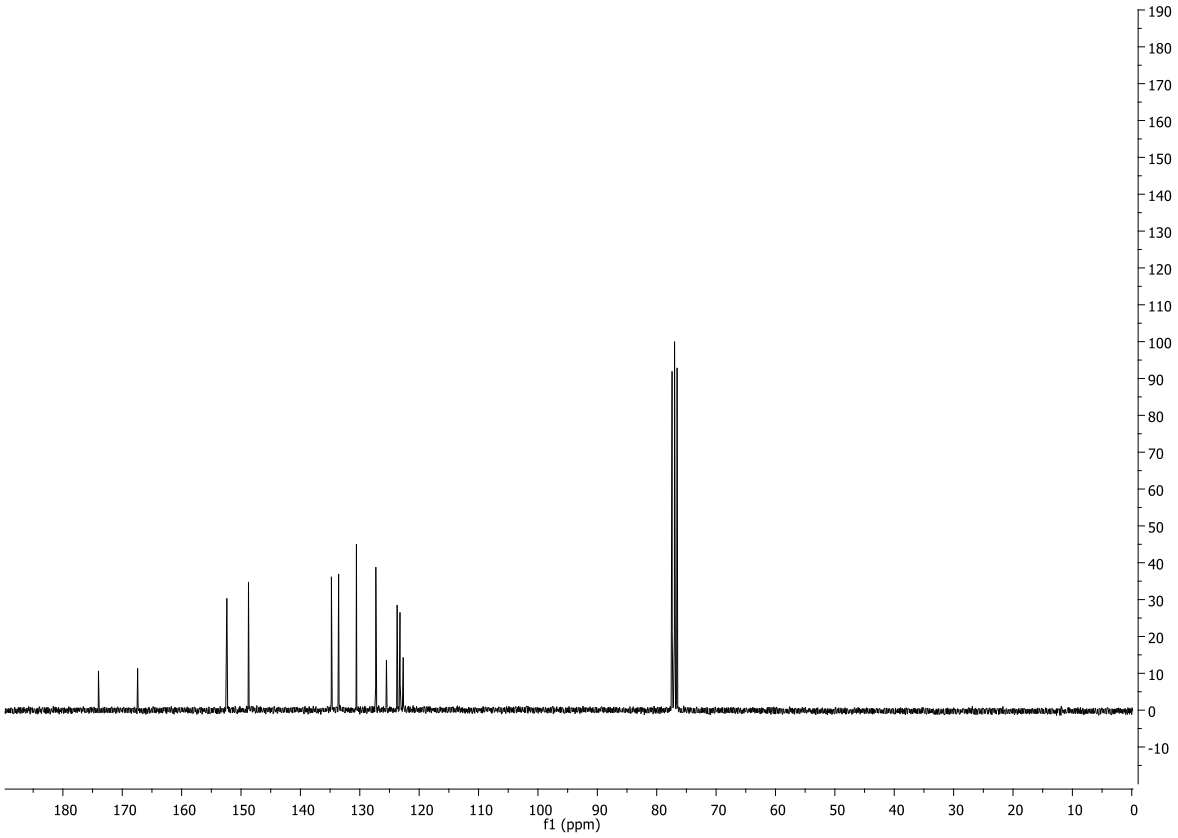

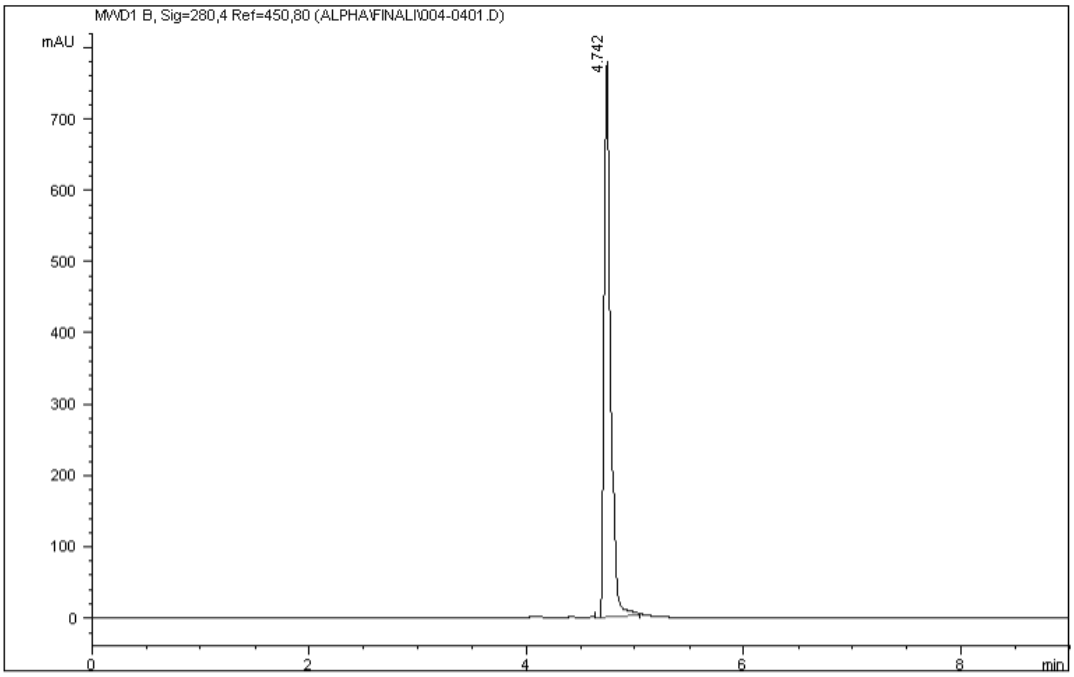

Signal 1: MWD1 B, Sig=280,4 Ref=450,80

Peak #	Area %	Area	RT [min]
1	100.000	3.234e3	4.742

Column: Supelcosil LC-SI (250x4.6 mm 5 µm)

Flow: 0.75 mL/min

Inj volume: 10 µL

Mobile Phase: EtOAc/MeOH 97.5/2.5

λ: 280 nm

Rt/12 min: 4.7 min

Purity: 100%

5-(4-nitrophenyl)-3-(pyridin-3-yl)-1,2,4-oxadiazole (**32**)

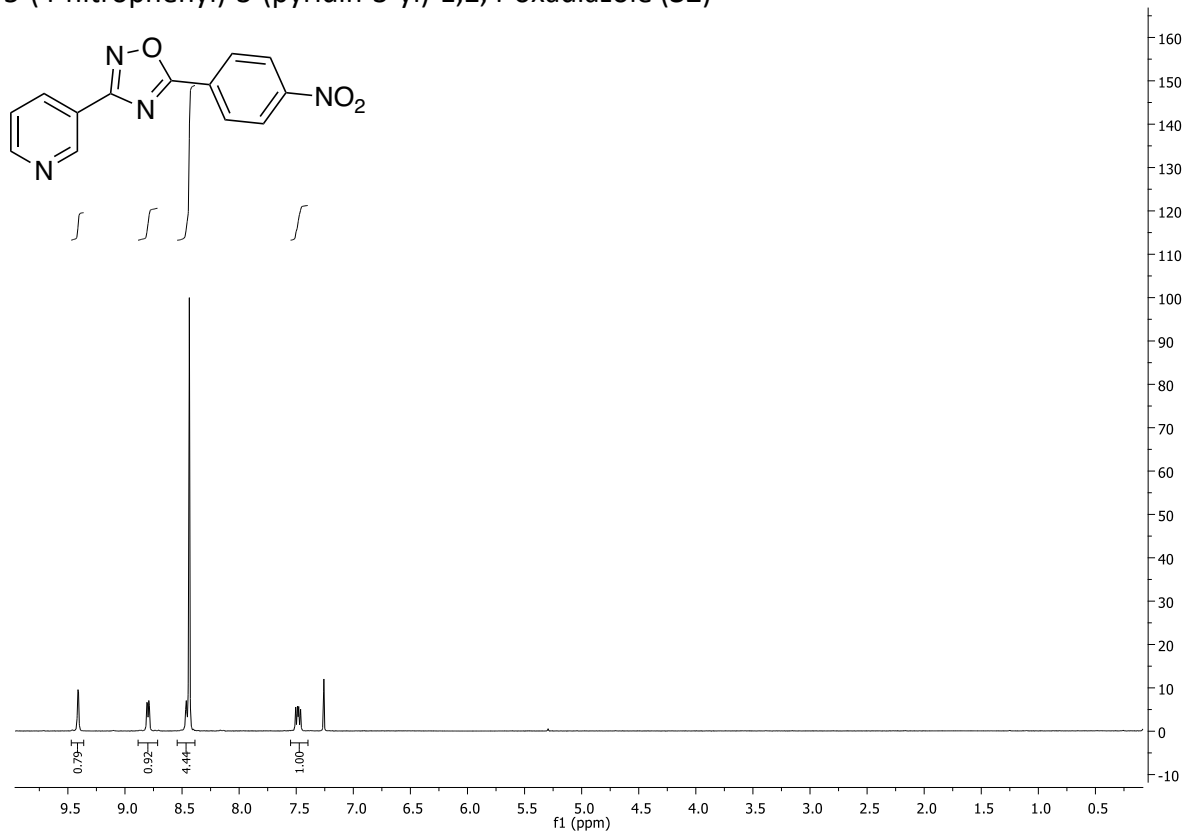

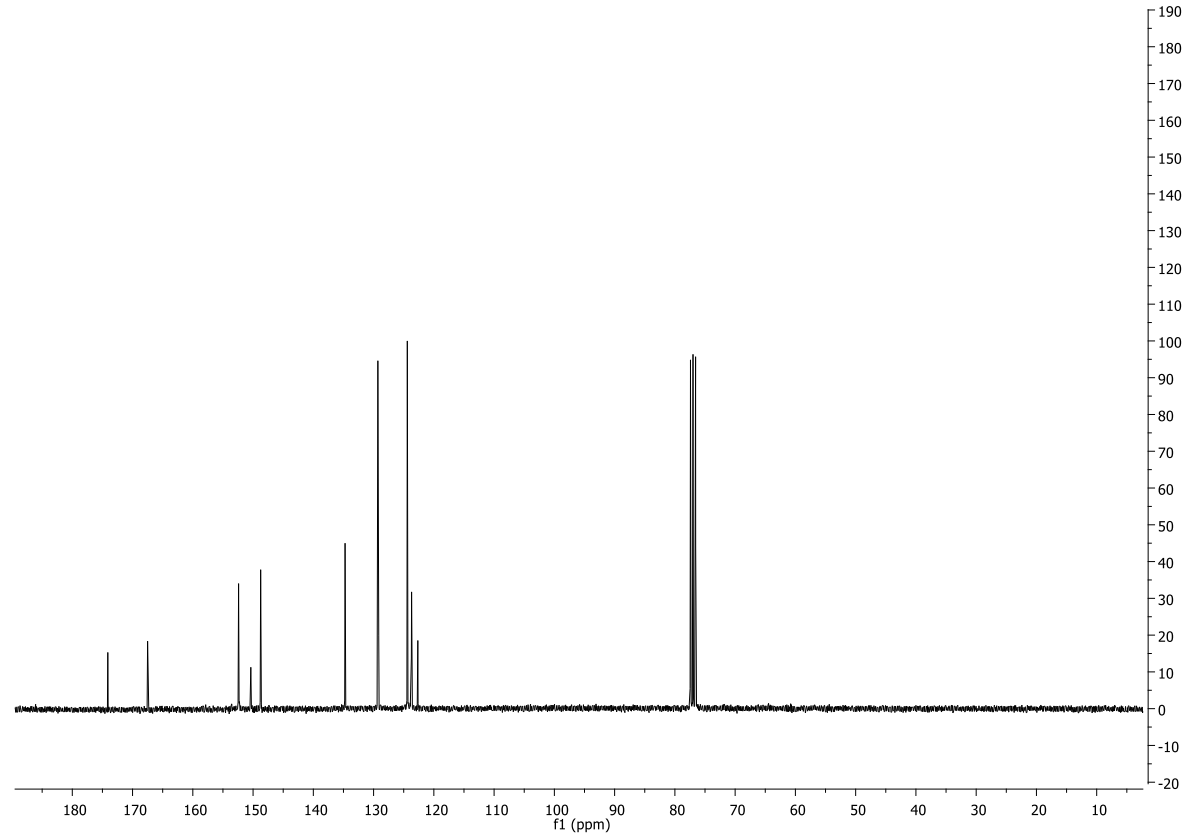

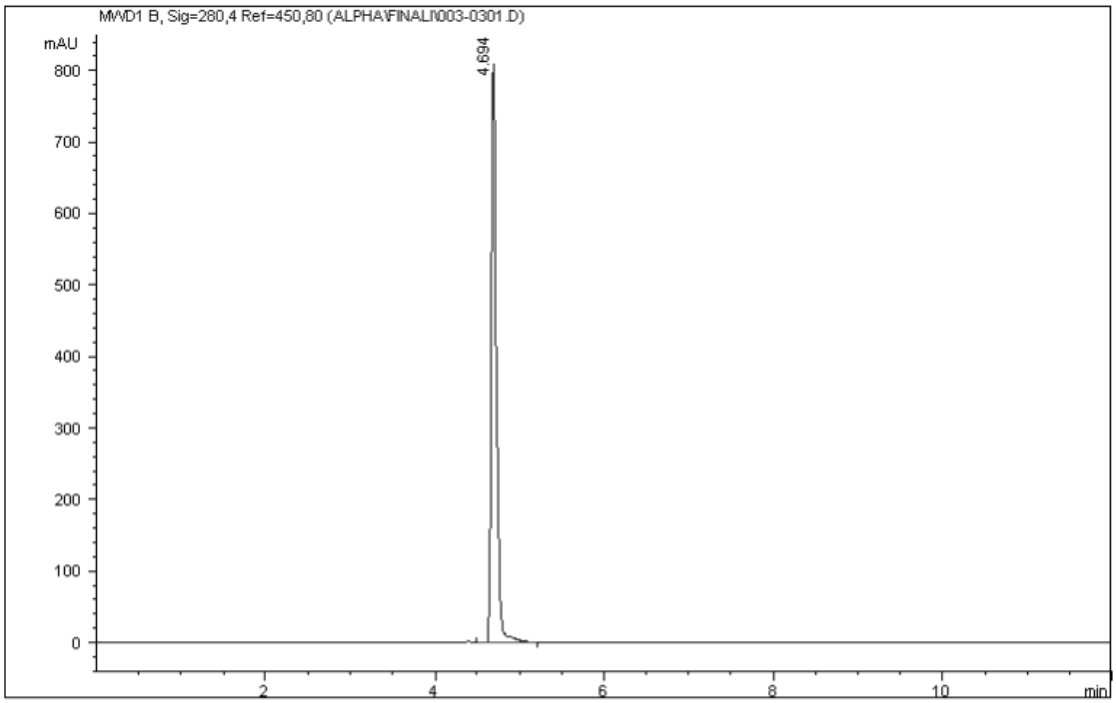

Signal 1: MWD1 B, Sig=280,4 Ref=450,80

Peak #	Area %	Area	RT [min]
1	100.000	3.458e3	4.694

Column: Supelcosil LC-SI (250x4.6 mm 5 µm)

Flow: 0.75 mL/min

Inj volume: 10 µL

Mobile Phase: EtOAc/MeOH 97.5/2.5

λ: 280 nm

Rt/12 min: 4.7 min

Purity: 100%

5-(3-fluorophenyl)-3-(pyridin-3-yl)-1,2,4-oxadiazole (**33**)

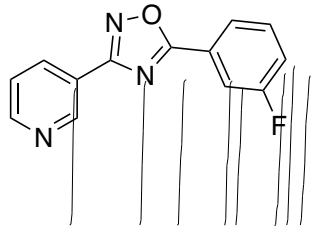

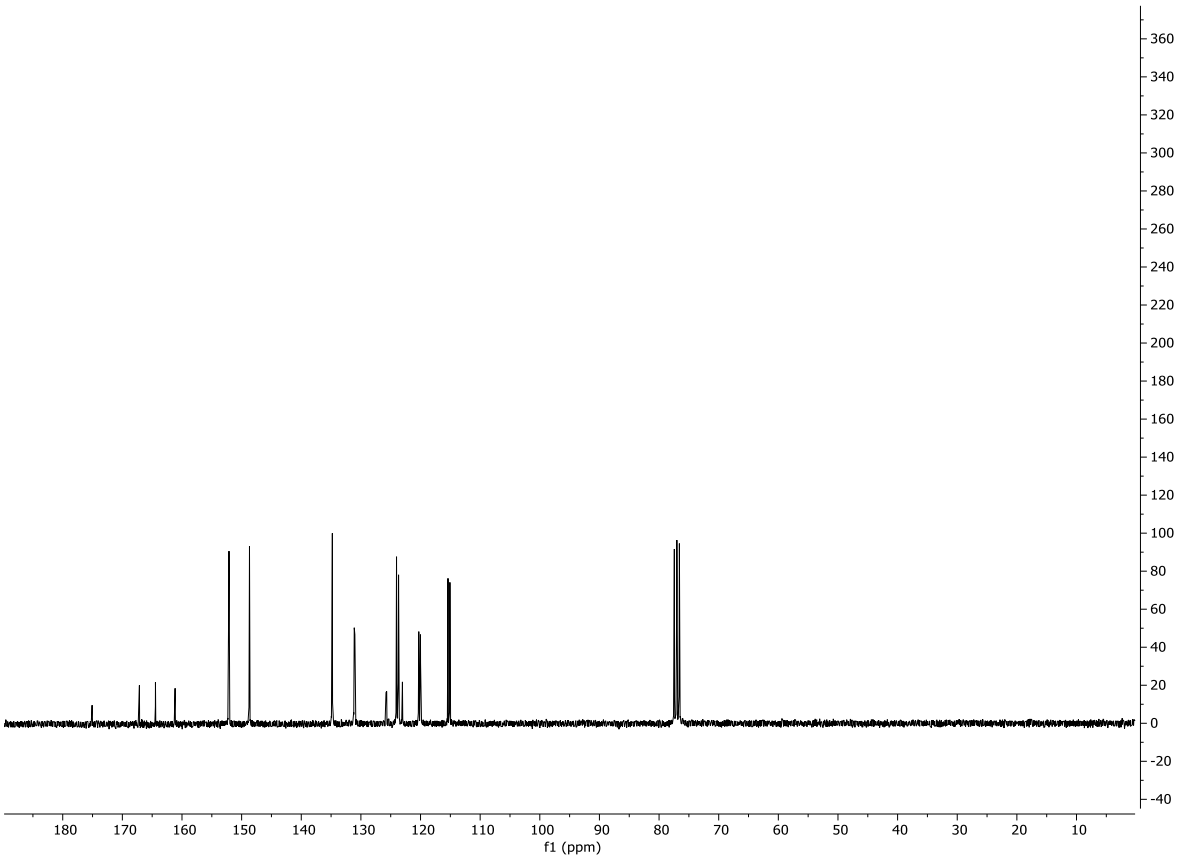

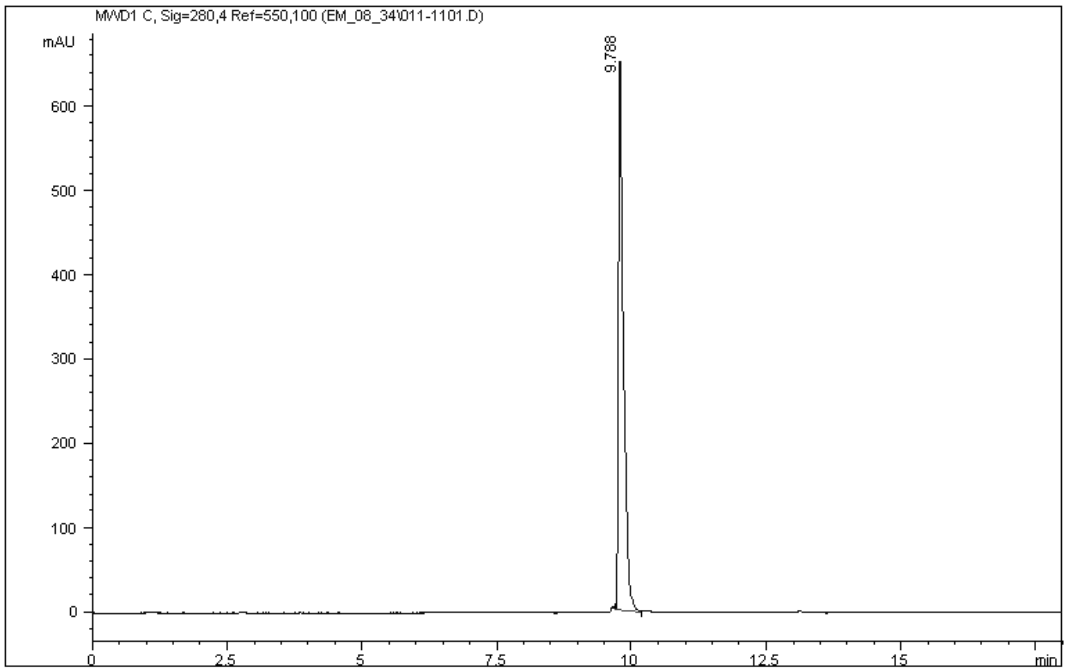

Signal 1: MWD1 C, Sig=280,4 Ref=550,100

Peak #	Area %	Area	RT [min]
1	100.000	4.337e3	9.788

Column: Hypersil BDS C18 (250x4.6 mm 5 µm)

Flow: 1.5 mL/min

Inj volume: 10 µL

Mobile Phase: H_2O/MeOH 70/30-95/5

λ: 280 nm

Rt/20 min: 9.8 min

Purity: 100%

5-(4-fluorophenyl)-3-(pyridin-3-yl)-1,2,4-oxadiazole (**34**)

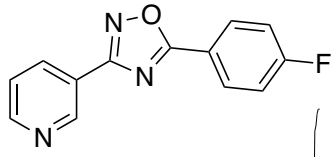

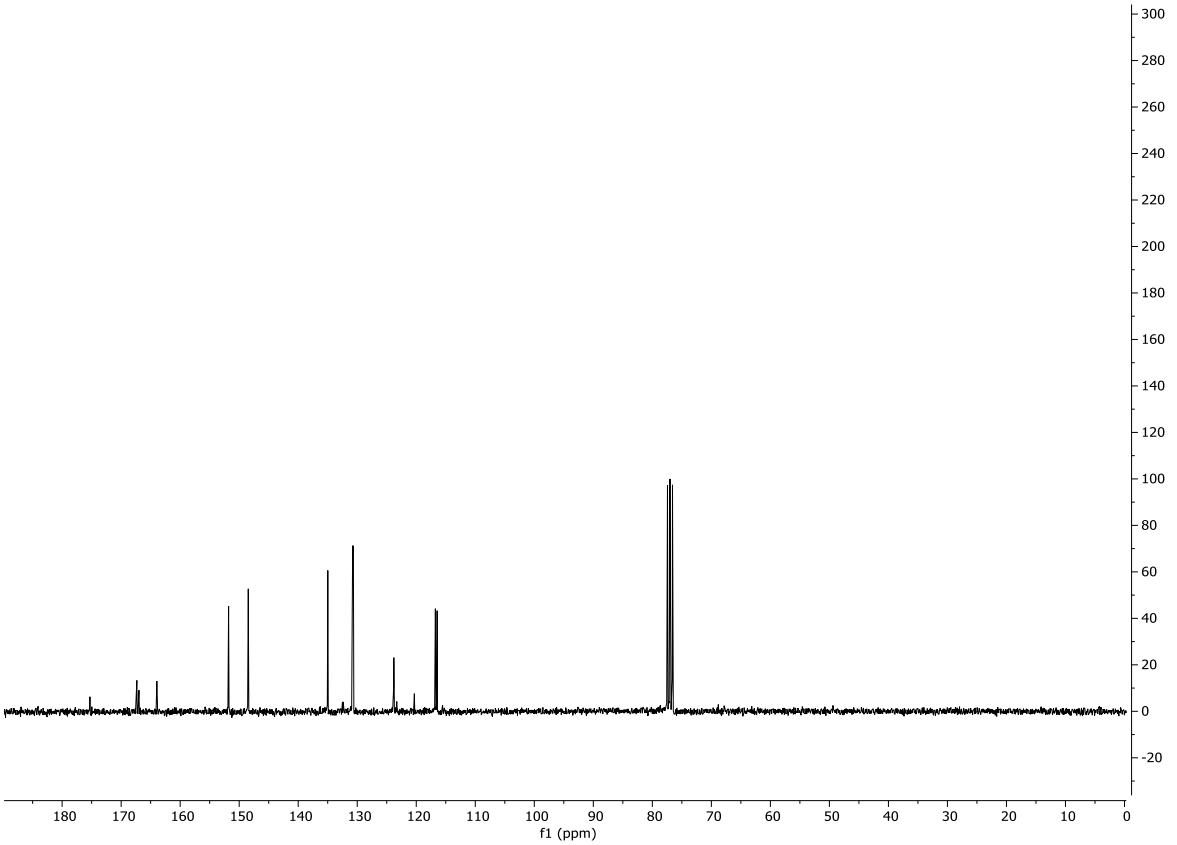

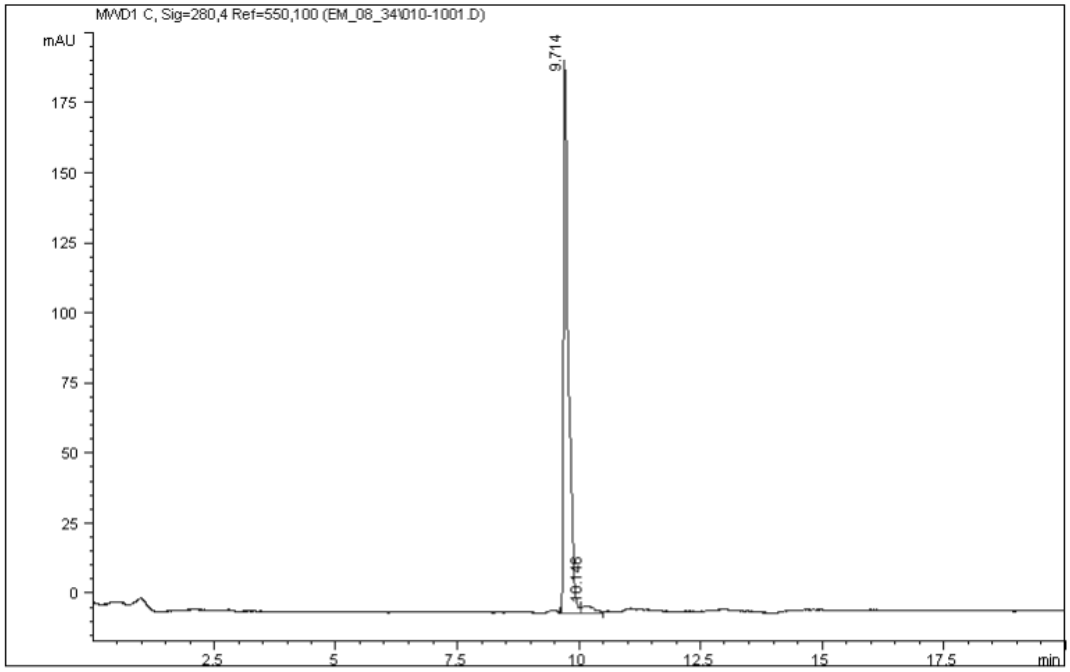

Signal 1: MWD1 C, Sig=280,4 Ref=550,100

Peak #	Area %	Area	RT [min]
1	96.968	1.283e3	9.714
2	3.032	40.132	10.146

Column: Hypersil BDS C18 (250x4.6 mm 5 µm)

Flow: 1.5 mL/min

Inj volume: 10 µL

Mobile Phase: H_2O/MeOH 70/30-95/5

λ: 280 nm

Rt/20 min: 9.7 min

Purity: 96.97%

5-(3,4-difluorophenyl)-3-(pyridin-3-yl)-1,2,4-oxadiazole (**35**)

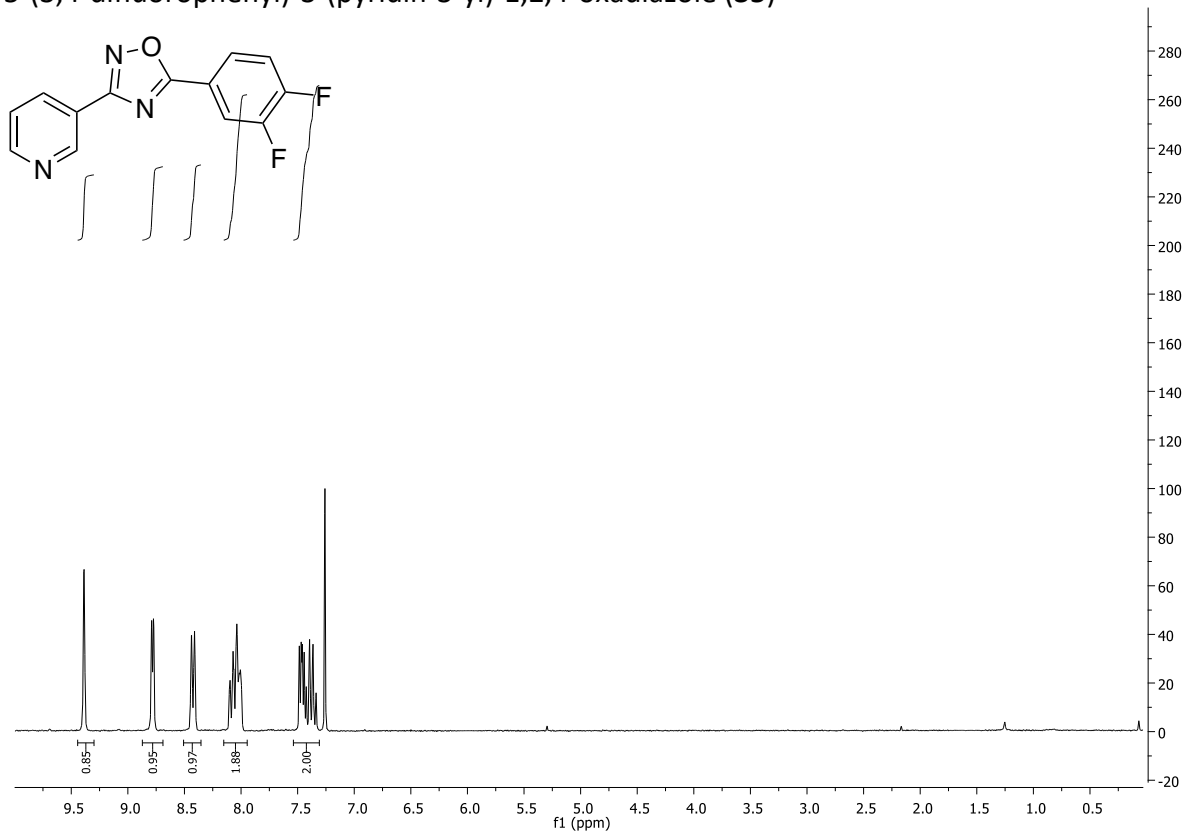

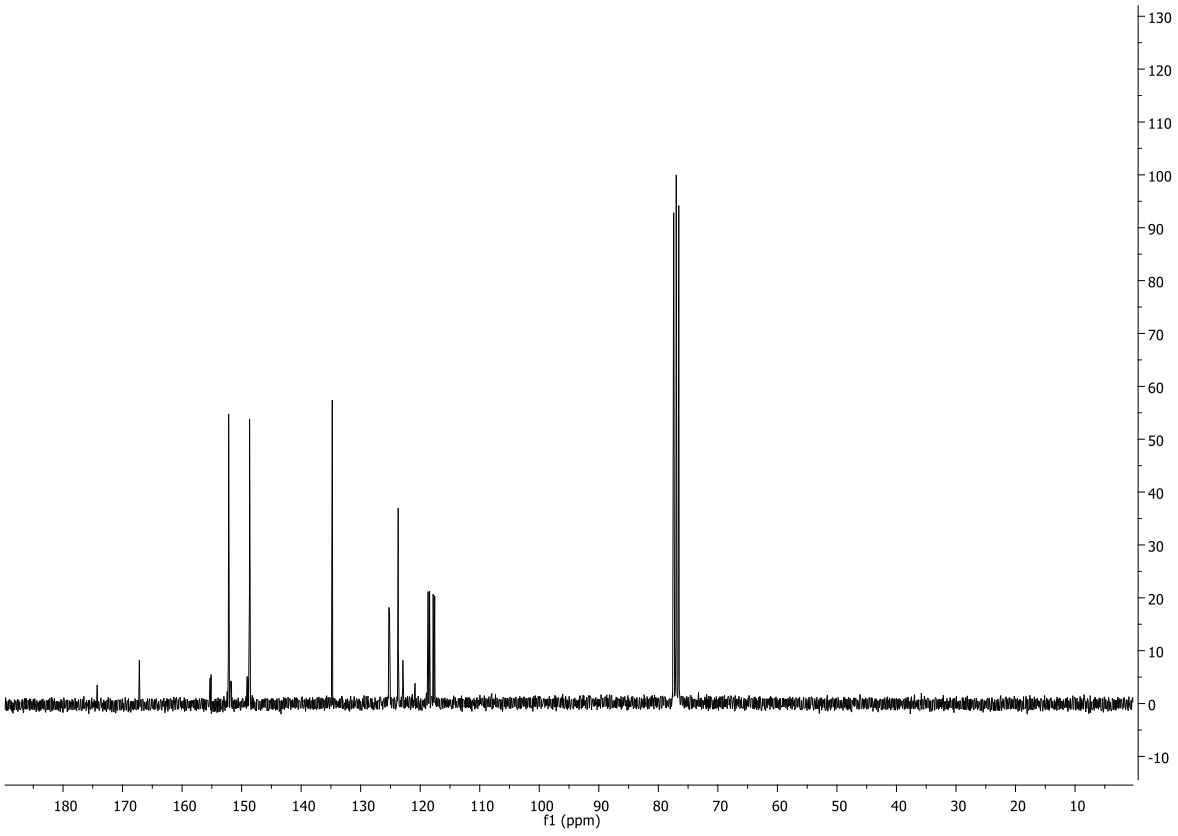

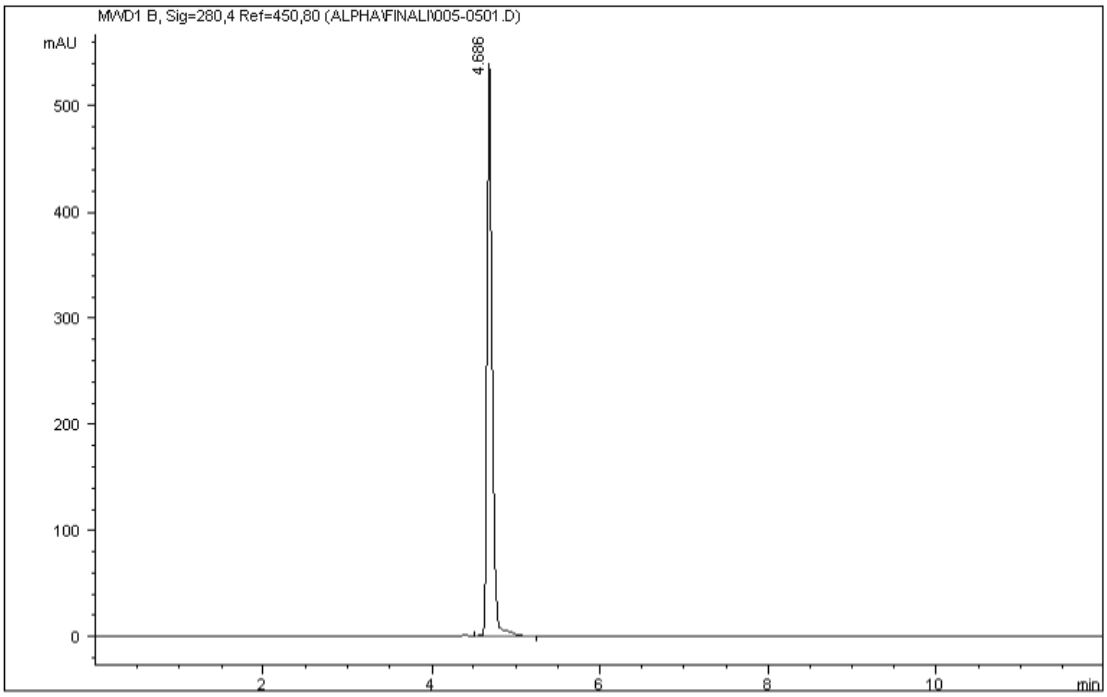

Signal 1: MWD1 B, Sig=280,4 Ref=450,80

Peak #	Area %	Area	RT [min]
1	100.000	2.371e3	4.686

Column: Supelcosil LC-SI (250x4.6 mm 5 µm)

Flow: 0.75 mL/min

Inj volume: 10 µL

Mobile Phase: EtOAc/MeOH 97.5/2.5

λ: 280 nm

Rt/12 min: 4.7 min

Purity: 100%

3-(pyridin-3-yl)-5-(2,3,4-trifluorophenyl)-1,2,4-oxadiazole (**36**)

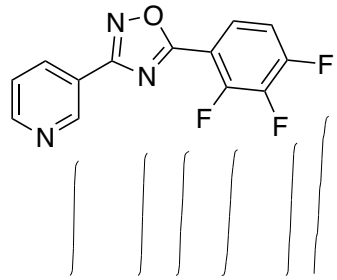

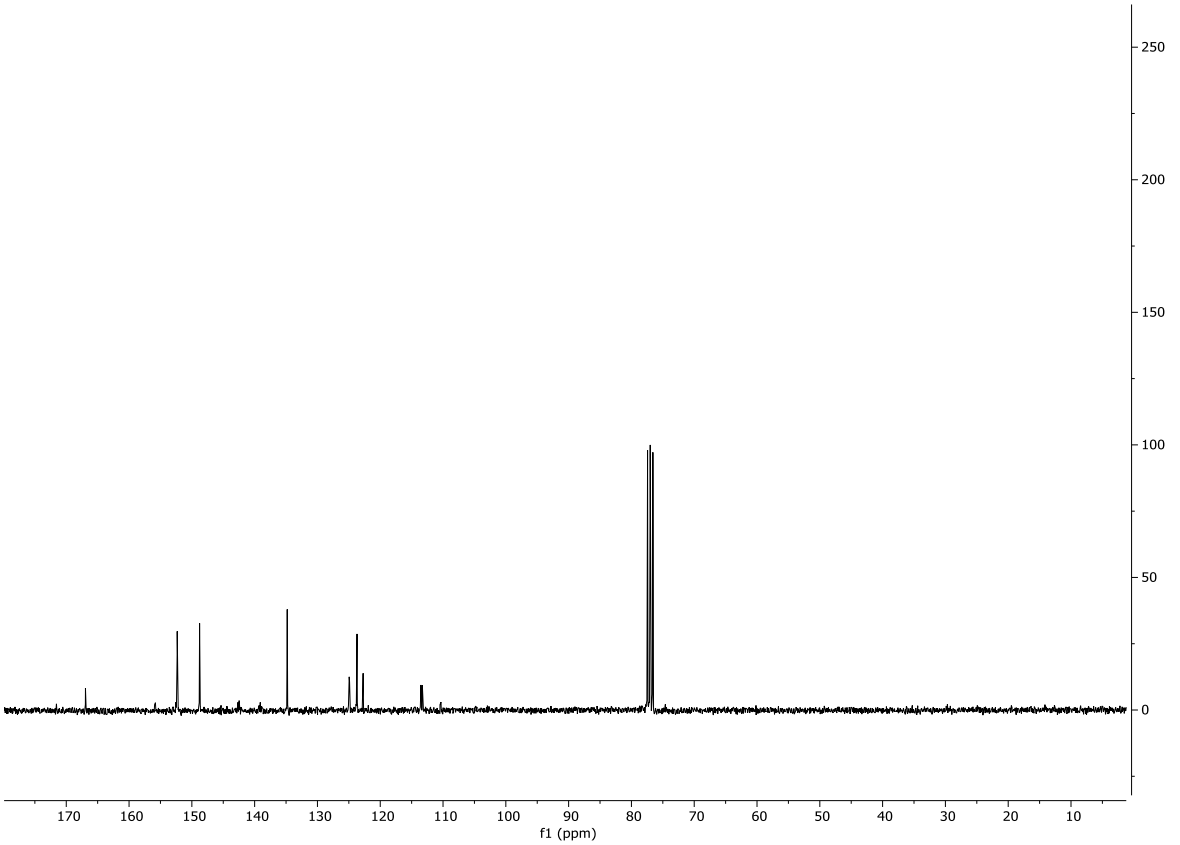

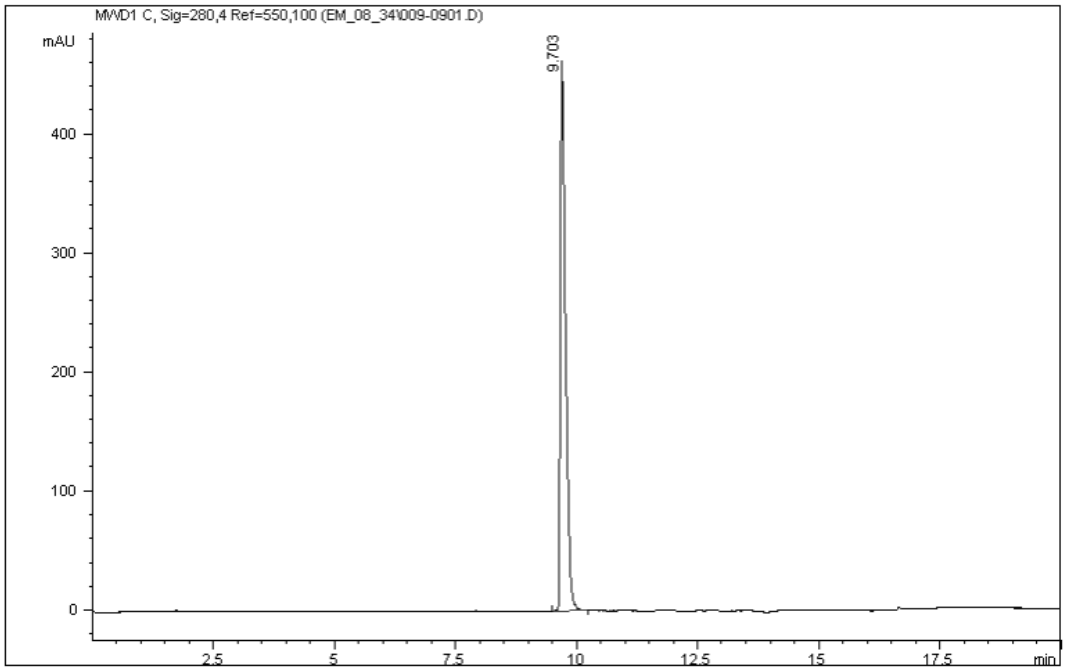

Signal 1: MWD1 C, Sig=280,4 Ref=550,100

Peak #	Area %	Area	RT [min]
1	100.000	3.129e3	9.703

Column: Hypersil BDS C18 (250x4.6 mm 5 µm)

Flow: 1.5 mL/min

Inj volume: 10 µL

Mobile Phase: H_2O/MeOH 70/30-95/5

λ: 280 nm

Rt/20 min: 9.7 min

Purity: 100%

3-(pyridin-3-yl)-5-(3,4,5-trifluorophenyl)-1,2,4-oxadiazole (**37**)

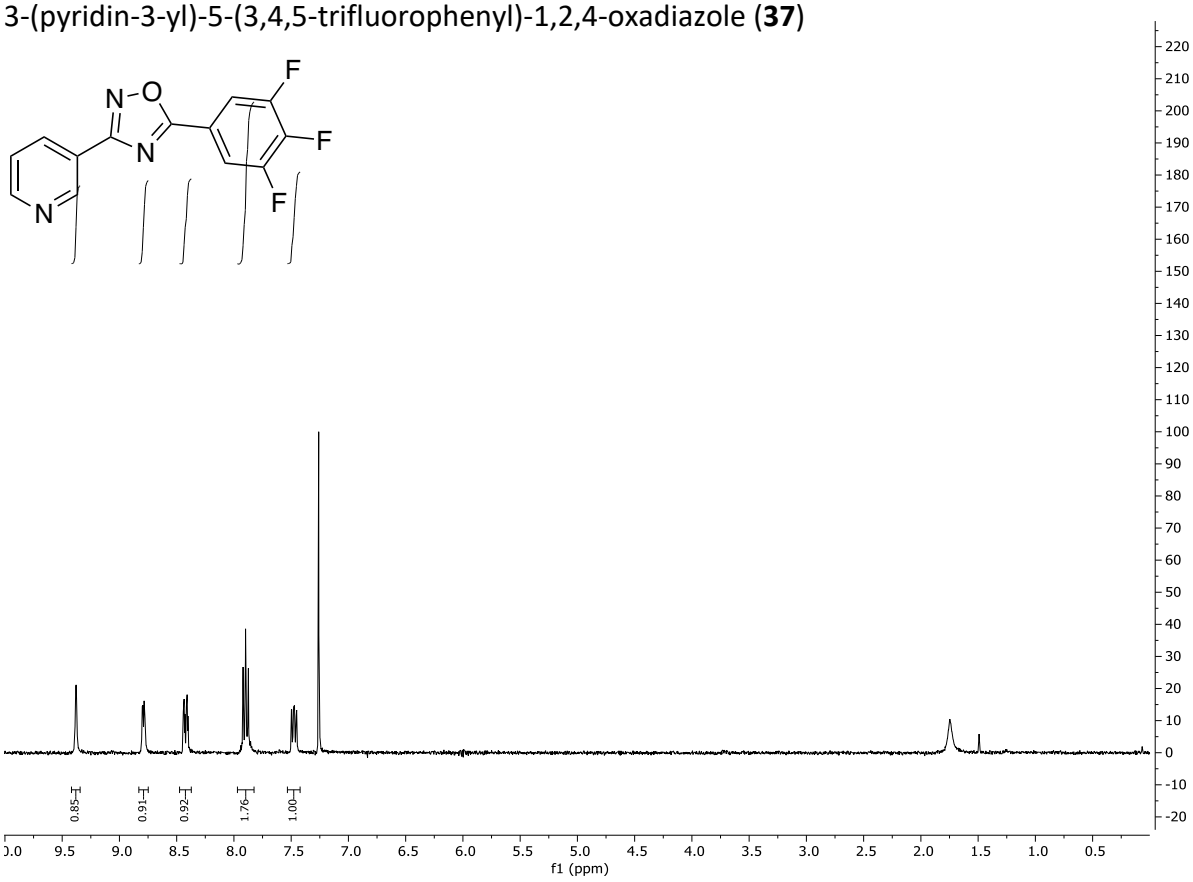

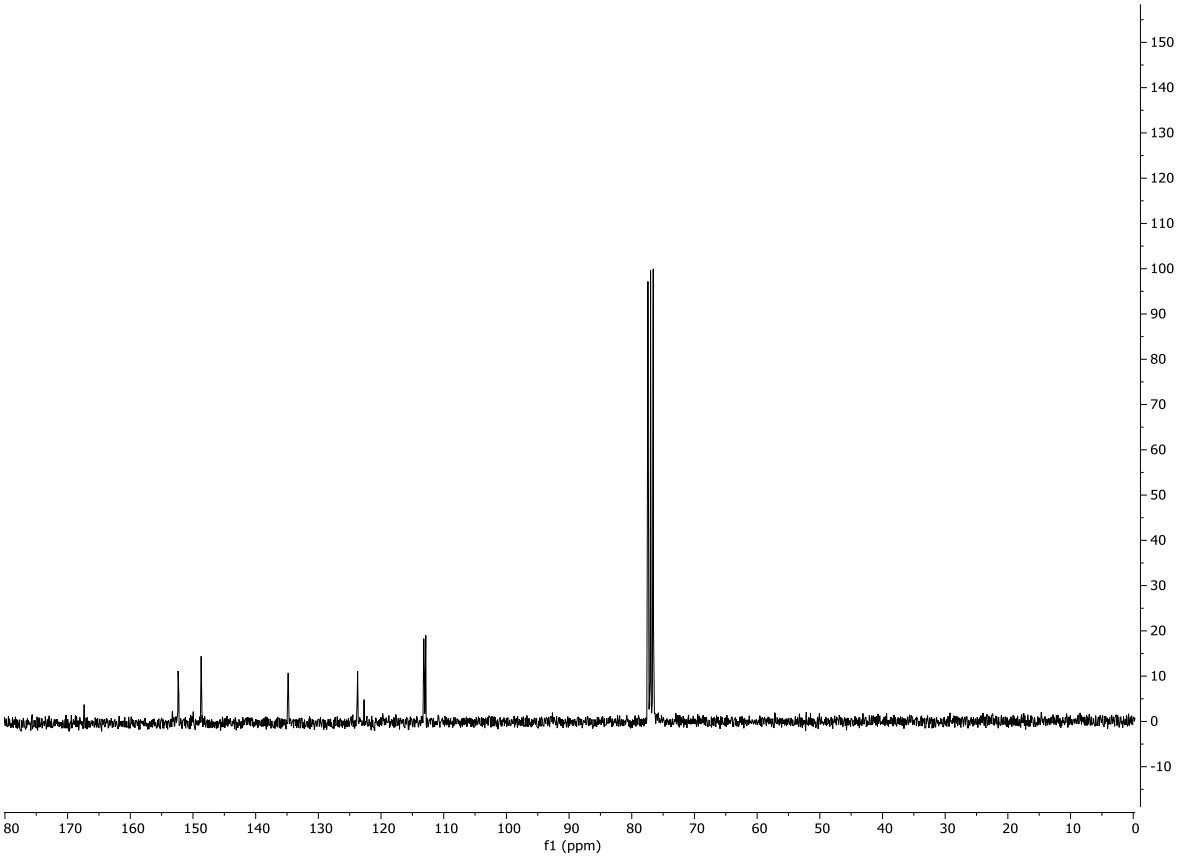

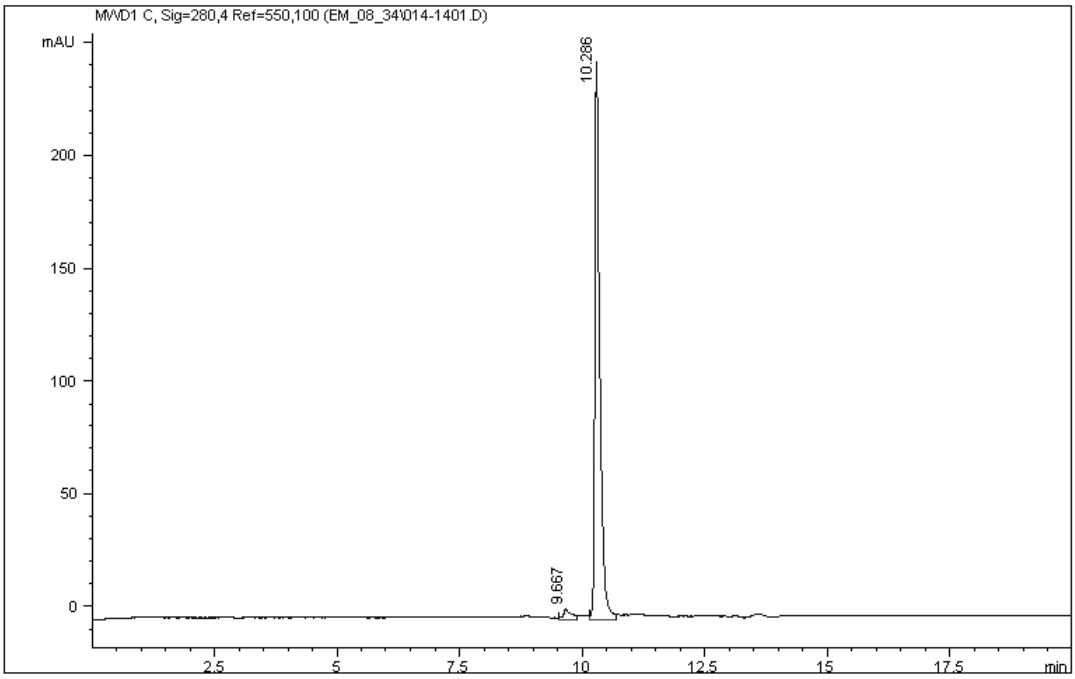

Signal 1: MWD1 C, Sig=280,4 Ref=550,100

Peak #	Area %	Area	RT [min]
1	3.273	61.093	9.667
2	96.727	1.805e3	10.286

Column: Hypersil BDS C18 (250x4.6 mm 5 µm)

Flow: 1.5 mL/min

Inj volume: 10 µL

Mobile Phase: H_2O/MeOH 70/30-95/5

λ: 280 nm

Rt/20 min: 10.3 min

Purity: 96.73%

3-(pyridin-3-yl)-5-(2,3,4,5-tetrafluorophenyl)-1,2,4-oxadiazole (**38**)

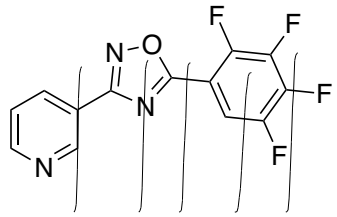

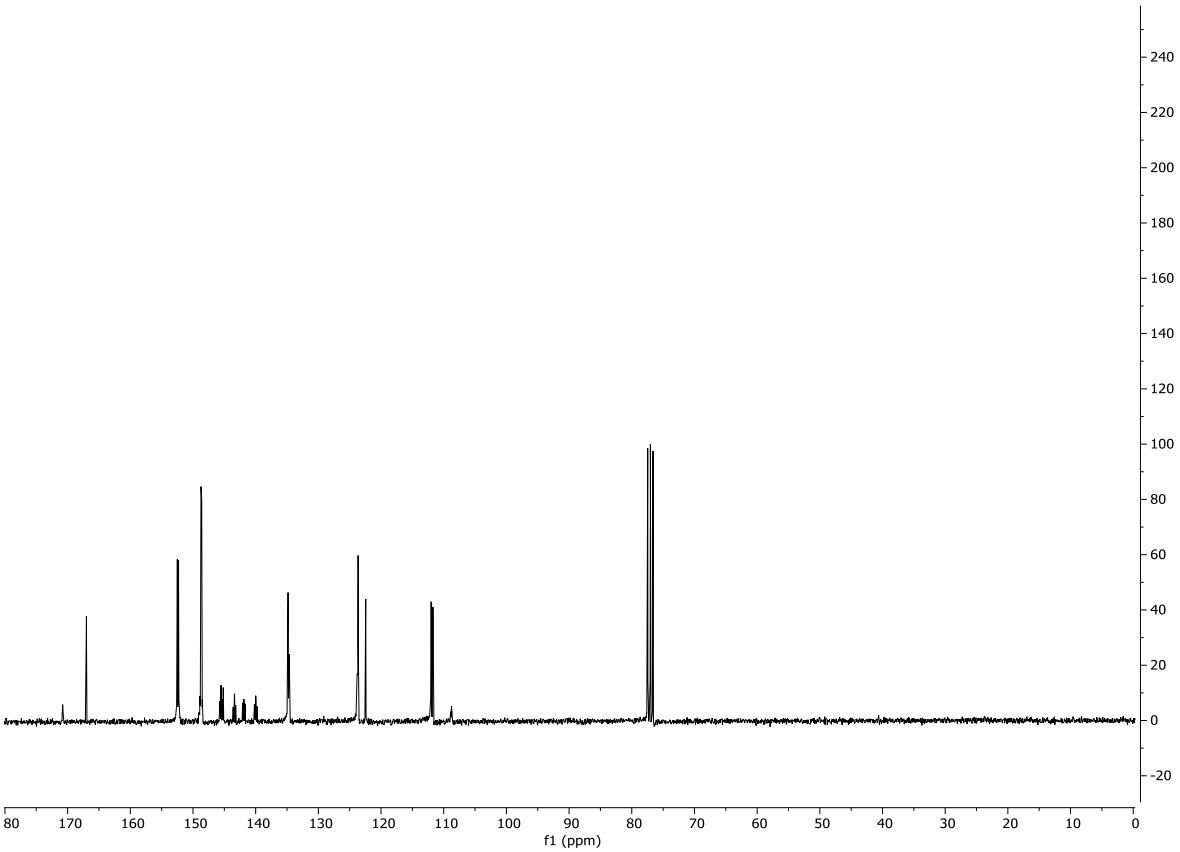

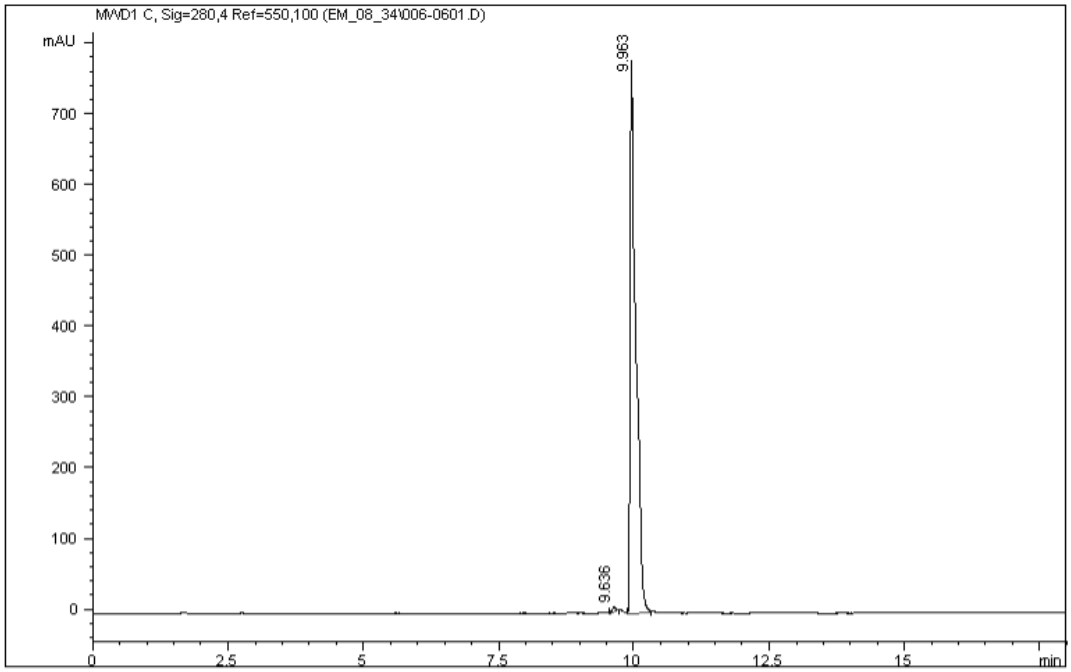

Signal 1: MWD1 C, Sig=280,4 Ref=550,100

Peak #	Area %	Area	RT [min]
1	0.646	36.246	9.636
2	99.354	5.576e3	9.963

Column: Hypersil BDS C18 (250x4.6 mm 5 µm)

Flow: 1.5 mL/min

Inj volume: 10 µL

Mobile Phase: H_2O/MeOH 70/30-95/5

λ: 280 nm

Rt/20 min: 9.7 min

Purity: 98.17%

5-(3-fluoro-4-nitrophenyl)-3-(pyridin-3-yl)-1,2,4-oxadiazole (**39**)

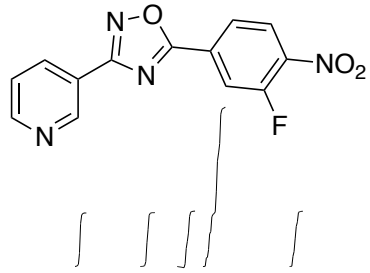

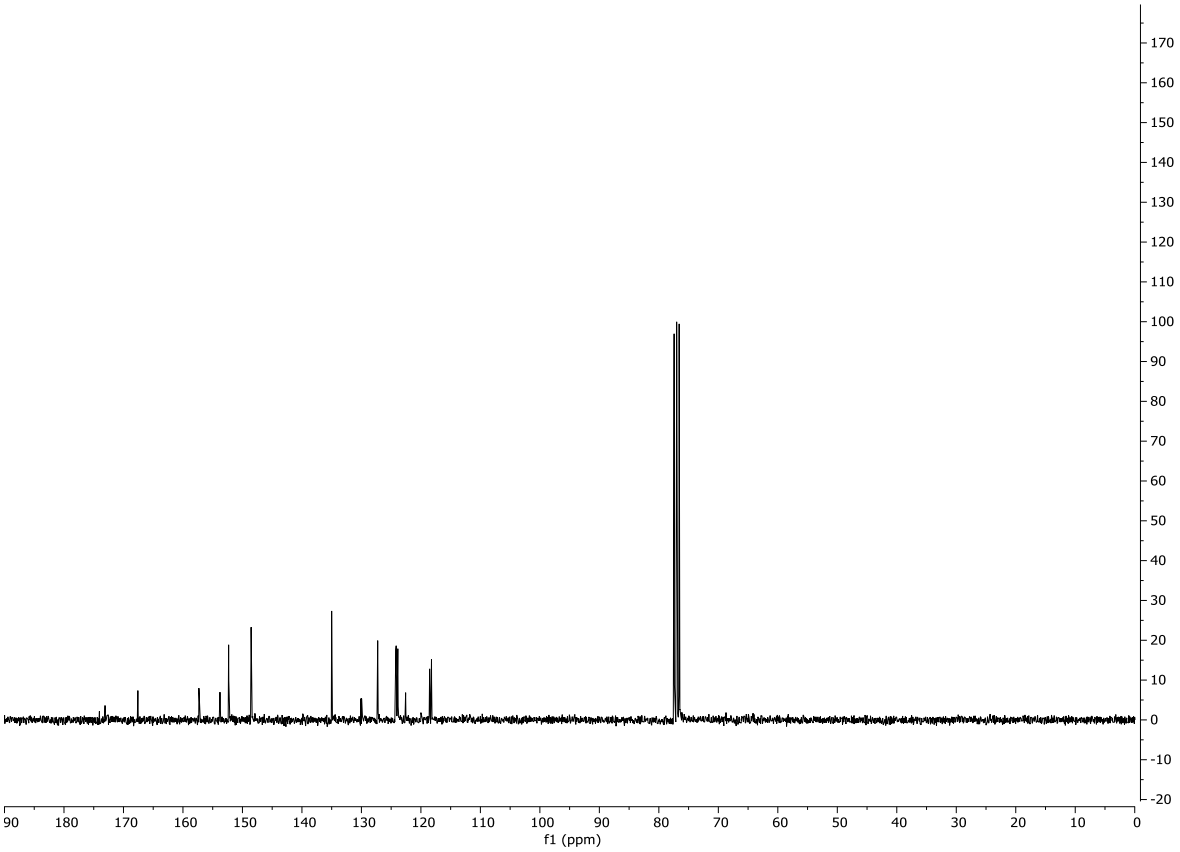

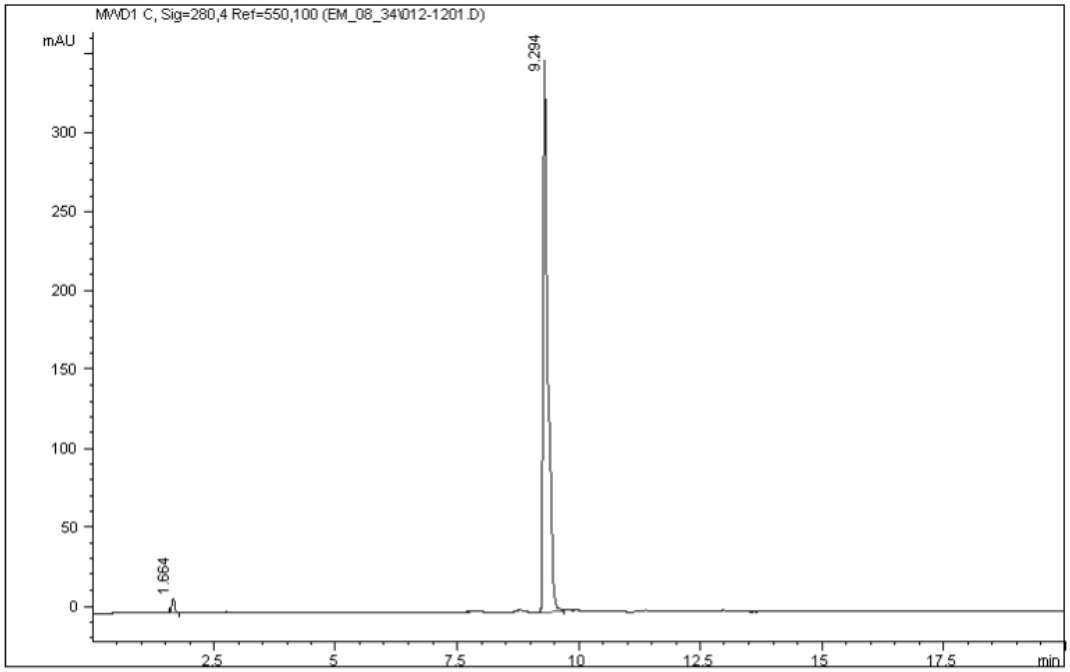

Signal 1: MWD1 C, Sig=280,4 Ref=550,100

Peak #	Area %	Area	RT [min]
1	1.647	37.386	1.664
2	98.353	2.232e3	9.294

Column: Hypersil BDS C18 (250x4.6 mm 5 µm)

Flow: 1.5 mL/min

Inj volume: 10 µL

Mobile Phase: H_2O/MeOH 70/30-95/5

λ: 280 nm

Rt/20 min: 9.3 min

Purity: 98.35%

5-(4-fluoro-3-nitrophenyl)-3-(pyridin-3-yl)-1,2,4-oxadiazole (**40**)

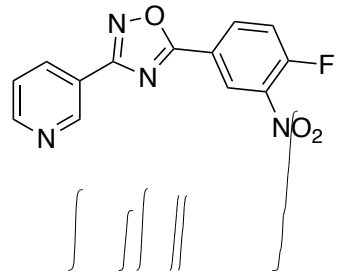

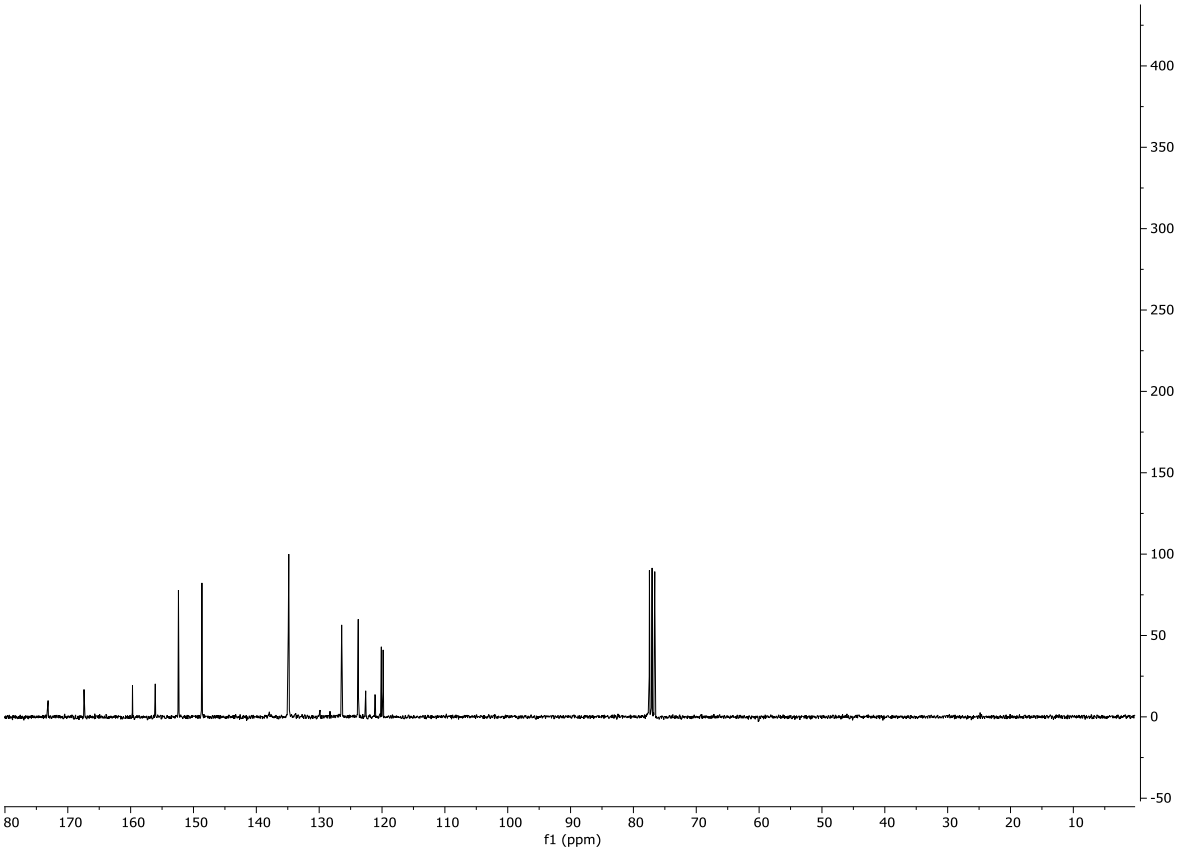

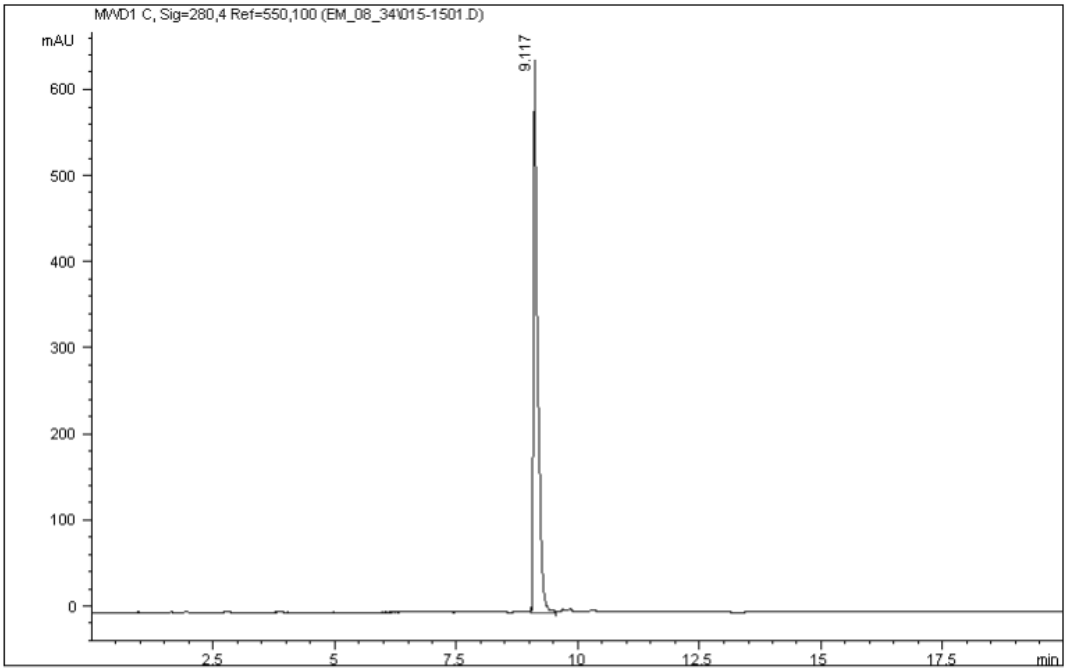

Signal 1: MWD1 C, Sig=280,4 Ref=550,100

Peak #	Area %	Area	RT [min]
1	100.000	3.937e3	9.117

Column: Hypersil BDS C18 (250x4.6 mm 5 µm)

Flow: 1.5 mL/min

Inj volume: 10 µL

Mobile Phase: H_2O/MeOH 70/30-95/5

λ: 280 nm

Rt/20 min: 9.1 min

Purity: 100%

5-(2-fluoropyridin-4-yl)-3-(pyridin-3-yl)-1,2,4-oxadiazole (**41**)

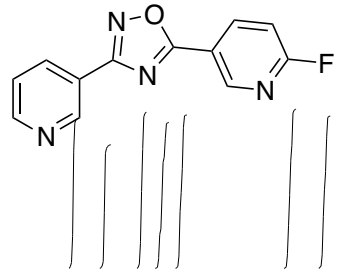

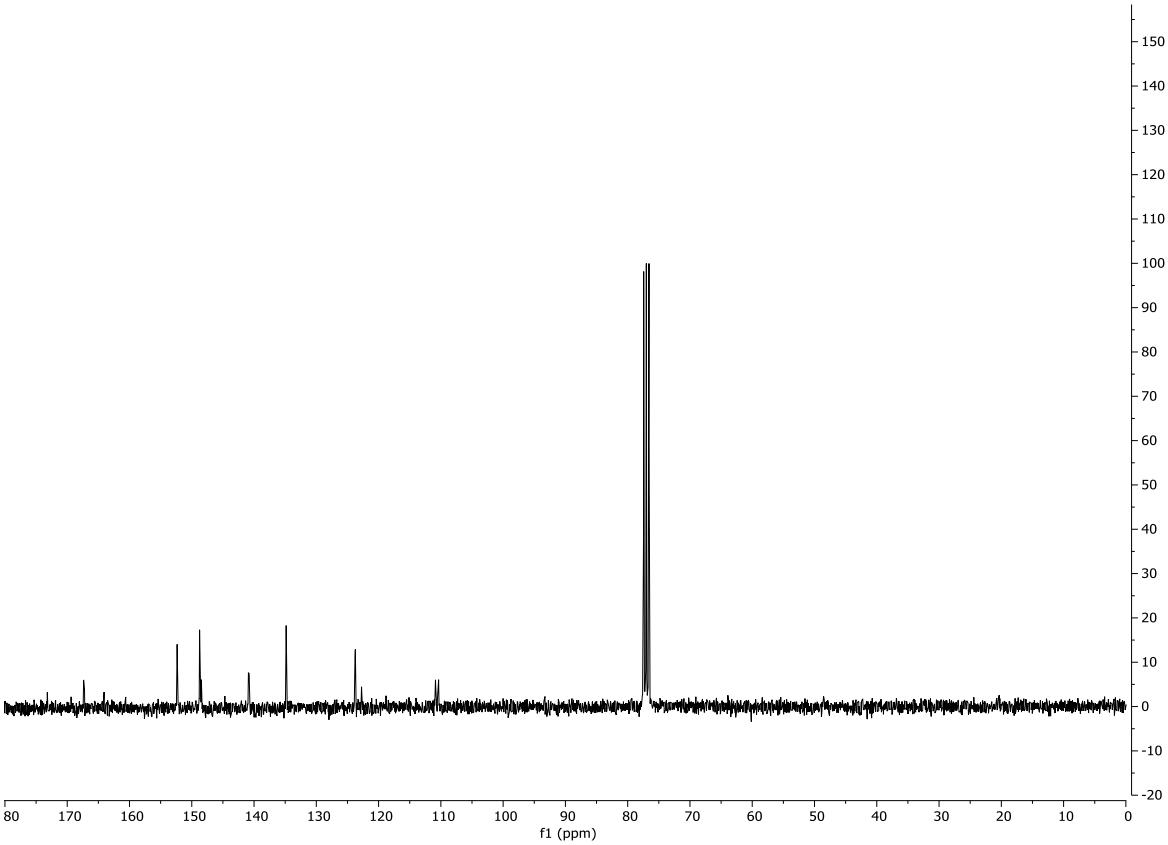

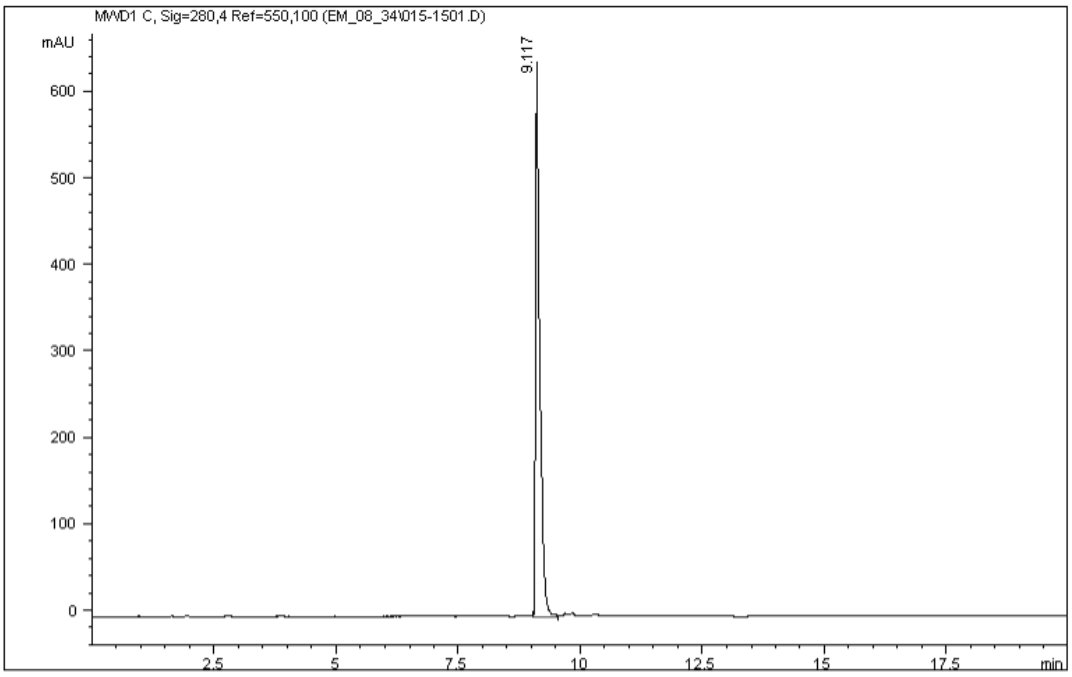

Signal 1: MWD1 C, Sig=280,4 Ref=550,100

Peak #	Area %	Area	RT [min]
1	100.000	3.937e3	9.117

Column: Hypersil BDS C18 (250x4.6 mm 5 µm)

Flow: 1.5 mL/min

Inj volume: 10 µL

Mobile Phase: H_2O/MeOH 70/30-95/5

λ: 280 nm

Rt/20 min: 9.1 min

Purity: 100%

3-(5-(3-cyanophenyl)-1,2,4-oxadiazol-3-yl)-benzoic acid (**42**)

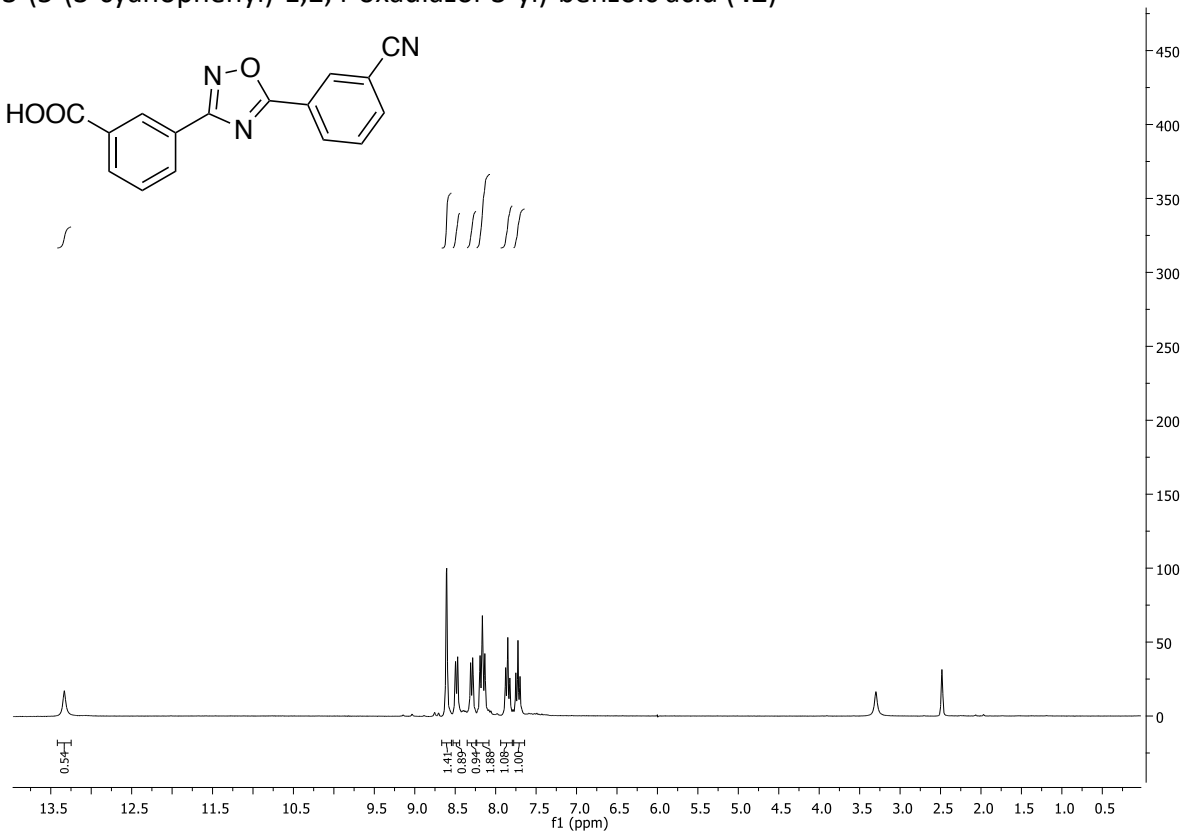

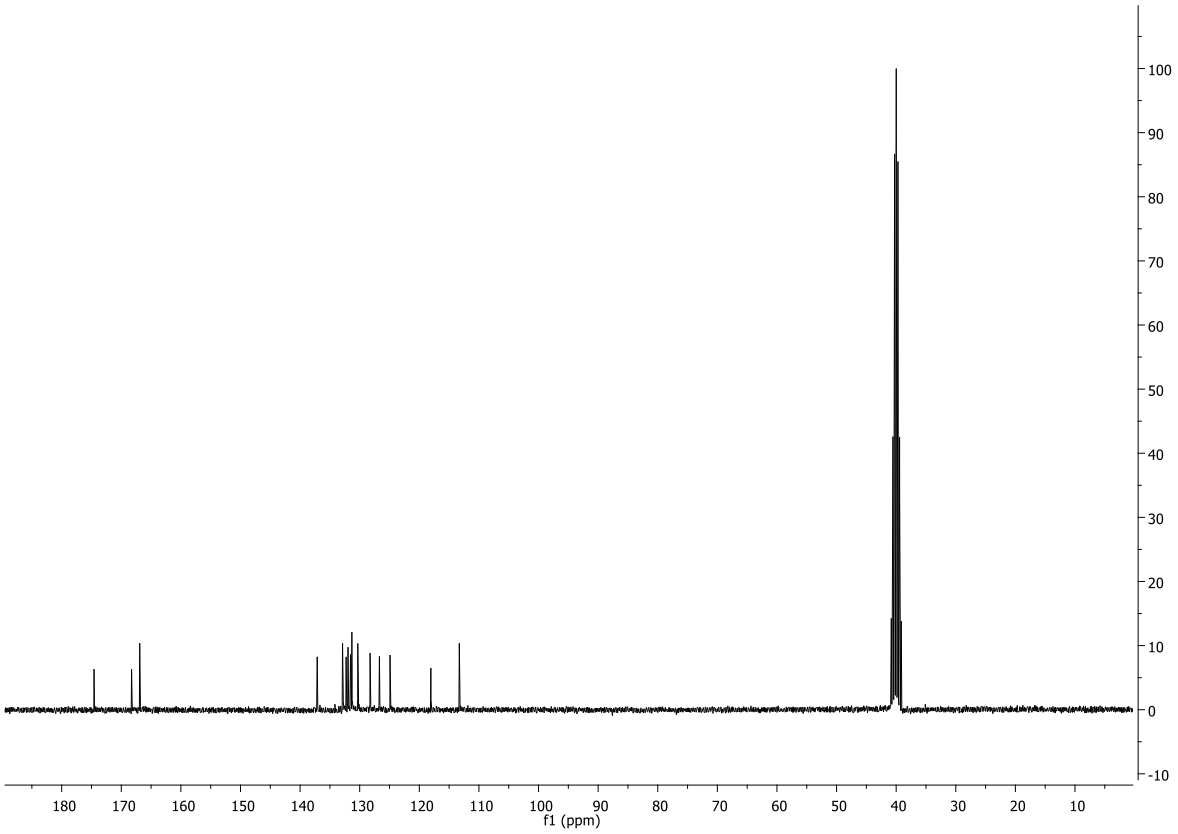

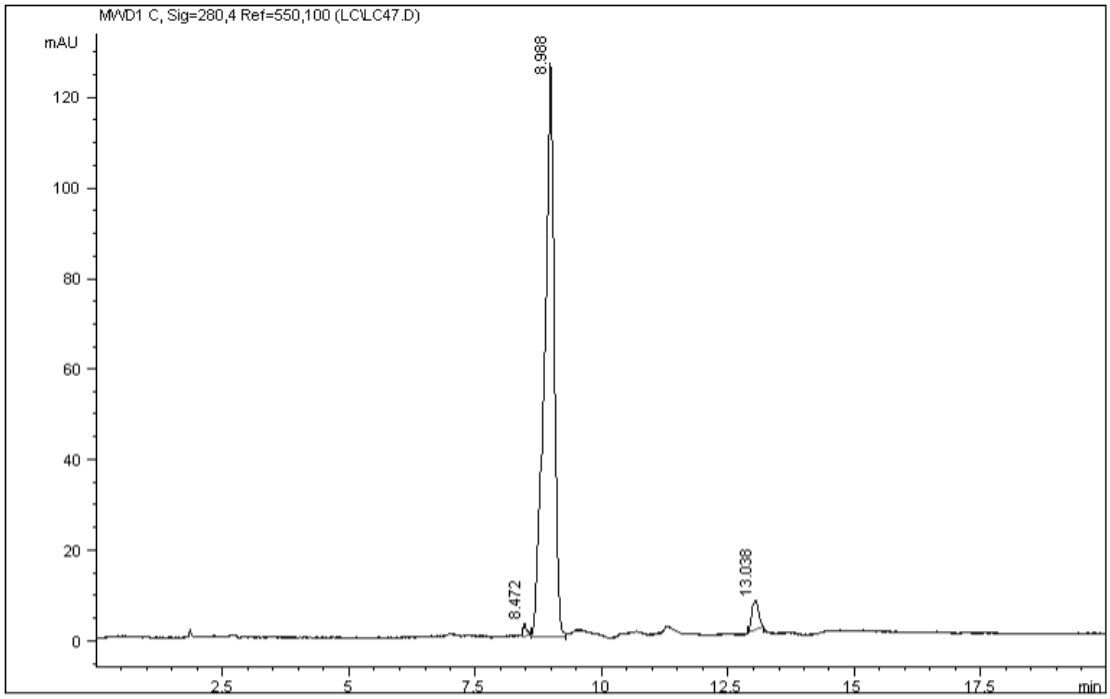

Signal 1: MWD1 C, Sig=280,4 Ref=550,100

Peak #	Area %	Area	RT [min]
1	0.755	13.420	8.472
2	96.004	1.705e3	8.988
3	3.240	57.559	13.038

Column: Hypersil BDS C18 (250x4.6 mm 5 µm)

Flow: 1.5 mL/min

Inj volume: 10 µL

Mobile Phase: H_2O/MeOH 70/30-95/5

λ: 280 nm

Rt/20 min: 8.6 min

Purity: 96.00%

3-(3-(pyridin-3-yl)-1,2,4-oxadiazol-5-yl)-sodium benzoate (**43**)

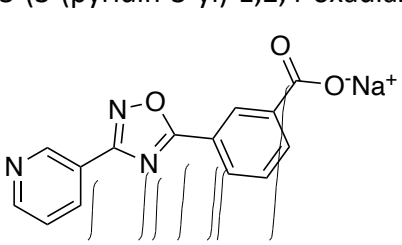

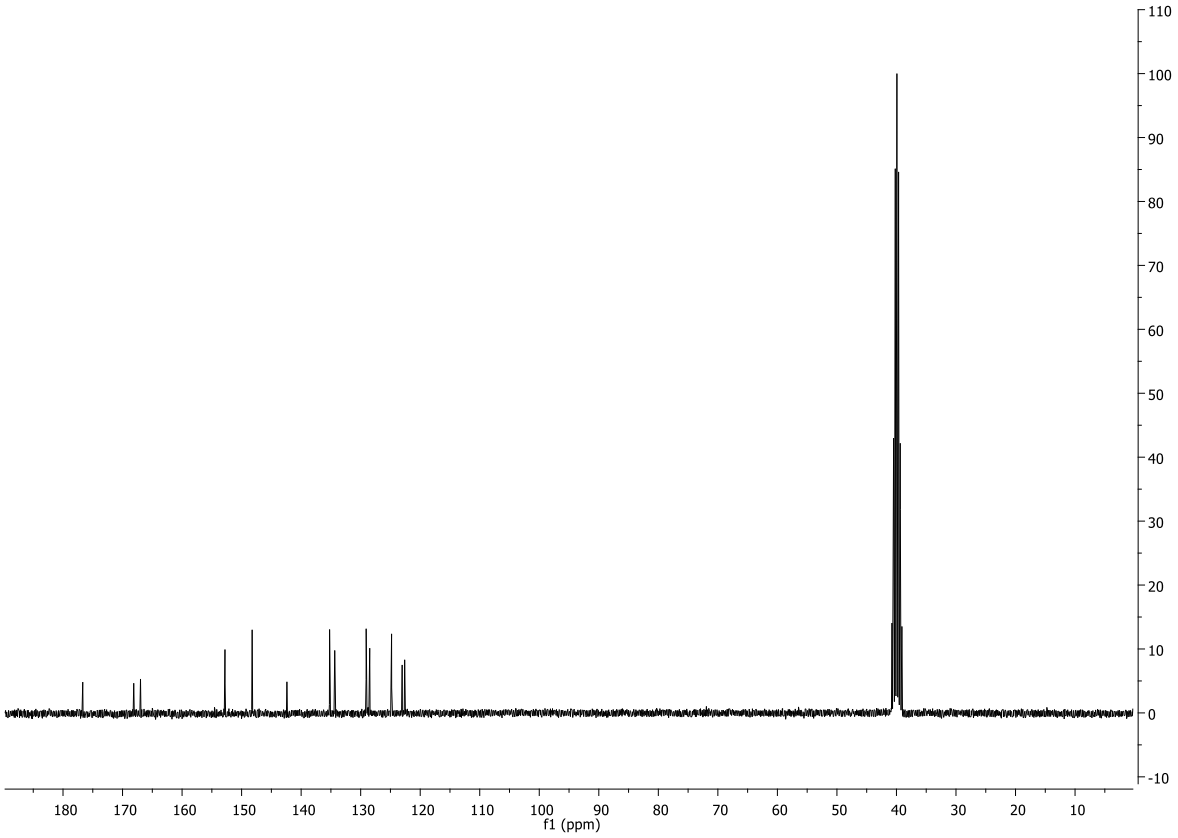

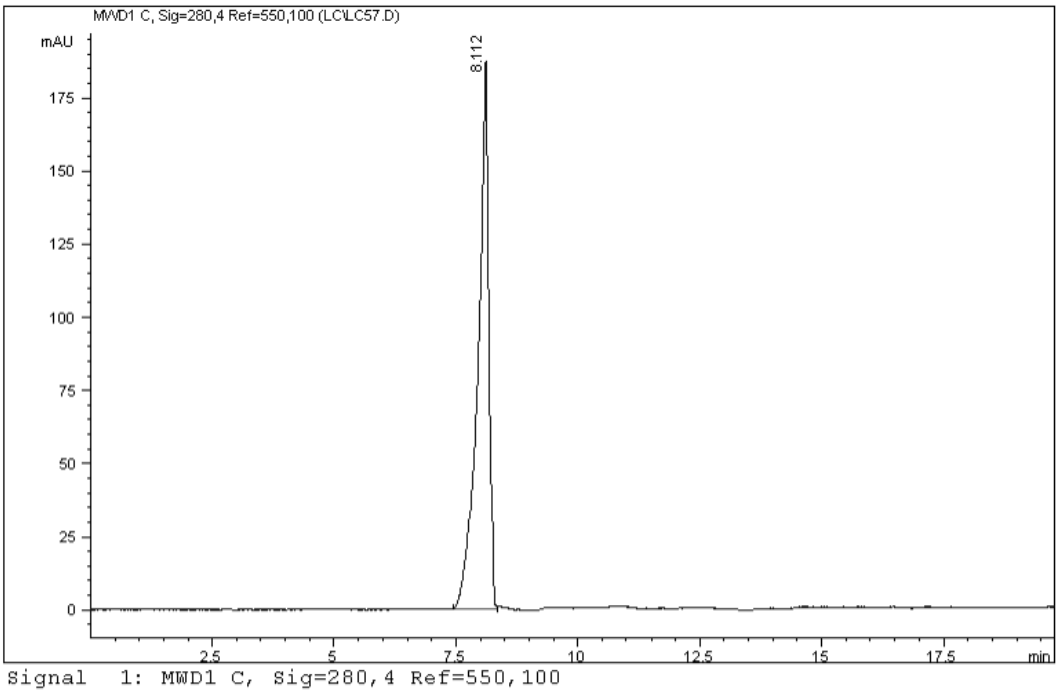

Signal 1: MWD1 C, Sig=280,4 Ref=550,100

Peak #	Area %	Area	RT [min]
1	100.000	2.892e3	8.112

Column: Hypersil BDS C18 (250x4.6 mm 5 µm)

Flow: 1.5 mL/min

Inj volume: 10 µL

Mobile Phase: H_2O/MeOH 70/30-95/5

λ: 280 nm

Rt/20 min: 8.1 min

Purity: 100%

5-(cyclohex-1-en-1-yl)-3-(pyridine-3-yl)-1,2,4-oxadiazole (**44**)

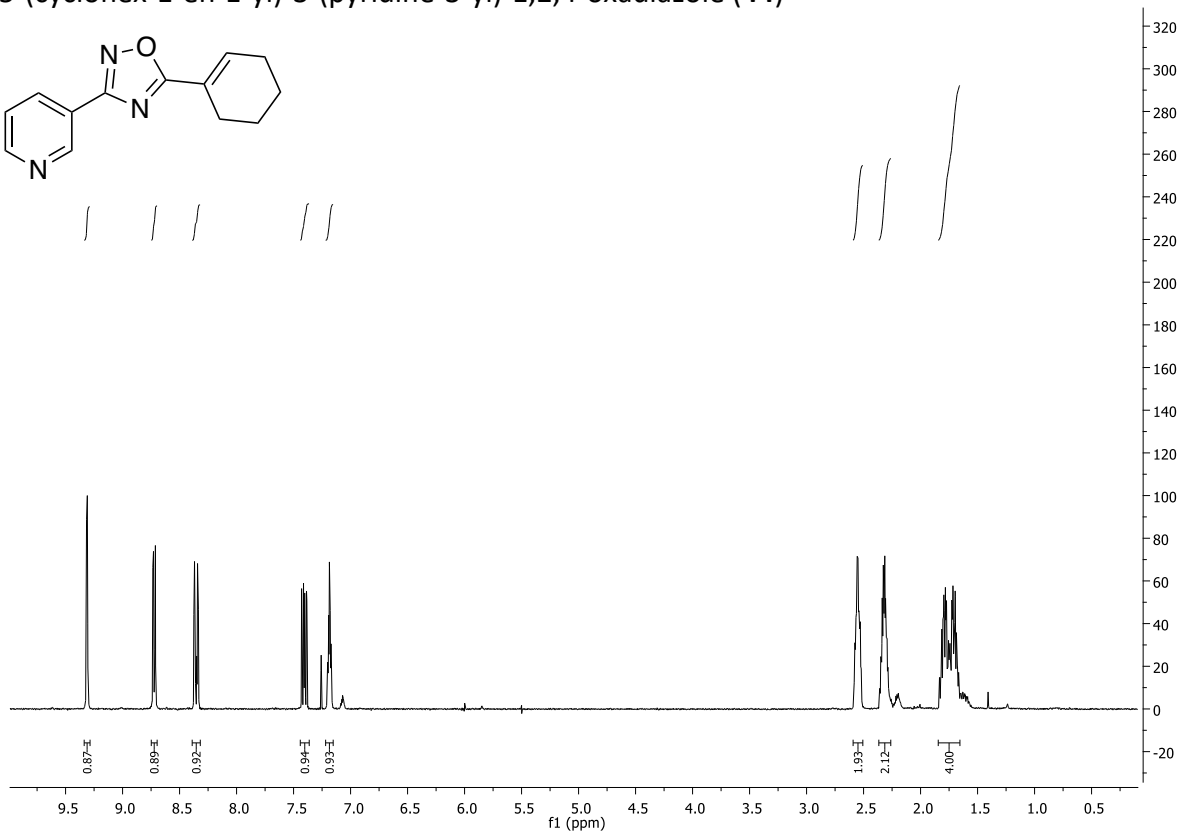

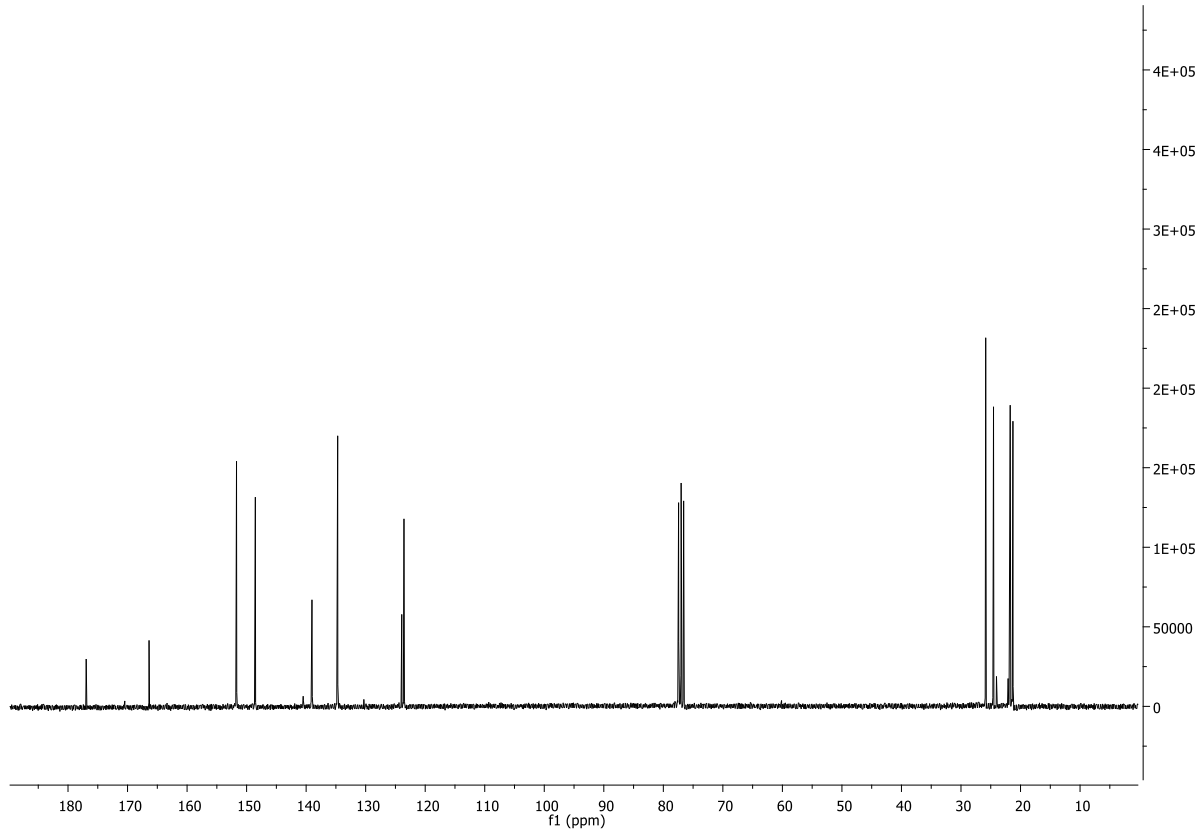

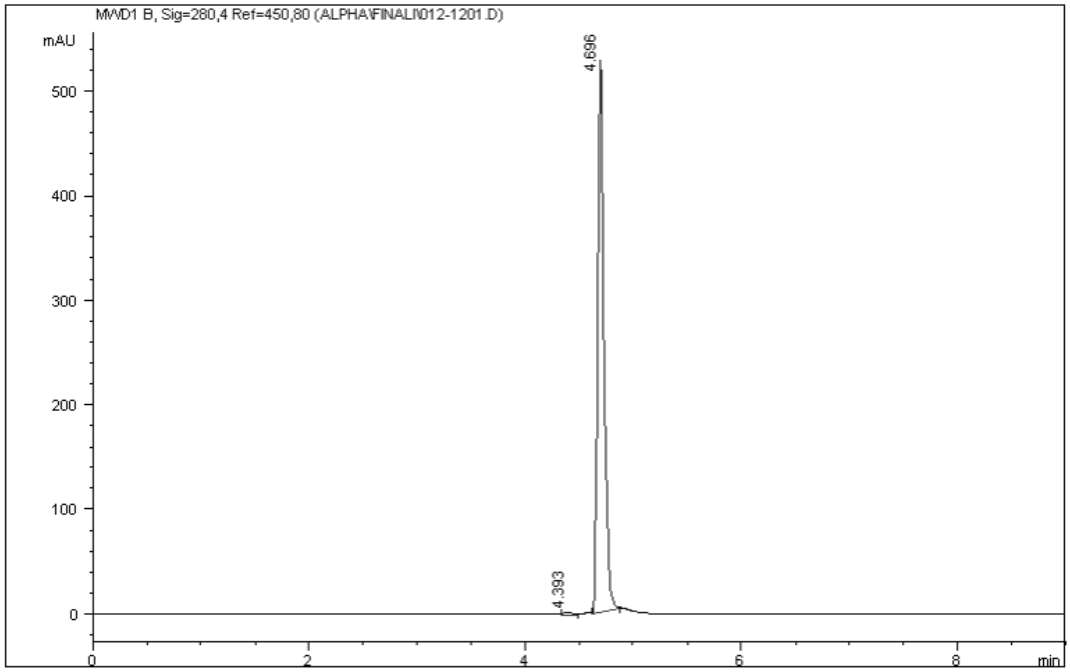

Signal 1: MWD1 B, Sig=280,4 Ref=450,80

Peak #	Area %	Area	RT [min]
1	0.830	17.773	4.393
2	99.170	2.123e3	4.696

Column: Supelcosil LC-SI (250x4.6 mm 5 µm)

Flow: 0.75 mL/min

Inj volume: 10 µL

Mobile Phase: EtOAc/MeOH 97.5/2.5

λ: 280 nm

Rt/12 min: 4.7 min

Purity: 99.17%

3-(3-(furan-3-yl)-1,2,4-oxadiazol-5-yl)-benzonitrile (**45**)

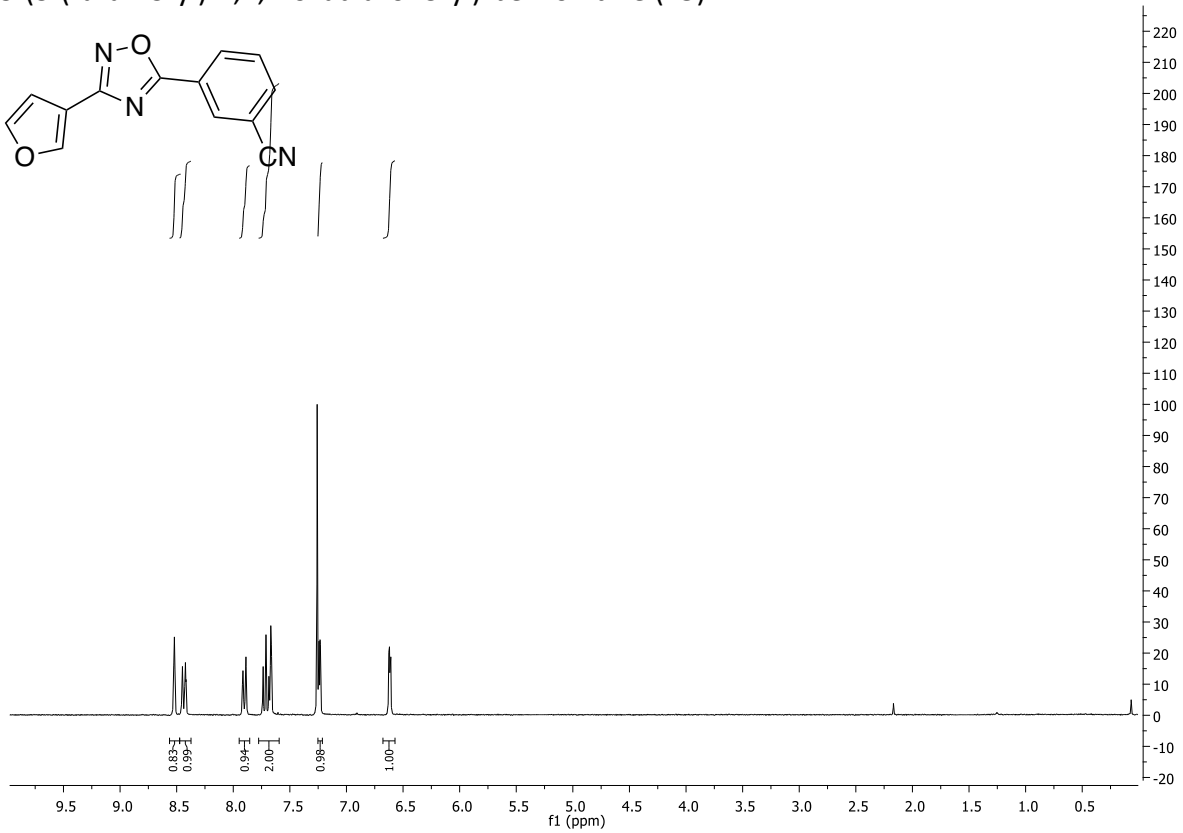

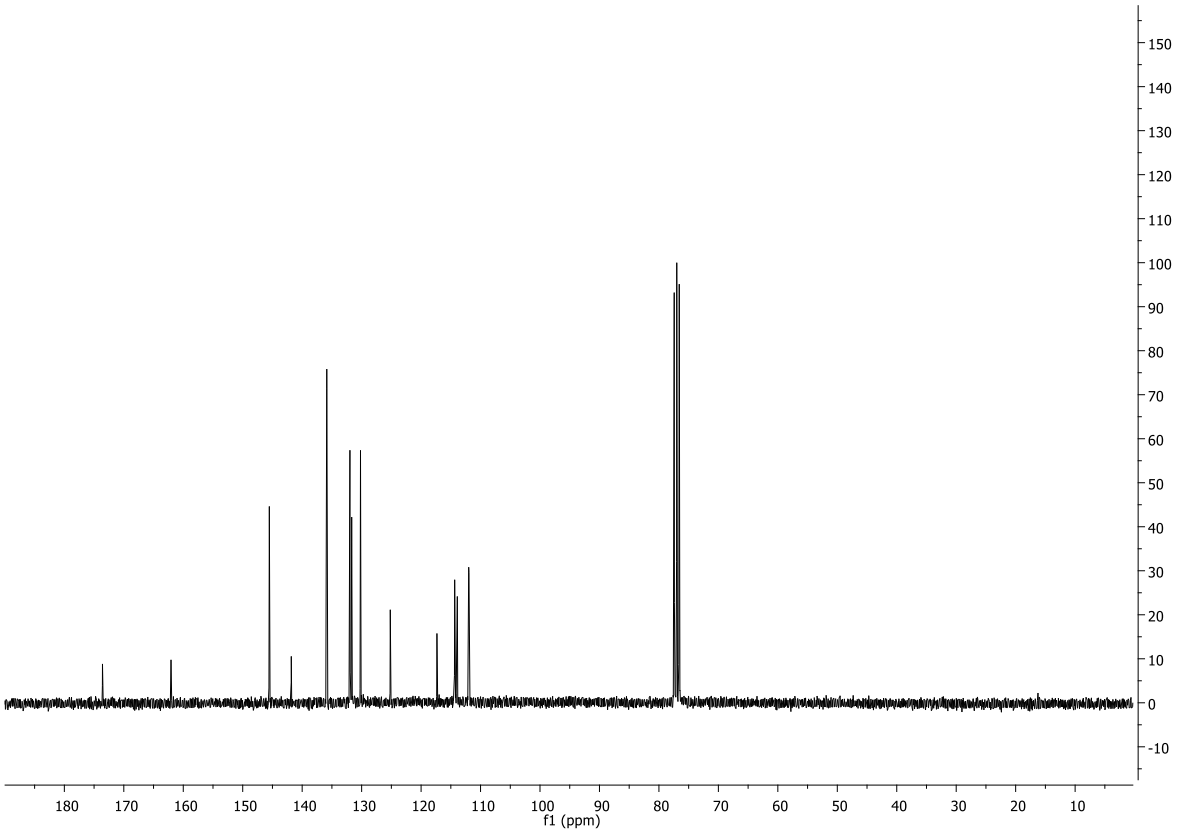

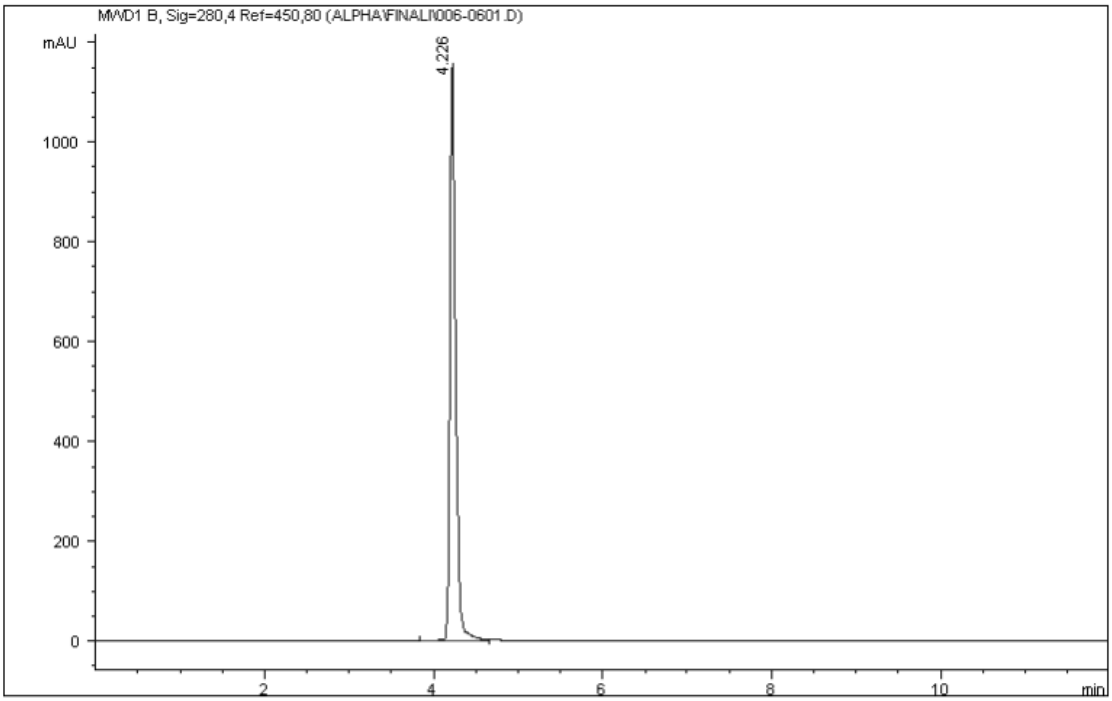

Signal 1: MWD1 B, Sig=280,4 Ref=450,80

Peak #	Area %	Area	RT [min]
1	100.000	5.252e3	4.226

Column: Supelcosil LC-SI (250x4.6 mm 5 µm)

Flow: 0.75 mL/min

Inj volume: 10 µL

Mobile Phase: EtOAc/MeOH 97.5/2.5

λ: 280 nm

Rt/12 min: 4.2 min

Purity: 100%

3-(3-cyclohexyl-1,2,4-oxadiazol-5-yl)-benzonitrile (**46**)

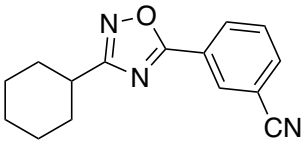

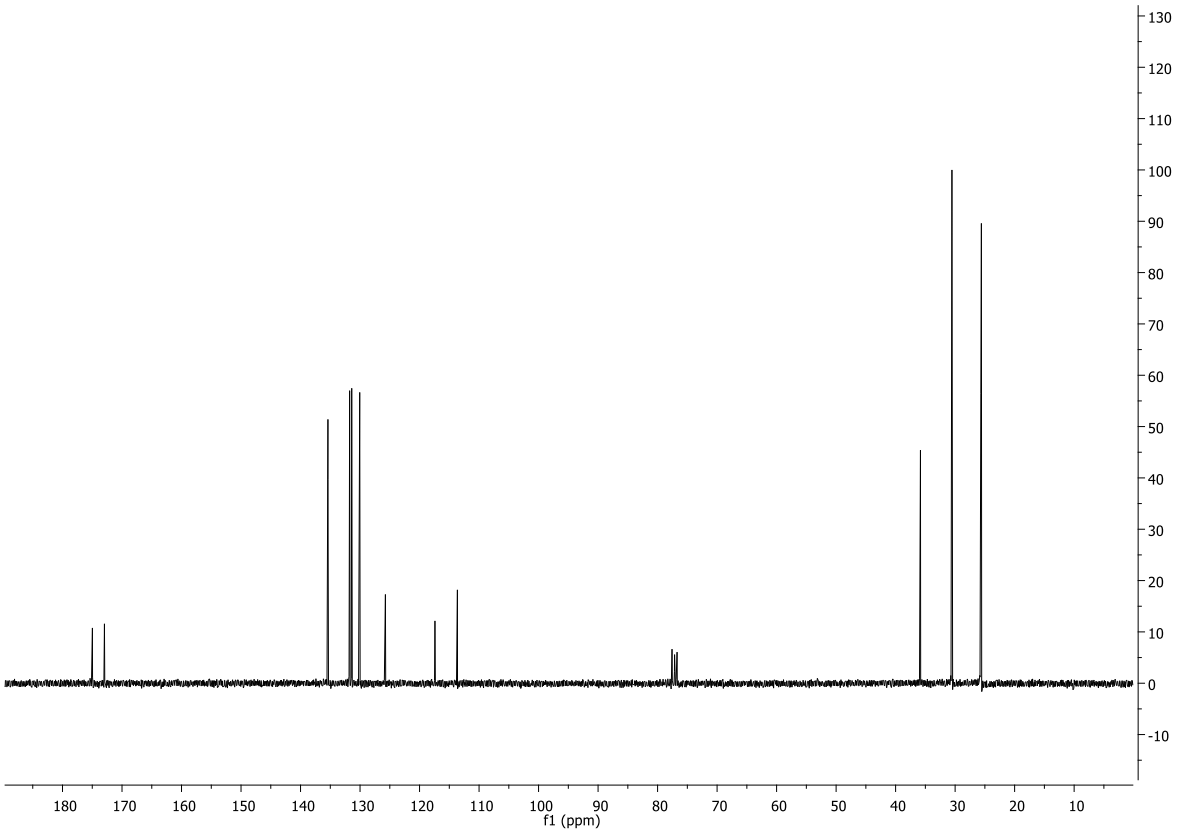

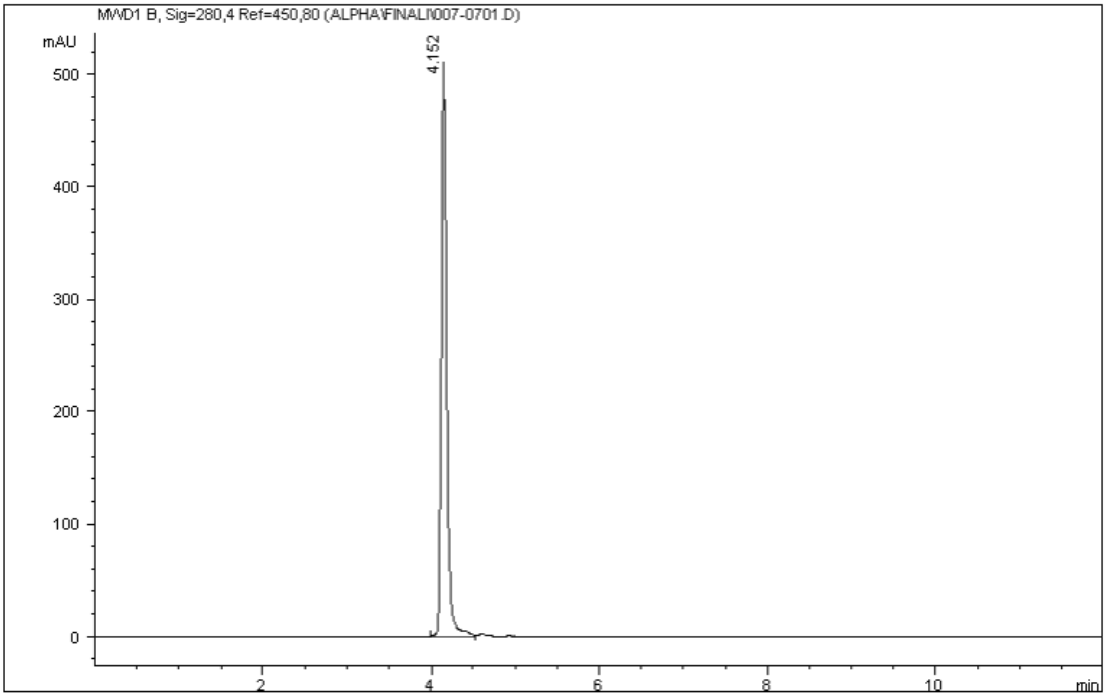

Signal 1: MWD1 B, Sig=280,4 Ref=450,80

Peak #	Area %	Area	RT [min]
1	100.000	2.345e3	4.152

Column: Supelcosil LC-SI (250x4.6 mm 5 µm)

Flow: 0.75 mL/min

Inj volume: 10 µL

Mobile Phase: EtOAc/MeOH 97.5/2.5

λ: 280 nm

Rt/12 min: 4.2 min

Purity: 100%

3-(3-(piperidin-1-yl)-1,2,4-oxadiazol-5-yl)-benzonitrile (**47**)

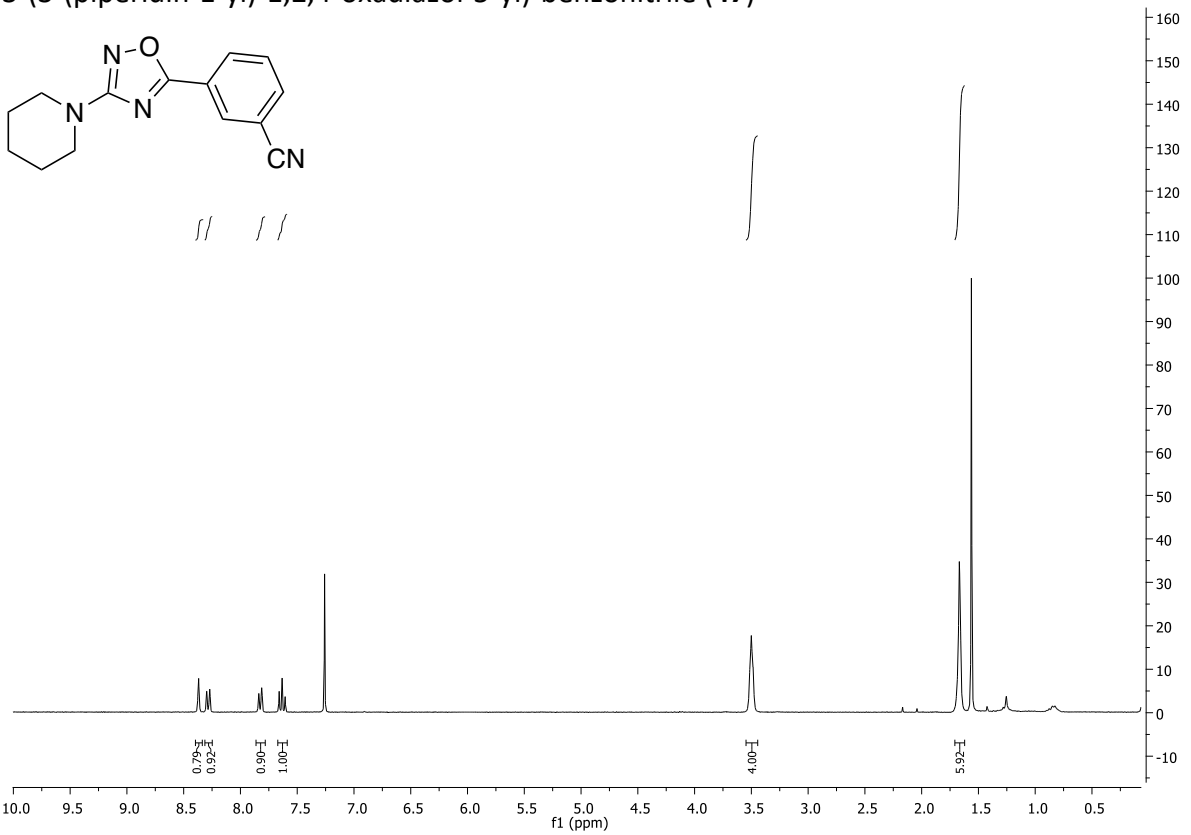

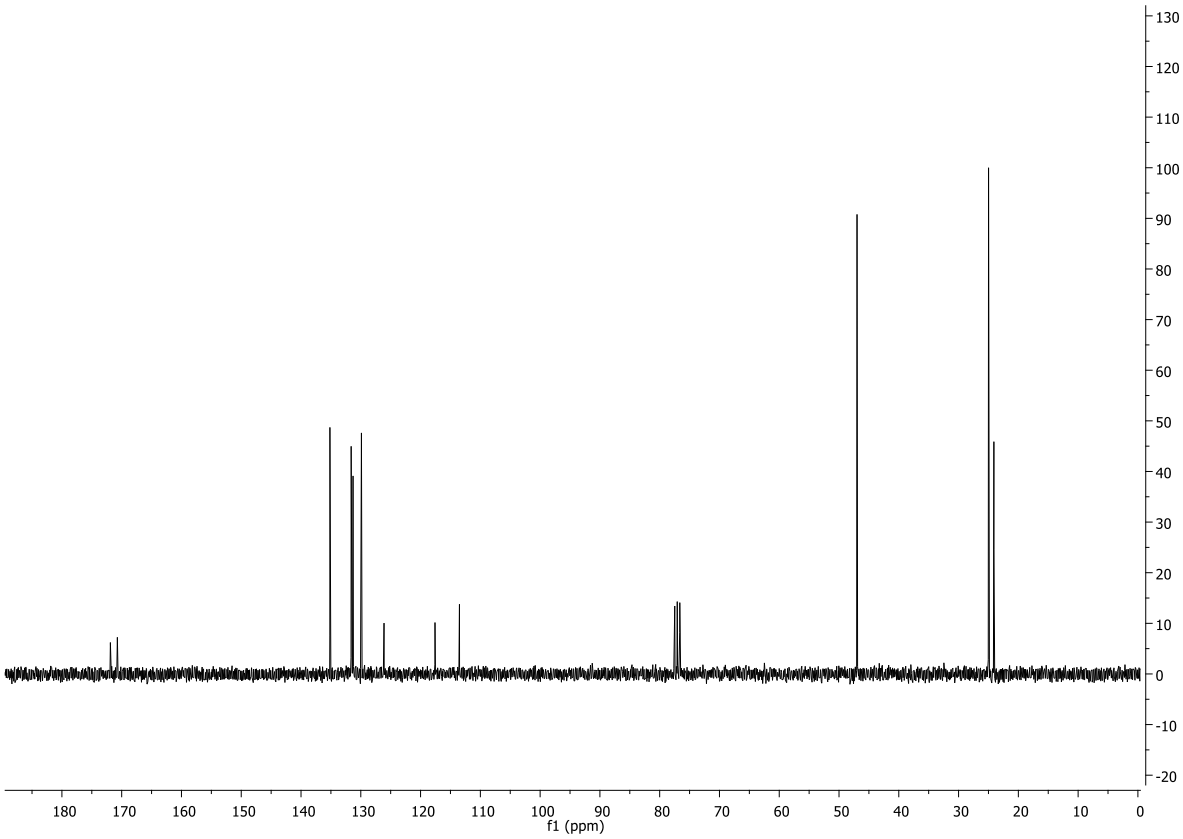

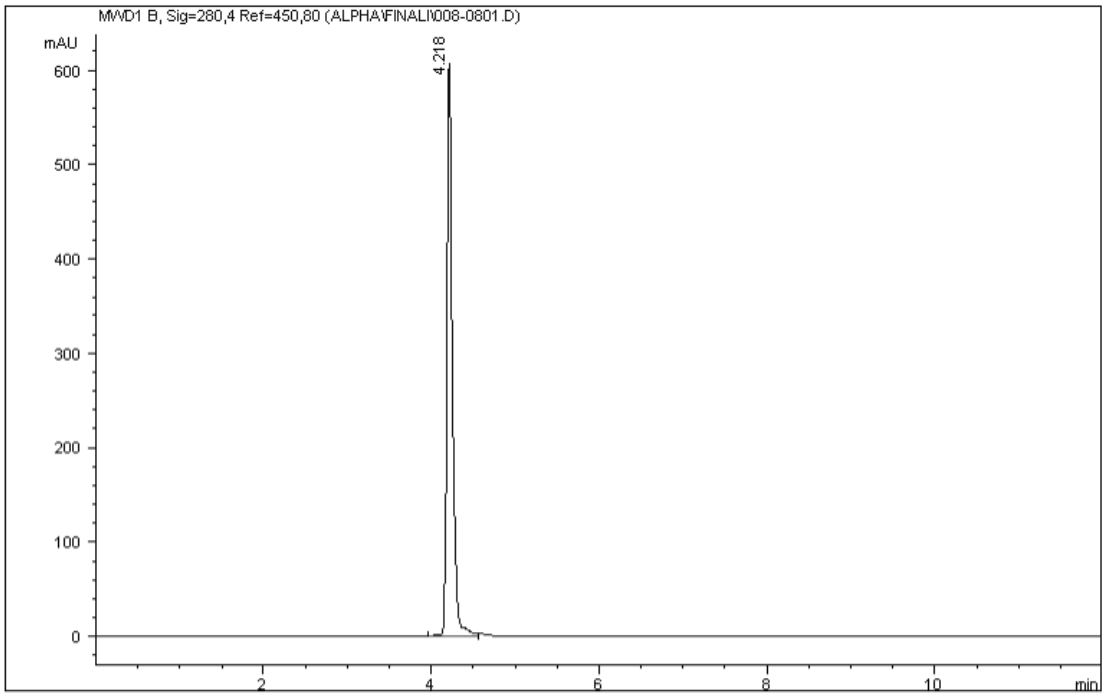

Signal 1: MWD1 B, Sig=280,4 Ref=450,80

Peak #	Area %	Area	RT [min]
1	100.000	2.725e3	4.218

Column: Supelcosil LC-SI (250x4.6 mm 5 µm)

Flow: 0.75 mL/min

Inj volume: 10 µL

Mobile Phase: EtOAc/MeOH 97.5/2.5

λ: 280 nm

Rt/12 min: 4.2 min

Purity: 100%

1-(3-(3-(pyridin-3-yl)-1,2,4-oxadiazol-5-yl)-pyperidin-1yl)ethan-1one (**48**)

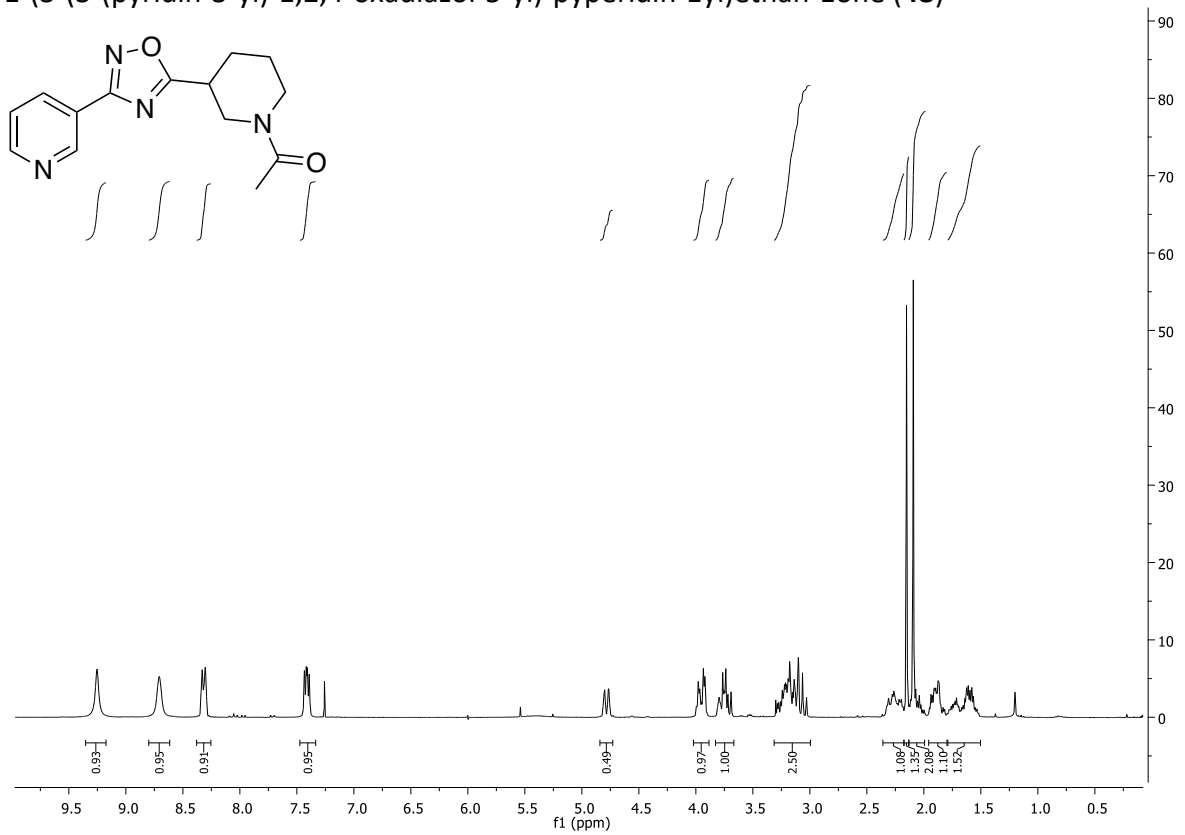

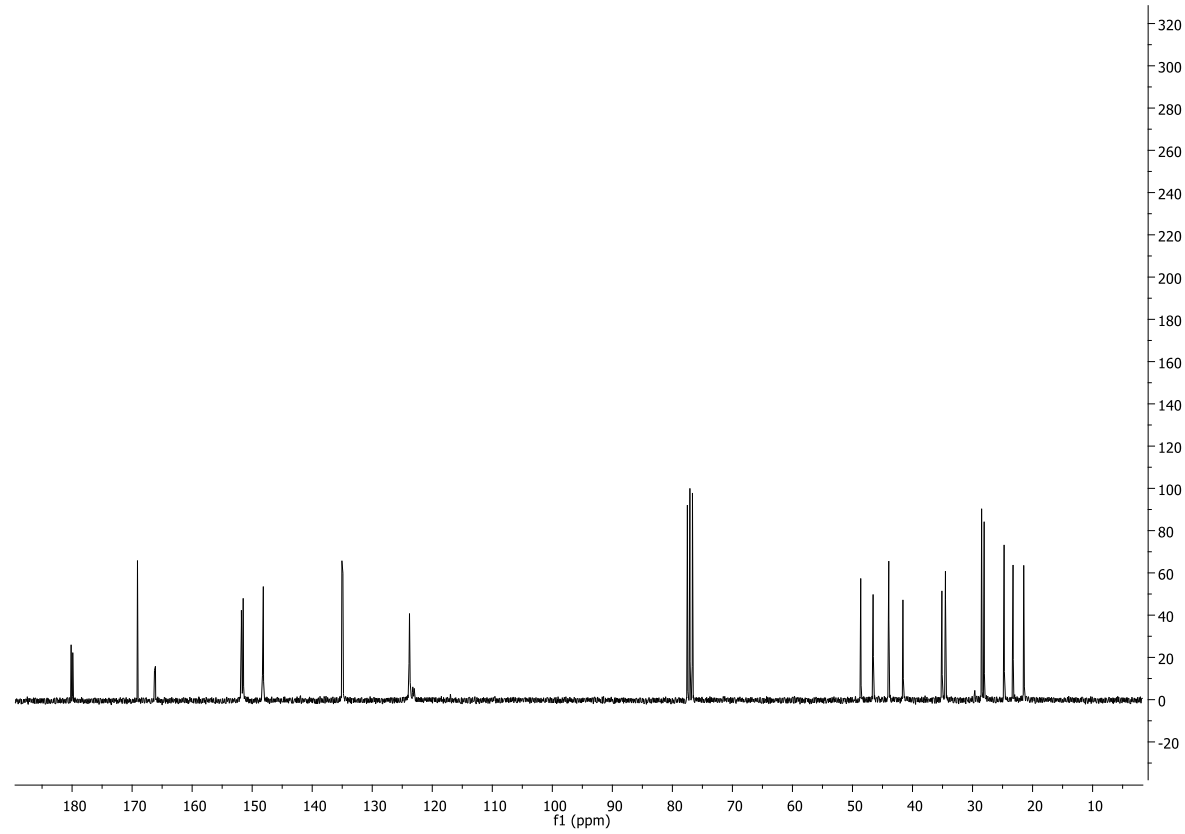

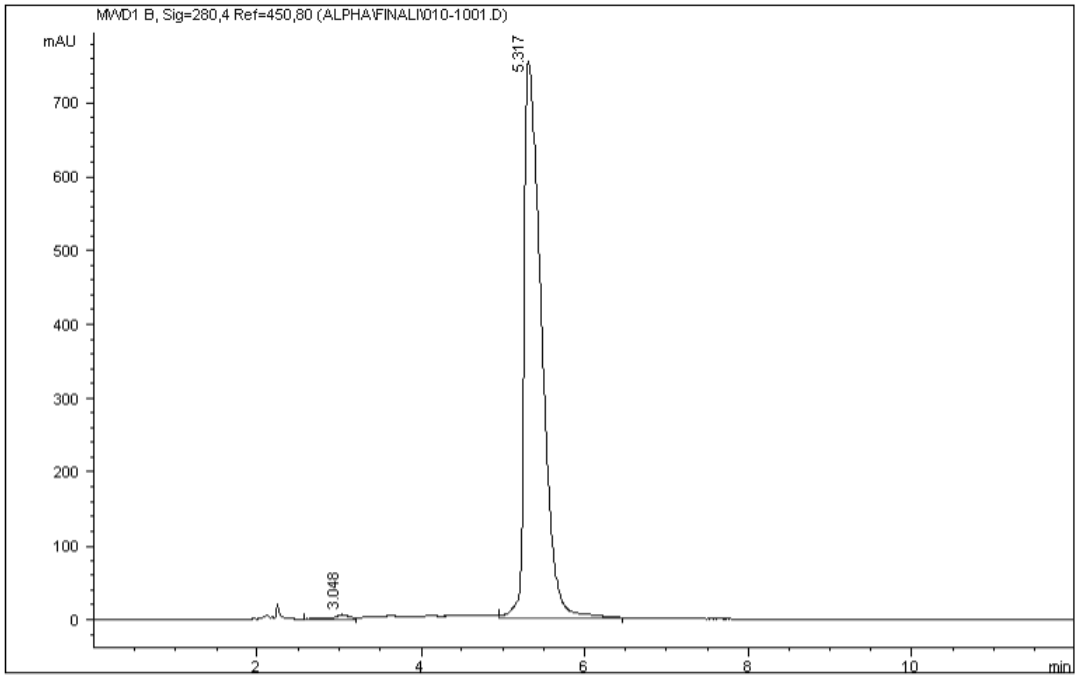

Signal 1: MWD1 B, Sig=280,4 Ref=450,80

Peak #	Area %	Area	RT [min]
1	0.852	95.632	3.048
2	99.148	1.113e4	5.317

Column: Supelcosil LC-SI (250x4.6 mm 5 µm)

Flow: 1.5 mL/min

Inj volume: 10 µL

Mobile Phase: EtOAc/MeOH 95/5

λ: 280 nm

Rt/12 min: 5.3 min

Purity: 99.15%

3-(3-(pyridin-3-yl)-1,2,4-oxadiazol-5-yl)pyperidin-1-carbaldehyd (**49**)

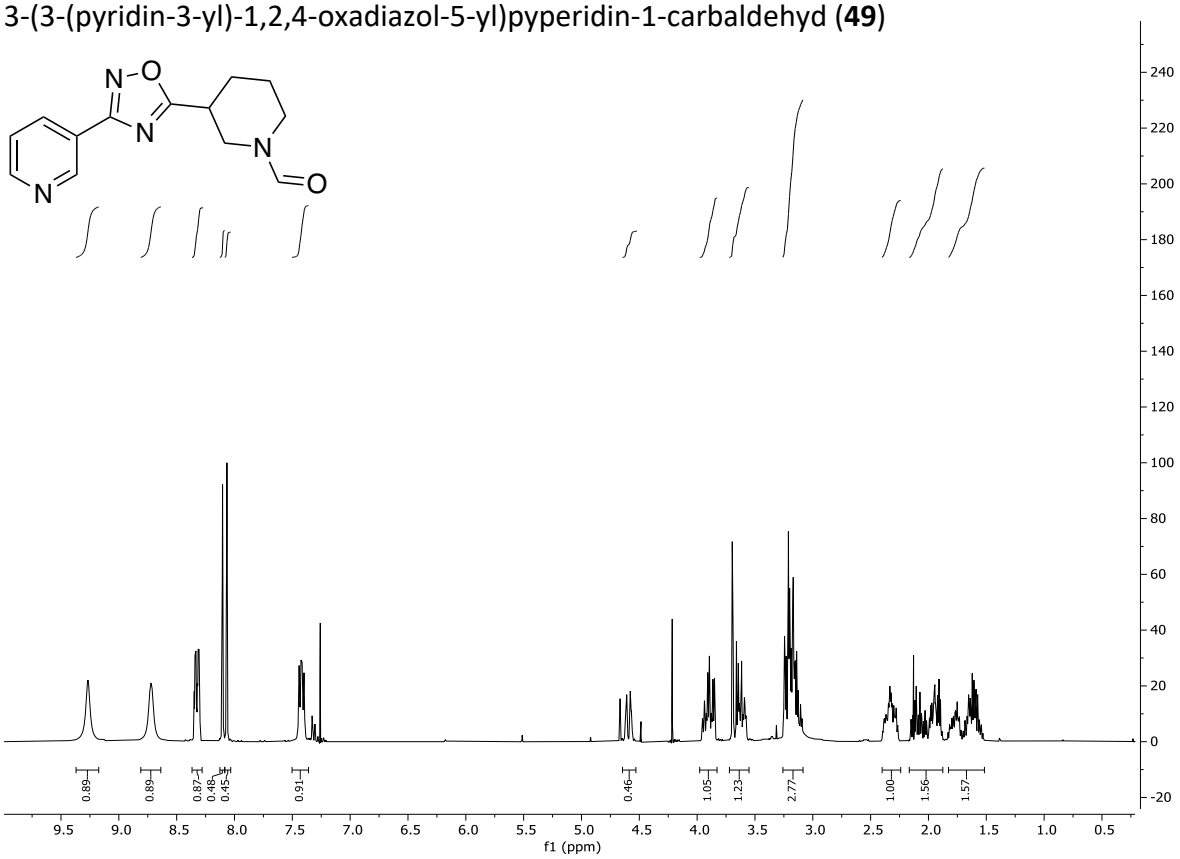

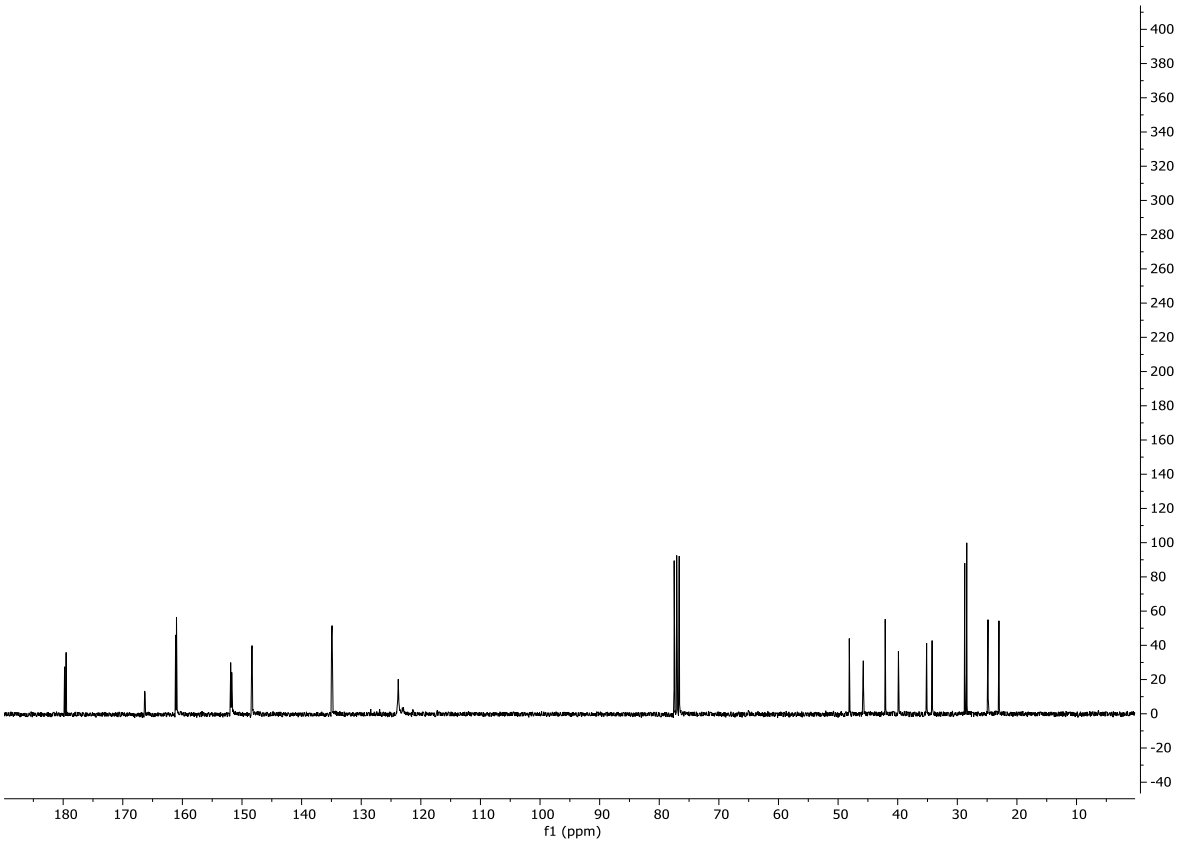

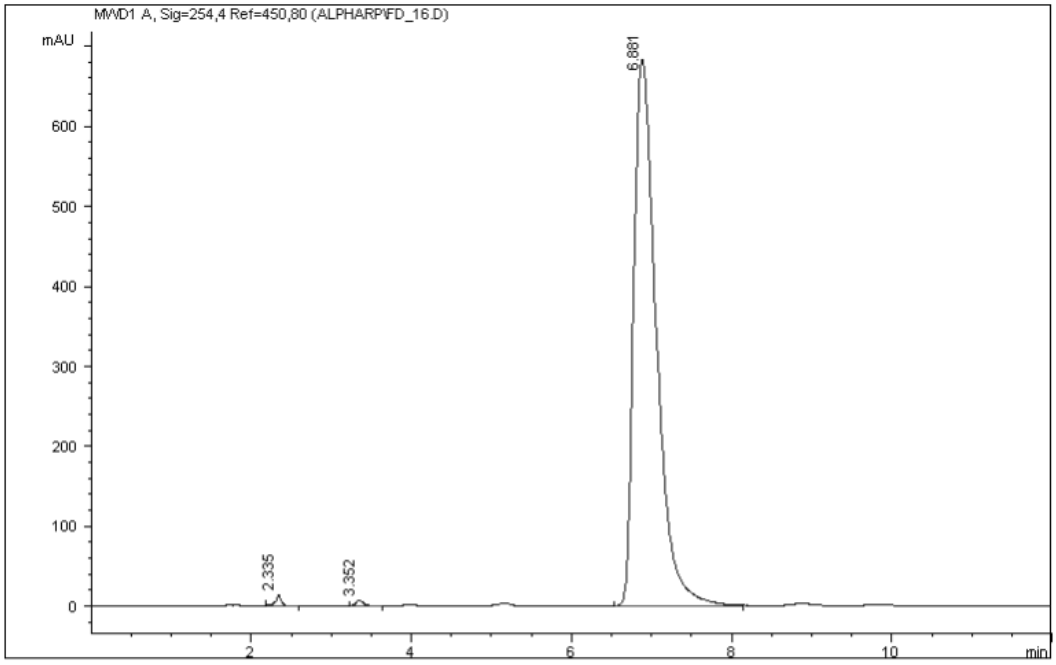

Signal 1: MWD1 A, Sig=254,4 Ref=450,80

Peak #	Area %	Area	RT [min]
1	0.533	71.587	2.335
2	0.409	54.940	3.352
3	99.058	1.330e4	6.881

Column: Hypersil BDS C18 (250x4.6 mm 5 µm)

Flow: 1.5 mL/min

Inj volume: 10 µL

Mobile Phase: MeOH 40%

λ: 254 nm

Rt/12 min: 6.8 min

Purity: 99.06%

1-(4-(3-(pyridin-3-yl)-1,2,4-oxadiazol-5-yl)-pyperidin-1yl)ethan-1one (**50**)

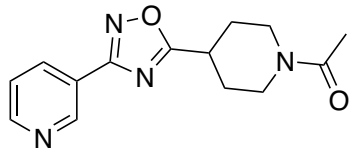

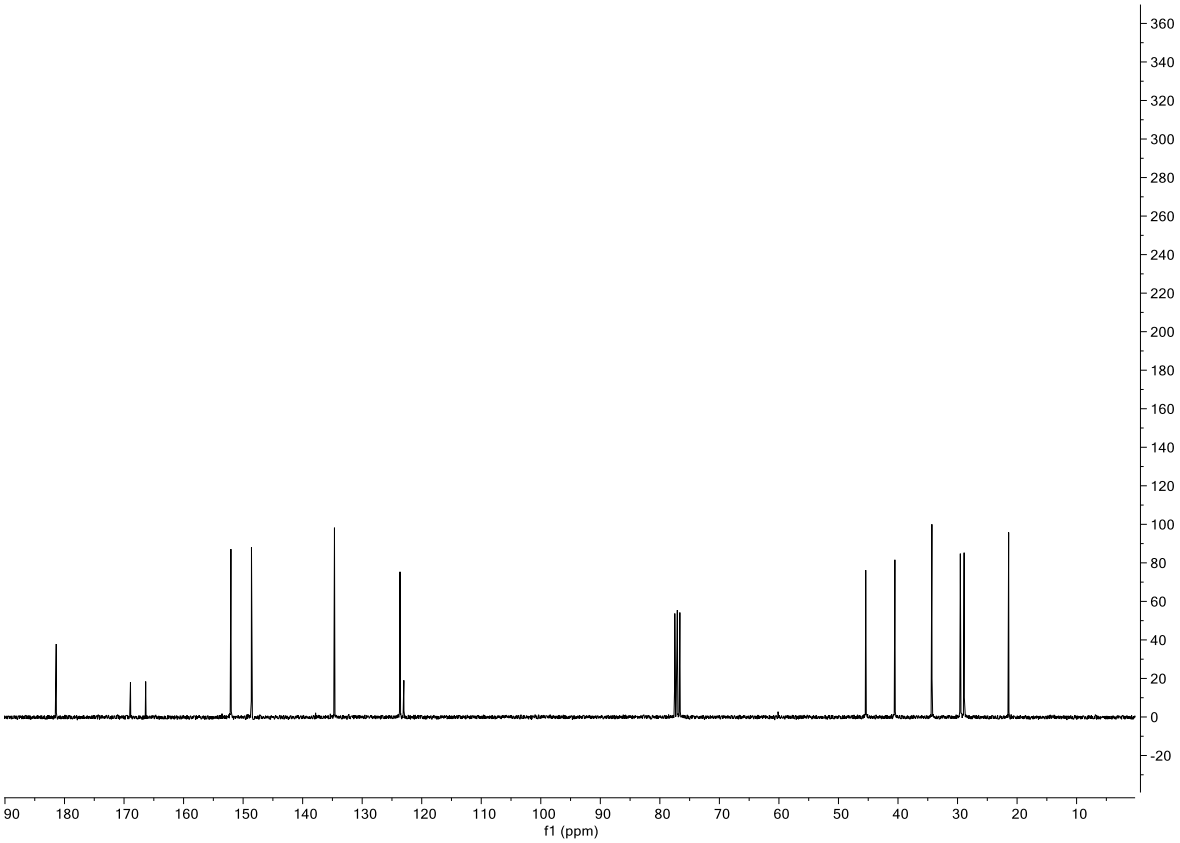

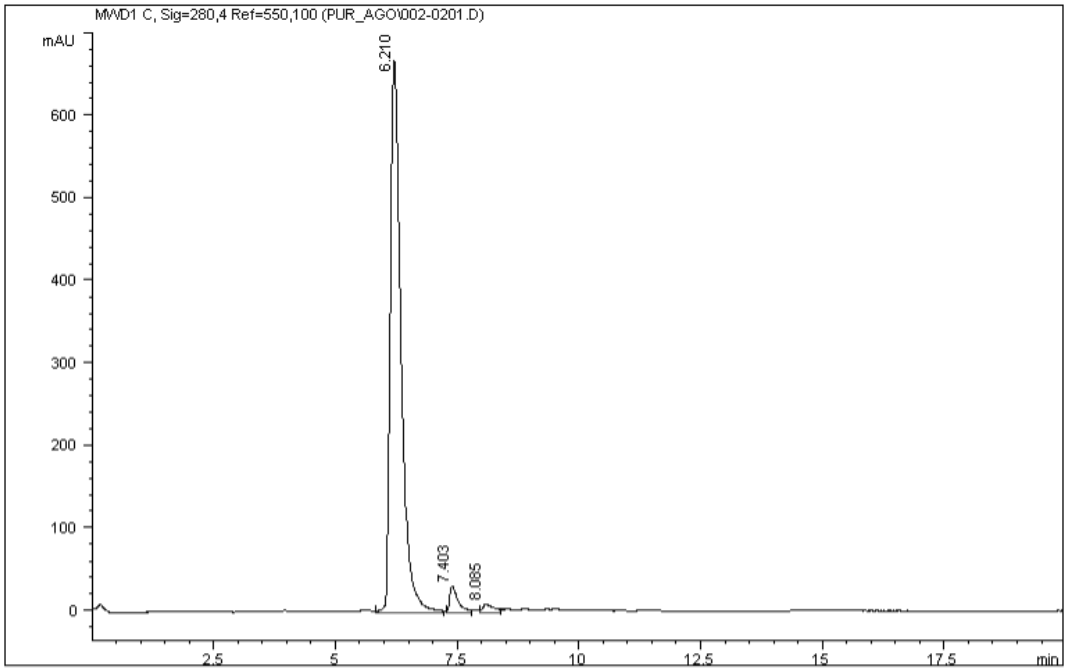

Signal 1: MWD1 C, Sig=280,4 Ref=550,100

Peak #	Area %	Area	RT [min]
1	95.150	1.050e4	6.210
2	3.408	376.122	7.403
3	1.442	159.185	8.085

Column: Hypersil BDS C18 (250x4.6 mm 5 µm)

Flow: 1.5 mL/min

Inj volume: 10 µL

Mobile Phase: H_2O/MeOH 70/30-95/5

λ: 280 nm

Rt/20 min: 6.2 min

Purity: 95.15%

4-(3-(pyridin-3-yl)-1,2,4-oxadiazol-5-yl)pyperidin-1-carbaldehyde (**51**)

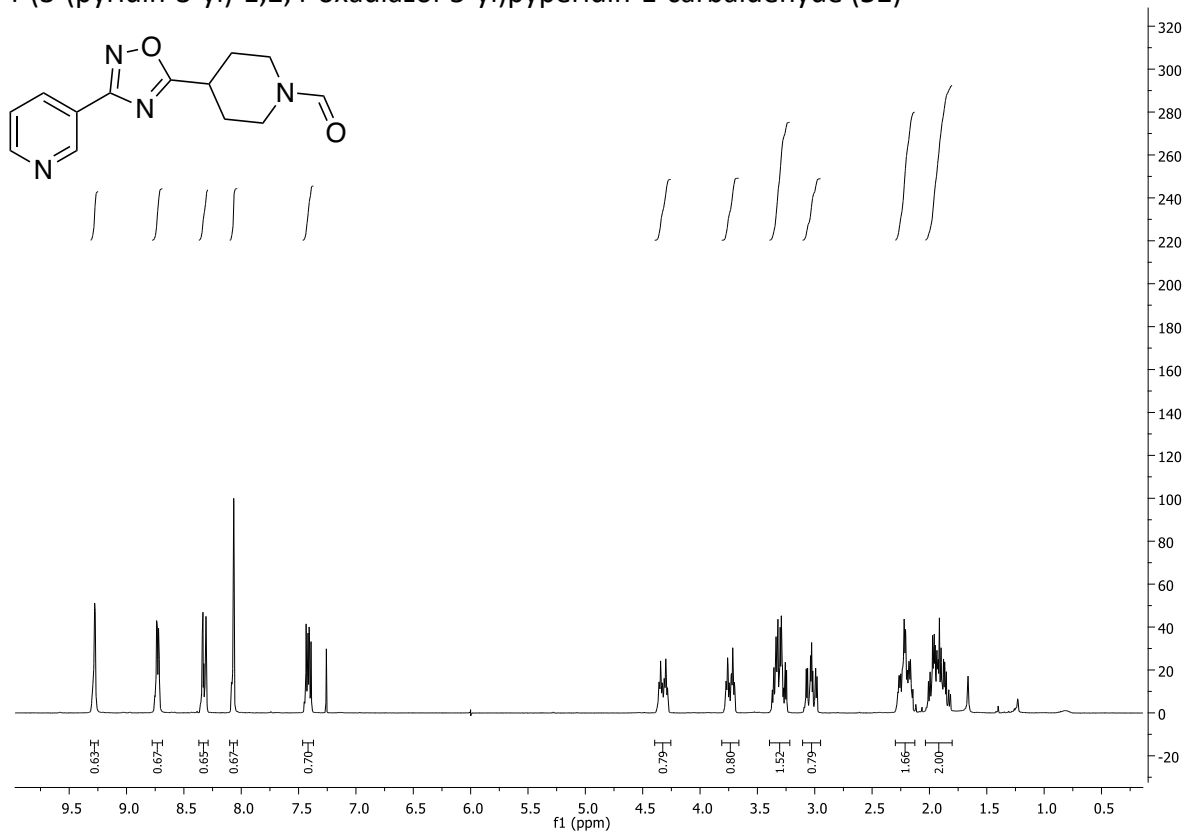

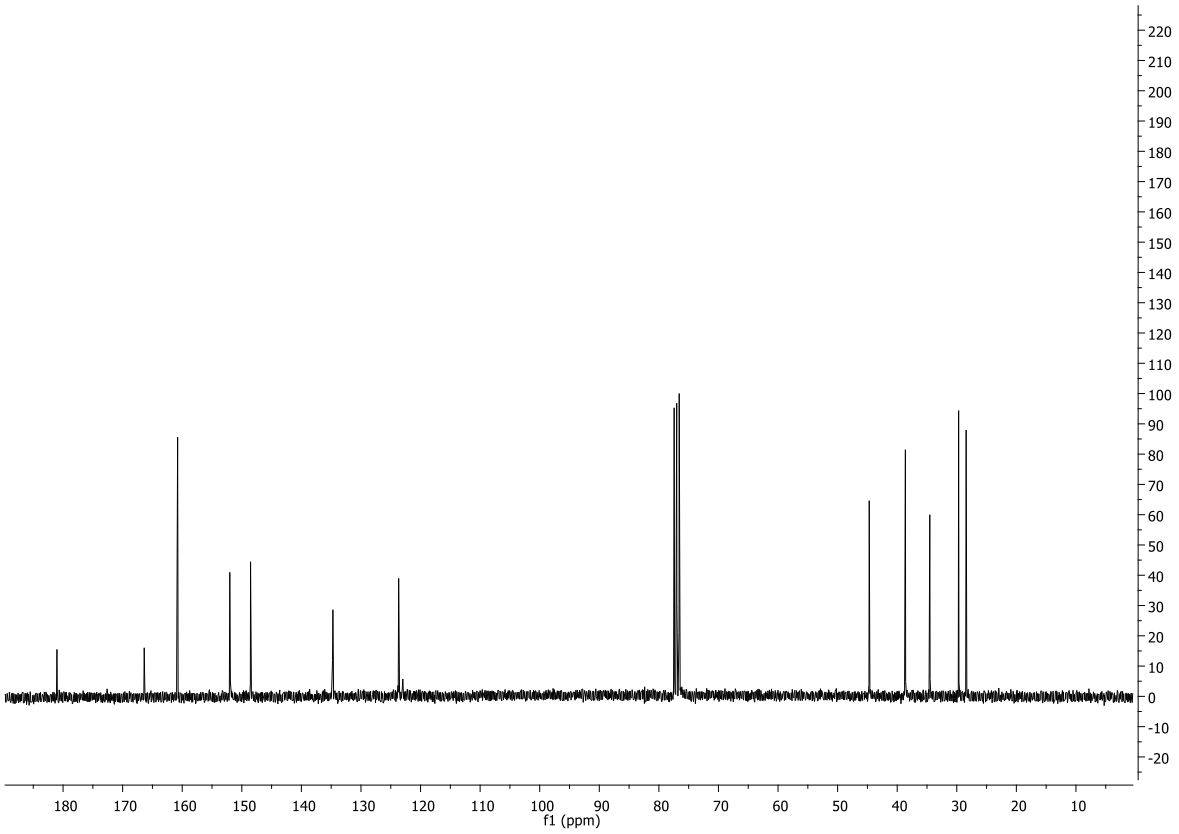

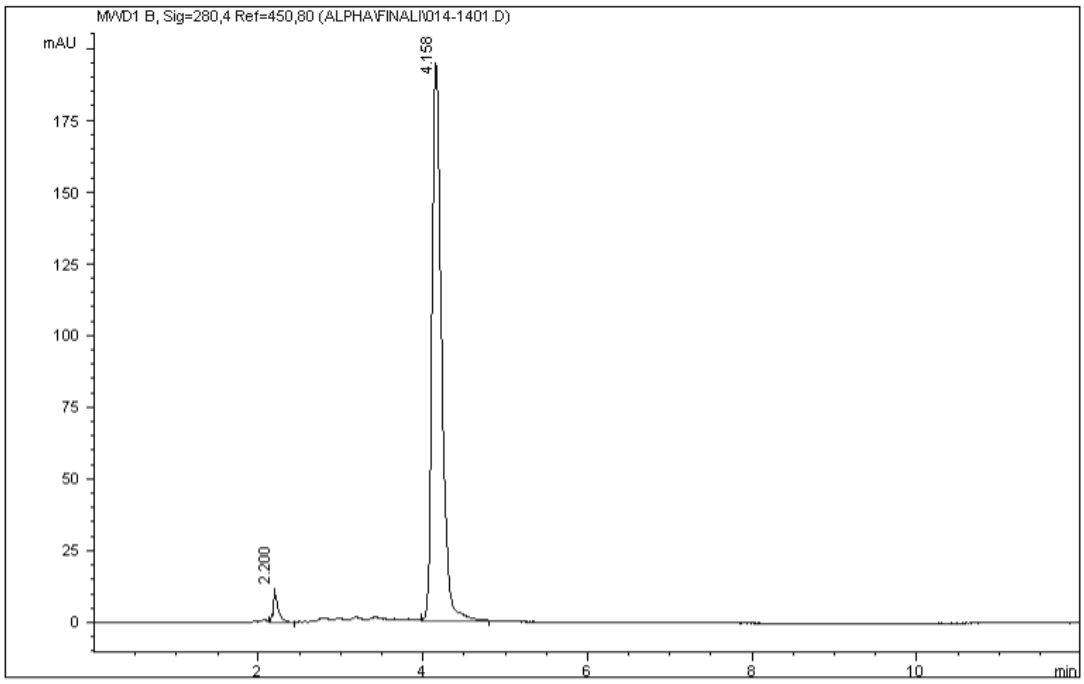

Signal 1: MWD1 B, Sig=280,4 Ref=450,80

Peak #	Area %	Area	RT [min]
1	2.740	45.306	2.200
2	97.260	1.608e3	4.158

Column: Supelcosil LC-SI (250x4.6 mm 5 µm)

Flow: 1.5 mL/min

Inj volume: 10 µL

Mobile Phase: EtOAc/MeOH 95/5

λ: 280 nm

Rt/12 min: 4.2 min

Purity: 97.26%

(2*S*)-1-((8-bromo-7-hydroxyquinolin-2-yl)methyl)-2-(((5-hydroxypyridin-3-yl)oxy)methyl)-1-methylpyrrolidin-1-ium methanesulfonate (**BHQ-(*S*)-V**)

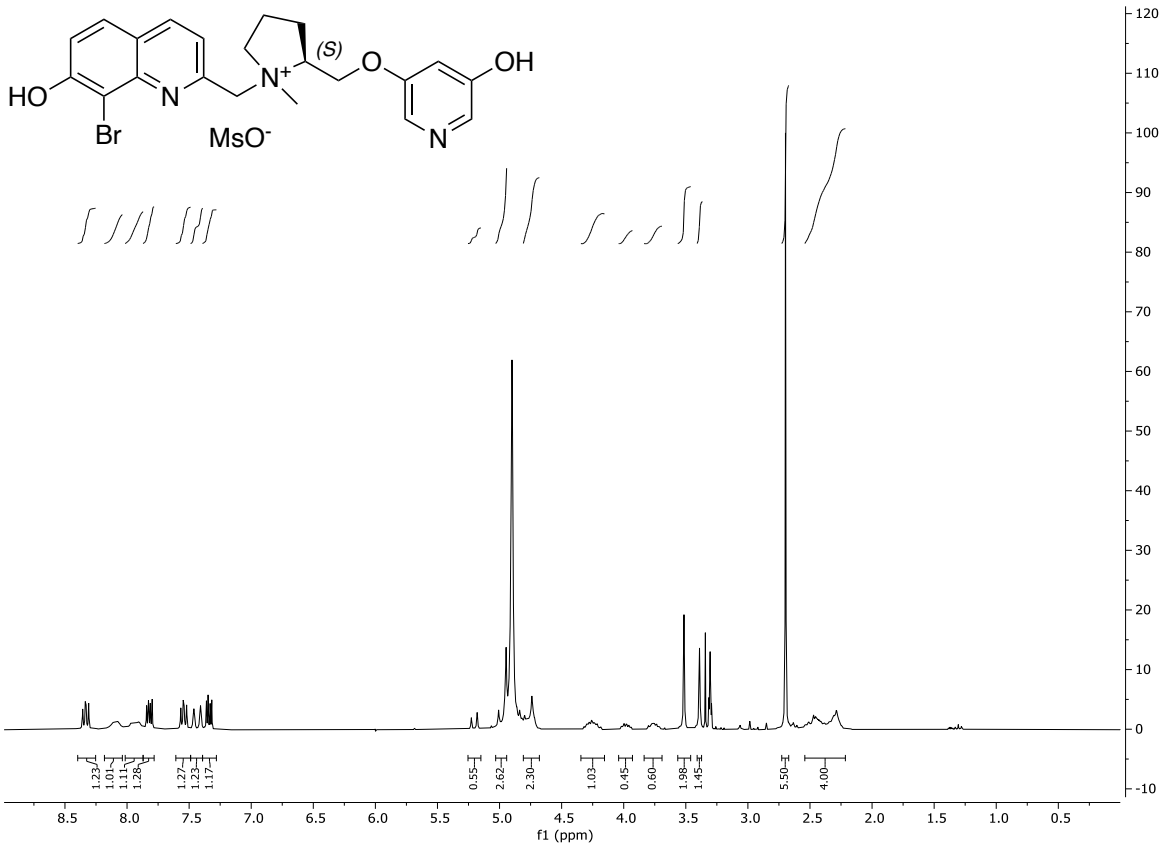

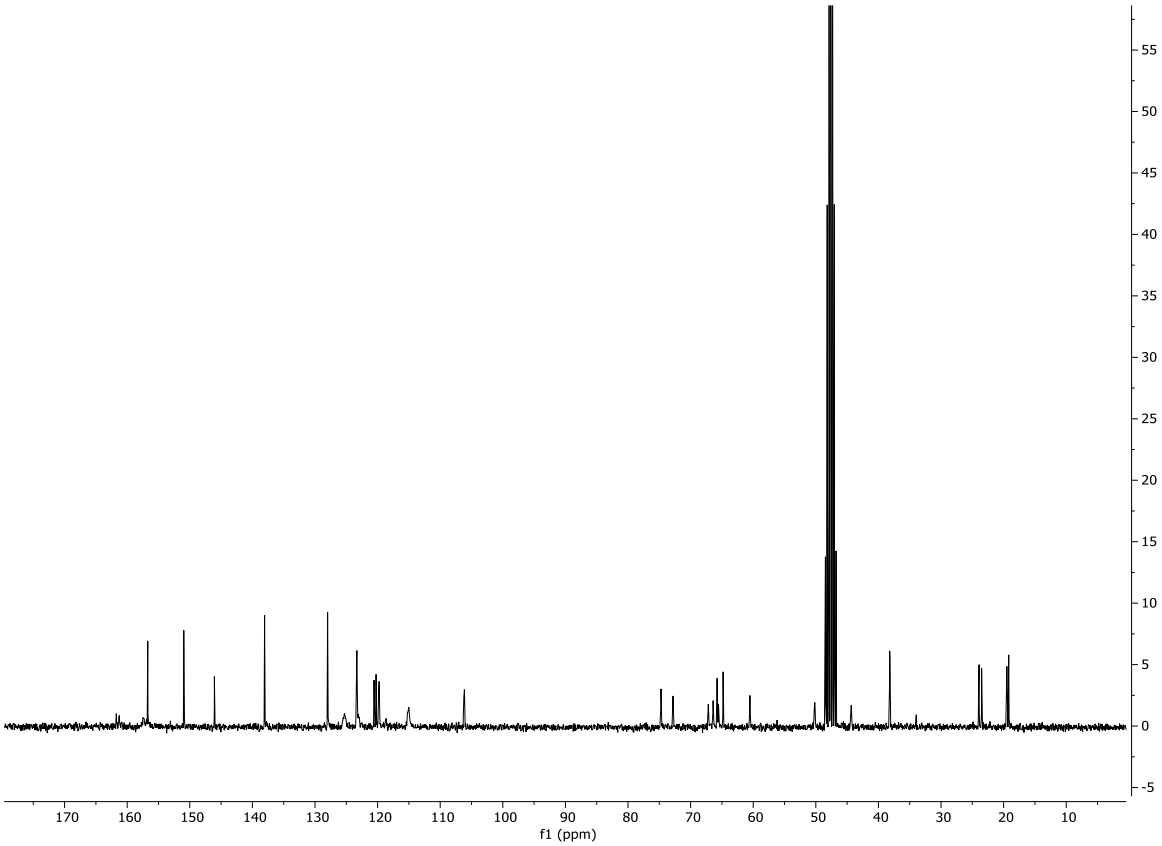

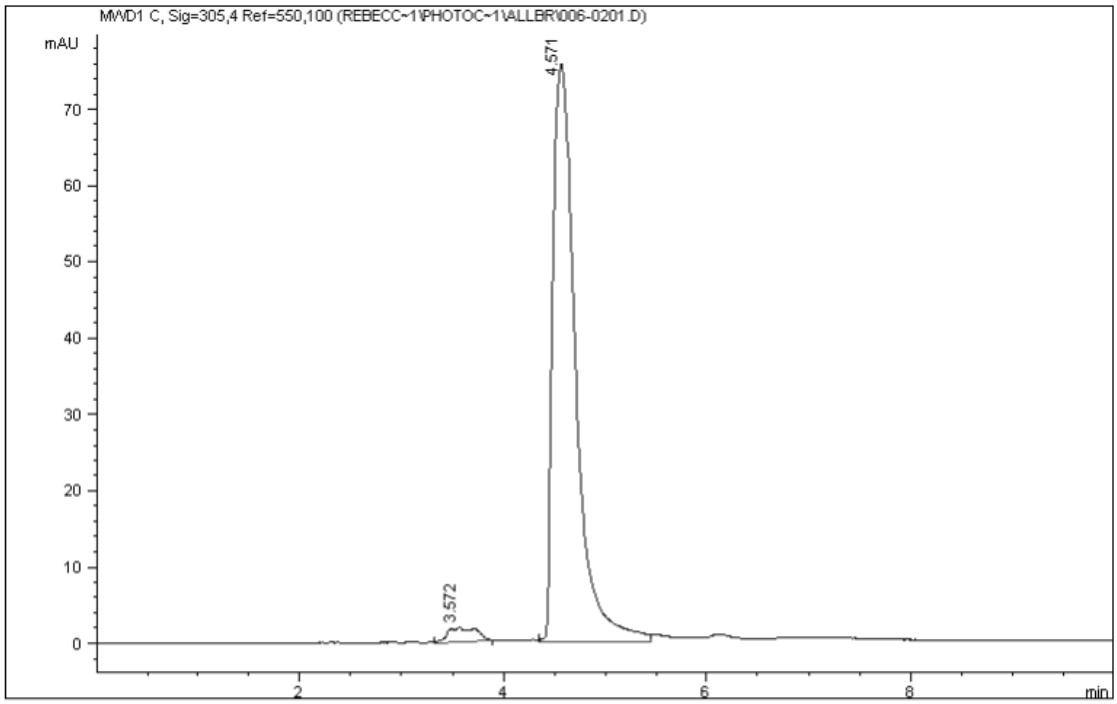

Signal 1: MWD1 C, Sig=305,4 Ref=550,100

Peak #	Area %	Area	RT [min]
1	2.719	33.120	3.572
2	97.281	1.185e3	4.571

Column: Hypersil BDS C18 (250x4.6 mm 5 µm)

Flow: 1 mL/min

Inj volume: 5 µL

Mobile Phase: 75:25 H_2O/CH_3CN + 0.1% TFA

λ: 240 nm

Rt/10 min: 4.57 min

Purity: 97.28%

(2*S*)-1-((8-cyano-7-hydroxyquinolin-2-yl)methyl)-2-(((5-hydroxypyridin-3-yl)oxy)methyl)-1-methylpyrrolidin-1-ium 2,2,2-trifluoroacetate (**CyHQ-(*S*)-VI**)

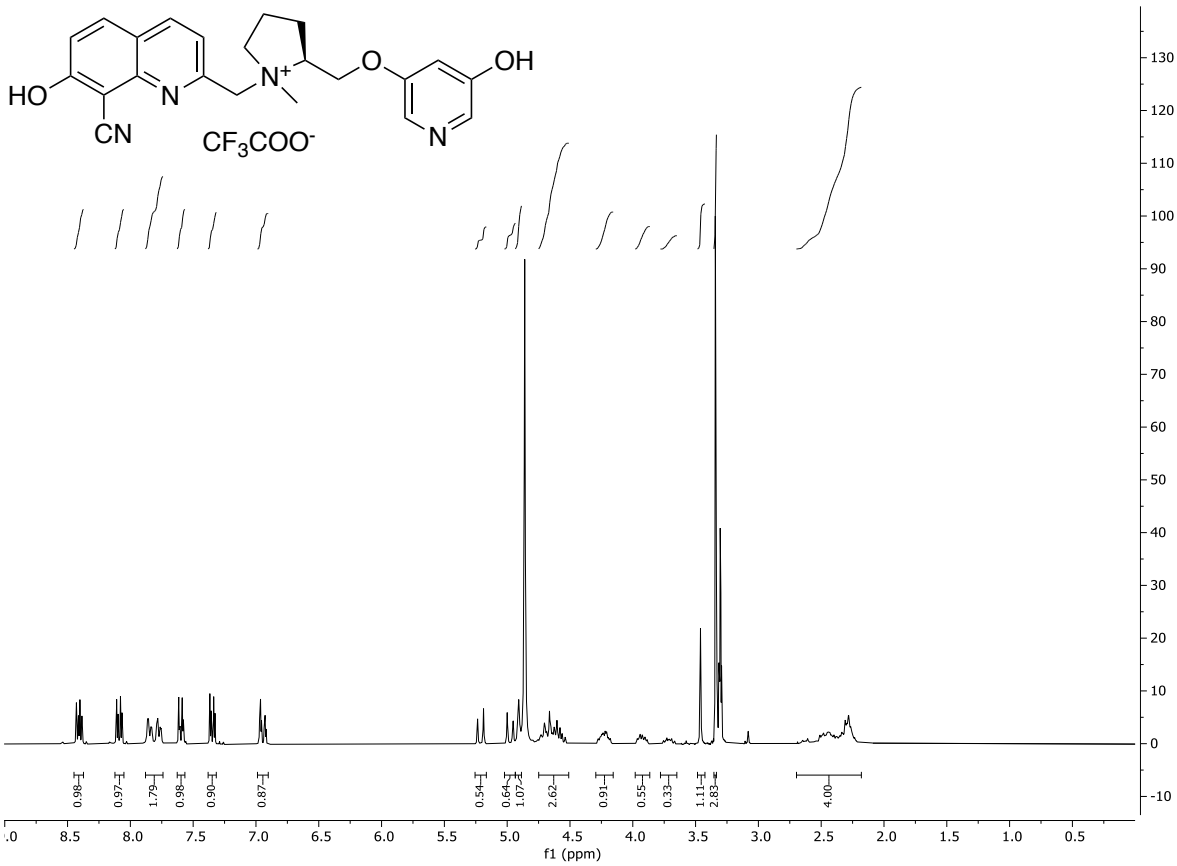

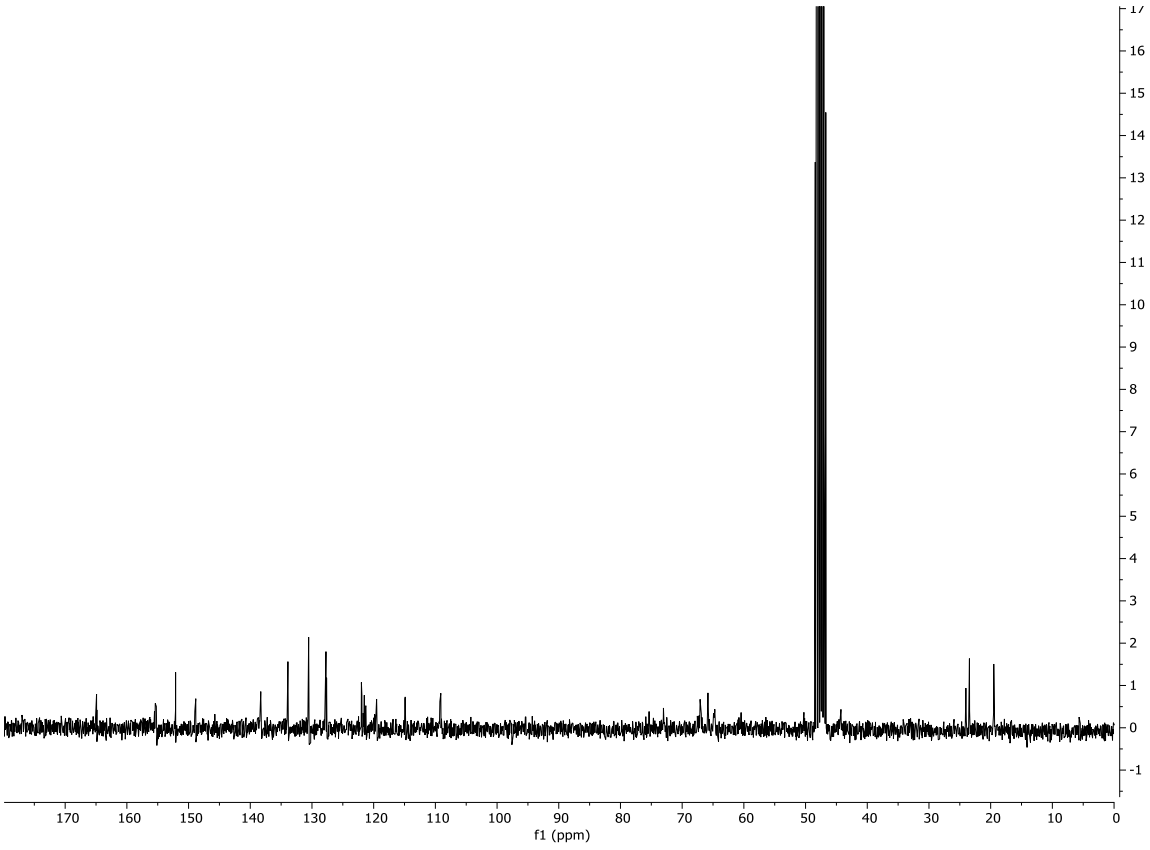

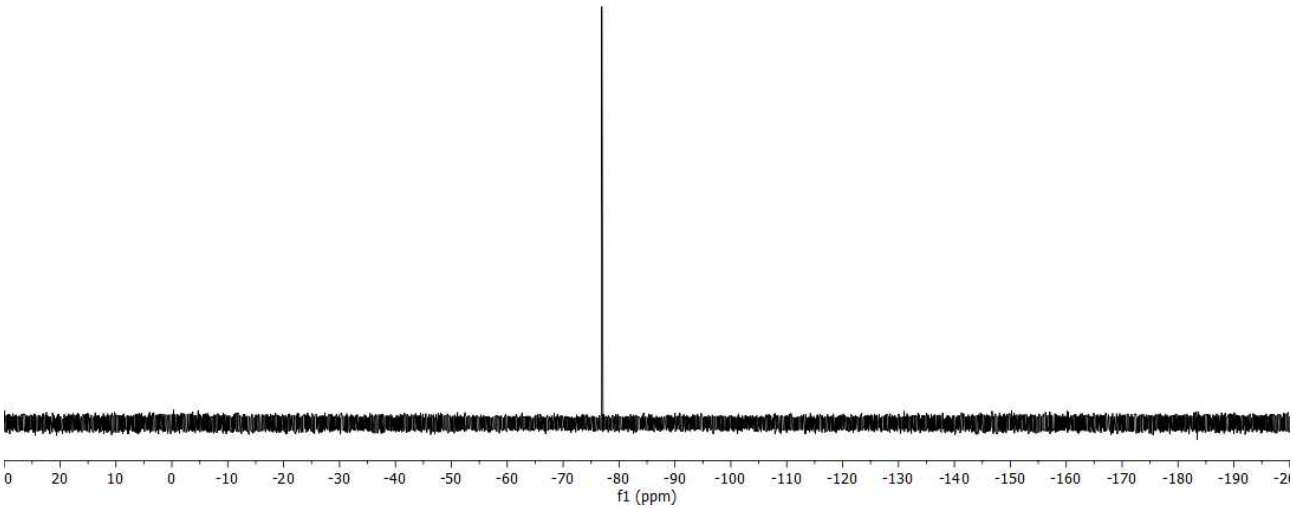
0 20 10 0 -10 -20 -30 -40 -50 -60 -70 -80 -90 -100 -110 -120 -130 -140 -150 -160 -170 -180 -190
f1 (ppm)

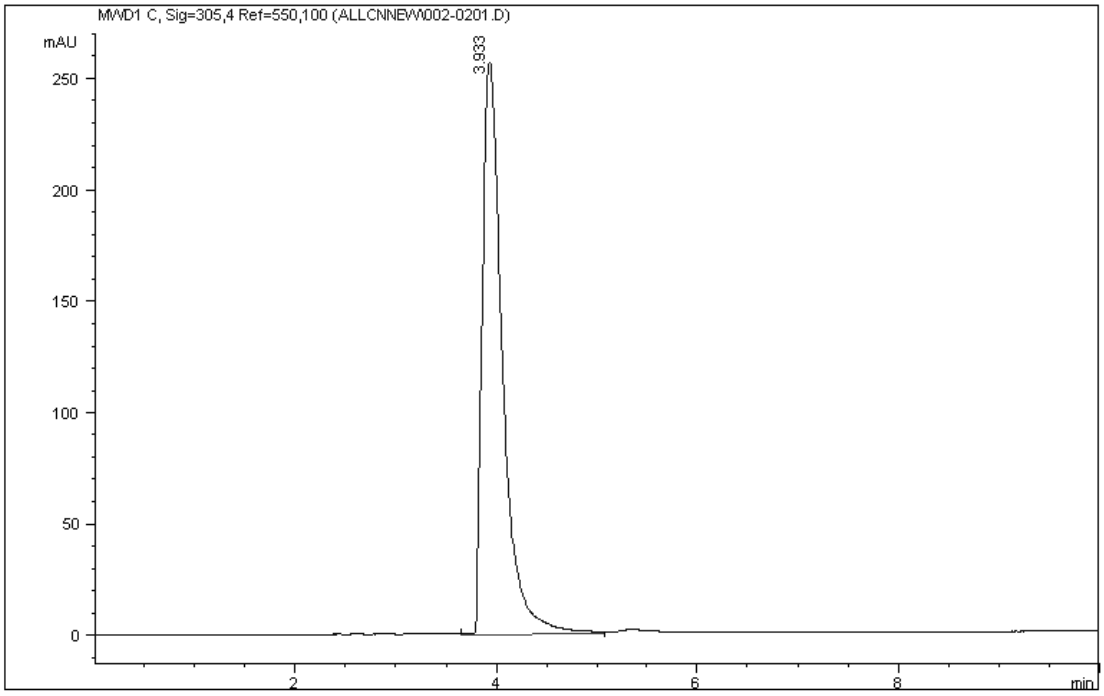

Signal 1: MWD1 C, Sig=305,4 Ref=550,100

Peak #	Area %	Area	RT [min]
1	100.000	3.582e3	3.933

Column: Hypersil BDS C18 (250x4.6 mm 5 µm)

Flow: 1 mL/min

Inj volume: 5 µL

Mobile Phase: 75:25 H_2O/CH_3CN + 0.1% TFA

λ: 240 nm

Rt/10 min: 3.61 min

Purity: 99.40%

Absorption spectra of 8-bromo-2-(hydroxymethyl)quinolin-7-ol (**138**)

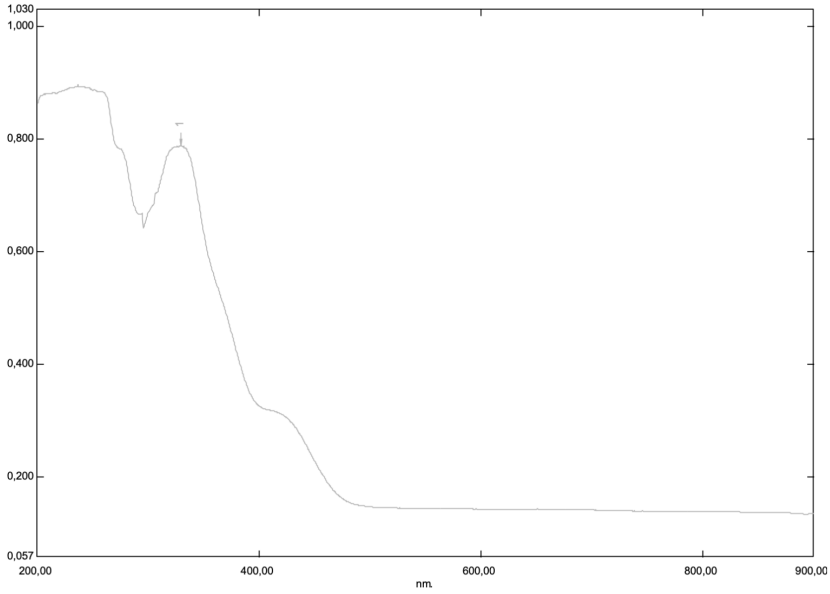

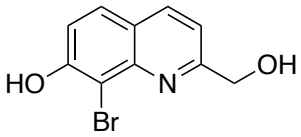

0.39 mM

No.	Wavelength nm.	Abs.
1	329.50	0.788

Absorption spectra of 8-cyano-2-(hydroxymethyl)quinoline-7-ol (**139**)

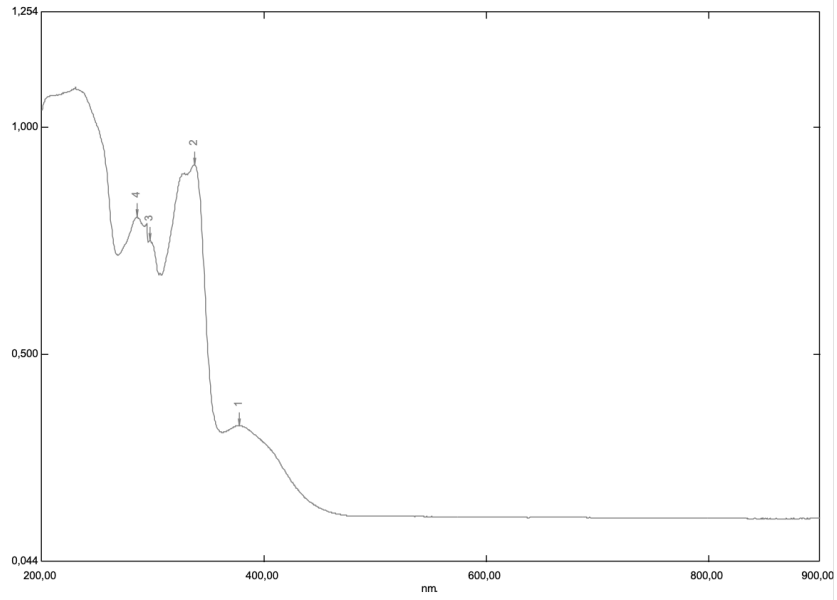

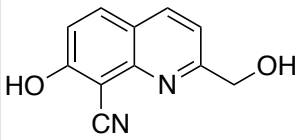

0.5 mM

No	Wavelength nm.	Abs.
1	377.50	0.343
2	337.50	0.918
3	297.50	0.751
4	285.50	0.803

Absorption spectra of (*S*)-5-((1-methylpyrrolidin-2-yl)methoxy)pyridin-3-ol (*S*)-**VI**

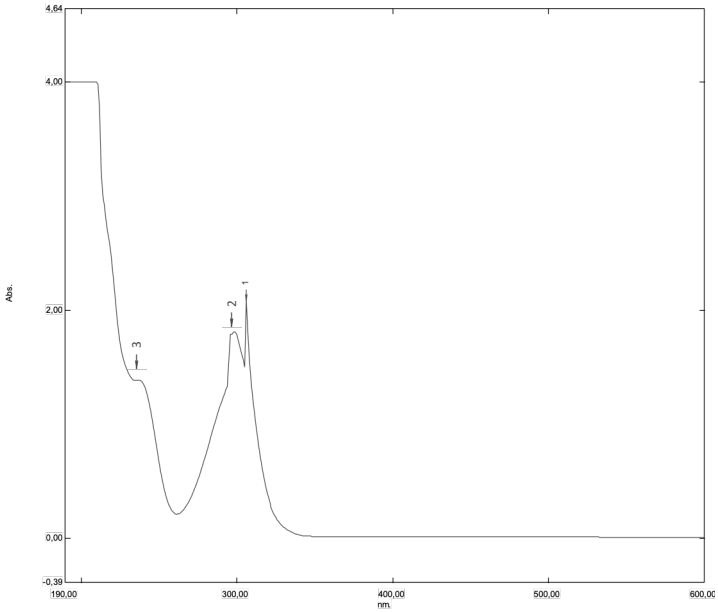

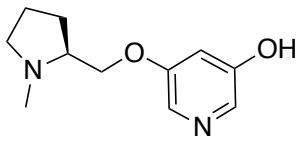

0.53 mM

No.	Wavelength nm.	Abs.
1	306.00	2.09
2	298.00	1.81
3	240.00	1.36

Absorption spectra of (2*S*)-1-((8-bromo-7-hydroxyquinolin-2-yl)methyl)-2-(((5-hydroxypyridin-3-yl)oxy)methyl)-1-methylpyrrolidin-1-ium methanesulfonate BrHQ-(*S*)-**VI**

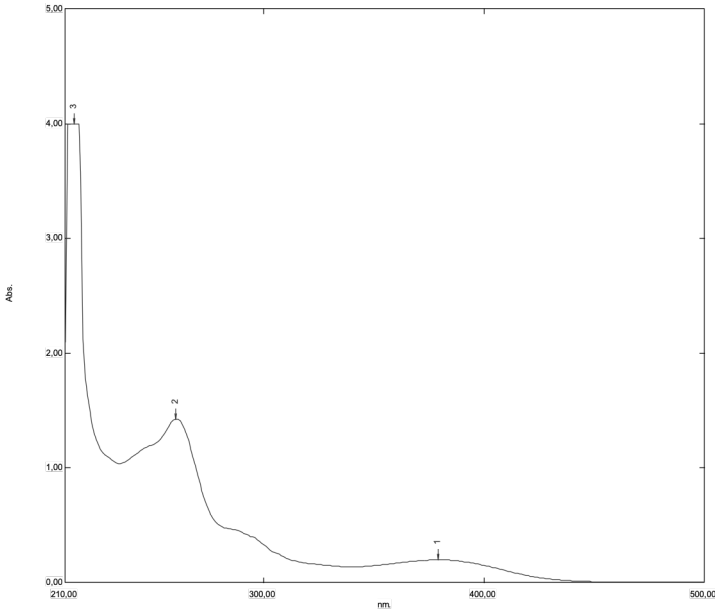

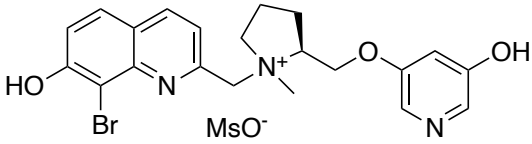

0.1 mM

No.	Wavelength nm.	Abs.
1	379.00	0.20
2	260.00	1.43
3	214.00	4.00

Absorption spectra of (2*S*)-1-((8-cyano-7-hydroxyquinolin-2-yl)methyl)-2-(((5-hydroxypyridin-3-yl)oxy)methyl)-1-methylpyrrolidin-1-ium 2,2,2-trifluoroacetate CyHQ-(*S*)-**VI**

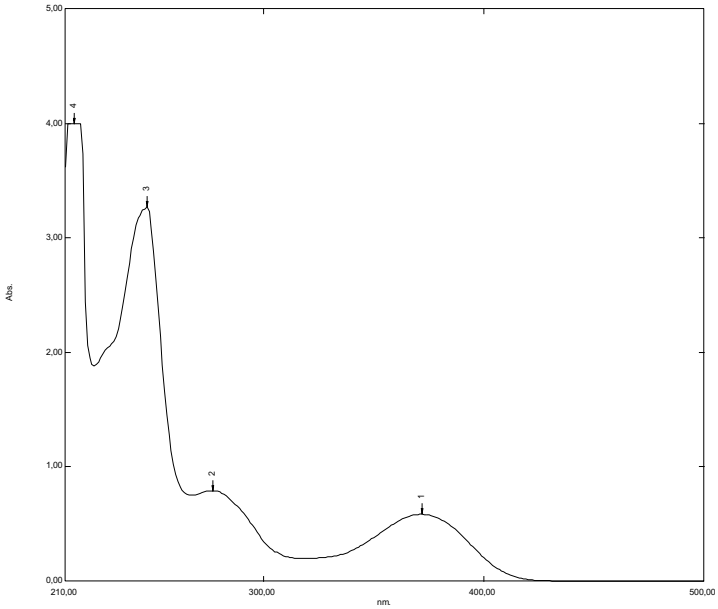

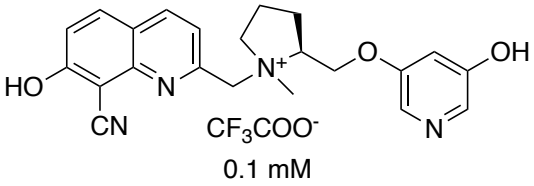

0.1 mM

No.	Wavelength nm.	Abs.
1	372.00	0.58
2	277.00	2.79
3	247.00	3.27
4	214.00	4.00

Photolysis reaction with 1-photon excitation (1PE) of compound BHQ-(*S*)-VI

Gradient elution (flow rate 1 mL/min) using as mobile phases (A) H2O and (B) CH3CN, both containing 0.1% of TFA; the elution was set as follows (%B): 0 min, 10%; 9 min, 20%; 12 min, 20%; 14 min, 10%; 16 min, 10%.

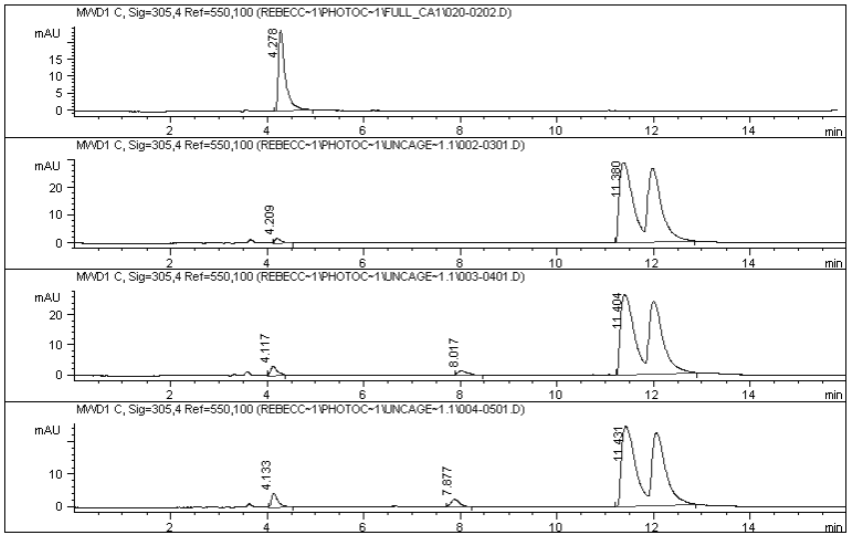

(*S*)-**VI**

BHQ-(*S*)-**VI** 0 sec

BHQ-(*S*)-**VI** 1 sec

BHQ-(*S*)-**VI** 2 sec

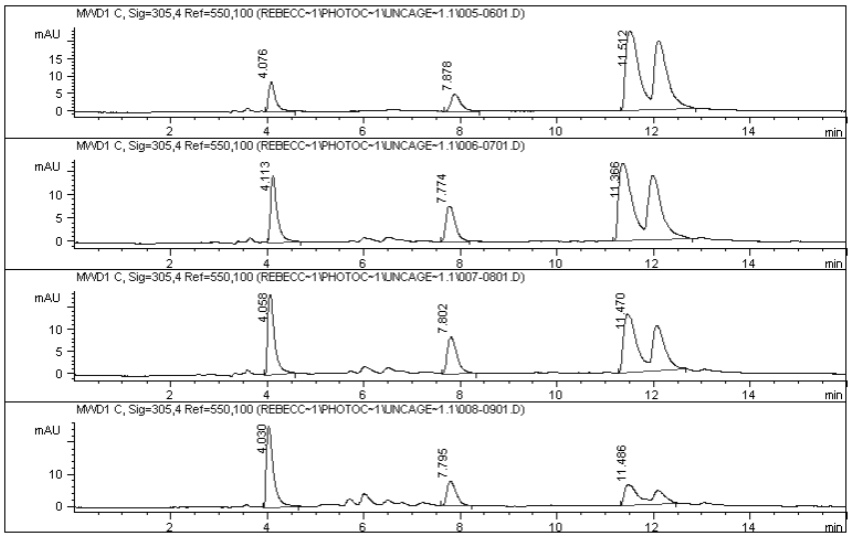

BHQ-(S)-**VI** 5 sec

BHQ-(*S*)-**VI** 10 sec

BHQ-(*S*)-**VI** 15 sec

BHQ-(*S*)-**VI** 30 sec

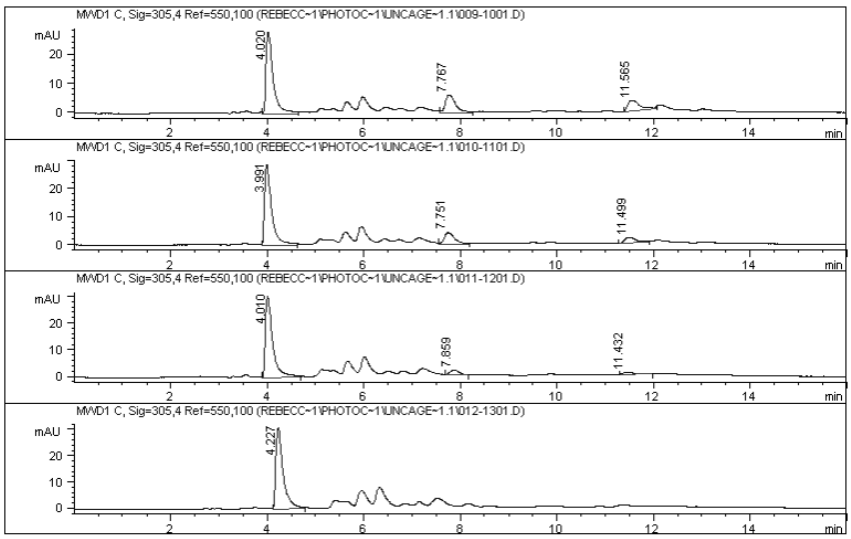

BHQ-(S)-**VI** 45 sec

BHQ-(*S*)-**VI** 60 sec

BHQ-(*S*)-**VI** 90 sec

BHQ-(*S*)-**VI** 120 sec

Photolysis reaction with 1-photon excitation (1PE) of compound CyHQ-(*S*)-VI

Gradient elution (flow rate 1 mL/min) using as mobile phases (A) H2O and (B) CH_3CN, both containing 0.1% of TFA; the elution was set as follows (%B): 0 min, 10%; 9 min, 20%; 12 min, 20%; 14 min, 10%; 16 min, 10%.

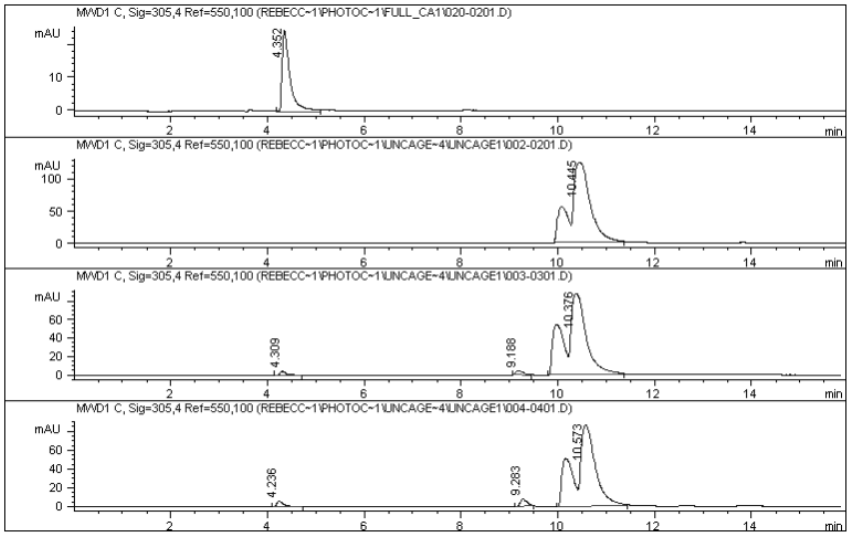

(*S*)-**VI**

CyHQ-(*S*)-**VI**
0 sec

CyHQ-(*S*)-**VI**
1 sec

CyHQ-(*S*)-**VI**
2 sec

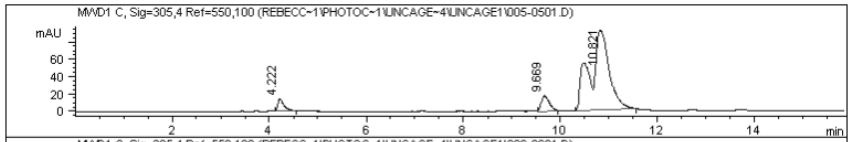

CyHQ-(S)-**VI**
5 sec

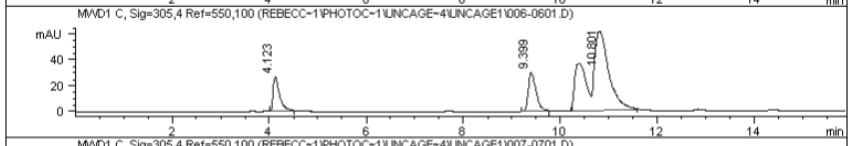

CyHQ-(*S*)-**VI**
10 sec

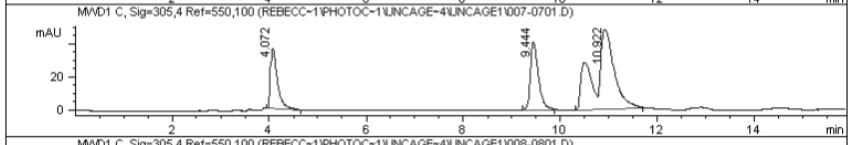

CyHQ-(*S*)-**VI**
15 sec

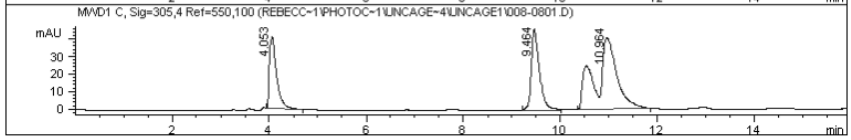

CyHQ-(*S*)-**VI**
30 sec

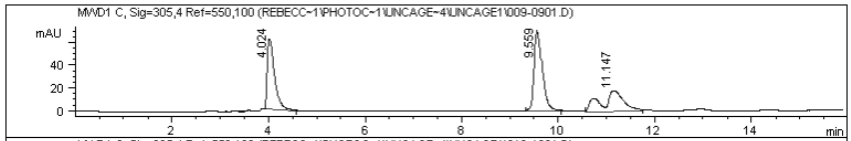

CyHQ-(S)-**VI**
45 sec

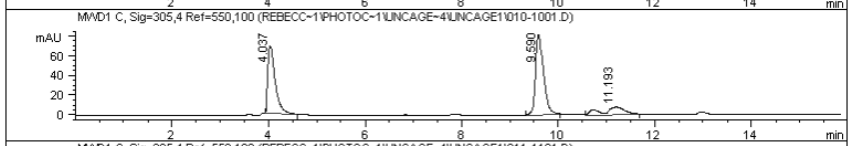

CyHQ-(*S*)-**VI**
60 sec

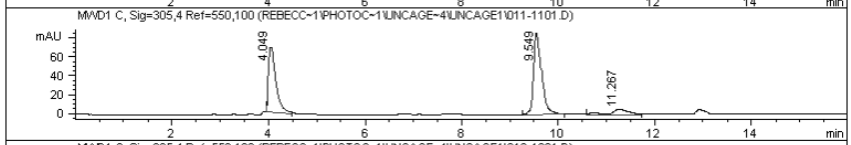

CyHQ-(*S*)-**VI**
90 sec

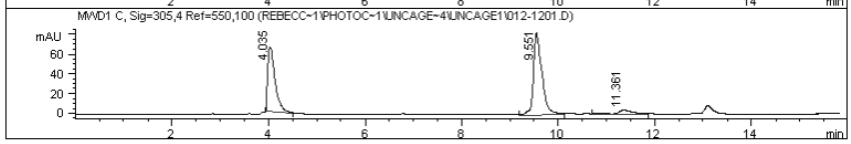

CyHQ-(*S*)-**VI**
120 sec

Ringraziamenti

Ed eccomi qui… alla fine di questo percorso. A volte, pensandoci, sembra sia iniziato ieri, altre volte, invece, sembra un tragitto lungo una vita. Sono passati tre anni ed in questi tre anni la mia vita è cambiata completamente, è stata stravolta e quasi niente è rimasto come prima. Sono stati tre anni magnifici, pieni, sì, di difficoltà, ma anche di gioie, amicizie, soddisfazioni personali e professionali, viaggi, esperienze che mai potrò dimenticare e, ovunque andrò, costudirò con gelosia questo bagaglio di emozioni e conoscenze. In questi ricordi porterò sempre anche le persone che mi sono state vicine, che mi hanno dato una mano dall'alto della loro saggezza, che mi hanno motivata, aiutata, spronata, supportata, che mi hanno fatta ridere quando meno volevo farlo e che non mi hanno mai abbandonata.

Il primo ringraziamento lo vorrei rivolgere ai miei professori, prof. Cristiano Bolchi e prof. Marco Pallavicini: se sono qui è soprattutto merito vostro. Grazie Cri per questi tre fantastici anni (in realtà di più, perché mi hai sopportato anche durante la laurea) assieme. Non è solo perché mi hai insegnato LA chimica, ma soprattutto perché hai creduto in me, ti sei fidato di me e mi hai lasciato tutto lo spazio di manovra di cui avevo bisogno per imparare a gestire un laboratorio, un progetto, anzi, più progetti assieme. Ma in tutto ciò non mi hai mai lasciata un momento da sola, non mi hai mai abbandonato ed il tuo occhio vigile era sempre su di me. Un grazie speciale va anche a lei, prof, per esserci sempre stato nel momento di difficoltà. Grazie per avermi dato questa opportunità, di avermi accolta nel suo gruppo di ricerca, di aver credo in me in tutto e per tutto. È stata un'esperienza magnifica per la quale le sarò sempre grata.

Ringrazio anche ogni singolo collega e studente che hanno condiviso con me i nostri 80m^2 di laboratorio. Marta, Jack, Ricky, Ge, Maya, Anna, Cate, Fra, Marty, Daria, Ali, Sofi, Edo, Bea, Andre, Ele, Vale, Ale, Camo! Mio Dio ragazzi, ma siete tantissimi! Non volevo dilungarmi troppo in questi ringraziamenti (con la crisi energetica, costa stampare pagine in più) ma credo che ognuno di voi sa di quanto io sia grata per il vostro tempo, per il vostro affetto e la vostra professionalità. Con alcuni ci sentiamo tuttora, con altri non ci sentiamo più, però avete fatto parte della mia vita e tutti mi avete fatta crescere. Vi voglio bene ragazzi!

Tra tutti i colleghi, vorrei però ringraziare a parte Francesco. Se non fosse per te, non sarei qui. Non avrei di certo fatto questo percorso e chissà come sarebbe stata la mia vita. Dal giorno di

quella famosa cioccolata, sei stato al mio fianco, sei stata la mia spalla in lab e se anche poi sei stato lontano, ho sempre avuto il tuo supporto. Questa tesi non sarebbe esistita senza di te!

Ci sono altre due persone molto speciali nella mia vita che non sono state presenti solo durante questi tre anni, ma che sono con me da ormai quasi dieci anni. Gaia e Sara. Ormai credo di avervi detto tutto e quello che non ho detto, lo sapete perché mi conoscete meglio di chiunque altro. Grazie per tutto quello che avete fatto e che continuate a fare per me. Ognuna è speciale a modo suo, ma se solo mancasse una di voi, il quadro della mia vita non sarebbe completo. Non potrei desiderare amiche migliori nella mia vita. Grazie!

Ringrazio anche Ale che in tutto ciò è quella che mi sopporta di più tempo. Mi dispiace che tu abbia deciso di cambiare scuola nel 2009, ti saresti risparmiata un'amica così rompipalle ma ormai mi tieni, così come sono! Anche se tra impegni vari riusciamo a vederci poco, so che tu ci sei sempre! Ti voglio bene mur!

Un grazie immenso va ad altre tre persone speciali che in questi tre anni sono entrati a far parte della mia vita. Siete la mia piccola Mountain Family che in effetti vedo più spesso della mia vera family. Come farei senza la mia Alice! Se non ci fossi tu a condividere il mio spirito antisportivo, le risate in parete o nel cane a faccia in giù e soprattutto i lamenti costanti in montagna. Beh, e tutto ciò sarebbe impossibile senza il nostro sommo maestro Garbelli. Grazie Tommy! Per tutti i paranchi, per tutte le risate, mangiate, sclerate… per tutti "Voglio la mia Alice". Siete stupendi! And last but not least, Brambo. Che dire... se l'unico che è riuscito a farmi correre in montagna (ok, per te non era corsa, ma io ero morta) senza che io mi lamentassi o piangessi. Ogni volta che faccio l'otto penso a te e cerco di farlo nella maniera più bella possibile. Grazie che, in modo tutto tuo, ci sei sempre!

E alla fine lascio i ringraziamenti più importanti in assoluto. Prima di tutto voglio ringraziare tutta la mia famiglia, senza distinzione che hanno sempre creduto in me, che mi sono sempre stati vicini e si sono sempre preoccupati per me! Vi voglio bene.

Ringrazio Piero, il mio amore. Ci siamo conosciuti poco dopo il mio ingresso in dottorato e quindi hai avuto la "fortuna" di assistermi in tutte le fasi emotive che ho passato. Mi sei sempre stato vicino, anche quando avrei voluto mollare tutto. Mi sei stato vicino quando mi

trovavo a quasi nove mila chilometri di distanza. Quando mi sentivo giù, hai sempre creduto in me e sei sempre stato e sei tutt'ora orgoglioso di me. Sei stato il supporto più grande che avrei potuto avere. Grazie amore mio!

Отдельное спасибо моей бабуле. Хоть ты и далеко, хоть мы и видимся редко, но я знаю, что ты всегда со мной, переживаешь за меня, любишь меня! Спасибо тебе, что, когда я приезжаю, я чувствую себя опять маленькой девочкой, с твоими блинчками, вареньем и супчками. Я тебя очень люблю!

Un altro grazie va a mio papà. Grazie che ci sei sempre per me, che credi in me anche quando io non ci credo più. Non mi hai lasciata sola neanche un momento di questo percorso e mi hai sempre dato conforto. Lo so, non sono la figlia più affettuosa del mondo, ma ti voglio immensamente bene e non sarei quello che sono diventata senza te. Grazie papino!

Мамулечка, мой самый любимый и дорогой человек на свете, чтобы я делала без тебя! Спасибо тебе за все, спасибо за жизнь, за жертвы, за любовь, за заботу, за то, что ты вырастила меня и дала мне все, лишь бы я исполнила свои мечты. Наконец-то, когда у тебя будут спрашивать про меня, ты сможешь сказать, что я закончила учиться! Я тебя люблю больше всего на свете и без тебя я бы никогда не добилась того, что у меня есть!

Beh, che dire. Alla fine, grazie a me! Che mi sono fatta in quattro ed ora sono qui, che finalmente posso mettere quel tanto sudato "PhD" dopo il mio nome, il resto lo so già.

Grazie UniMi per questi anni, sei stata una casa ma ora è giunto il momento di nuove avventure! Chissà se un giorno ci rivedremo. Per ora non me la sento di darti un addio, ma un semplice….

Ciao.